

Geomechanically coupled modelling of fluid flow partitioning in fractured porous media.

SANAEE, R.

2015

The author of this thesis retains the right to be identified as such on any occasion in which content from this thesis is referenced or re-used. The licence under which this thesis is distributed applies to the text and any original images only – re-use of any third-party content must still be cleared with the original copyright holder.

Geomechanically Coupled Modelling of Fluid Flow Partitioning in Fractured Porous Media

Reza Sanaee

A dissertation submitted in partial fulfilment of the
requirements of The Robert Gordon University for the degree of
Doctor of Philosophy

November 2015



Geomechanically Coupled Modelling of Fluid Flow Partitioning in Fractured Porous Media

Principal Supervisor: Dr. Gbenga Oluyemi

Supervisors' details:

Dr. Gbenga Oluyemi, Dr. Mamdud Hossain and Prof. Babs Oyeneyin

School of Engineering, Riverside East Building, Robert Gordon University,
Garthdee, Aberdeen, UK AB10 7GJ

Funding Institute:

IDEAS Research Institute, Robert Gordon University, Aberdeen, United
Kingdom

Acknowledgement

Intimate moral and technical support and cooperation of my family, supervisors and research colleagues made this challenging research an enjoyable and fruitful experience for me. On behalf of all those who contributed to this success, I would like to thank a few here.

I express my gratitude to my supervisors, **Dr. Gbenga Oluyemi**, **Dr. Mamdud Hossain** and **Prof. Babs Oyeneyin** for their support and beneficial comments throughout my research journey. Owing to their trust, I could develop my industrial skills alongside my academic record. I am also indebted to great financial and administrative support of **Mrs. Virginia Dawod** and **Prof. Susan Crow of IDEAS research Institute** of Robert Gordon University.

I got also benefitted from scientific guidance of other universities' academics such as **Prof. Z. Karpyn of Penn State University** and **Dr. Adriana Paluszny of Imperial College London** and would like to convey my appreciation to their kind cooperation.

My lack of experience in designing and building an experimental set-up was significantly compensated thanks to the technical comments of **Mr. Robert Grey of Corex**, **Mr. Amir Farzaneh of Herriot-Watt University**, and **Mr. Kevin Legge of Pmac** in addition to RGU technicians **Mr. Martin Johnstone** and **Mr. Andy Ross**. I sincerely appreciate their guidance. I also have to acknowledge cherished collaboration of **Dr. David Healy of University of Aberdeen** for authorizing my sonic measurements.

Finally I owe all my lifetime triumphs to everlasting emotional support of my family and friends. I wouldn't be able to make this research without you. Thank You!

Dedication

This dissertation is dedicated to my Father, my Mother, my Brother and my Sister for their patience and spiritual encouragement.

Abstract

Reza Sanaee

PhD dissertation: Geomechanically coupled modelling of fluid flow partitioning in fractured porous media

Naturally fractured reservoirs are characterised with complex hydro-mechanical dynamics. Hydrocarbon can be stored and produced from rock matrix, the fracture network or both, in these reservoirs. Normally the fracture network is depleted much faster than the matrix blocks due to its increased hydraulic conductivity; consequently, the recovery factor is low for these reservoirs. Additionally, in-situ stress profile changes with reservoir depletion and affects fluid flow dynamics of the fractured reservoir. Therefore dynamic characterisation of fractured reservoirs is considered as a challenging task responsible for inefficient exploitation of their reserves. This dissertation focuses on characterising matrix-fracture fluid flow partitioning subjected to variable overburden stress loading. Understanding of the matrix-fracture hydro-mechanical interaction would assist in developing optimum production plans to maximize fractured reservoirs recovery.

Initially three different fracture implementation techniques of simulating fracture as an equivalent porous medium, implementing it as a sub-dimensional feature within the porous matrix and considering fracture domain as an open channel were evaluated using a set of published laboratory core flooding data. The best fracture simulation approach was identified to be fracture implementation as an open channel interacting with matrix block. This approach takes into consideration the coupling of Darcy flow equation in the matrix domain to Navier-Stokes flow formulation in the fracture. The efficiency of this fracture simulation approach was significantly enhanced when coupled further with poro-elasticity physics and stress dependent permeability.

In the next step, the coupled open channel fracture simulation approach was applied to perform a sensitivity analysis on effect of all parameters of the governing equations on fracture and matrix flow. The results of this analysis were statistically analysed, with specific attention to the analytical formulation

of the governing equations, to develop coupled empirical flow models for fracture and matrix. These empirical models incorporate both flow physics of matrix and fracture as well as mechanical loading impacts. An analysed multiphase flow scenario demonstrated the compatibility of the coupled simulation approach with multiphase flow investigations in fractured porous media.

A novel core flooding set-up, capable of separated fracture and matrix flow measurement, was designed and built to enable laboratory evaluation of the developed empirical models. This set-up enabled monitoring of pressure front within matrix and fracture taking the advantages of several differential pressure transducers along the core plug length. Variation of the matrix and fracture flow in response to different stress loading scenarios was investigated in laboratory. Furthermore, laboratory validation indicated that matrix flow model is capable of predicting laboratory measurements with an acceptable accuracy; however, fracture flow model seemed to need more improvement. Probable factors that could have caused inaccuracy in fracture flow model were discussed and improving actions were recommended as an extension to this research. Application of the empirical models in fractured porous medium characterisation simulations reduces the coupling-related numerical complexities.

The coupled empirical models can predict flow dynamics of fractured reservoirs under various stress regimes. They demand much less computational effort and as they incorporate geometrical factors they can be up scaled conveniently. In terms of production planning for fractured reservoirs, the empirical models can assist engineers to manage matrix and fracture production efficiently based on overburden stress variations.

Table of Contents

ACKNOWLEDGEMENT	III
DEDICATION	IV
ABSTRACT.....	V
TABLE OF CONTENTS	VII
LIST OF FIGURES	X
LIST OF TABLES	XIV
NOMENCLATURE	XV
SUBSCRIPTS AND MATHEMATICAL OPERATORS.....	XVIII
CHAPTER 1.0.....	1
INTRODUCTION	1
1.1 BACKGROUND.....	1
1.1.1 <i>Naturally Fractured Reservoirs</i>	1
1.1.2 <i>Fracture-Matrix flow interaction</i>	3
1.1.3 <i>Poro-elasticity</i>	5
1.2 JUSTIFICATION FOR RESEARCH	6
1.3 RESEARCH AIM AND OBJECTIVES	9
1.4 RESEARCH METHODOLOGY	10
1.4.1 <i>Numerical modelling</i>	10
1.4.2 <i>Statistical and analytical investigations</i>	11
1.4.3 <i>Laboratory experiments</i>	11
1.5 CONTRIBUTION TO KNOWLEDGE	12
1.6 DISSERTATION LAYOUT.....	13
CHAPTER 2.0.....	15
LITERATURE REVIEW	15
2.1 INTRODUCTION	15
2.2 ANALYTICAL STUDIES	17
2.3 NUMERICAL SIMULATIONS.....	23
2.4 LABORATORY EXPERIMENTAL INVESTIGATIONS	29
CHAPTER 3.0.....	34
FRACTURE MODELLING WITHIN POROUS MEDIA	34
3.1 INTRODUCTION	34
3.2 FRACTURE AS AN EQUIVALENT POROUS DOMAIN	34
3.2.1 <i>Governing equations</i>	38
3.2.2 <i>fracture-matrix hydraulic interaction</i>	39
3.3 FRACTURE AS (N-1) DIMENSIONAL FEATURE WITHIN POROUS MATRIX	43
3.3.1 <i>Discrete fracture implementation in COMSOL</i>	43
3.3.2 <i>Darcy law Governing equations and fracture flow boundary condition</i>	45
3.3.3 <i>N-1 dimensionally modelled fracture analysis results</i>	46
3.4 REALISTIC OPEN CHANNEL FRACTURE	50

3.4.1	<i>Open channel fracture geometry and discretisation</i>	50
3.4.2	<i>Open channel fracture modelling concept governing equations</i>	52
3.4.3	<i>Open channel fracture simulation efficiency</i>	53
3.4.4	<i>Matrix-fracture cross flow characterisation</i>	58
3.5	OPEN CHANNEL FRACTURE COUPLED WITH PORO-ELASTICITY AND STRESS DEPENDENT PERMEABILITY.....	59
3.5.1	<i>Poro-elasticity and stress dependent permeability physics</i>	60
3.5.2	<i>Coupled open channel fracture modelling outcomes</i>	62
3.5.3	<i>Cross flow modelling applying coupled open channel fracture approach</i>	68
3.6	DISCUSSION.....	70
CHAPTER 4.0		73
MECHANISTIC EMPIRICAL MATRIX AND FRACTURE FLOW MODELS		73
4.1	INTRODUCTION	73
4.2	NUMERICAL EVALUATION OF HYDRO-MECHANICAL PARAMETERS.....	75
4.2.1	<i>Porous matrix cross section area open to flow</i>	75
4.2.2	<i>Initial rock matrix permeability</i>	79
4.2.3	<i>Core plug length</i>	82
4.2.4	<i>Fluid dynamic viscosity</i>	86
4.2.5	<i>Differential pressure</i>	88
4.2.6	<i>Overburden stress</i>	90
4.2.7	<i>Biot-Willis coefficient</i>	94
4.2.8	<i>Poisson’s ratio</i>	98
4.2.9	<i>Young’s Modulus</i>	102
4.2.10	<i>Pore pressure</i>	107
4.2.11	<i>Fluid density</i>	111
4.2.12	<i>Initial fracture aperture</i>	114
4.3	COUPLED EMPIRICAL MODELS FOR FRACTURE AND MATRIX FLOW	119
4.3.1	<i>Matrix flow model</i>	119
4.3.2	<i>Fracture flow model</i>	123
4.4	EXTENSION OF COUPLING APPROACH TO TWO-PHASE FLOW MATRIX-FRACTURE INTERACTION	126
4.4.1	<i>Two-phase flow governing equations</i>	127
4.4.2	<i>Two-phase scenario physics coupling</i>	131
CHAPTER 5.0		136
LABORATORY ANALYSIS OF MATRIX-FRACTURE FLOW INTERACTION UNDER MECHANICAL LOADING		
CONDITIONS		136
5.1	INTRODUCTION	136
5.2	LABORATORY FRACTURED POROUS MEDIA FLOW ANALYSES BACKGROUND.....	137
5.3	CORE FLOOD RIG DESIGN AND IMPLEMENTATION	138
5.4	MATRIX-FRACTURE FLOW PARTITIONING LABORATORY ANALYSIS PROCEDURE	145
5.4.1	<i>Plug samples physical properties</i>	145
5.4.2	<i>Brine preparation</i>	147
5.4.3	<i>Laboratory fractured core flooding tests</i>	148
5.5	EXPERIMENTAL ANALYSIS RESULTS AND EMPIRICAL MODELS VALIDATION.....	153
CHAPTER 6.0		159
DISCUSSION, CONCLUSIONS AND RECOMMENDATION FOR FURTHER RESEARCH		159
6.1	INTRODUCTION	159

6.2 DISCUSSION.....	159
6.2.1 <i>Coupling techniques of open fracture modelling approach</i>	159
6.2.2 <i>Parametric numerical analysis and empirical models</i>	161
6.2.3 <i>Laboratory validation of the developed empirical models</i>	163
6.3 CONCLUSIONS.....	165
6.4 RECOMMENDATION FOR FURTHER WORK	167
REFERENCES	169
APPENDIX A: PUBLICATIONS	189

List of Figures

Figure 1-1: Snapshot of a fractured formation outcrop in south of Iran-----2

Figure 1-2: An illustration of simultaneous fracture and matrix production in the near-wellbore region-----6

Figure 2-1: Stress affected fracture and matrix permeability models-----21

Figure 2-2: Schematic demonstrating a laboratory set-up for brine-flooding of an artificially fractured core plug-----32

Figure 3-1: Core flooding of an artificially fractured core plug under confining overburden stress-----35

Figure 3-2: Fractured core plug created and meshed using Ansys Fluent-----36

Figure 3-3: Vertical cross section of fluid velocity z component-----40

Figure 3-4: Flow paths visualization which demonstrates a drainage scenario-----41

Figure 3-5: Matrix-fracture flow partitioning results derived from equivalent porous medium approach simulation-----42

Figure 3-6: Two-dimensional fracture implementation within core plug geometry-----44

Figure 3-7: Velocity field arrow diagram superimposed on the pressure iso-surface contours-----47

Figure 3-8: Overburden stress effect on fracture flow while modelling fracture as a sub-dimensional boundary using COMSOL Darcy’s law interface-----49

Figure 3-9: Geometry created for the open channel fracture modelling concept utilizing symmetry boundary condition-----51

Figure 3-10: Velocity contours indicating flow velocity profile evolution and flow exchange quality along the core length-----54

Figure 3-11: Open channel fracture-matrix flow partitioning-----56

Figure 3-12: Fracture flow partitioning variation in response to overburden stress loading calculated using the sub-dimensional fracture implementation and open channel fracture modelling approach-----57

Figure 3-13: Matrix-fracture cross flow-----58

Figure 3-14: Total matrix displacement slice diagram-----63

Figure 3-15: Total matrix displacement plot-----64

Figure 3-16: Coupled open channel fracture-matrix flow partitioning-----65

Figure 3-17: Matrix flow variation in the coupled simulation-----66

Figure 3-18: Cross flow variation in coupled open channel fracture simulation approach-----69

Figure 3-19: Fracture modelling approach validation-----70

Figure 3-20: Fracture flow partitioning in coupled analysis-----71

Figure 4-1: Matrix displacement in response to overburden stress-----76

Figure 4-2: Stress affected fracture closure for various matrix plug sizes----77

Figure 4-3: Fracture and matrix flow versus plug radius-----78

Figure 4-4: Fracture-matrix cross flow variation due to cross section area alterations-----79

Figure 4-5: Incremental fracture flow response to various matrix permeabilities-----80

Figure 4-6: Cross flow infinitesimal change versus matrix permeability-----81

Figure 4-7: Matrix flow for various matrix permeabilities-----82

Figure 4-8: Core plug length effect on the mechanical displacements-----83

Figure 4-9: Fracture and matrix flow evolution versus core plug length-----84

Figure 4-10: Cross flow variation as the plug length increases-----85

Figure 4-11: Effect of dynamic viscosity on fracture and matrix flow-----86

Figure 4-12: Effect of dynamic viscosity on fracture-matrix cross flow-----87

Figure 4-13: Matrix displacement versus differential pressure-----88

Figure 4-14: Fracture and matrix flow versus differential pressure-----89

Figure 4-15: Cross flow as a function of differential pressure-----90

Figure 4-16: Matrix displacement in response to overburden stress-----91

Figure 4-17: Fracture and matrix flow variation under different overburden stresses-----92

Figure 4-18: Matrix flow as a function of overburden stress-----93

Figure 4-19: Cross flow change due to overburden stress variation-----94

Figure 4-20: Biot-Willis coefficient driven matrix displacement-----95

Figure 4-21: Fracture flow response to Biot-Willis coefficient-----96

Figure 4-22: Effect of Biot-Willis coefficient variation on matrix flow-----97

Figure 4-23: Cross flow alteration due to Biot-Willis coefficient change-----98

Figure 4-24: Poisson’s ratio effect on matrix displacement under overburden stress-----99

Figure 4-25: Poisson’s ratio effect on matrix flow-----	100
Figure 4-26: Poisson’s ratio effect on fracture flow-----	101
Figure 4-27: Matrix-fracture cross flow change due to various Poisson’s ratio values-----	102
Figure 4-28: Less matrix displacement for higher young’s modulus values--	103
Figure 4-29: Minor increase of matrix flow for higher young’s modulus core plugs-----	104
Figure 4-30: Young’s modulus effect on fracture and matrix flow-----	105
Figure 4-31: Significant increase of cross flow rate as Young’s modulus increases-----	106
Figure 4-32: Pore pressure effect on matrix displacement-----	107
Figure 4-33: Matrix flow increases due to pore pressure rise-----	108
Figure 4-34: Fracture flow increases due to higher pore pressures-----	109
Figure 4-35: Matrix-fracture cross flow versus pore pressure-----	110
Figure 4-36: Matrix flow for various fluid densities-----	111
Figure 4-37: Incremental increase of fracture flow with fluid density-----	112
Figure 4-38: Matrix-fracture cross flow affected by fluid density-----	113
Figure 4-39: Matrix flow variation for different initial fracture aperture sizes-----	115
Figure 4-40: Matrix and fracture flow characterisation for different initial fracture aperture sizes-----	115
Figure 4-41: Matrix-fracture flow exchange evolution for various initial fracture aperture sizes-----	116
Figure 4-42: Sensitivity of various parameters appearing in governing equations on fracture, matrix and cross flow-----	118
Figure 4-43: Matrix flow modelling pseudo parameters-----	120
Figure 4-44: Matrix flow regression model residual magnitudes-----	122
Figure 4-45: Fracture flow modelling pseudo parameters-----	124
Figure 4-46: Fracture flow fitted model residuals’ statistics-----	125
Figure 4-47. Typical relative permeability model implemented in the two-phase flow equations within core plug matrix-----	128
Figure 4-48: Outlet boundaries incorporated for the two-phase Darcy law physics -----	132
Figure 4-49: Oil saturation profile versus time within matrix-----	134

Figure 4-50: Oil saturation profile versus time within fracture-----134

Figure 4-51: Two phase flow fracture and matrix flow partitioning for oil phase-----135

Figure 5-1: Cut core plugs-----139

Figure 5-2: Set metallic shim-----140

Figure 5-3: Metallic flow accumulating plugs-----141

Figure 5-4: Sandstone half plugs attached to the flow accumulating plugs ready for flooding test-----142

Figure 5-5: Core flood rig design-----143

Figure 5-6: Core flood rig equipped with digital pressure monitoring -----144

Figure 5-7: Rock mechanical properties of Buff Berea sandstone-----147

Figure 5-8: Laboratory implemented initial and boundary conditions for the flooding tests-----149

Figure 5-9: Typical differential pressures while flooding-----150

Figure 5-10: Matrix and fracture laboratory flow measurements-----154

Figure 5-11: Matrix flow model evaluation-----155

Figure 5-12: Fracture flow model evaluation-----156

List of Tables

Table 2-1: Back calculated fracture aperture magnitudes for an artificially fractured core plug flooded under overburden stress-----	33
Table 3-1: Simulated fractured core plug and flooding fluid properties-----	37
Table 3-2: Equivalent porous media approach simulation (eq. Porous) results versus cumulative outflow laboratory measurements of stalker et al. -----	41
Table 3-3: Comparison of flow partitioning results considering sub-dimensional implementation of fracture (disc. Frac) versus the equivalent porous medium modelling strategy (eq. Porous) for the 21.4 MPa confining stress-----	48
Table 3-4: Comparison of flow partitioning results considering sub-dimensional implementation of fracture (disc. Frac) and the open channel fracture (open Frac) simulation approach under 21.4 MPa confining stress-----	54
Table 3-5: Flow partitioning results for coupled open channel fracture simulation approach-----	67
Table 3-6: Comparison of the simulation specification for each of the fractured porous medium simulation approaches-----	67
Table 4-1: Modelling data for the numerical sensitivity analysis-----	74
Table 5-1: Buff Berea sandstone plugs and laboratory used brine specification-----	146
Table 5-2: Brine composition after McGuire et al., 2005-----	147

Nomenclature

Symbol	Description
A	Cross sectional area [m^2]
b	Fracture aperture [m]
C_o	Drag coefficient for oil droplets
c	Mass fraction
D_{md}	Turbulent dispersion coefficient [m^2/s]
d_o	Equivalent diameter of oil droplets [m]
E	Young's modulus [Pa]
F	Any additional body force [N]
$FFLOW$	Fracture flow [m^3/s]
g	Acceleration of gravity [m/s^2]
\bar{H}	Effective fracture aperture [m]
k, K	Permeability [m^2]
k_n	Fracture stiffness [N/m]
k_r	Relative permeability
L	Length of fracture/core [m]
M	Inverse of Darcy storage coefficient

$MFLOW$	Matrix flow [m^3/s]
m_{ob}	Oil to brine(continuous) phase mass transfer rate [kg/s]
P	Pressure [Pa]
P_p	Pore pressure [Pa]
Q, q	Volumetric flow rate [m^3/s]
Q_m	Mass source term [$kg/m^3.s$]
Re	Reynolds number
S	Saturation; Source term in momentum equation [N/m^3]
s	Fracture spacing [m]
t	Time [s]
u	Displacement [m]
v	Velocity [m/s]
V_c	Compressional wave velocity [m/s]
V_R	Node volume [m^3]
V_s	Shear wave velocity [m/s]
v_{slip}	Relative velocity vector between two phase
α	Pressure coefficient
α_B	Biot-Willis coefficient

γ	Transmissivity term [m^2/s]
Δ_n	Actual thickness of porous domain grids [m]
$\Delta\varepsilon$	Total body strain
$\Delta\sigma$	Total stress change [Pa]
θ	Tortuosity
μ	Viscosity [Pa.s]
μ_T	Turbulent viscosity [Pa.s]
ϑ	Poisson's ratio
ξ	Fluid content
ρ	Density [kg/m^3]
τ	Fracture/matrix transfer term [m^3/s]
τ_{Gm}	Summation of viscous and turbulence stresses [Pa]
φ	Effective porosity
∇D	Unit vector in gravity direction [m]
C	Inertial resistance factor [1/m]
\aleph	Exponential recovery constant [1/s]

Subscripts and Mathematical Operators

Symbol	Description
b	Brine
c	Connate saturation
D_c	Diffusion coefficient
e	Effective
f	Fracture value
fma	Fracture-matrix interface
i, j, k	Unit vectors of x, y and z axis
j, β	Phase
ma	Matrix value
o	Oil
P	Particle
R	Grain radius
r	Relative/Residual
T	Tangential plane of fracture
t	Time
tp	Two phase

Vol	Volumetric
w	Water
x, y, z	Coordinate directions
\rightarrow	Vector
$,$	Partial differentiation with respect to the following index
∇	Nabla differential operator
0	Initial

Chapter 1.0

Introduction

More than half of the past century has been involved with various theoretical, experimental and numerical analyses to characterise flow dynamics within petroleum reservoirs. Occurrence of natural fractures within the reservoirs adds to the complexity of petroleum accumulation, migration and production. Variable in-situ stress regime, due to reservoir depletion as it is being exploited, alters the quality of fractured reservoirs flow regimes and further complicates reservoir dynamic characterisation.

Applications of numerical simulations assisted significantly in understanding hydro-mechanical behaviour of these reservoirs. However geometry complexity can result in excessive numerical run-time in fractured formations analysis. This dissertation is focused on developing and validating empirical models that can alleviate the aforementioned numerical complexities of fractured reservoirs flow characterisation.

1.1 Background

1.1.1 Naturally Fractured Reservoirs

Naturally fractured petroleum reservoirs have been challenged for about half a century in development, drilling and completion, production and enhanced recovery stages worldwide. As a critically important category of challenging hydrocarbon resources, they account for almost 60 percent of the world oil remaining reserves (Elfeel et al., 2010). Figure 1-1 shows a typical fractured formation outcrop in Middle East region.



Figure 1-1. Snapshot of a fractured formation outcrop in south of Iran.

Characterisation and evaluation of fluid flow (Sarkar et al., 2002; Paul et al., 2007; Unsal et al. 2010; Barton et al., 2013), particles transfer (Di Donato and Blunt, 2004; Stalgorova and Babadagli, 2012), heat exchange (Suzuki et al. 2014) and mechanical deformation (Settari et al., 2001; Rutqvist et al., 2002; Elkhoury et al., 2013) phenomena within this type of reservoirs have been extensively investigated in various disciplines ranging from petroleum engineering and hydro-geology to nuclear waste disposal. Fractures flow and mechanics characterisation is critical in storage and waste disposal operations as they provide leakage pathways and consequently can result in the operation failure (Fleming and Haggerty, 2001).

Existence of fractures as highly conductive channels within the formation along with their varying mechanical conditions due to active in-situ stress regimes is the main source of these reservoirs complexity. Once a wellbore intrudes a fractured formation, encountering various pressure abnormalities is inevitable. This is due to the fact that the rock mass is not acting as a continuum. Drilling instability issues (Zhang et al., 2003; Jamshidi and Amani, 2014) will be encountered among the most imminent complications in early stages of a fractured reservoir development.

Having drilled a successful wellbore, the next immediate concern for petroleum engineers would be the completion design and implementation. Since the fractures possess significant permeabilities, they will be depleted much faster

than the rock matrix which in itself will lead to immature reservoir abandonment or costly stimulation treatments (Chacon and Tiab, 2007). Fractures as the source of permeability heterogeneity would enforce complex fluid contact levels, pressure drawdown trends and recovery magnitudes (Matthai et al., 2007). Maximizing fractured reservoir deliverability depends on wise completion designs and such designs cannot be achieved without a comprehensive overview of the fracture-rock matrix hydro mechanical interaction. Natural depletion of the reservoir will alter the in-situ stress regime as the reservoir continues to produce; consequently the geometry of the fractures will change and the cross flow (the flow exchange between rock matrix and fracture at the matrix-fracture interface) between matrix masses and fracture network will be affected. Therefore production scenarios from the reservoir require consistent monitoring throughout the production life cycle.

Eventually these reservoirs similar to the conventional ones will require stimulation and enhanced recovery treatments in order to exploit the unrecovered reserves remaining in the large matrix blocks despite depleted fracture network. However presence of the naturally fracture network once again jeopardizes the probability of a successful operation. This is due to the fact that minimum resistance to the treatment fluid within fractures results in low reservoir sweep efficiency and undesired breakthrough into the adjacent formations.

1.1.2 Fracture-Matrix flow interaction

Fracture network and rock matrix act as inter-related hydrocarbon storage and production systems and as mentioned before, optimum engineering approaches demand comprehensive understanding of fracture-matrix flow exchange mechanism. Fracture-matrix hydraulic interaction is of prime importance in naturally fractured reservoirs type III (Nelson, R. A., 2001) in which fractures provide an assistance in reservoir fluid flow additional to the feasible intrinsic reservoir matrix permeability.

This hydraulic interaction changes with reservoir depletion that in its turn alters dynamic in-situ stress state, fracture network geometry, pore space and capillary pressure. One more challenging issue is the fact that fracture network

unlike the rock matrix cannot be precisely characterised; parameters such as fractures aperture, connectivity, wall friction, propagation and half-length which form the fracture network hydraulic characteristics are difficult to measure (Agar et al., 2010).

A considerable amount of research has been conducted so far to characterize flow (Slough et al., 1999; Lee et al., 2000), mass transfer (Reynolds and Kueper, 2001) and heat transfer (Pruess and Wu, 1991; Wu et al., 2002) within fractured formations. However oil and gas industry still considers developing these reservoirs as a high risk task due to their unknown time dependent, multi-physics coupled behaviour.

Multiple physical fundamentals contribute to the fracture-matrix flow interaction. The major flow governing equation in rock matrix is the Darcy law equation while free flow Navier-Stokes equation illustrates flow in fracture channels. At the matrix-fracture interface the continuity of pressure and fluid velocity is persistent until the two systems start to flow independently. Furthermore, multiphase flow and time dependent flow regime evolution should be considered when investigating most realistic flow scenarios. On the other hand, when the reservoir is undergoing stress regime alteration, all the mentioned physics should be considered coupled to the mechanistic models to account for the matrix pore space as well as fractures geometry variation.

In summary, analysing fracture-matrix flow interaction under varying mechanical loading represents a complicated multi-physics problem requiring precise physics coupling in addition to robust construction of boundary conditions especially at the fracture matrix interface.

1.1.3 Poro-elasticity

As described previously, in comparison to the conventionally stable systems which could be comprehensively analysed using Darcy equation, the quasi-static hydraulic investigation of a fractured porous medium under unstable stress state demands the application of more sophisticated coupled governing equations. The required descriptive coupled analysis should account for stress dependent hydro-dynamic characteristics of the fractured formation.

Imposing a porous medium to a loading/unloading condition would result in pore fluid pressure fluctuations due to the induced dilation or contraction of the pore space provided that the pores fluid containment is prevented from an equivalent-rate discharge (Detournay and Cheng, 1993). Monitoring the coupled diffusion-deformation mechanisms has been extensively explored in geomechanical problems such as consolidation (Griso and Rohan, 2007) and subsidence (Gambolati et al., 2001), in-situ stress profiling (Sanaee et al., 2010), saturated rock mass failure mechanisms and pressurized wellbore induced instabilities (Sanaee et al., 2010; Van Oort, 1994; Mogilevskaya et al., 2000).

The first analytical one dimensional formulation that enabled incorporation of effects of fluid pressure in soil consolidation process was developed by Terzaghi (Terzaghi, 1923). However it was Biot (Biot, 1941) who introduced a linear theory called poro-elasticity which defines effective overburden stress for porous materials containing fluid saturation. His initial theory has been revised several times by him (Biot, 1955; Biot, 1956a; Biot, 1956b; Biot, 1962) and other researchers (Rice and Cleary, 1976). The defined parameters of this theory, as will be detailed in literature review, were later coupled to the mechanical stress-strain relationships to enable analytical investigation of fluid containing porous rocks mechanical behaviour under loading scenarios.

1.2 Justification for Research

As illustrated in Figure 1-2, reservoir fluid production in the near-wellbore region is complicated within naturally fractured reservoirs type III. The complexity which arises from fracture-matrix interaction and the resulted complicated near-wellbore flow regime, also encountered within tight reservoirs which are stimulated for production via hydraulic fracturing. The only difference in the latter case is the horizontal reservoir entry and wellbore completion (Fig. 1-2). As mentioned previously, the near-wellbore production quality is also affected by reservoir depletion and consequent in-situ stress regime alteration.

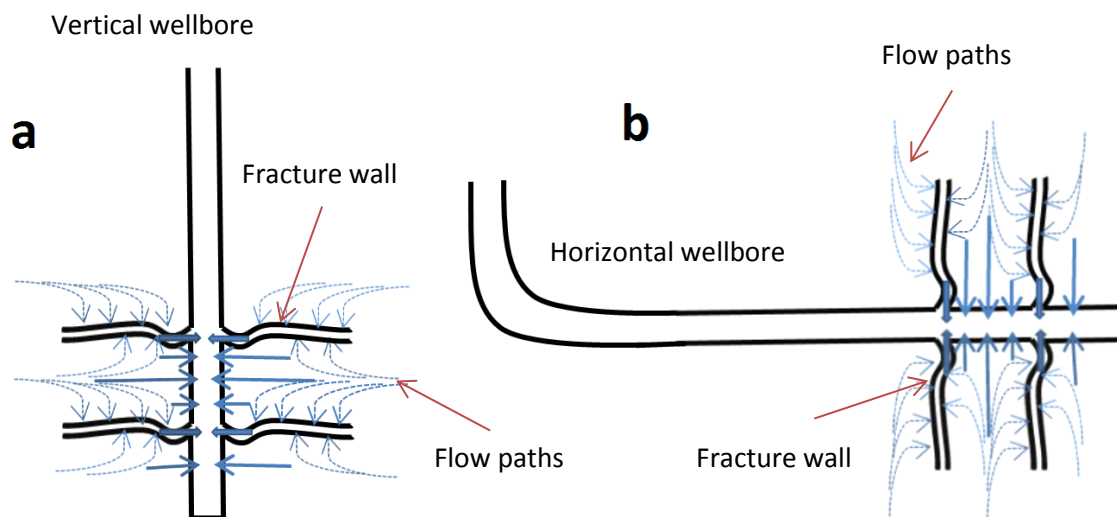


Figure 1-2. An illustration of simultaneous fracture and matrix production in the near-wellbore region; a) vertical wellbore in naturally fractured reservoir b) an stimulated tight reservoir.

Poro-elasticity serves as an efficient descriptive formulation in illustrating fluid-containing porous materials' response to loading; however present conductive hydraulic pathways in fractured reservoirs respond to loading through geometry variations.

A conventional approach was to consider the fractures as representative porous media assuming large permeability and porosity magnitudes while using Darcy equations (Kazemi et al., 1992; Dutra and Aziz, 1992; Bai et al.,

1997). These assumptions are far from the real case flow in fractured reservoir blocks and the calculated cross flow magnitudes between fractures and adjacent reservoir blocks using this approach are flawed.

Discrete fracture modelling technique, as an improved modelling approach, was utilized in fractured formations hydro-mechanical characterisation in more recent analyses (Lee et al., 2000; Hughes and Blunt, 2001; Voelker, 2004; Elfeel et al, 2010). This strategy is extensively applied in most field scale investigations as it is more realistic than the conventional approach and can be specifically adjusted to be reasonably efficient with regard to numerical complexities. However, it requires the definition of transfer functions in order to evaluate fracture-matrix flow exchange. These transfer functions are based on some assumptions, which are discussed in the literature survey, that limit the applicability of the method and reduce its validity. On the other hand, Mechanical effects cannot be precisely coupled with fracture geometry as fractures are modelled as sub-dimensional features in the model geometry. Therefore, although discrete fracture modelling technique is considered numerically efficient, it suffers from fracture geometry simplifications.

Prevailing models applied extensively in field-scale simulators like Computer Modelling Group (CMG), which model fracture permeability as an exponential decay function of the effective normal stress to the fracture aperture, whether rely on empirical laboratory measurements of fracture stiffness, like Barton-Bandis correlation (Bandis et al., 1983; Barton et al., 1985) or suffer from not considering the rock matrix comparable permeability to the fracture permeability like the model introduced by James Rice in 1992 (Rice, 1992). Each one of these models may well be indicative of fractured porous media flow in specific fields, like for fractured low permeable carbonate formations, however, they cannot be generally used for hydraulic switching flow systems between rock matrix and fracture due to the overburden stress alteration. Achieving a precise predictive fracture permeability model requires consideration of fracture aperture and permeability evolution based on the mechanical movement measurements of the fracture walls.

In order to achieve most realistic simulations of flow partitioning (the contribution of total formation inflow into a wellbore from matrix or fracture in

an open-hole completion in which both fracture and matrix are able to flow into the wellbore) behaviour between fracture and matrix in response to overburden stress variations, fractures need to be modelled as free flow channels hydraulically connected to the matrix blocks. Subsequently, this modelling concept requires the coupling of poro-elasticity calculated volume strain magnitudes to the fracture geometry as well as the coupling of Darcy flow within the rock matrix pore spaces to the free Navier-stokes flow in the aperture variant fractures (Sanaee et al., 2013). Flow velocities should also maintain continuity over the fracture matrix interface to provide a hydraulically integrated formation response to stress regime variation. Moreover, the stress-strain interactions of the fractured rock mass affect the permeability in both systems which need to be addressed in an integrated modelling approach.

Coupling various physics of flow and stress-strain between two hydraulically distinct systems -matrix and fracture- possessing distinctive permeabilities have been tried in some previous investigations (Bai and elsworth, 1994; bai et al., 1997; Ozkan et al., 2010). However these trials suffer from some simplifications, which are discussed in the following chapter, adopted to overcome numerical instability which will be resulted in tackling such complicated simulations. Moreover, these numerical efforts lack laboratory evaluation.

This study concentrates on developing empirical models for fracture and matrix flow contributions in fractured reservoirs, based on most realistic coupled numerical analysis, which can be calculated with reduced numerical efforts and can be up scaled much more conveniently. The coupled numerical analyses covered Darcy and Navier-Stokes flow regimes within matrix and fracture respectively, while flow continuity was maintained at the matrix-fracture interface. These flow regimes are also coupled with poro-elasticity formulations to enable evaluation of overburden stress variation effects. The developed empirical models were further examined against experimental data obtained from a series of laboratory flooding tests taking the advantages of a novel custom-designed fracture-matrix flow partitioning analysis rig.

1.3 Research aim and objectives

Significance of optimizing tectonically active fractured reservoirs production and consequent successful implementation of enhanced recovery methods necessitates comprehensive recognition of fracture-matrix hydro-mechanical interactions.

The aim of this research is to develop laboratory evaluated empirical flow partitioning models that benefit from less numerical complexity while maintaining enhanced reliability. The development is based on the most realistic flow and geomechanical governing equations.

Several objectives were considered to facilitate reaching the desired empirical models as follows:

1. Evaluation of various numerical fracture modelling approaches and adoption of the most precise one for a coupled numerical analysis.
2. Implementation of geomechanically coupled numerical modelling of single phase laboratory fractured core flooding data.
3. Development of empirical fracture and matrix flow models based on the existing mechanistic models and statistical analysis of sensitivity study results
4. Design and implementation of a special laboratory core flooding set-up to generate laboratory data to evaluate the developed models efficiency.

This dissertation entails the undertaken steps in fulfilling the requirements of achieving the mentioned objectives following an extensive fractured porous medium characterisation literature review.

1.4 Research methodology

In order to investigate geomechanical dynamics of fracture-matrix system, advantages of numerical simulations were taken into consideration. Numerical modelling provided the opportunity to perform a sensitivity analysis of the fracture-matrix dynamics-governing parameters of fractured porous medium. Furthermore, numerical simulations established the design specifications of a laboratory set-up which was required to evaluate the modelling results.

In the next stage, the sensitivity analysis results were statistically analysed to develop fracture and matrix empirical coupled flow models consistent with the analytical governing equations of the sensitivity analysis. Consequently, laboratory experiments using the novel-designed set-up were performed to assess the reliability of the developed models. Applied techniques in promoting each phase of the research methodology are further illustrated in this section.

1.4.1 Numerical modelling

Numerical analysis constitutes the basis of methodological research in this dissertation. Accuracy of the numerical simulations were optimized via appropriate discretization of the problem geometry, setting adequate initial and boundary conditions as well as monitoring the residual errors during each calculation step, not to exceed a pre-defined appropriate tolerance.

Governing equations of appropriate physics were implemented and their couplings were checked to maintain consistency. The simulation results were checked against published data to ensure practical functionality and accuracy of the meshing and simulations. Symmetry boundary conditions and parametric studies were employed to facilitate sensitivity analyses. In case of running time dependent analysis, the model was initialized using a steady state flow stage in advance.

A sensitivity analysis of the coupled governing equations' parameters was implemented to assist in developing empirical flow partitioning models. Initial analyses were accomplished using ANSYS FLUENT software; however, implementing fracture in more vigorous simulation approaches lead to utilization of COMSOL Multi-Physics software. Purposefully implemented

modules of COMSOL such as subsurface flow, geomechanics and CFD facilitated coupling of physics and used for the majority of the numerical analyses in this dissertation.

1.4.2 Statistical and analytical investigations

Sensitivity analysis results were analysed using non-linear multi-parameter regression analysis in order to develop empirical flow partitioning models. Several pseudo-parameters were generated based on the analytical governing equations to facilitate the regression fitting procedure. Non-linear models were introduced to the Newton-Raphson based regression algorithm in line with the non-linear relationships present in the governing equations with specific attention to the numerical couplings.

Individual models covering the individual parameters/pseudo-parameters effects were all checked based on their mean squared error indices before implementing in the regression algorithm. All the possible models generated by the algorithm, were evaluated against statistical criteria to ensure their accuracy and prediction capability. The final empirical models were selected based on the residual magnitudes and distribution of their prediction.

1.4.3 Laboratory experiments

Laboratory experiments were employed as a validation tool in assessing the predictive capability of the empirical models. A novel core flooding set-up that meets the requirements for laboratory study of flow partitioning between matrix and fracture was designed and built for this purpose.

Laboratory analysis followed the standard core flooding procedures while taking into consideration the novel rig functionality requirements. Plug samples were vacuum saturated initially and artificial fractures were generated in a way to have minimum fracture walls asperities. Flow accumulating plugs, designed as part of the rig, were machined and attached to the core plugs to capture and accumulate matrix flow.

Parameters such as flow rate and differential pressure were used to monitor and characterise the flooding front movement and fracture-matrix flow dynamics. Flooding experiments were analysed under various overburden stresses exerted by means of a hydraulic hand pump to enable investigation of stress variation on the fractured core plugs flow dynamics.

1.5 Contribution to knowledge

The current research provides novel numerical couplings in fractured porous media flow characterisation as well as coupled empirical flow equations for matrix and fracture flow. In addition, a novel experimental set-up was designed and built which provided fracture-matrix flow partitioning data.

A comprehensive coupled geomechanical numerical modelling was accomplished in which the mechanistic governing equations of poro-elasticity were coupled to the flow equations of porous media, Darcy law, and Navier-Stokes channel flow within fractures. This coupling was performed through incorporation of fracture geometry alteration in response to overburden stress change in the Navier-Stokes flow equation. Such couplings provided a robust realistic numerical modelling that resulted in a comprehensive sensitivity study of all the relevant parameters involved in a stressed fractured porous media flow modelling.

Further to the enhanced accuracy that this multi-coupling approach offered in fractured rocks flow characterisation, fracture-matrix flow interaction specifically under overburden loading conditions could be analysed. Understanding matrix-fracture flow dynamics provides opportunities to design and implement stress relief techniques in order to optimize hydrocarbon discharge into fracture network within mature fields in which fracture network is depleted despite considerable reserves in the reservoir formation matrix.

Empirical geomechanistic models were also developed that can be further utilized in up-scaled fractured formations flow analysis with reduced demand for computational efforts. These models were further validated against laboratory data. The validation confirmed that the matrix flow model is much

more reliable than the fracture flow model in predicting fractured formation dynamic behaviour under overburden stress loading conditions.

In addition, a novel core flooding set-up that meets the requirements for laboratory study of flow partitioning between matrix and fracture was designed and commissioned. This rig allows for differentiation between matrix and fracture flow contributions to total flow in fractured reservoirs under various overburden stress loadings owing to implementation of novel steel flow accumulating plugs inside the core holder sleeve.

The rig configuration also provides the chance to monitor flow front within both matrix and fracture and analyse the flow regimes occur while flooding a fractured core plug. This functionality which eliminates the cost and complexity of utilizing a micro computed tomography (micro-CT) scanning device, was achieved through consideration of several differential pressure transducers along the core holder length capable of indicating hydraulic pressures within the core holder sleeve. Some operational considerations in the design of the rig enable its convenient augmentation in order to analyse multi-phase flow and flooding under tri-axial stress loading regime for fractured core plugs.

1.6 Dissertation layout

First chapter of the dissertation provided a brief introductory to the research subject outlining its background and justification. Research aim and considered milestones in its accomplishment are mentioned to deliver an overview of the study phases. This introduction chapter followed by the adopted and designed numerical and experimental investigation methodology and finally culminated in a summary of the research novelties and its potential benefits in optimizing fractured reservoirs hydrocarbon recovery

Chapter 2 presents a comprehensive literature review which provides an overview of the previously published relevant investigations focusing on the fracture-matrix flow dynamics. Previous scientific studies are criticised in three category of analytical, numerical and laboratory analyses.

Following to the literature review, chapter 3 examines various approaches in modelling fractured porous medium such as simulation of fracture domain as an equivalent porous media, a sub-dimensional feature or an open channel. The chapter describes the process used in selecting the best numerical approach that was considered for analyses presented in chapter 4.

Chapter 4 presents an extensive numerical sensitivity study that sets the scene for the development of empirical matrix-fracture flow partitioning models. The chapter also illustrates the statistical analysis of the parametric study results and how the results were applied to develop a suite of empirical models for fracture and matrix flow. Application of the adopted numerical approach in analysing time dependent multi-phase flow scenarios is also addressed briefly in this chapter.

Laboratory design, implementation and validation of the empirical models presented in chapter 4, are discussed in the chapter 5. Challenges associated with the design of the novel core flood rig and developing robust experimental procedures are addressed and followed by interpretation of flow regimes inferred from differential pressure readings during a representative fractured core flooding experiment. The measurement technique applied in the laboratory experiments is also described and the capability of the developed empirical models in predicting laboratory measurements is evaluated.

Chapter 6 presents a comprehensive discussion of the dissertation achievements and their drawn conclusions. Eventually several invaluable research extension opportunities are recommended owing to the numerical and laboratory infrastructures developed in this study.

Chapter 2.0

Literature review

2.1 Introduction

Fractured reservoirs constitute the vast majority of the world oil and gas reserves specifically in carbonates. Despite the significant reserve, natural fractured reservoirs suffer from low recovery rates and constrained life span comparing to the non-fractured counterparts (Beydoun, 1998; Burchette, 2012; Montaron, 2008).

Generally reservoir intact matrix blocks are the main source of original oil in place while the existing fracture network forms the initial permeability facilitating hydrocarbons production to the producing wells. However, a dense fracture network can be considered as a hydrocarbon containing porosity and permeable rock matrices can compete with fractures in terms of production into the wellbore. This makes selecting best representing reservoir model of single porosity, dual porosity or dual permeability, a complicated requirement.

Moreover, there are several uncertainties associated with modelling this type of reservoirs. Capturing fractures' density, geometry and connectivity raises as a challenge in static modelling and consequently fracture permeability and quality of matrix-fracture hydraulic interaction are encountered as significant complexities in reservoir dynamic modelling. In addition, Reservoir depletion alters the in-situ stress state and this stress disturbance in its turn results in variation of fractures structure and matrix-fracture dynamic interaction mechanism.

Significant progresses in geophysics specifically in seismic and visual wellbore logging has improved static modelling of fractured reservoirs tremendously however, the matrix-fracture flow partitioning and its dynamic nature in response to in-situ stress variation still demands more thorough investigation. Several approaches that have been applied in characterisation of fractured reservoirs are addressed and criticised in this chapter based on their analytical, numerical or laboratory research methodology.

Generally the fracture network occurrence pattern within formation matrix blocks dictates the fractured reservoir modelling approach. Geometric characteristics of the fractures along with their connectivity should be considered in deciding for dual porosity or dual permeability modelling techniques to be adopted. Dual porosity model may well be able to illustrate a dense, disconnected fractured formation however, larger-scale connected fractures demand a dual porosity dual permeability modelling (Bourbiaux et al., 2002). Having reached an appropriate modelling approach, implementation of the precise flow and fracture parameters is the next challenge to deal with. The introduction of discrete fracture network (DFN) modelling assisted in implementation of crucial parameters such as fracture system porosity, fractures transmissivity, directional fracture network permeability and matrix-fracture interaction parameters (Dershowitz et al., 2000). Discrete fracture modelling significantly improved analysis of fractures connectivity and scale-dependent heterogeneity effects when coupled with dual porosity/permeability models. However, there are crucial coupling complexities which jeopardizes the reliability of the simulation results and sometimes computer intensive explicit modelling of fractures and matrix blocks is inevitable.

It has been revealed that although the applied techniques have considerably improved petroleum engineers understanding, coupling of the physics in modelling fractured porous medium flow can still be more accurate and numerically efficient empirical approaches can facilitate the mechanically-coupled simulation of fractured porous medium flow regime.

2.2 Analytical studies

The first analytical efforts geared towards illustrating the flow behaviour within fractured reservoir are those which consider both fracture and matrix as an integrated equivalent porous medium. Flow characteristics of this conceptual formation are considered as a representation of the combined characteristics of the porous rock matrix and the existing fractures (Kazemi et al., 1992). This approach can assist in analysing sparsely fractured reservoirs considered isotropic in which the fractures are constrained in geometry and do not form a conductive flow network which dominates matrix flow. Furthermore, variation of the flow characteristics within small reservoir sections is one of the controversial challenges in modelling fractured porous media that cannot be addressed using this approach. Due to the significant limitations highlighted, the realistic approach to treat these reservoirs as multi-porosity, multi-permeability formations have been taken into consideration.

Generally flow within the rock matrix follows the conventional characteristic flow physics of Darcy law depending on reservoir conditions and wellbore/completion strategy; However within the fractures it can be best analysed applying modifications of Navier-Stokes flow equations. In some initial analytical works, generalized Darcy equations have been adopted to describe the fracture flow velocity using some statistical analyses and assuming relatively small fluid velocities within both matrix and fracture (Evans, 1982):

$$\vec{v}_{fj} = - \frac{K_{rjf} \bar{k}_f}{\mu_{jf}} [\nabla P_{fj} + \rho_{jf} \left(\frac{\partial \vec{v}_{fj}}{\partial t} \right) - g \nabla D] \quad (2-1)$$

The only difference in this model in comparison with the original Darcy law is the velocity term in the right hand side of equation 2-1: $\frac{\partial \vec{v}_{fj}}{\partial t}$; this is the variation of the fracture velocity with time that is considerable in non-steady state flow regimes; This was considered to promote the functionality of the equation to the scenarios in which non-Darcy flows are occurring within the fractures delivering Reynolds numbers more than 2100. Fracture fluid content charging from adjacent matrix blocks was accommodated via consideration of a fluid interaction term and anisotropic nature of fractures distribution was addressed using statistical functions of space and orientation. Such

approaches might illustrate the transient regimes but no experimental or field data validation has been offered for their application.

Recovery mechanisms from fractured reservoirs significantly rely on the fracture network characteristics; viscous displacement of oil by gas or water is not often a dominant mechanism due to the relatively small pressure gradient across individual matrix blocks. Instead, solution gas drive, gravity drainage and water imbibition are considered the most effective recovery mechanisms (Kazemi and Gilman, 1993).

In later researches, attention was paid to the cross flow between fracture and matrix and attempts were made to incorporate empirical relationships to the flow equations. Specifically when water imbibition is the dominant recovery mechanism such transfer functions can be implemented in a dual-porosity formulation assuming that reservoir volumetric rate of oil recovery from the matrix is equal to the volumetric rate of imbibed water and defined in terms of water saturations within fracture (S_{wf}) and matrix (S_{wma}) as shown in equation 2-2 (Kazemi et al., 1992):

$$\tau_o = \frac{V_R \phi_{ma} \aleph}{5.6146} [S_{wf}(1 - s_{orma} - s_{wcma}) - (S_{wma} - s_{wcma})] \quad (2-2)$$

τ_o is the flow rate between fracture and matrix and \aleph is a constant equal to the reciprocal of the time required to recover 63% of recoverable oil. This flow transfer function is useful for one dimensional flow problems within dual porosity formations. The mathematical analyses were continued on the flow transfer functions and some new double porosity formulations have been obtained which could describe the multi-dimensional large-scale problems through finite difference discretization (Dutra and Aziz, 1992).

Although conventional dual-continuum approach is more convenient to implement in a reservoir scale simulation and is less demanding computationally, generally, the fracture-matrix flow interaction is calculated based on fracture relative permeability concept within this approach. Paying attention to the fact that fracture relative permeability is a hydraulic property along the fracture plane while fracture-matrix interaction is governed by the matrix-driven flow perpendicular to the fracture plane, the accuracy of this approach become limited. Considering a multiphase simulation, a mass

balance equation (eq. 2-3) should be implemented for each phase β (Wu et al., 2004):

$$\frac{\partial}{\partial t}(\varphi S_{\beta} \rho_{\beta}) = -\nabla \cdot (\rho_{\beta} v_{\beta}) + q_{\beta} \quad (2-3)$$

Where the Darcy velocity of phase β is defined by equation 2-4:

$$v_{\beta} = -\frac{k k_{r\beta}}{\mu_{\beta}} (\nabla P_{\beta} - \rho_{\beta} g \nabla D). \quad (2-4)$$

In these equations ρ_{β} is the density of phase β under reservoir conditions; φ is the effective porosity of the medium; μ_{β} is the viscosity of phase β ; S_{β} represents the saturation of phase β . P_{β} is phase β pressure and $k_{r\beta}$ is the relative permeability of phase β .

These equations will be applied in combination with constitutive equations such as those relating relative permeability values to the capillary pressure and other PVT data. In order to incorporate the fracture-matrix flow interaction Wu et al. utilised a transmissivity term as given in eq. 2-5 below:

$$\gamma_{ij} = \frac{A_{fma} k_{ma}}{l_{fma}} \quad (2-5)$$

Where A_{fma} is the interfacial area between fracture and matrix; k_{ma} is the absolute matrix permeability along the fracture–matrix connection boundary and l_{fma} is a characteristic length for flow crossing the interface in a double porosity model. Fracture-matrix flow has been calculated based on the local equilibrium of fracture and matrix capillary pressures.

These formulations could improve the understanding of flow partitioning within the fractured reservoirs but they were not coupled solutions which can illustrate mechanically affected flow behaviours.

Mechanistic models for flow behaviour within fractured media have been introduced through rock mechanical concepts of stress-strain relationships. For this purpose, the concept of hydraulic conductivity for flow through parallel fracture surfaces which is also referred to as the cubic law, as in equation 2-6, was adopted (Bai and Elsworth, 1994):

$$K = \frac{\rho g b^3}{12s\mu} \quad (2-6)$$

This relationship (eq. 2-6) suggests that the conductivity of a smooth-walled fracture, neglecting turbulent flow, is proportional to the fracture aperture b by a power of three. Bai and Elsworth (1994) also derived the field expression of poro-elasticity that can be coupled to the conductivity equation as shown in eq.2-7:

$$\frac{E}{2(1+\nu)} u_{i,jj} + \frac{E}{2(1+\nu)(1-2\nu)} u_{k,ki} + \alpha p_{p,i} = 0 \quad (2-7)$$

where u is displacement, E is the elastic modulus, ν is Poisson's ratio, p is pore pressure and α is pressure coefficient. They considered a cubic grain packing model and, based on Kozeny theory, obtained the equation shown in eq. 2-8 (Bai et al., 1995).

$$K = \frac{2}{\pi^2} R^2 \left(\frac{\rho g}{\mu} \right) \quad (2-8)$$

R denotes the model grain radius. Based on these calculations they derived coupled formulation shown in equation 2-9 for stress related permeability in which $\Delta\varepsilon$ is the total body strain and k_n is fracture stiffness.

$$\Delta K = \frac{\rho g b^3}{12s\mu} \left[1 + \Delta\varepsilon \left(\frac{k_n b}{E} + \frac{b}{s} \right)^{-1} \right]^3 \quad (2-9)$$

Such coupling was further developed for radial coordinates by using fluid pressure gradients as a body force (Bai et al., 1995). These formulations can be further generalized to achieve a dual permeability model for both fracture and matrix (equations 2-10 & 2-11) (Bai et al., 1997)

$$\Delta K_{ma} = K_0 \left\{ 1 \mp \frac{1}{2} \left[\frac{9(1-\nu^2)}{2} (\pi \Delta\varepsilon_{ma})^2 \right]^{\frac{1}{3}} \right\}^2, \quad \Delta\varepsilon_{ma} = \frac{\Delta\sigma}{E} \quad (2-10)$$

$$\Delta K_f = \frac{1}{12s} [b + (s + b)\Delta\varepsilon_f]^3, \quad \Delta\varepsilon_f = \frac{\Delta\sigma}{K_n(s+b)} \quad (2-11)$$

These formulations were further expanded for the cases in which the main permeability directions are not coincident with the major strains (Bai et al., 1999).

Analytical approach, up to this point, seemed to be quite applicable since coupled formulations have been achieved for both fracture and matrix domains. However, this approach was based on the assumption that there is no cross flow between these two systems. Moreover there is a need to validate their effectiveness and efficiency with experimental data. In addition, they are merely applicable to single phase flow scenarios and as can be inferred from Figure 2-1, the cubic model of fracture permeability (Eq. 2-6) and the dual permeability expansion of that (Eq. 2-11) provides different trends of fracture permeability evolution in response to stress induced fracture aperture variation. Equation 2-10 is widely accepted to be illustrative of matrix permeability alteration due to normal stresses and it is used in our numerical experiments for the matrix domain however, the coupled adopted approach in accounting for stress-driven fracture permeability variation in our numerical experiments is independent of both models depicted in Figure 2-1 for fracture permeability and it will be more elaborated in the next chapter.

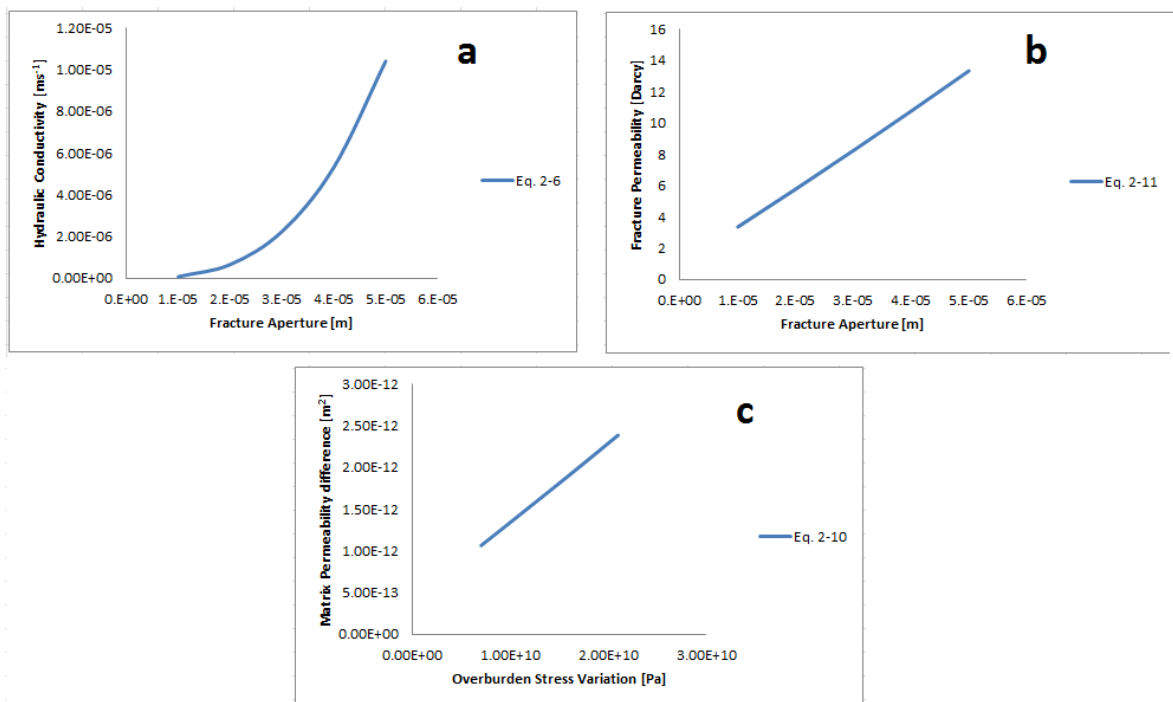


Figure 2-1. Stress-affected fracture and matrix permeability models. a) the cubic model of a parallel-plate fracture type hydraulic conductivity b) dual permeability expansion for fracture permeability c) stress-dependent matrix permeability model

Further analytical efforts have been reported in the literature to account for the interactions and phase partitioning between fracture and matrix, in the field of chemical engineering (Slough et al., 1999). There were also some analytical investigations to extend these dual permeability formulations to a fracture network or to non-uniform fractures. One approach was to use hierarchical pattern of fracture length and connectivity and consider specific flow solutions for the representative aperture values (Lee et al., 2000)

Another aspect of flow physics investigations within fractured formations is the non-steady state flows and time dependency of the flow regime evolution. There were considerable progress in proposing analytical solutions for pseudo steady state single phase flow through a triple porosity formation (matrix, fractures and cavities) (Liu et al., 2003); although the solutions were numerically verified, flow was considered through fractures network exclusively while cavities and matrix accounted for storage and drainage into the conductive fractures.

Improvements in designing novel experimental set-ups, made it possible to recognize various fracture filling processes using diffusion equations for one-dimensional imbibition and derive time-dependent equations for flow in fractured media (Rangel-German and Kovscek, 2001). The weak point of these models is that they assume incompressible fluid and matrix and as a result they cannot be coupled with mechanical models. Besides, these models were based on saturation profiles measurement rather than a flow partitioning measurement, hence they are not suitable for flow partitioning applications.

Recently further coupled analyses were done to investigate the chemical dissolution effects on flow within these reservoirs which is an indication of the importance and complexity of this flow partitioning problem among other disciplines. Mechanical-chemical coupled flow models enabled investigating the effect of temperature and chemical dissolution of fracture asperities on the flow behaviour (Min et al., 2009). Tracers have also been used a lot in flow characterisation experiments; attempts have also been made to couple the partial differential equations for pressure and tracer concentration to characterise the flow partitioning within fractured media (Paluszny, 2009). This recent work focuses on the coupled effects based on the propagation of

the fractures and investigates the immature fractures within a porous media. Fracture matrix flow partitioning has been also mathematically analysed for other flow regimes such as turbulent flow within the fractures in the presence of confining stresses in fractured cores (Oluyemi and Ola, 2010).

Coupled analytical works have recently attracted a lot of scientific interests. In 2010, the stress-related permeabilities were coupled to the diffusivity equations within radial coordinate systems to monitor the flow partitioning between matrix and fracture (Ozkan et al., 2010). This analytical model has been tested in a fractured shale gas reservoir and is seen to be applicable in predicting cumulative flow through a fractured system.

In summary most of the analytical solutions of flow partitioning within a fractured media do not consider the mechanical effects of in-situ stress variation which is a very important aspect of production from any reservoir. In addition, most of these solutions suffer from absence of experimental verifications. Related numerical and laboratory works will be also addressed in following sections and their thorough review demonstrates lack of a comprehensive validated study in analysing realistic scenarios of flow distribution within fractured reservoirs.

2.3 Numerical simulations

All the analytical modelling efforts for flow partitioning within discontinuous porous media as addressed in previous section, are based on some engineering and simplifying assumptions; therefore they need to be tested to establish their field applicability. Laboratory experiments for fractured porous media have always been very hard to design due to the complexity, time and budget constraints. As a result, many of the experts took the advantage of numerical simulations which are extensively more convenient, fast and cost effective to run. Numerical modelling also enables large-scale modelling which is an outstanding advantage.

Finite difference method as a mathematical technique has been used to solve flow problems within fractured media. It has been applied within fractures which are a source of discontinuity, along with analytical matrix-fracture

transfer models to characterise flow (Pruess and Wu, 1991). Early finite difference analyses were 2D analyses of matrix blocks containing single fracture (Han, 1996). These were based on initial experimental works and assisted in differentiating longitudinal and transverse fracture orientation effects on flow. Software packages like Eclipse have been used to investigate single phase flow (Keller, 1996) and two-phase flow (Akin and Kovscek, 1998; Schembre et al., 1998) within fractures.

More complicated fracture networks have been analysed using finite element discretization and unstructured meshing capabilities in the field of hydrogeology (Taniguchi and Fillion, 1996; Matthai et al., 2007; Piri and Karpyn, 2007; Petchsingto and Karpyn, 2009; Petchsingto and Karpyn, 2010). Main investigation issue in these research works was the effect of complexity of a fracture network on fluid production however, the fracture network complexity should be analysed in combination with the rock mechanical failure criteria and rock matrix reflection to variable stress regimes to provide an accurate fracture-matrix hydraulic interaction analysis. Density-driven fracture flow simulations have also been performed using other software packages, for example RockFlow3 (Thorenz, 2001); Such numerical simulations investigated more complex fracture geometries and permeability profiles; however they were just fracture flow studies which did not consider any coupled mechanical models.

There are also a variety of field-scale simulations performed taking the advantage of parallel schemes which allowed investigation of production for multiphase flow within fractured reservoirs (Wu et al., 2002; Coumou et al., 2008) and for large fracture networks (Sarda et al., 2002). The acceptable error margin in these field-scale investigations is more widespread and so they are not accurate analytical models. However the discrete fracture network modelling concept that is used in Eclipse (Voelker, 2004; Elfeel et al., 2010) seems to provide the best results especially when the effects of mechanical stress are considered (Baghbanan, 2008). Discrete fracture network approach is considered as a reliable technique to characterise hydraulic parameters of fractured porous medium flow scenarios in which flow occurs in fractures dominantly and the matrix blocks serve as hydrocarbon source accounting for the fracture network charging.

Fracture-matrix hydraulic interaction was also implemented in discrete fracture network scheme through various definitions of flux and pressure continuity at the interface; for instance, Ito and Seol (2003) performed 3D discrete fracture network analysis considering fracture-matrix flow interaction based on defining specific rock properties to the fractures connected to the surrounding rock blocks. Fracture and matrix were considered as two separate continua (multi continuum concept, Aziz and Settari, 1979) in any single volume element of the geometry. This requires defining a representing elementary volume (REV) and setting the problem domain volume elements greater than this REV. Such an assumption is not valid for limited number of fractures in large rock mass blocks. Fracture in such modelling concept, is a mathematical element possessing a "fracture permeability" however, through defining interfacial surface in fracture-matrix cross-cutting elements, fracture-matrix flow interaction is calculated; This approach is successful in analysing minor flow interaction via monitoring the variation in permeability and interfacial surface at fracture-matrix interface.

Similarly, various porosity and permeability scenarios have been tested along with fracture aperture sizes to investigate the flow regimes that may develop within fractured formations (Matthai and Belayneh, 2004). In pace with the development of coupled analytical mechanistic flow models, the models were examined through finite element simulations for fractured porous media in such a way that porous media flow physics were used for both fracture and matrix in Cartesian (Bai et al., 1997) and in radial coordinates (Bai et al., 1999). Single-well 2D models that include the effects of stress on permeability values have also recently been analysed to investigate Darcy and Non-Darcy flow regimes (Rubin, 2010). These simulations are useful coupled studies but again they are not validated by laboratory experiments that can provide an insight of the coupling strategies robustness. Furthermore, they used the same porous media physics within both –the matrix and fracture domains.

Statistical techniques and programming languages like FORTRAN have been also used to investigate more specific boundary conditions especially in chemical engineering for solute transport and diffusion problems (Fleming and Haggerty, 2001) and tracer flow experiments (Reynolds and Kueper, 2001; Frampton, 2010). These simulations are based on diffusion equations; and

although they can be useful in understanding flow problems, however they do not consider viscous flow.

One technique that has been used to include fractures within the porous medium simulations without any conflict with the continuum based physics, which is the fundamental concept behind majority of simulator software, was the inclusion of fractures as attached 2D lattices to the 3D matrix blocks (Hughes and Blunt, 2001; Hoteit and Firoozabadi, 2008; Weatherill et al., 2008; Paluszny, 2009; Jaffre et al., 2011). This simplification is efficient in flow simulations but the main shortcoming is that the cross flow between matrix and fracture need to be addressed using saturation based correlations based on various assumptions; furthermore the fracture aperture mechanical hysteresis under overburden stress cannot be investigated utilizing such problem geometry and physics settings.

Although numerical discretisation methods like finite difference and finite element have been extensively used in fractured reservoirs simulations but their applicability to a large extent relies on the physics settings and fracture-matrix interface saturation and pressure formulation. Finite element discretisation is unable to describe saturation discontinuity at the fracture-matrix interface. This is mainly due to the fact that capillary pressure between fracture and matrix is discontinuous and such capillary pressure contrast, in most severe two phase flow cases, will even challenge the assumption of fractures as the main flow containing regions. Very fine mesh sizing is also needed at the fracture-matrix interface especially in solute transport studies of discrete fracture networks in which diffusion rate is very slow (Weatherill et al., 2008).

On the other hand, finite difference technique is restricted to horizontal or vertical fractures only. Moreover, in vertex centered Finite volume method coupled to discrete fractures, accuracy of the results depends on the grid size of matrix adjacent to the fracture (Hoteit and Firoozabadi, 2008). It is worth mentioning that in specific cases where fracture can be considered as flow source, integral finite difference in conjunction with control volume discretisation resulted in analytically verified through-fracture injection modelling based on capillary pressure continuity at the fracture-matrix

interface (Wu and Pruess, 2005; Wu and Qin, 2009). Capillary pressure continuity enables calculation of fracture relative permeability values at the interface grid cells.

Considering fractures as $(n-1)$ features within n dimensional porous domain, as mentioned previously, is a remedial step which can assist to overcome these shortcomings to some extent. Hoteit and Firoozabadi extended MFE (mixed FE) to account for fracture matrix interaction in simulating two-phase flow in fractured reservoir. In their approach, degrees of freedom for saturation and pressure in a fracture grid cell were not the same as neighbouring matrix grid cell. Having considered a constant potential along the width of fracture grid cells and cross flow equilibrium merely across fractures, they were able to alleviate the size constraint of the grids in the vicinity of the fractures and volumetric flux between fracture and matrix has been calculated using a transfer function.

Time discretization is also as important as space discretization in stabilizing the fractured porous medium flow simulations. The prevalent proper IMPES (implicit pressure and explicit saturation) approach which uses previous time step saturation values in pressure equation, facilitates solving pressure and saturation equations sequentially via decoupling them (Hoteit and Firoozabadi, 2008; Jaffre et al., 2011). Combination of these techniques offers the possibility of introducing different rock types in the vicinity of a fracture as well.

Even in these novel simulation approaches, fractures were characterized by equivalent porosity and permeability values and therefore still a double porosity double permeability concept was applied which is far from the real cases in terms of evolved flow regimes and hydraulic interactions. It is worth mentioning that there were several mechanistic flow analyses in fractured reservoirs which were focused on fracture initiation and propagation mechanics (Philip et al., 2005; Paluszny, 2009); These investigations revealed so many aspects of evolution of a fractured reservoir as well as the hydraulic fracture generation during a stimulation treatment however, they do not deal with the production profile variation and fracture matrix flow interaction in

response to stress and fracture aperture alterations as they consider modified average permeability magnitudes for the fracture-matrix containing grid cells.

On the other hand, there were also some recent finite volume analyses which considered poro-elasticity to account for the mechanical coupling of flow in fractured porous media (Tran and Ravoof, 2007; Sanaee et al., 2013). Poro-elasticity relates the effect of stress on the saturation through volumetric strain; although this term is robust in evaluating stress affected hydraulics in rock matrix, it is not sufficient to illustrate fracture flow variation due to the aperture size disturbance.

Very recently flow partitioning has been studied within a fractured matrix numerically in which different flow regimes have been tested for the matrix and fracture. Laminar single phase Navier-Stokes equations were used for fracture system and Darcy equations for porous medium (Crandall et al., 2010; Sanaee et al., 2012; Sanaee et al., 2013). The effect of fracture roughness was also incorporated in Fracture flow (Q_f) through Reynolds number (Re) (equation 2-9) (Crandall et al., 2010):

$$q_f = \frac{\bar{H}^3}{61.5(1+\theta)(1+0.12Re_{\bar{H}}^{0.687})} \frac{\Delta P}{\mu L} \quad (2-12)$$

\bar{H} is the modified fracture aperture. Although this model is a useful fracture flow partitioning model, however it is based on 2D fracture profiles and does not encompass the coupled effects of stresses. Moreover the fracture walls were assumed to be impermeable and so the model does not account for cross flow between the matrix and the fracture. The model also lacks an experimental validation. Laboratory validation has however been performed for two-phase fracture flow scenario simulated by a model of spherical pores and cylindrical throats (Ferer et al., 2011). This simulation is however not coupled with mechanistic models.

Therefore it is evident that although numerous simulations have been done on fractured systems, there is very few comprehensive analyses that include mechanical effects and consider the cross flow between the two sub-systems of fracture and matrix which can be used for practical flow partitioning analysis in fractured reservoirs.

2.4 Laboratory experimental investigations

As mentioned before, the number of laboratory experiments for fractured porous medium flow partitioning analysis is very limited. Particularly there hasn't been any specifically designed laboratory set-up capable of separate measurement of fracture and matrix flow partitioning magnitudes, reported in the literature. Porous rocks flooding tests are performed using core flooding cells and they have been designed for non-fractured cores as a standard.

Original fractured core plugs laboratory investigations were analysing hydro mechanical characteristics of cores containing a fracture intersecting the core axis (Raven and Gale, 1985) in conventional rock mechanical apparatuses. Such normal to core axis fractures collect the flow from the core inlet to their permeable walls and so they are not useful for flow partitioning investigations in which the amount of flow contribution through each type of porosity is desired; artificially generated longitudinal fractures can also be analysed within similar cells and the routine core flooding cells, which can exert stresses as a confining pressure on the sample (Han, 1996; Hughes and Blunt, 2001; Souley et al., 2007), however the major challenge is how to measure the outflow from fractures and matrix separately. In addition, thermally fractured core plugs were also hydraulically characterised in the conventional tri-axial cells to provide an insight into the evolution of permeability in response to stress variations (Faoro et al., 2013). Although such investigations were pretty beneficial in understanding field scale production changes, they were unable to provide distinctive illustration of the hydraulic behaviour of fracture and formation matrix.

Despite the lack of fracture-matrix flow partitioning laboratory investigations, there are lots of laboratory works that investigated flow merely through fractures channels. To achieve this aim in primitive experimental efforts, transparent set-ups were used along with CCD cameras (Detwiler et al., 1999) that could provide fracture filling regimes concentrations and saturations (Rangel-German and Kovscek, 2001). Even complex fracture aperture profiles (Detwiler et al., 2000; Ferer et al., 2011) were built using transparent glasses and multiphase flow scenarios (Detwiler et al., 2002) were studied using similar set-ups. In the more developed type of these experiments stress effects have been investigated. This was achieved by covering the internal

faces of the glass-made fracture by reactive chemicals that could alter the fracture aperture as a result of a chemical reaction (Detwiler, 2008). Such studies helped a lot in understanding the flow mechanism within fractures but the obvious limitation for these set-ups is that they are not applicable to flow partitioning studies since matrix phase was entirely absent in the set-up.

There are also more advanced investigations of fracture permeability under various stress regimes in natural core plugs which enable diffusion into the rock matrix. These experiments explain the fracture flow alteration as a result of shear (Faoro et al., 2009) and normal stresses (Faoro et al., 2012). However, these studies, just like the previous category, were designed and performed to understand fracture hydraulics without any quantitative implications of the flow partitioning between fracture and matrix.

CT scanning techniques have been used to determine fracture geometries that can be used in more accurate numerical simulations (Keller, 1996) and in combination with a core flooding cell to monitor saturation profiles, relative permeabilities and capillary pressures in multiphase flow scenarios (Rangel-German et al., 1999; Kovscek et al., 2000). Using a CT scan device-mounted core flooding cell, Ameri Ghasrodashti et al. investigated effects of several parameters such as flow rate, fracture aperture and fluids rheological characteristics on miscible two phase flow, considering the annular space between the core and the core holder as the fracture aperture in 2013. CT scanning capability also enabled investigating various flow regime and sweep efficiency for non-uniform fracture aperture profiles (Alajmi and Grader, 2000). X-ray CT scans have been also used to investigate one dimensional imbibition from a single fracture to investigate time dependent imbibition invasion zone evolution (Tidwell et al., 1995).

CT scanning systems have the limitation of not being able to scan continuously and can only provide cross sections of flow through the core; this problem can be solved for imbibition-type problems for small cores that can be implemented vertically in imbibing cells (Akin and Kovscek, 1998; Kovscek et al. 2000; Rangel-German and Kovscek, 2000; Rangel-German and Kovscek, 2001). These analyses assisted in understanding the various flow regimes that develop during different stages of flooding process. The flow regime detected

at early stages was “fracture-filling” which indicates a variable plane flow source due to relatively slow water flow through fracture. The second observed regime was “Instantly-filled fracture” where the time to fill fracture is much less than imbibition time and a constant plane source imbibition will be resulted. Although they are good for relative permeability measurements or saturation front monitoring, they cannot provide the volume of flow which passes through rock matrix and through fracture for flow partitioning analysis.

In addition, some laboratory trials have been performed on heterogeneous matrix systems targeting cross flow between two different matrixes rather than between a matrix and a fracture system. Two different methodologies were used for this experimental set-up. The first entails having a matrix in the central space of the flooding cell and another type of matrix in the annulus space between this central core and the flooding cell casing (Apaydin et al., 1998; Bertin et al., 1999). The second entails making different artificial matrixes using various sizes of glass beads (Zinn et al., 2004).

The other problem that appears to weigh heavily against performing laboratory experiments on fractured rock substrates is the phenomenon of fracture aperture healing, especially when the experiment entails the application of overburden stress. The fracture aperture may change in response to stress loading. Such changes would need to be considered within the coupled models. Spacers or shims application has been reported in the literature to ensure a constant aperture throughout the whole fracture length (Rangel-German et al., 1999; Rangel-German and Kovscek, 2000; Rangel-German and Kovscek, 2001). However the challenge with the use of spacers and shims is that they may penetrate the cores under high stress loading as they are metallic spacers with a thickness of tens of microns range in accordance with prevailing initial fracture aperture sizes. It is therefore important to evaluate the mechanical properties of the rock at the experimental set-up design stage, particularly when no averaging technique is used to consider the non-uniform change of fracture aperture under extensive loading conditions even in the presence of shims. Micro computed tomography (MCT) technique (Karpyn et al., 2009) that can quantify micro-scale apertures has also been used to measure fracture aperture; this technique is however quiet costly.

The most recent successful attempts have considered the effects of stresses on flow through fractured cores (Wang et al., 2011; Liu et al., 2011) but the problem of measuring flow contributions from matrix and fracture separately still remains unsolved and necessitated custom-design of a laboratory set-up.

In order to be able to design and implement a rig that enables measurement of fracture-matrix flow partitioning, a routine core flooding experiment (Stalker et al., 2009) was considered as the pilot study. This laboratory study was based on brine-flooding through a longitudinally cut core plug to simulate an artificial fracture (Fig. 2-2).

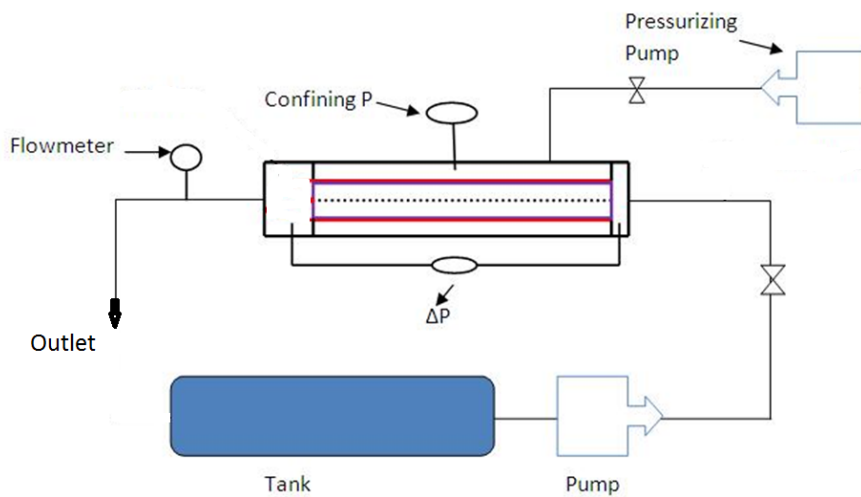


Figure 2-2. Schematic demonstrating a laboratory set-up for brine-flooding of an artificially fractured core plug.

A back-calculation of fracture permeability and fracture aperture based on the overall measured fractured core plug permeability magnitudes was performed (Table 2-1) to analyse the effect of persistent confining stress on the fracture geometry and hydraulics. Following chapters entail how the outcome of this research was utilized as a benchmark in achieving best physics coupling strategy in a realistic numerical investigation.

Table 2-1. Back calculated fracture aperture magnitudes for an artificially fractured core plug flooded under overburden stress (Stalker et al., 2009).

Overburden (Psi)	Fracture Aperture (micron)		
1000	60.6	Core plug length (cm)	7.54
1600	45.7	Core plug Diameter (cm)	3.79
2200	38	Matrix porosity	0.154
2800	31.3	Matrix permeability (mD)	315

In this dissertation, fracture-matrix flow partitioning is modelled numerically taking the advantages of a coupled approach. Subsequently the numerical analysis outcome is evaluated using laboratory measurements. Chapter 3 describes the procedure of selecting the appropriate numerical modelling approach.

Chapter 3.0

Fracture modelling within porous media

3.1 Introduction

Extensive literature review demonstrated a range of methods applied to implement fractures within a porous medium in fractured formations flow and structural deformation analyses. In order to develop applicable empirical models, adopting most precise fracture modelling approach is of prime importance. Three prevalent strategies of fracture consideration as an equivalent porous medium, an (n-1) dimensional feature and a free flow channel interacting with the matrix have been examined in this chapter and validated against published laboratory results by Stalker et al. (2009). The approach which considers fracture as a free flow channel interacting with rock matrix proved to be the most accurate, particularly when coupled with appropriate mechanistic governing equations, and was consequently adopted in sensitivity simulations of the following chapter.

3.2 Fracture as an equivalent porous domain

Having concentrated on developing empirical models for stress-affected flow through rock matrix and fracture, core scale analyses were scrutinized in our investigations. In order to fulfil detailed simulations of flooding through fractured core plugs, Ansys-Fluent code, as an extensively applied commercial one in porous media studies (Cito, 2009; Piller et al., 2014; Tamayol and Bahrami, 2008) was initially sanctioned for our core scale investigations. Fluent is a C based computational fluid dynamics (CFD) code that provides the user with the flexibility of introducing C-implemented user defined subroutines of non-standard boundary conditions. Implementation of fractures within porous medium necessitates defining capillary pressure/saturation continuity at the interface which can be problematic using standard codes associated modules.

Core flood test through a Clashach sandstone core plug containing a uniform longitudinal smooth-walled fracture under confining overburden stress constitutes the basis for our numerical analyses (Fig. 3-1). This base case scenario has been sanctioned due to availability of published laboratory data for validation purposes.

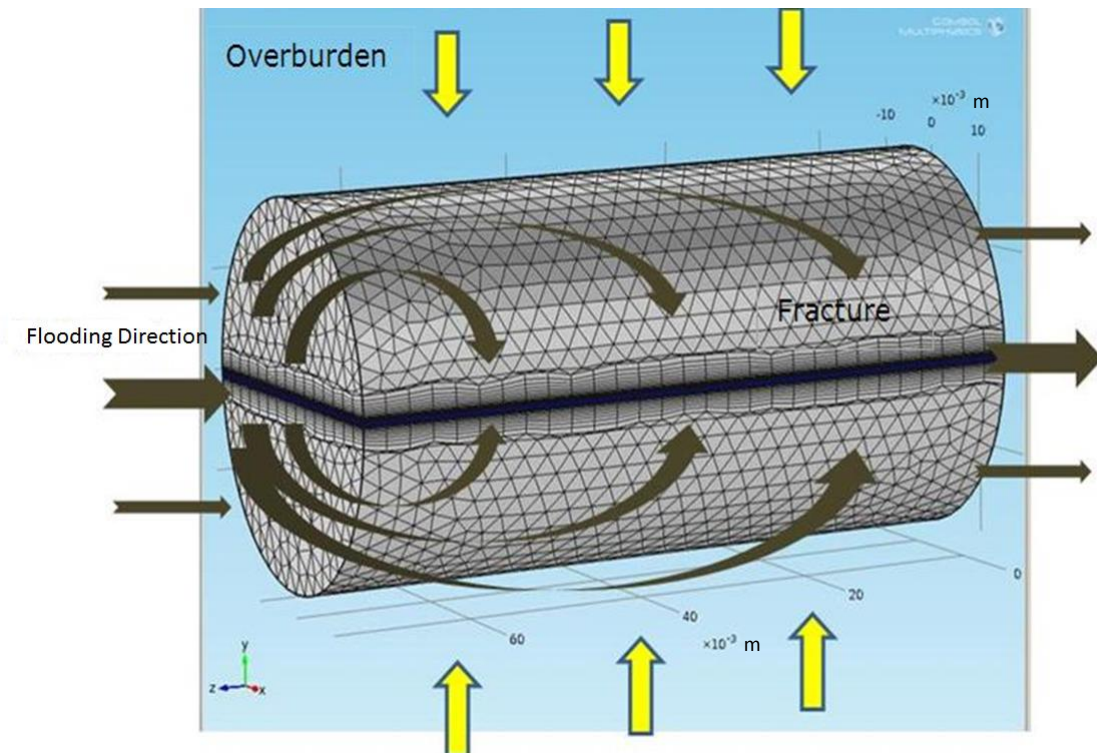


Figure 3-1. Core flooding of an artificially fractured core plug under confining overburden stress.

The first fracture modelling approach was investigated via generation of a thin equivalent cuboid porous domain splitting a porous core plug into two halves in the middle longitudinally (Fig. 3-2). In order to achieve a robust discretisation, the Fluent generated geometry was transferred to Ansys ICEM and fine-meshed using that module. The discrepancy between the fracture and the plug matrix domains' dimensions demands a gradual decrease from the coarser matrix grid size to the finer fracture grid size to alleviate large differentials in the continuity calculations at the fracture-matrix interface.

Ansyz ICEM enables fine meshing and the perfectly discretised geometry can be linked to Fluent for the mathematical analysis.

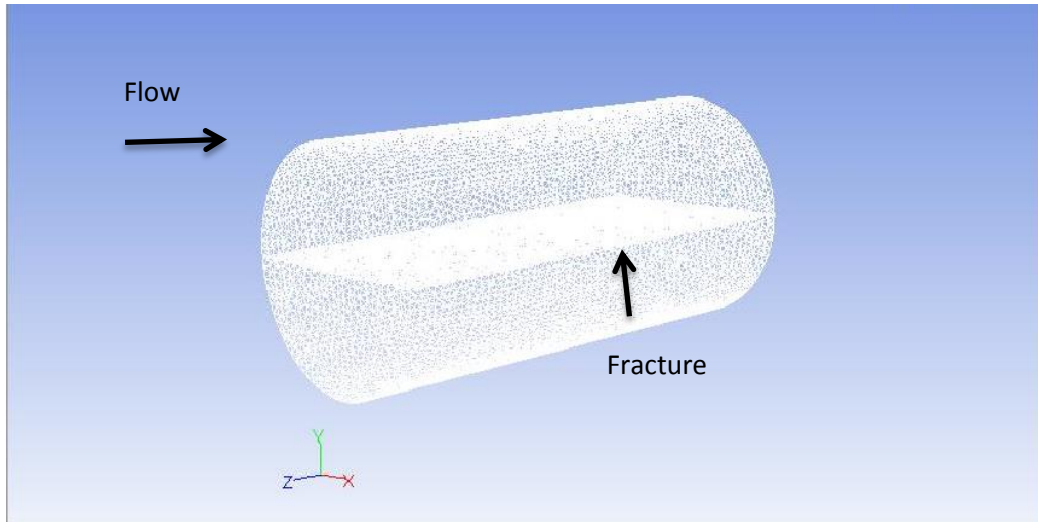


Figure 3-2. Fractured core plug created and meshed using Ansys Fluent. Note the denser meshed cuboid fracture domain splitting the core plug into two halves.

According to the validation requisites of the flooding analysis, published data of an artificially fractured core plug (Stalker et al., 2009) set the basis for our simulation initialization. Table 3-1 illustrates the simulated Clashach sandstone core plug properties flooded under various overburden stresses. It is worth mentioning that the provided rock mechanical data in Table 3-1 which was utilised in the coupled analyses of following sections of this chapter was derived from various literature sources (Crawford et al., 1995; Jones and Somerville, 2001; Ojala, 2003). The referenced core flood laboratory experiment involved flooding of a Clashach sandstone core plug which was longitudinally cut in halves under various overburden stress intensities to analyse hydraulic properties of a fractured sandstone core plug. The published experimental data does not provide the fracture and matrix flow magnitudes separately, however the summation of fracture and matrix out flow simulation results were decided to be compared against the outflow laboratory measurements of the available publication. This approach was adopted due to

the lack of any available published data of segregated fracture and matrix flow measurements.

Table 3-1. Simulated fractured core plug and flooding fluid properties.

<i>Simulation test data</i>	
Plug diameter	3.79x10 ⁻² m 7.54x10 ⁻² m
Plug length	
Matrix Porosity	0.154
Matrix Permeability	3.10874x10 ⁻¹³ m ²
Fluid Viscosity	0.001 Pa.s
Young's Modulus	4.0x10 ¹⁰ Pa
Poisson's Ratio	0.14
Fluid Compressibility	3.0x10 ⁻¹⁰ Pa ⁻¹

As evident from table 3-1, fracture domain is defined as a distinct porous medium interacting with the core plug matrix. Stalker et al. (2009) accounted for fracture aperture based on a back calculation method. This method estimates fracture aperture based on the comparison of the laboratory flow measurements with the amount that Darcy equation delivers for the equivalent porous material consisting of the matrix and an additional virtual porous region within the fracture domain subjected to the measured differential pressures (the difference between the exerted injection pressure at the core holder inlet and the observed pressure at the core holder outlet) across the core plug under each overburden stress. This virtual porous fracture domain has a fracture porosity based on the fracture volume to the whole core plug volume ratio, and a permeability calculated by the Schechter equation (Eq. 3-1). Initially a fracture aperture is guessed and permeability of the fracture is calculated and the whole fractured core plug volumetric average permeability is compared with the laboratory-derived core plug permeability

and the initial guess is corrected accordingly. Following such an iterative correction cycle the fracture aperture is back calculated. These estimated fracture aperture values were applied to construct fracture geometry in our simulations. Fracture porosity was calculated based on the fracture to total core plug volume ratio and fracture permeability (k_f) was calculated based on the Schechter equation according to the fracture aperture values (b) (eq. 3-1); (Stalker et al., 2009):

$$k_f = 8.45 \times 10^9 b^2 \quad (3-1)$$

The published experimentally measured differential pressures were considered as the reference for initial and boundary conditions. Based on the laboratory constraints of the published data, steady state laminar linear flooding through core plug was implemented.

3.2.1 Governing equations

Simplistic homogenous porous media is modelled through incorporating a momentum source term within the standard fluid flow equations. This source term (Eq. 3-2) consists of a viscous loss term which is known as Darcy equation (first right-hand side term; eq. 3-2) and an inertial loss term (second right- hand side term; eq. 3-2):

$$S_i = -\left(\frac{\mu}{K} v_i + C \frac{1}{2} \rho \bar{v} v_i\right) \quad (3-2)$$

Where S_i is the source term for the i^{th} (x , y or z) momentum equation, \bar{v} is the magnitude of velocity and C is the inertial resistance factor. This momentum sink contributes to the pressure gradient in any modelled porous cell accounting for a pressure drop which is proportional to the fluid velocity in the cell.

In case of linear laminar flow through porous media and low flow velocities such as our desired investigation scenario, the inertial resistance factor can be considered negligible and pressure drop would be dominantly proportional to the velocity. Ignoring diffusivity and convective effects, the porous media model reduces to Darcy law (eq. 3-3) which relates the total flow velocity to the product of intrinsic permeability of the porous medium and the total

pressure drop divided by the fluid viscosity and the length over which the pressure drop occurs:

$$\nabla P = -\frac{\mu}{k} \vec{v} \quad (3-3)$$

Taking the advantage of the above governing equation, the simulation of the fractured core plug was performed by defining fixed pressure boundaries according to the laboratory measured differential pressure magnitudes for every overburden stress level and corresponding fracture aperture size.

3.2.2 Fracture-matrix hydraulic interaction

The benchmarking laboratory experiments of Stalker et al. were performed using fully saturated core plugs to enable presuming steady state linear flow regime within the characterisation calculations. Since validation of flow partitioning between fracture and matrix was the main concern the highest overburden loading test scenario of Stalker et al. experiments, flooding under 21.4 Mpa (3100 psi) overburden stress, was numerically simulated. Intensive overburden stress enforces minimum fracture aperture size and hence the least flow bypass magnitude through fracture; this will promote the matrix capability to compete with limited conductivity of fracture in terms of flow.

Flow velocity field was visualized using Fluent post processing capabilities (Fig. 3-3) along with Techplot (Fig. 3-4) to achieve a robust concept of fracture-matrix flow exchange. As can be seen in Figure 3-3, the maximum fluid velocity is observed within the fracture domain, the green and blue region in the middle, and matrix flow is dominant in the immediate vicinity of the more permeable fracture. High velocity region in the middle of the velocity cross section, indicates higher conductivity of the fracture in comparison to the adjacent matrix; flooding takes place in the z direction and Fig. 3-3 shows the z component of the flooding velocity to assist in highlighting the fracture conductivity significance. A minimum turbulent effect is apparent at the fracture tip which occurs due to the presence of a double inlet, fracture and matrix, with different hydraulic characteristics.

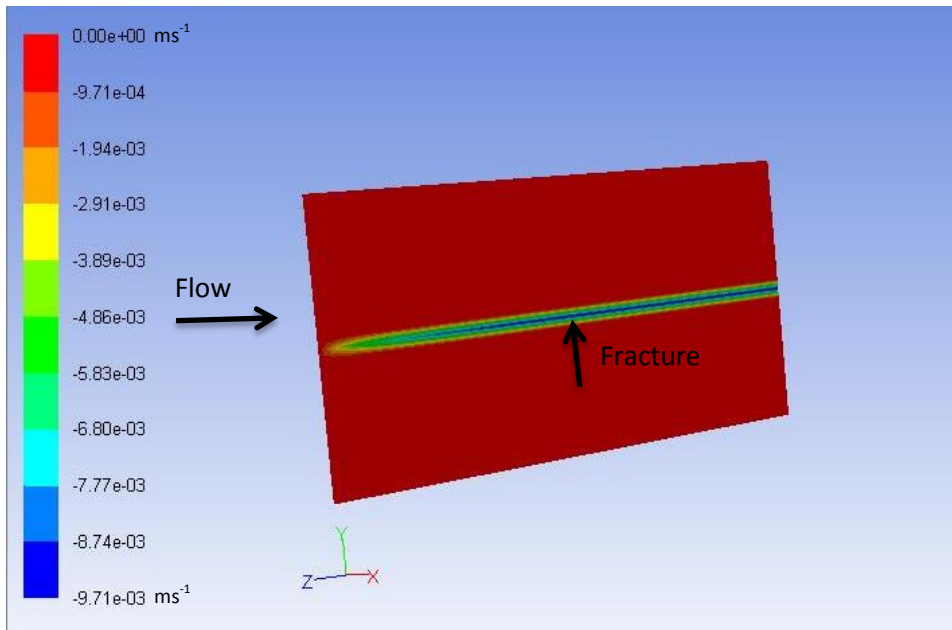


Figure 3-3. Vertical cross section of fluid velocity z component. Flooding direction is in contrary to the positive z coordinate.

Figure 3-4 illustrates the convergence of flow paths toward fracture as flow front travels farther from the inlet face. Colour-legend Pressure drop field over the core plug is provided to assist in understanding the evolution of the flow paths within the flooded fractured core plug. Consequently the analysis is dominantly a drainage problem analysis due to the injection through both fracture and matrix simultaneously. Flooding under decreased overburden pressures that allows larger fracture aperture sizes can result in imbibition scenarios due to the dominant fracture intake as a result of its enhanced permeability and significantly limited resistance to flow.

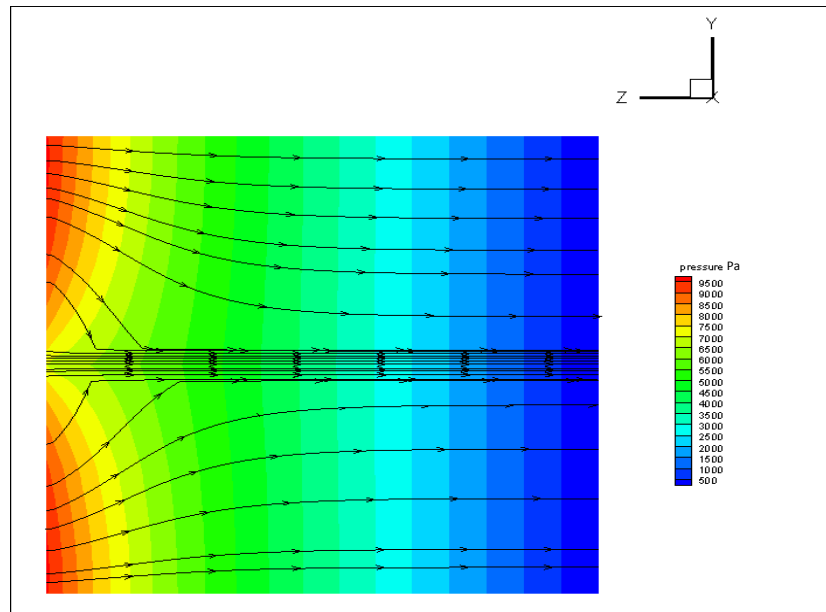


Figure 3-4. Flow paths visualization which demonstrates a drainage scenario.

Although fracture and matrix outflow contributions (flow partitioning) were calculated during the numerical analyses, as discussed previously, the published laboratory accumulated outflow measurements could merely be utilised for validation purposes due to the lack of any laboratory measured fracture-matrix flow partitioning data. Equivalent porous medium simulation approach of fractured Clashach sandstone for the most intensive overburden pressure of 21.4 Mpa (3100 psi) ,which delivers the most accurate laboratory flow partitioning measurements, indicates one order of magnitude difference with the accumulated outflow experimental data (Fig. 3-5; Table 3-2).

Table 3-2. Equivalent porous media approach simulation (Eq. Porous) results versus cumulative outflow laboratory measurements of Stalker et al.

Overburden 21.4 Mpa		Flow rate (m ³ /s)			
		Fracture	Matrix	Cumulative	% Difference
Flow rate (m ³ /s)	ΔP (pascal)	Eq. Porous	Eq. porous	Eq. Porous	Eq. Porous
3.3x10 ⁻⁸	5171	1.0x10 ⁻¹⁰	2.34x10 ⁻⁹	2.44x10 ⁻⁹	92.6
1.0x10 ⁻⁷	17030	3.29x10 ⁻¹⁰	7.68x10 ⁻⁹	8.009x10 ⁻⁹	92.0
6.7x10 ⁻⁸	11170	2.16x10 ⁻¹⁰	5.04x10 ⁻⁹	5.256x10 ⁻⁹	92.2
5.0x10 ⁻⁸	8412	1.63x10 ⁻¹⁰	3.8x10 ⁻⁹	3.963x10 ⁻⁹	92.1
3.3x10 ⁻⁸	5447	1.05x10 ⁻¹⁰	2.46x10 ⁻⁹	2.565x10 ⁻⁹	92.2

Such a significant error margin demonstrates the limited application of the applied simulation approach.

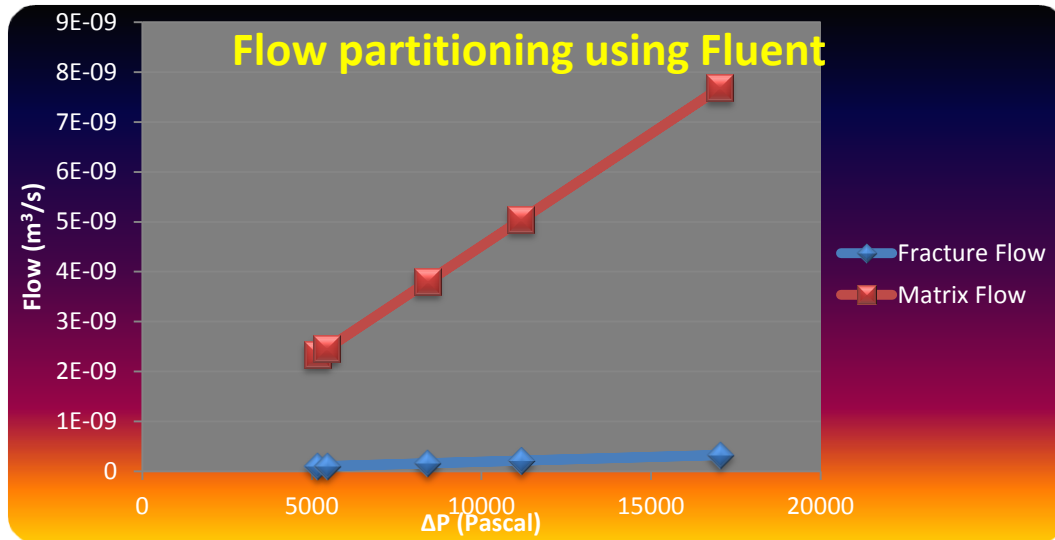


Figure 3-5. Matrix-fracture flow partitioning results derived from equivalent porous medium approach simulation.

Although the flow measurements difference seems to be infinitesimal by magnitude, the discrepancy between the simulation results and the experimental data is significant considering the core scale case study. Robustness of the simulation mesh was improved by applying various capabilities of conforming mesh generation of Fluent; However the refined mesh results remained consistent with the coarser mesh size case despite variation in computation time scale.

Consequently treating fracture as a discrete boundary within the core plug porous geometry has been attempted in order to distinguish the advantages of this more extensively applied simulation approach.

3.3 Fracture as (n-1) dimensional feature within porous matrix

In order to study the treatment of fracture as a sub dimensional feature, COMSOL Multi-physics finite element analysis software was utilized. COMSOL Multi-physics, known formerly as FEMLAB, is finite element analysis simulation software which provides several predefined physics interfaces to handle engineering problems. The software has been developed based on several differential equations that have been studied in mathematics department of KTH University in Sweden.

COMSOL in-built sub surface flow module offers variety of interfaces suitable to investigate porous subsurface formation static and dynamic coupled hydro-mechanical scenarios. Its multi-physics functionalities facilitate coupling structural mechanics models with laminar and turbulent flow regimes. Furthermore the integrated package would cover a wide range of post processing features making the software independent of any supplementary product to accomplish a comprehensive study. These advantages in combination with the convenient capability of introducing novel formulation to COMSOL solver resulted in its vast application in coupled porous media fluid flow publications (Bayani Cardenas and Wilson, 2007; Zhu et al., 2007; Diaz-Viera et al., 2008). COMSOL software suite also provides geomechanics and structural mechanics modules which can be coupled to fractured porous media flow equations in order to achieve fully coupled descriptive models of stress affected fracture-matrix flow partitioning.

3.3.1 Discrete fracture implementation in COMSOL

The same laboratory experimental data was used in the evaluation of discrete fracture concept in this section. Problem geometry and discretisation were significantly simplified due to the elimination of fracture domain. Implementing fracture as a two-dimensional boundary within the core plug geometry (Fig. 3-6) eliminated the aspect ratio contrast between fracture and matrix domains and consequently reduced variable discretisation, truncation errors and computational efforts in solving equations at the fracture-matrix interface. A sensitivity analysis on the model mesh proved the independency of the

solution results from the grid size; consequently a sufficiently fine grid appropriate for a typical non-fractured porous medium flow analysis was generated.

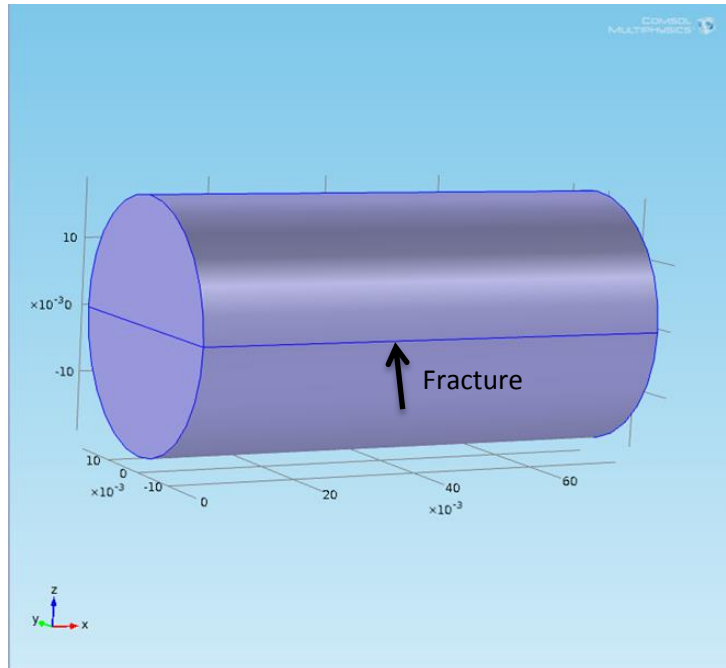


Figure 3-6. Two-dimensional fracture implementation within core plug geometry.

Considering the consistency of the simulations, the modelled fracture is longitudinal along whole core length with a uniform aperture throughout its length identical to what has been investigated in previous case. The core was flooded from left to the right and both matrix and fracture were open to flow at the inlets and outlets in the simulation initialization phase.

3.3.2 Darcy law Governing equations and fracture flow boundary condition

The most convenient interface of COMSOL software package to analyse flow within a porous medium is Darcy's law interface. Darcy law physics are implemented in this module which takes the effects of fluid pressure gradient, viscosity and the flow trajectory into consideration to calculate fluid velocity field variation while traveling through a porous medium as presented in eq. 3-4:

$$v = -\frac{k}{\mu}(\nabla P + \rho g \nabla D) \quad (3-4)$$

v in the above equation denotes the fluid Darcy velocity, k represents porous medium permeability, μ is the fluid dynamic viscosity, ∇P is the pressure gradient, ρ is the fluid density, g is the gravitational acceleration and ∇D is the unit vector in the direction over which the gravity would take effect. Gravity effects have been neglected in our plug scale analyses for all fractured porous media flow simulations in this chapter; therefore, the pressure gradient acts as the sole source of fluid movement in the core plug. Equation (3-4) is combined with the continuity equation in COMSOL Darcy Law interface to provide the generalized governing equation given by equation 3-5:

$$\frac{\partial}{\partial t}(\rho\varphi) + \nabla \cdot \rho \left[-\frac{k}{\mu}(\nabla P + \rho g \nabla D) \right] = Q_m \quad (3-5)$$

φ in these equation represents the porous material porosity and Q_m is a mass source term. Based on the fully saturated plug flooded in these analyses, a steady state linear flow scenario with no flow accumulation within the plug was considered.

The fracture flow boundary condition feature contributes to the problem physics through fracture flow interface of COMSOL Multiphysics. This interface uses tangential derivatives to calculate the flow along the interior boundary representing the fracture within the model. Fracture flow interface takes the advantage of a tangential form of Darcy's law (equation 3-6):

$$q_f = -\frac{k_f}{\mu} b (\nabla_T P + \rho g \nabla_T D) \quad (3-6)$$

The subscript f represents the fracture parameters, q_f is the volumetric flow rate per unit length of the fracture, b is the fracture aperture and subscript T

indicates that the gradient is measured on the tangential plane of the fracture. Fracture permeability (k_f) has been calculated according to the aperture size using the same procedure as in equivalent porous media simulation approach investigation. Equation 3-6, in combination with the continuity equation, provides an identical governing equation similar to the Darcy's law governing equation for the sub-dimensional fracture flow calculations as presented in eq. 3-7:

$$b \frac{\partial}{\partial t} (\varphi_f \rho) + \nabla_{\mathbf{T}} \cdot (\rho \mathbf{q}_f) = b Q_m \quad (3-7)$$

Fracture porosity (φ_f) has also been calculated based on the fracture domain volume to the whole fractured porous medium volume ratio (Van Golf-Racht, 1982).

3.3.3 N-1 dimensionally modelled fracture analysis results

Although fracture is defined as a boundary in the geometry, in the solution process, as can be inferred from the governing equations its aperture has been taken into account and the flow rate through the fracture was computed indirectly by applying tangential component of Darcy law along the fracture.

Despite the fact that the analysed problem is not directly mechanically-coupled, similar to the previous fracture modelling approach, the effect of stresses was considered in terms of fracture aperture magnitudes following the same aperture calculation method described in previous section (Stalker et al., 2009).

Available pressure drop values from the modelled experimental data were also applied in defining pressure boundaries, just like in Fluent simulations, and the outflow fluxes were monitored as the results.

Pressure isosurface contours and velocity diagrams derived from this simulation approach do not show any vertical flow path lines as matrix-fracture cross flow which is a consequence of defining fracture as a boundary within the model geometry (Fig. 3-7).

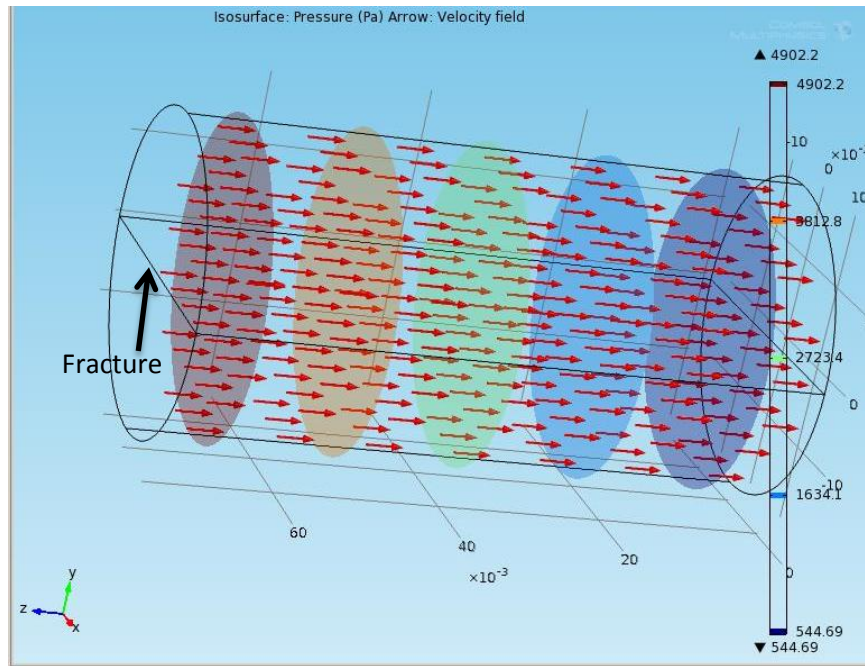


Figure 3-7. Velocity field arrow diagram superimposed on the pressure iso-surface contours.

In contrast with the outflow simulation results from the equivalent porous medium approach, the observed outflow magnitudes in sub-dimensional fracture modelling approach (Disc. Frac in table 3-3) demonstrated much improved match with laboratory measurements in terms of cumulative outflow especially for matrix domain. As table 3-3 indicates sub-dimensional implementation of fracture delivers much more reliable results than fracture treatment as an equivalent porous domain due to the decreased error percentages in the simulation results from almost 92% to approximately less than 20% for the 21.4 MPa (3100 psi) confining stress case.

Table 3-3. Comparison of flow partitioning results considering sub-dimensional implementation of fracture (Disc. Frac) versus the equivalent porous medium modelling strategy (Eq. Porous) for the 21.4 MPa confining stress.

Overburden 3100 Psi, 21.4 MPa		Flow rate (m3/s)							
		Fracture		Matrix		Cumulative		% Difference	
Flow rate (m3/s)	ΔP (Pascal)	Disc. Frac	Eq. Porous	Disc. Frac	Eq. Porous	Disc. Frac	Eq. Porous	Disc. Frac	Eq. Porous
3.3×10^{-8}	5171.1	1.83×10^{-9}	1.0×10^{-10}	2.405×10^{-8}	2.34×10^{-9}	2.589×10^{-8}	2.44×10^{-9}	21.55697	92.606061
1.0×10^{-7}	17030	6.04×10^{-9}	3.29×10^{-10}	7.921×10^{-8}	7.68×10^{-9}	8.525×10^{-8}	8.009×10^{-9}	14.7496	91.991
6.7×10^{-8}	11170	3.96×10^{-9}	2.16×10^{-10}	5.196×10^{-8}	5.04×10^{-9}	5.592×10^{-8}	5.256×10^{-9}	16.543433	92.155224
5.0×10^{-8}	8411.6	2.98×10^{-9}	1.63×10^{-10}	3.913×10^{-8}	3.8×10^{-9}	4.211×10^{-8}	3.963×10^{-9}	15.786	92.074
3.3×10^{-8}	5446.9	1.93×10^{-9}	1.05×10^{-10}	2.534×10^{-8}	2.46×10^{-9}	2.727×10^{-8}	2.565×10^{-9}	17.375758	92.227273

Implementation of fracture as an internal boundary within COMSOL Darcy law interface enabled performing a parametric sweep type of fracture flow analysis exposed to varying overburden stress magnitudes as provided in figure 3-8. Furthermore, the simulation runtime for the parametric sweep analysis happened to be just few minutes which is a considerable improvement in running a porous media flow simulation in presence of fractures. Since the poro-elasticity effect hasn't been taken into consideration at this stage, the overburden stress did not exhibit any direct impact on the matrix flow contributions.

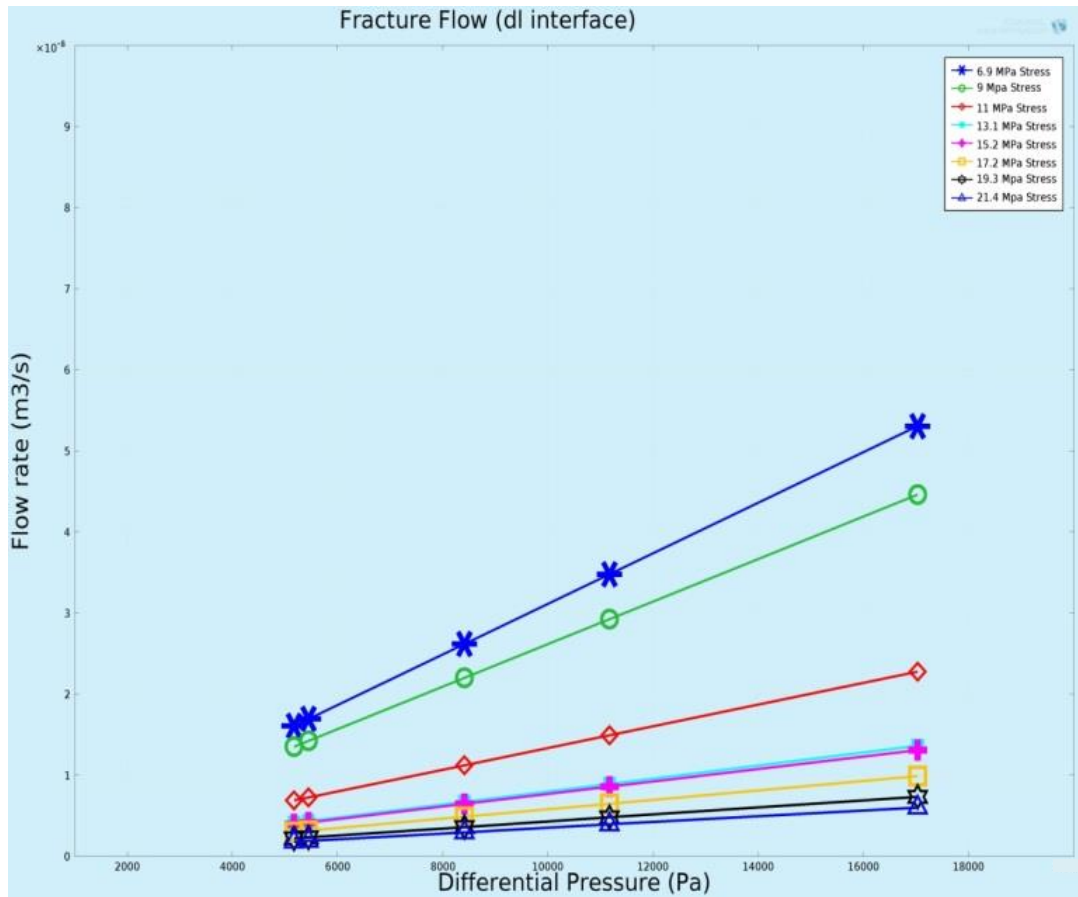


Figure 3-8. Overburden stress effect on fracture flow while modelling fracture as a sub-dimensional boundary using COMSOL Darcy’s law interface.

As expected, variation of fracture flow copes with Darcy law and enhanced pressure drop results in increased fracture flow as it is calculated as a tangential component of Darcy flow. Enhanced overburden stress intensities results in decreased fracture flow rates for any constant differential pressure between the core plug inlet and outlet. This effect is indeed a direct sequence of reduced fracture apertures corresponding to increased overburden stresses. Figure 3-8 also indicates that fracture flow partitioning dependency on overburden stress, illustrated as the slope of fracture flow rates versus differential pressure magnitudes, demonstrates an inconsistency at approximately 11 MPa overburden stress. Such an inconsistency can be inferred as a symptom of fracture closure, however, a proper mechanically-coupled analysis needed to be performed to enable identification of decisive stress levels at which fracture hydraulic behavior alters.

Implementing fracture as a sub-dimensional feature within a porous media flow analysis proved to provide more accurate results while reducing the computational efforts and runtime, however with regard to governing equations, it is evident that actual cross flow between fracture and matrix and its variation with overburden stress loading still cannot be analyzed using this simulation approach.

3.4 Realistic open channel fracture

In order to achieve the most realistic approach of fracture modelling in fractured porous media flow study, the advantages of free and porous media flow interface of COMSOL were taken into consideration. The underpinning governing equations of this interface enables modelling free Navier-Stokes flow adjacent to porous media flow while maintaining the pressure and velocity field consistency. Applying such a realistic fracture modelling approach facilitates monitoring of fracture-matrix cross flow subjected to varying overburden stress loadings and its simulated flow magnitudes should align the most with laboratory core flooding data.

3.4.1 Open channel fracture geometry and discretisation

The two previously examined fracture implementation techniques were simplifications applied to overcome the extensive computational effort needed for considering fracture as an open channel discontinuity within a porous medium. Extensive computations are direct results of large aspect ratio between fracture aperture size (in microns in current analysis) and the core plug dimensions (in Centimeters for current analysis) which cause excessive runtime and a low memory-efficient solution.

The advantages of introducing symmetry boundary conditions enabled simulation of the same analysed core flood experiment while modelling fracture as a laminar Navier-Stokes flow domain interacting hydraulically with the adjacent porous matrix domain through computation of flow dynamics for a quarter of the whole fractured plug geometry (Fig. 3-9).

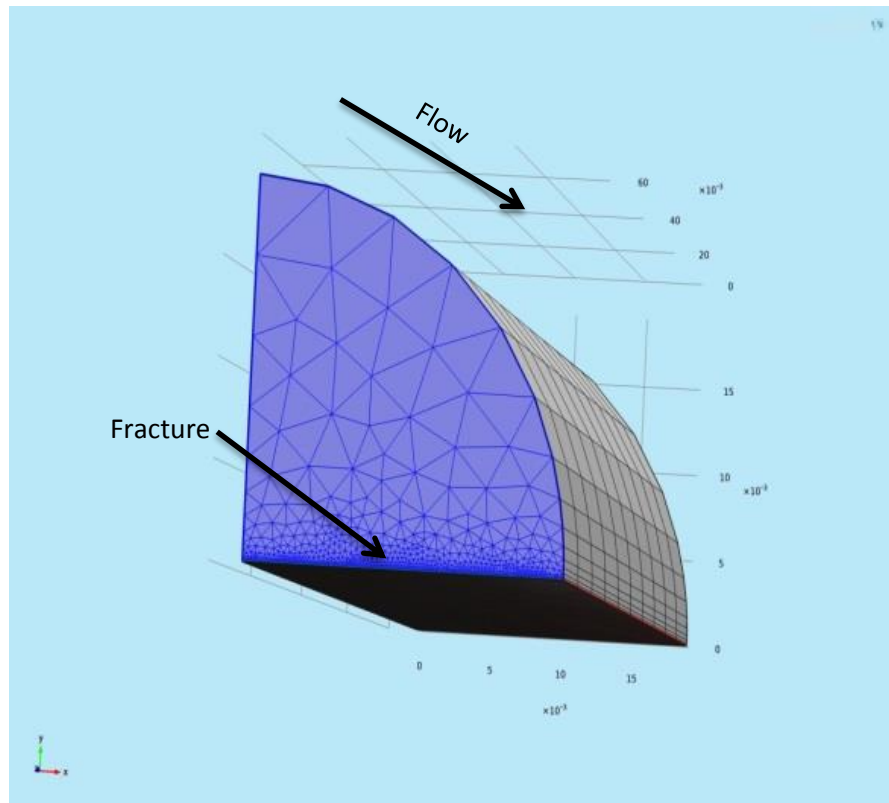


Figure 3-9. Geometry created for the open channel fracture modelling concept utilizing symmetry boundary conditions.

Advantages of utilizing symmetry boundary conditions reduced the complexity of numerical operations and truncation errors which promoted the efficiency of the solver. Furthermore the matrix-fracture cross flow quality could be characterized through assigning velocity probes on the interface.

Continuity of the pressure and velocity fields is further illustrated in the following section along with the governing equations of flow within fracture and matrix domains.

3.4.2 Open channel fracture modelling concept governing equations

Similar to the previous modelling efforts, within the rock matrix, Darcy law was applied as the governing equation for flow and therefore the analytical formulation of this law (Eq. 3-4) and the accompanying continuity equation (Eq. 3-5) is not restated in this section.

On the other hand, the governing equation utilized within fracture domain and its coupling with the Darcy formulation of matrix domain interface grids are what more accredited in the open channel fracture simulation concept.

Laminar form of Navier-Stokes equations applied within the fracture domain as it was considered a free flow channel; this can be represented mathematically for an incompressible, constant viscosity fluid as (Eq. 3-8):

$$\nabla P = -\rho \frac{Dv}{Dt} + \rho g + \mu \nabla^2 v \quad (3-8)$$

Where the substantial time derivative is defined as:

$$\rho \frac{Dv}{Dt} = \rho \frac{\partial v}{\partial t} + \rho(v \cdot \nabla)v \quad (3-9)$$

It is worth mentioning that COMSOL general formulation is simplified for our steady state flow scenarios. Also implementing general Navier-Stokes flow physics within the fracture domain facilitates the incorporation of turbulence within the fracture channel; this is an advantage for generalization of the simulation to the larger fracture apertures which exhibit enhanced discrepancy in terms of permeability comparing to the adjacent formation matrix.

In order to maintain a continuous velocity and pressure field in the interface of a porous medium and a free flow domain, Brinkman equation which is an extension of Darcy law was adopted. Brinkman equation for a steady-state flow neglecting the inertial forces and any mass generation or accumulation can be rephrased as Eq. (3-10) (Martys and Hagedom; 2002):

$$\nabla P = -\frac{\mu}{k} v + \mu_e \nabla^2(v) \quad (3-10)$$

In this equation μ_e is the effective viscosity of the fluid in the porous medium and free flow domains. μ_e was determined on the assumption that $\mu \frac{du}{dy}$ in free

flow domain equals $\mu_e \frac{du}{dy}$ in the porous medium domain when $y = 0$ represents the interface between the domains.

3.4.3 Open channel fracture simulation efficiency

All the initial and boundary conditions applied to the stress affected core flood scenarios maintain the consistency with the previous simulation approaches. This procedure was intentionally adopted to achieve an understanding of the optimum fracture modelling approach in fractured porous media simulations.

Figure 3-10 exhibits the flow velocity field distribution along the core length; the distribution clearly indicates a major proportion of flow paths converge into the fracture, marked with orange color indicating higher flow velocities, in accordance with previous simulation approaches. The evolution of the flow paths convergence cannot be visualized along the core plug length as the outer circumference of the plug is covered with zero velocity, in blue, in accordance with the no slip stress boundary condition requirements. In addition, the streamlines at the inlet only converge into the fracture at its external edge and flow contribution which passes through core plug central part converge into fracture volume at a further distance from the inlet.

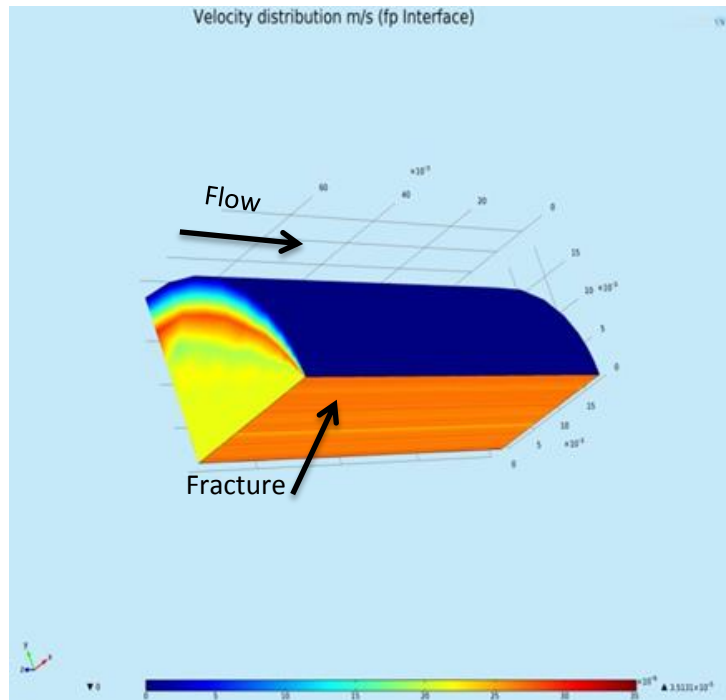


Figure 3-10. Velocity contours indicating flow velocity profile evolution and flow exchange quality along the core length.

The utilized flow equations provided a continuous flow between the rock matrix and the fracture and allows the cross flow between the two systems. As can be inferred from table 3-4, modelling fracture as an open channel exchanging flow with matrix provided more reliable outcomes. Although the improvement may seem infinitesimal, special attention should be paid to the fact that the current analysis is a plug scale one and the insignificant improvement can demonstrate massive accuracy in field scale studies.

Table 3-4. Comparison of flow partitioning results considering sub-dimensional implementation of fracture (Disc. Frac) and the open channel fracture (Open Frac) simulation approach under 21.4 MPa confining stress.

overburden 21.4 MPa (3100 Psi)		Flow rate (m3/s)							
Experimental Data		Fracture		Matrix		Cumulative		% Difference	
flow rate (m3/s)	ΔP (psi)	Disc. Frac	Open Frac	Disc. Frac	Open Frac	Disc. Frac	Open Frac	Disc. Frac	Open Frac
3.3×10^{-8}	0.75	1.83×10^{-9}	5.32×10^{-9}	2.41×10^{-8}	2.204×10^{-8}	2.59×10^{-8}	2.736×10^{-8}	21.55697	17.090909
1.0×10^{-7}	2.47	6.04×10^{-9}	1.752×10^{-8}	7.92×10^{-8}	7.24×10^{-8}	8.53×10^{-8}	8.992×10^{-8}	14.7496	10.08
6.7×10^{-8}	1.62	3.96×10^{-9}	1.148×10^{-8}	5.2×10^{-8}	4.76×10^{-8}	5.59×10^{-8}	5.908×10^{-8}	16.54343	11.820896
5.0×10^{-8}	1.22	2.98×10^{-9}	8.64×10^{-9}	3.91×10^{-8}	3.584×10^{-8}	4.21×10^{-8}	4.448×10^{-8}	15.786	11.04
3.3×10^{-8}	0.79	1.93×10^{-9}	5.6×10^{-9}	2.53×10^{-8}	2.32×10^{-8}	2.73×10^{-8}	2.88×10^{-8}	17.37576	12.727273

Similar to the findings of discrete fracture modelling approach, fracture flow decreases as the overburden stress increases with identical trends as can be seen in Fig. 3-11. Fracture flow results exhibit a rather close trend for fracture flow rates under overburden stress loading above 11 MPa while below this stress loading, the flow rate trends are more dispersed; this can be an indication of a shift in stress effects. The other inference from the study which is worth noting is that fracture flow exceeds matrix flow at low stress regimes and reduces drastically with increase in overburden stress loading. Consequently a stress threshold is reached beyond which the fracture flow does not change significantly. This is considered as the fracture healing pressure. However a more comprehensive poro-elasticity coupled modeling is required to achieve more practical and realistic results.

The dashed marker-free blue line in figure 3-11 represents matrix flow; and since stress dependent permeability was not accounted for, it is unchanged for all the stress loadings. Therefore, stress-dependent permeability has proven to be another physics-promoting feature to be implemented in the modelling investigation and it would be considered later to further improve the numerical analysis.

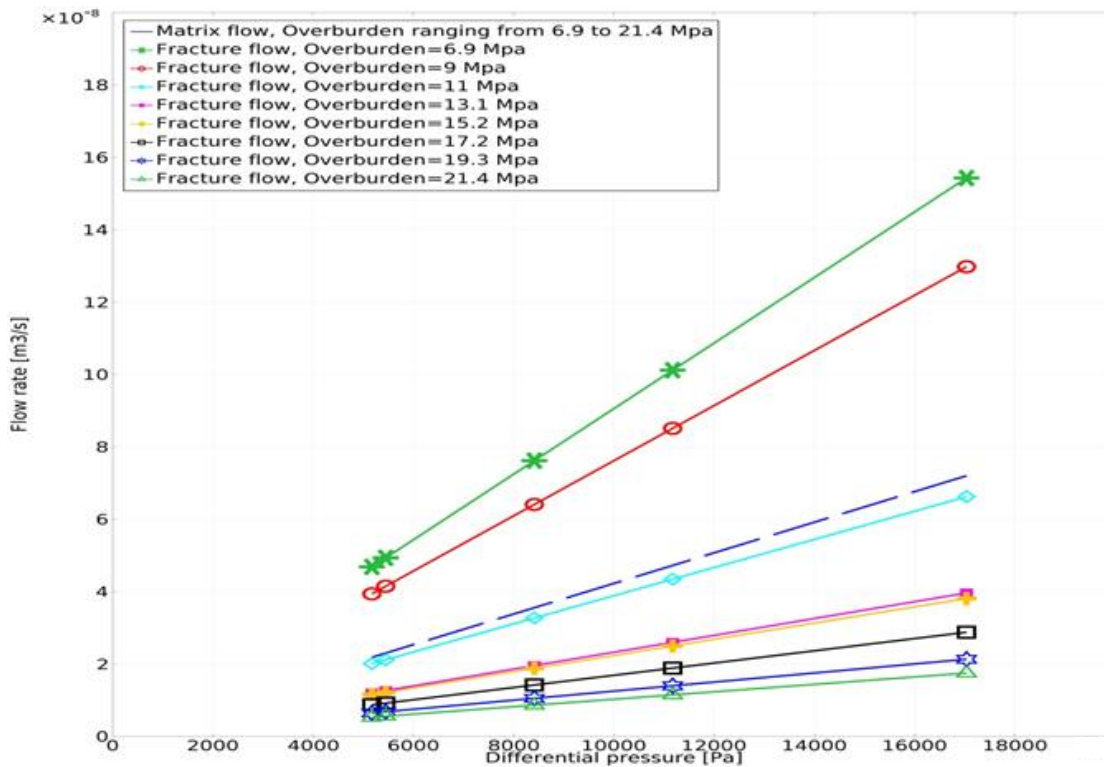


Figure 3-11. Open channel fracture-matrix flow partitioning; overburden stress effect on matrix and fracture flow while modelling fracture as an open channel interacting with matrix.

The cumulative flow rates calculated while applying open channel fracture simulation methodology (Table 3-4) are higher due to the larger fracture flow partitioning magnitudes, the fraction of cumulative flow that travels through fracture domain, as shown in figure 3-12. These higher fracture flow partitioning results can be interpreted as both an indication of more realistic Navier-Stokes flow within the fracture volume compared to a tangential derivation of Darcy flow in the former approach and a representation of the cross flow occurring between porous rock matrix and more permeable fracture channels.

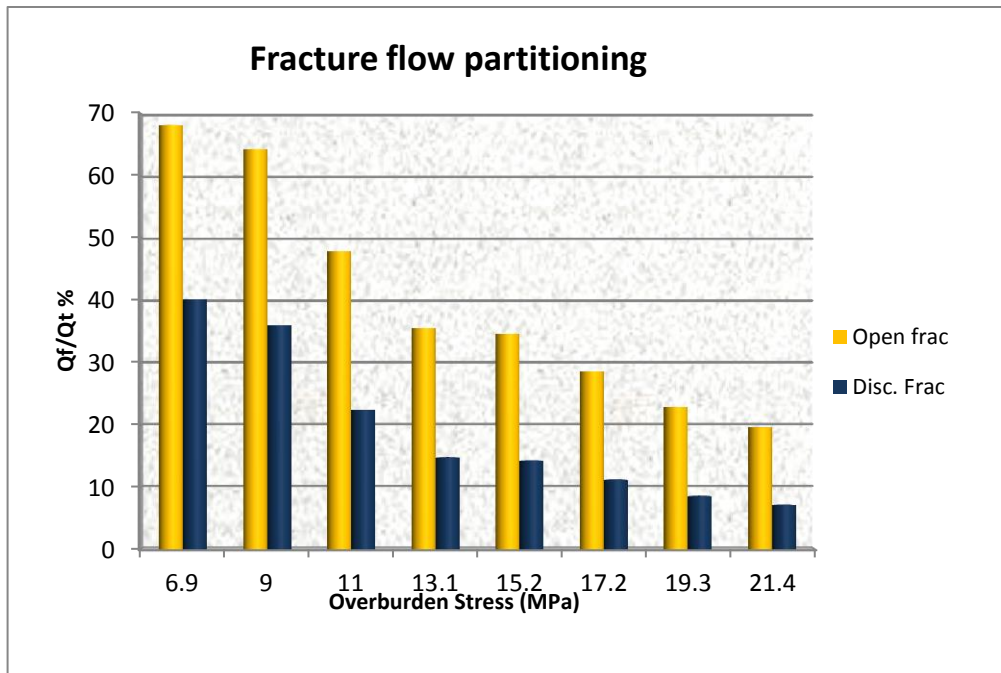


Figure 3-12. Fracture flow partitioning variation in response to overburden stress loading calculated using the sub-dimensional fracture implementation and open channel fracture modelling approaches.

Careful consideration of flow partitioning results obtained during open channel fracture modelling reveals that the dominant flow path for stresses under 11MPa is the fracture which accounts for more than 50 percent of the overall flow whereas discrete fracture modelling flow partitioning results indicate that even for the lowest stress magnitude the dominant flow path is the matrix responsible for minimum of about 60 percent of the overall flow (Note that based upon zero flow accumulation assumption, summation of fracture and matrix flow partitioning equals the total inflow). This inconsistency emphasizes the need for laboratory experimental flow partitioning data to ensure the accuracy and reliability of the numerical simulation approaches results.

3.4.4 Matrix-fracture cross flow characterisation

Simulating fracture as a volumetric domain in the open channel fracture modelling approach enabled cross flow measurement between the porous rock matrix and fracture. Cross flow is the vertical flow exchange in the interface between matrix and fracture as provided in figure 3-13 for various overburden stress loading levels for which the fracture flow variation has been monitored in previous section.

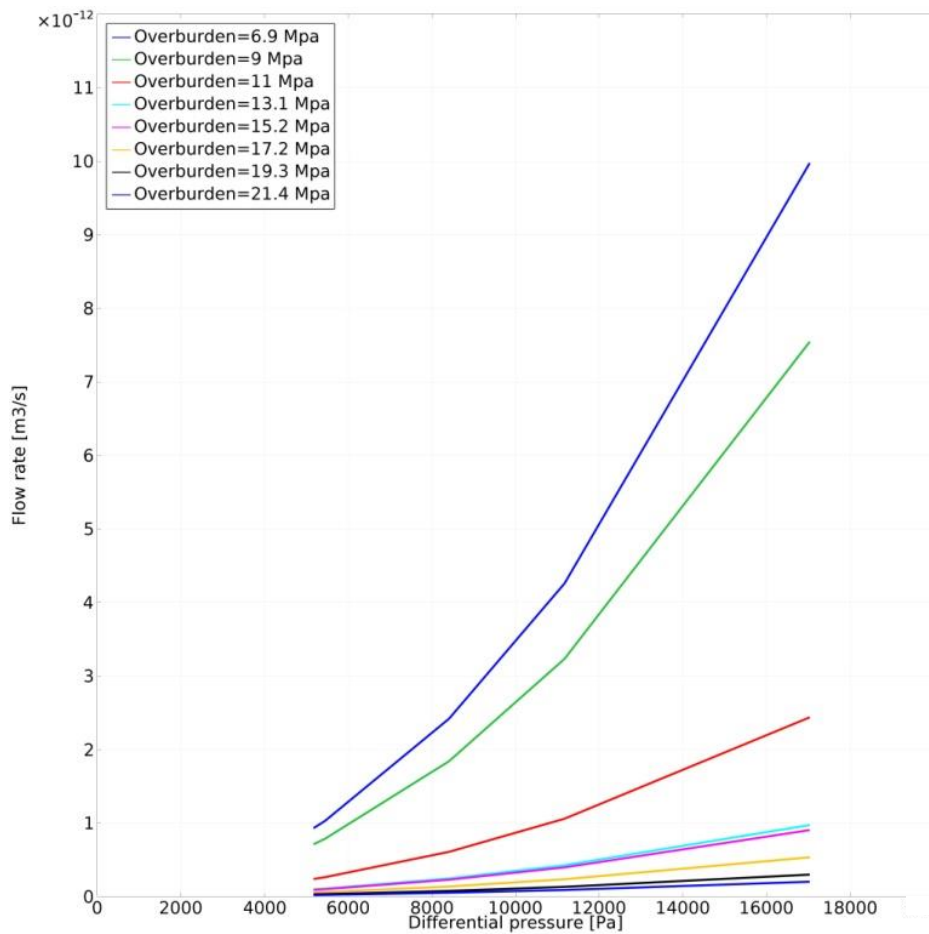


Figure 3-13. Matrix-fracture cross flow; variation of matrix-fracture cross flow against differential pressures under alternating overburden scenarios.

As can be seen in figure 3-13, similar to the fracture flow rate results, cross flow magnitudes also decrease in response to increased overburden stress. Cross flow measurements indicate that especially for high differential pressure magnitudes, cross flow severely changes in response to overburden stress.

This is much more significant again for stress loading levels below 11MPa. Furthermore, for these lower stresses, cross flow varies exponentially with differential pressures and is several orders of magnitudes higher.

It is worth mentioning that the indicated cross flow rates in Fig. 3-13 translates into 3-300 cc/day flow exchange per unit area of matrix blocks. Such normalization reveals the significance of fracture-matrix cross flow in a field scale production scenario particularly for lower overburden stress levels and higher differential pressures across the bulky field scale matrix blocks.

The cross flow measurements in combination with the fracture flow partitioning investigations proved that at a certain overburden stress level (between 11 MPa to 13 MPa for current analysis), the fracture can be considered as a semi-closed fracture. After this stress level the cross flow between rock matrix and fracture volume would reduce tremendously and the developed pressure drop within the fracture is not large enough to overcome the capillary effects in the rock matrix pore spaces, therefore, the flow partitioning for these overburden stresses are more affected by viscous forces.

3.5 Open channel fracture coupled with poro-elasticity and stress dependent permeability

Open channel fracture modelling approach driven results revealed that while the modelled flow partitioning magnitudes matched the experimental data within 10-17 % error margin (table 3-4), there is still more opportunity to upgrade the modelling technique.

Other than stress dependent permeability physics augmentation which was discussed in section 3.3 while interpreting the matrix flow behaviour, the stress affected fracture aperture variation could also be modelled via implementing structural mechanics and poro-elasticity physics coupled to the open channel fracture model. This approach appears to be the most realistic one providing the most precise flow characterisation of a fractured porous medium.

3.5.1 Poro-elasticity and stress dependent permeability physics

The overburden stress has a twofold effect on the fractured porous medium flow. It influences the fracture flow by exerting changes to the fracture aperture and on the other hand it affects matrix flow through alteration of pore volumes and the initial permeability of the rock. Both of these effects need to be accommodated in the flow characterization to achieve reliable results.

Poro-elasticity combines a transient type of Darcy equation with the elastic stress-strain geomechanical factors. A major constitutive equation in this physics is the Biot's equation (Eq. 3-11) which relates total stress to the total strain and pore pressure:

$$\sigma = E\varepsilon - \alpha_B P_p \quad (3-11)$$

In this equation σ is the stress tensor, ε is the strain tensor, E is the elasticity matrix for drained condition, α_B is the Biot-Willis coefficient and P_p is the pore pressure.

Biot's theory (Biot, 1962) delivers the other important constitutive model of poro-elasticity (as given in Eq. 3-12) which relates the change in the fluid content (ξ) to the volumetric strain (ε_{vol}) and incremental pore pressure:

$$P_p = M(\xi - \alpha_B \varepsilon_{vol}) \quad (3-12)$$

The coefficients α_B and M have been measured by Biot and Willis (Biot, 1962) as a function of drained, solid and fluid compressibility values. M is the inverse of storage coefficient which is the ratio of fluid added to the system per unit aquifer volume divided by the change in pore pressure; this relationship enables the coupling of poro-elasticity equation with Darcy equation in porous medium.

Poro-elasticity physics calculates strains due to the exerted overburden stress; consequently the computed strain magnitudes take effect as the fracture aperture variation. To consider the changes in the fracture flow, a moving mesh capability was adopted to couple the strain-driven displacements to the fracture geometry in the Navier-Stokes flow equations.

Moving mesh is an automatic re-meshing functionality of COMSOL that assisted in moving the mesh nodes at each step of the numerical solution when the model geometry was moving, without the need to regenerate the whole meshing process. The interface between fracture and matrix was allowed to move in prescribed directions and the model automatically perturbed the mesh nodes to conform the moved boundaries. It is worth mentioning that the material properties also extrapolate in the newly generated grids and in this way the material was also moving in accordance with the mesh while the mass balance was kept stable. As the mesh moved at each overburden stress based on the displacements from poro-elasticity calculations, the new conformed mesh was used for the flow calculations.

On the other hand, a stress dependent permeability model (Eq. 3-13) was used for the matrix flow based on the differential stress and geomechanical properties of the rock for every overburden stress corresponding to the fracture flow calculations (Bai and Elsworth, 1994):

$$k = k_0 \left\{ 1 \mp \frac{1}{2} \left[\frac{9(1-\nu^2)}{2} \left(\frac{\pi \Delta \sigma}{E} \right)^2 \right]^{\frac{1}{3}} \right\}^2 \quad (3-13)$$

In this equation k_0 represents the initial permeability of the rock matrix, ν is the Poisson's ratio, $\Delta \sigma$ is the differential volume stress and E is the Young's modulus of the drained rock matrix.

In summary, the vertical displacements of the fracture walls (derived from Eq. 3-11 and Eq. 3-12 calculations) were updating the fracture aperture while moving mesh capability was adjusting the mesh according to the deformed fracture geometry. The updated fracture was used in the same flow equations applied in the open channel fracture approach to compute the fracture flow for each overburden stress. Simultaneously Eq. 3-13 delivered updated matrix flow by changing the matrix permeability according to the overburden stress. This updated matrix permeability was utilized within the same matrix domain flow equations discussed in open channel fracture modelling section.

3.5.2 Coupled open channel fracture modelling outcomes

The same laboratory experiment (from Stalker et al., 2009) was simulated again using the poro-elasticity and stress dependent permeability coupled flow physics. 1 MPa pore pressure was defined as the laboratory experiments were done at this pore pressure.

All the initial and boundary conditions were set consistent to the previous analyses in accordance with the discussed Stalker et al. laboratory experiments in section 2.4 and the initial fracture aperture was assumed to be about 1.3×10^{-4} m. In order to be able to measure the fracture aperture variation under overburden stress, the simulated matrix domain had to be constrained along the external fracture wall (Fig. 3-14). This fixed fracture domain boundary provided the appropriate boundary condition for fracture walls displacement calculations in accordance with structural mechanics physics. The considered initial aperture size was assumed in a way to provide the published back calculated laboratory data for average fracture aperture for the benchmark exerted overburden stress, the 21.4 MPa stress loading case, due to the lack of any laboratory measured aperture data.

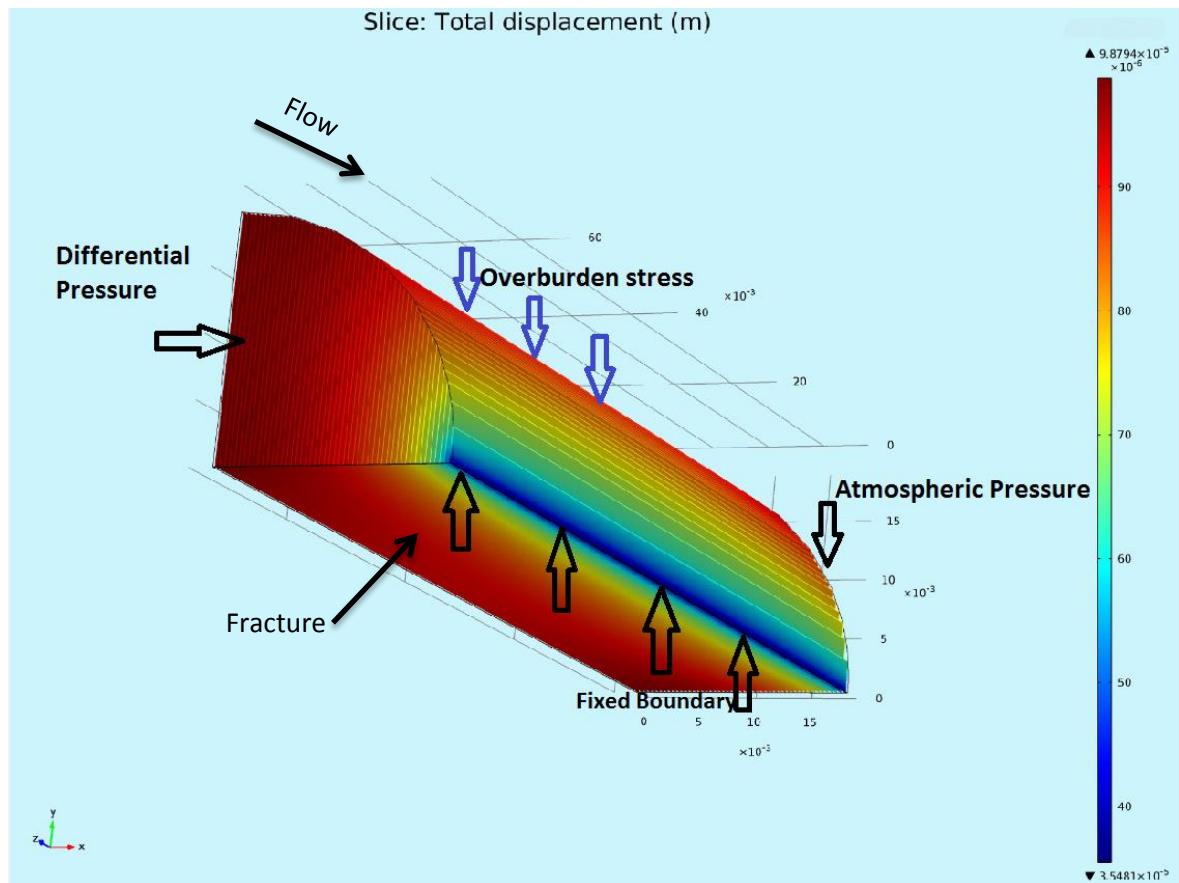


Figure 3-14. Total matrix displacement slice diagram including boundary conditions; vertical slices indicating vertical displacement of fracture walls; Note the fixed external fracture wall from which the displacement increases toward plug center line.

The numerical constraint of fixing external fracture wall is in line with the laboratory requirement to keep the fracture open through positioning metallic shims at the edge of fractured plug at the initial stage of flooding. Metallic shims were used in the experimental validation phase and will be discussed in detail in chapter 6. Existence of asperities or proppants in fracture is the realistic example of partially-fixed fracture walls in the field scale scenarios.

Having set the initial and boundary conditions, the overburden stress was increased incrementally from 6.9 MPa to 21.4 MPa and the geometrical displacements were monitored as shown in Fig. 3-15. Zero x coordinate represents the center of the core plug in which the displacement magnitudes were maximum. As evident in Fig. 3-15, the vertical displacements increased as the overburden stress increased. Computed displacement average over the

fracture plane was subtracted from the initial aperture and the remaining aperture was used for flow calculation in each stress loading scenario.

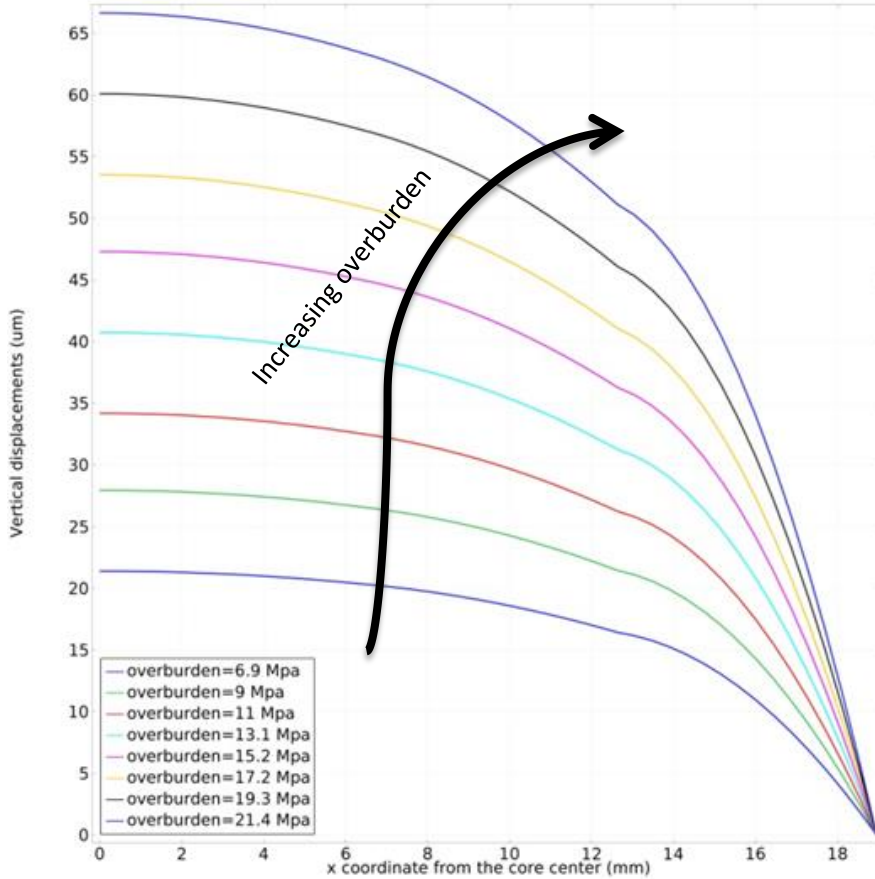


Figure 3-15. Total matrix displacement plot; vertical displacement of matrix under various overburden stress loading levels across fracture width; Note the zero displacement at the external edge of fracture.

Having coupled the stress dependent permeability for the matrix and updated poro-elasticity driven displacements in fracture geometry by means of re-meshing capability of COMSOL, the simulations were performed for different stress loading scenarios with the aim of investigating the change in the flow between the fracture and the matrix. It is worth mentioning that as the mesh regenerated to accommodate the decrease of fracture aperture, in each calculation step, the material properties were also extrapolated for the newly created grids. Mesh adjustment for each overburden stress is required as the physical geometry of the fracture changes as a result of structural stress-

strain physics; such a geometry change necessitates also considering the fixed boundary in the simulations (Fig. 3-14) and applying an averaging fracture aperture calculation method to provide the correct re-adjusted fracture geometry for the fluid flow physics within the fracture and at the matrix-fracture interface. The results of these simulations are presented in Fig. 3-16.

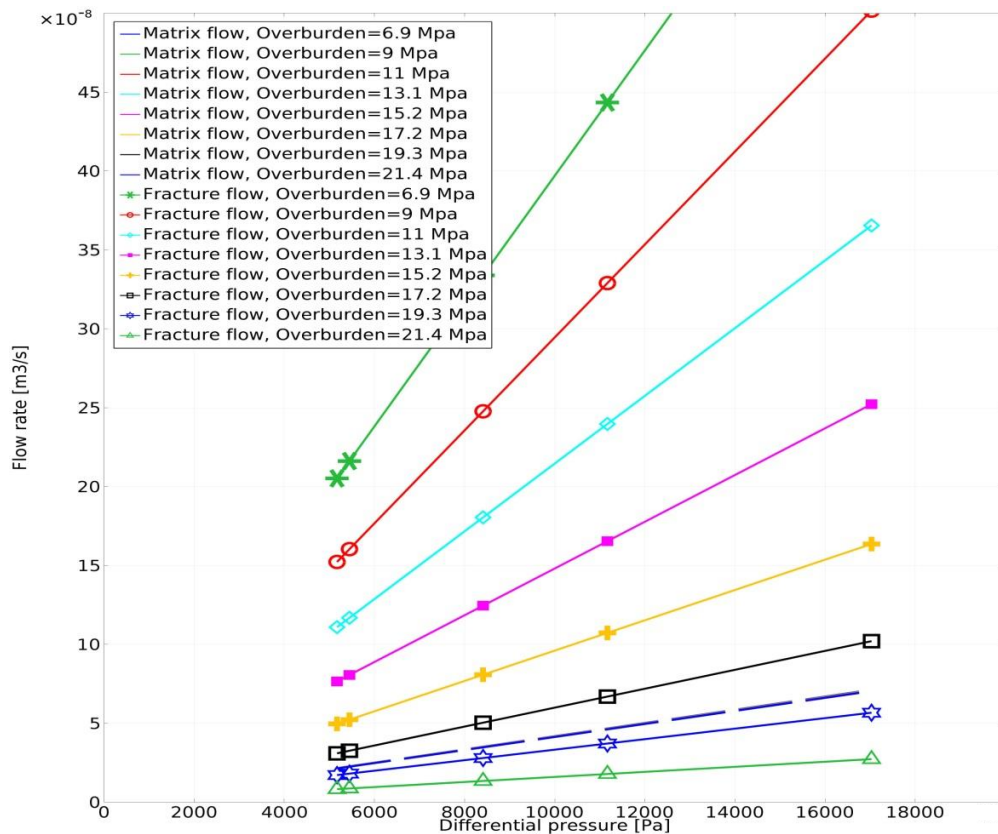


Figure 3-16. Coupled open channel fracture-matrix flow partitioning; overburden stress effect on matrix and fracture flow while modelling fracture as an open channel interacting with matrix coupled with poro-elasticity and stress dependent permeability.

Figure 3-16 indicates not only are the fracture flow partitioning results higher by tens of mm³/s for such a plug-scale investigation in the coupled open channel fracture simulation approach but also more interestingly, fracture flow exceeds matrix flow for the lower stress loading magnitudes. This fact emphasizes that laboratory experiments are needed to obtain the most realistic physics that can illustrate flow behavior in fractured porous media and

also to confirm the critical overburden stress beyond which fracture flow would not decrease significantly and can be considered as a threshold for fracture closure.

On the other hand, the matrix flow results change infinitesimally in the coupled approach. Although matrix flow partitioning results from coupled open channel fracture modeling approach seem to be identical to the results from Open channel fracture approach (when comparing Fig. 3-16 with Fig. 3-11), it must be noted that this similarity is only as a result of scale effects on fracture flow plots in Fig. 3-16. To emphasize the change in the matrix flow for the coupled modeling analysis, the resulting flow rates for the extreme cases of overburden stresses are plotted in Fig. 3-17. The change is not so impressive for the current core plug case; never the less, it can be so significant for large blocks of reservoir rock in highly stressed regions.

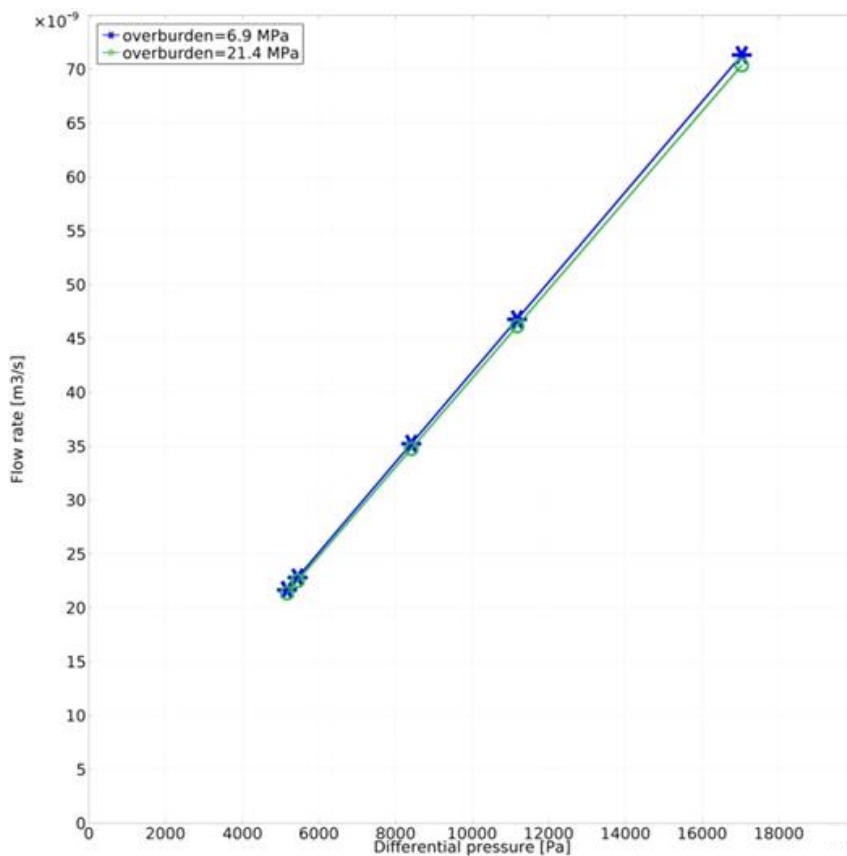


Figure 3-17. Matrix flow variation in the coupled simulation. Matrix flow discrepancy in response to overburden stress when stress dependent permeability is coupled with the porous media flow physics.

Cumulative flow magnitudes comparison against the laboratory measurements confirmed the superior accuracy of the coupled approach in simulation of mechanically coupled porous media flow problems (Table 3-5). The error margin decreased to less than 11 percent from less than 18 percent in the non-coupled simulation approach.

Table 3-5. Flow partitioning results for coupled open channel fracture approach. Comparison of flow partitioning results considering Coupling of poro-elasticity and stress dependent permeability (C. Open Frac) as opposed to the non-coupled open channel fracture (Open Frac) simulation approach under 21.4 MPa confining stress.

Overburden 21.4 Mpa 3100 Psi		Flow rate (m3/s)							
Experimental Data		Fracture		Matrix		Cumulative		% Difference	
flow rate (m3/s)	ΔP (psi)	Open Frac	C. Open Frac	Open Frac	C. Open Frac	Open Frac	C. Open Frac	Open Frac	C. Open Frac
3.3×10^{-8}	0.75	5.32×10^{-9}	8.30×10^{-9}	2.204×10^{-8}	2.14×10^{-8}	2.736×10^{-8}	2.97×10^{-8}	17.1	10.1
3.3×10^{-9}	2.47	1.752×10^{-8}	2.73×10^{-8}	7.24×10^{-8}	7.04×10^{-8}	8.992×10^{-8}	9.77×10^{-8}	10.1	2.3
3.3×10^{-10}	1.62	1.148×10^{-8}	1.79×10^{-8}	4.76×10^{-8}	4.62×10^{-8}	5.908×10^{-8}	6.41×10^{-8}	11.8	4.3
3.3×10^{-11}	1.22	8.64×10^{-9}	1.35×10^{-8}	3.584×10^{-8}	3.48×10^{-8}	4.448×10^{-8}	4.83×10^{-8}	11.0	3.5
3.3×10^{-12}	0.79	5.6×10^{-9}	8.74×10^{-9}	2.32×10^{-8}	2.25×10^{-8}	2.88×10^{-8}	3.13×10^{-8}	12.7	5.3

Table 3-6, provides a comparison of the discussed four various simulation approaches and the average error margin range between the simulation results against the experimental data clearly indicates that the coupled open fracture approach delivers the most precise outcome; in addition the grid resolution for each individual simulation approach illustrates how much the approaches are numerically efficient.

Table 3-6. comparison of the simulation specification for each of the fractured porous medium simulation approaches.

Simulation Approach	Physics		Boundary condition	Approximate Grid resolution	Error margin range
	Matrix	Fracture			
Eq. Porous	Darcy	Darcy	Pressure boundaries	300,000 Hexahedron	92%
Disc. Frac	Darcy	Darcy tangential	Pressure boundaries	18,000 tetrahedral	15%
Open Frac	Darcy	Navier-Stokes	Pressure boundaries	150,000 tetrahedral	11%
C. Open Frac	Coupled Darcy	Coupled Navier-Stokes	Pressure boundaries	150,000 tetrahedral	4%

It is worth mentioning that for all the numerical simulations in every adopted modelling approach, some numerical verification checks were made in order to ensure the authenticity of the results and achieving most efficient modelling approach. The numerical checks included gradual grid refinement until the point that the results were not showing any significant improvement despite the increased simulation runtime. In addition, the numerical results were monitored to be within the expected range that the analytical physics were predicting for a rough calculation over a similar domain.

3.5.3 Cross flow modelling applying coupled open channel fracture approach

As illustrated in section 3.4.4, an important privilege of considering fracture as a flow exchanging domain interacting with rock matrix is indeed its potential application in analyzing the alteration of cross flow between the fracture and the matrix. This capability is especially outstanding when reservoir engineers try to achieve an understanding of the quality of flow charging from large matrix blocks into the existing fracture networks in order to maintain reservoir deliverability. Coupling of Brinkman flow equation to the Darcy's law and Navier-Stokes equation at the interface between the fracture and the matrix augmented with poro-elasticity and stress dependent permeability provides the chance to monitor the cross flow and also follow its variation in a fully geomechanically-coupled simulation. Figure 3-18 presents the cross flow magnitude fluctuation in response to overburden stress for the coupled analysis.

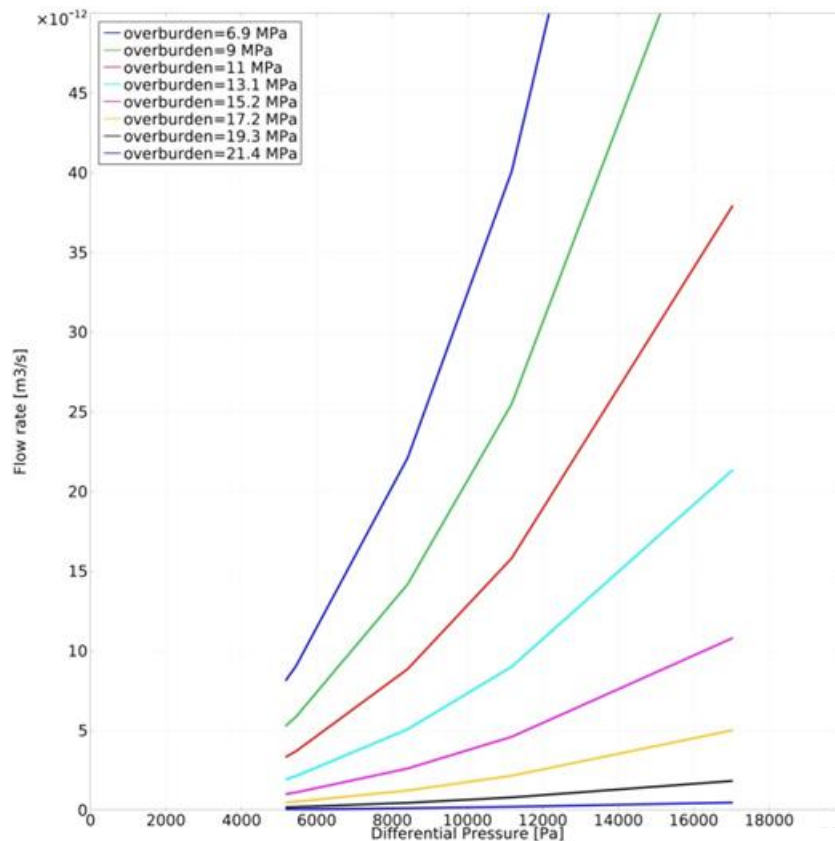


Figure 3-18. Cross flow variation in coupled open channel fracture simulation approach. Cross flow variation versus differential pressures under various overburden stresses.

Cross flow monitoring in both approaches reveals that primarily the flow discharge from matrix to the fracture decreases as the overburden stress increases. In fact at some excessive overburden stress, this flow exchange ceases and both systems flow individually. Being aware of the stress threshold beyond which matrix and fracture behave hydraulically independent will assist the engineers to formulate and implement appropriate stress relief strategy especially in highly-stressed fractured reservoir rocks to facilitate fracture networks hydrocarbon charging. This critical overburden stress beyond which cross flow varies linearly with differential pressures can be distinguished about 13 MPa in open channel fracture approach (Fig. 3-13), whilst it can hardly be determined for the coupled open channel fracture simulations (Fig. 3-18). This difference is an indication of the necessity of flow partitioning experimental data in which separate matrix and fracture flow rates are presented, as a more reliable validation mean.

Comprehensive understanding of cross flow variation due to overburden stress magnitudes is especially of prime importance in dual permeability models where the wellbore is producing from both fracture and matrix systems. However more laboratory validation is required and these simulation results utilized to precisely design for fracture-matrix flow partitioning laboratory investigations as will be discussed in chapter 6.

3.6 Discussion

A comparison of the flow partitioning results achieved through applying the four investigated fracture modelling approaches, approves the coupled open channel fracture strategy as the most accurate one (Fig. 3-19). This approach provides the closest flow rates to the laboratory data by an error margin of less than 11 percent.

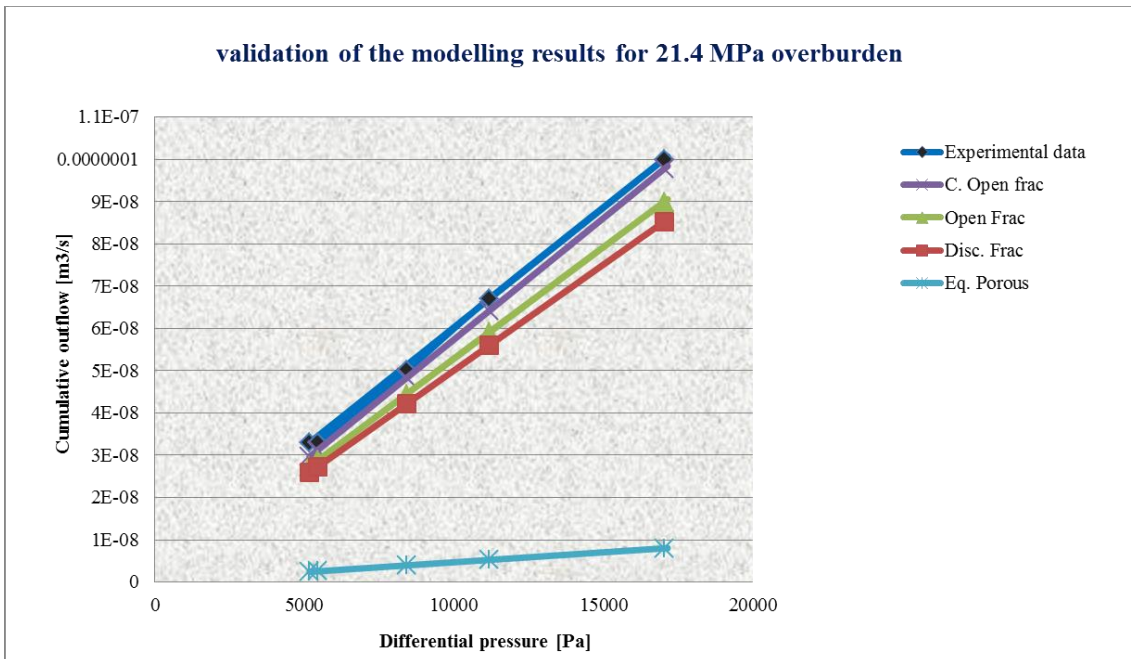


Figure 3-19. Fracture modelling approach validation. Comparison of various fracture modelling simulation strategies with the laboratory data.

The validation of the numerical results could merely be done in terms of cumulative flow. As was discussed previously the analyzed fracture modelling approaches provide different fracture, matrix and cross flow rates. The difference between these flow rates can be misleading in evaluating the behavior of a fractured formation under varying overburden stress. Figure 3-20 exhibits the fracture flow partitioning results derived from the coupled open channel fracture simulation. Comparison of this plot with figure 3-12, illustrates how dominant flow path differs for the overburden stresses when considering distinct fracture modelling approaches. It can be inferred from figure 3-20 that even for overburden stresses up to 18 MPa, fracture remains the dominant flow path while open channel fracture modelling approach indicated for overburden stress levels beyond 10 MPa matrix competes with fracture in terms of flow, accounting for more than 50 percent of the cumulative outflow from the fractured plug.

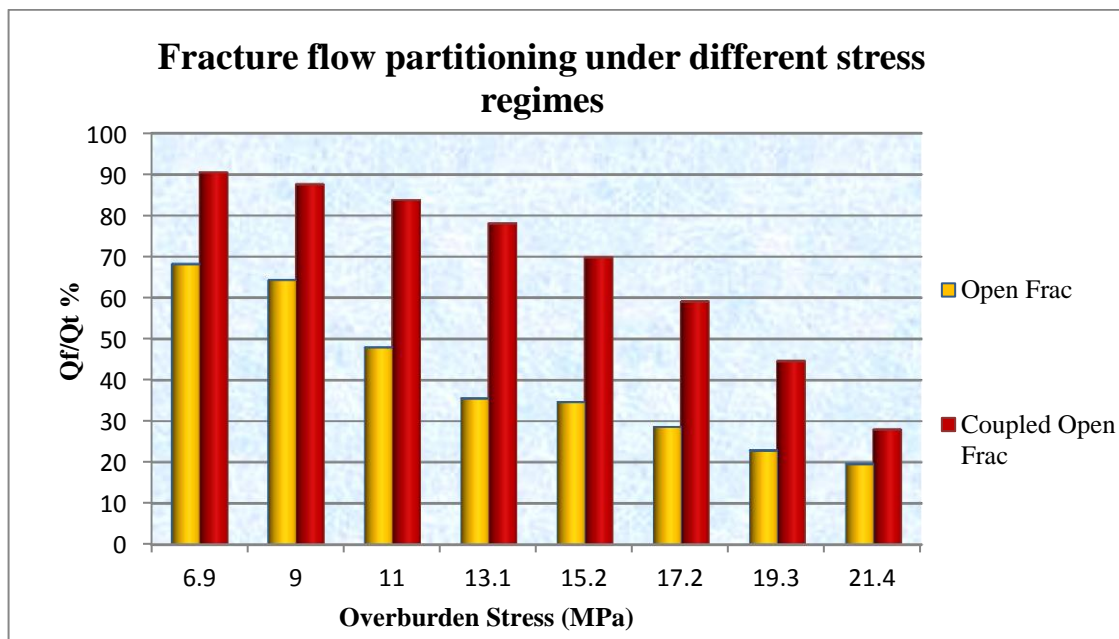


Figure 3-20. Fracture flow partitioning in coupled analysis. Fracture flow partitioning using Coupled and non-coupled open channel fracture approaches.

Therefore there is a requirement for design and execution of laboratory tests which can provide the measurement capability of these flow rates separately. The analyzed outcomes of the coupled fracture modelling approach, as the most precise one, set the basis for design and implementation of a capable laboratory set-up which will be discussed in detail in chapter 6.

Although coupled open channel fracture modelling approach is not as numerically efficient as sub-dimensional fracture implementation, as the purpose of our analyses is to develop empirical mechanically coupled models for fracture and matrix flow, this much more accurate simulation approach has been adopted for our sensitivity analyses in the next chapter.

Chapter 4.0

Mechanistic empirical matrix and fracture flow models

Having evaluated the various fracture implementation techniques in fractured porous media flow analysis in chapter 3, the coupled open channel fracture modelling approach was adopted to investigate effects of all geometric, hydraulic and mechanical parameters involved in matrix-fracture flow partitioning. The sensitivity analysis results were further modelled statistically with regard to the utilized analytical physics to develop mechanistic empirical matrix and fracture flow models.

4.1 Introduction

All the constitutive parameters in the governing equations of the open channel fracture modelling approach discussed in chapter 3 were analysed in a sensitivity analysis in order to be able to define their individual effect on matrix and fracture flow in a comprehensive hydro-mechanical mathematical model that can be descriptive of stressed fractured porous media flow.

In this chapter sensitivity analysis of all the relevant parameters are presented on fracture and matrix flow. Consequently the parameters effects were categorized with regard to their mathematical regression and the governing analytical formulations into physical constitutive expressions of the developed empirical models.

The sensitivity analysis and the developed models assume laminar flow within the fracture in accordance with the open channel fracture implementation approach and analysed for single phase flow through porous media. Geometric parameters like core plug length, cross section area and initial aperture were investigated in order to facilitate up scaling of the developed empirical models for fracture and matrix flow. On the other hand, in addition to the considered hydraulic parameters such as fluid dynamic viscosity, density and pressure drop appearing in porous media flow physics, developed

models account for mechanical parameters such as Young’s modulus, Poisson’s ratio and Biot-Willis coefficient that incorporate poro-elasticity and stress-dependent permeability into flow partitioning phenomenon.

Table 4-1 provides the base investigation case parameters along with the individual parameters’ range of variation for all the sensitivity analyses performed in this chapter; the applied data are whether the published values for Clashach sandstone or sandstones in general where specific Clashach data was not available in the literature (Jones and Somerville, 2001; Ojala, 2003; Crawford et al., 1995; Palciauskas and Domenico, 1989; Shafer et al., 2008; Malik et al., 1998; Berryman, 2004; Laurent et al., 1993; Franquet and Abass, 1999; Vasquez et al., 2009). In order to evaluate the individual effects of the constitutive parameters, a parametric study was investigated for the desired parameter.

Table 4-1. Modelling data for the sensitivity analysis.

<i>Sensitivity Parameters</i>	<i>Base case</i>	<i>Range</i>
Plug diameter Plug length	3.79×10^{-2} m	3×10^{-2} m - 4.4×10^{-2} m
Initial Matrix permeability	7.54×10^{-2} m	7.54×10^{-2} m - 1.4×10^{-1} m
	3.10874×10^{-13} m ²	2.5×10^{-13} m ² - 3.9×10^{-13} m ²
Matrix Porosity	0.154	0.05 - 0.47
Biot-Willis Coefficient	0.8	0.15 - 0.9
Fluid Viscosity	0.001 Pas	8×10^{-4} Pas - 3×10^{-3} Pas
Fluid Density	850 kgm^{-3}	$650 \text{ Kg} \text{m}^{-3}$ - 1050 kgm^{-3}
Young’s Modulus	4.0×10^{10} Pa	3.5×10^{10} Pa - 6.0×10^{10} Pa
Poisson's Ratio	0.14	0.1 - 0.35
Overburden	21.4×10^6 Pa	6.9×10^6 Pa - 21.4×10^6 Pa
Differential pressure	17030 Pa	5171 Pa - 17030 Pa
Pore Pressure	1×10^6 Pa	1×10^5 Pa - 2.0×10^7 Pa

4.2 Sensitivity analysis of hydro-mechanical parameters

4.2.1 Porous matrix cross section area open to flow

Since Darcy law accounts for flow within the rock matrix as discussed before in chapter 3, the constitutive parameters of Darcy equation were sanctioned for sensitivity analysis for their effects to be examined in the mechanically-coupled numerical simulations.

The porous surface area open to flow is one of the major parameters affecting the flow in porous media. On the other hand, modelling the effect of surface area open to flow variation, would enable up scaling the finally-derived flow models to field scale investigations.

The same described coupled-physics numerical model was adopted in this section to evaluate the effects of varying cross section area open to flow in the simulated core plug matrix. Initially the displacement of fracture walls, the fracture aperture, due to the exerted overburden stress is being affected by altering the cross section area of the flooded plug (Fig. 4-1). Consequently the updated interface surface averaged geometry and mesh was applied in the coupled physics to provide the fracture and matrix fluxes.

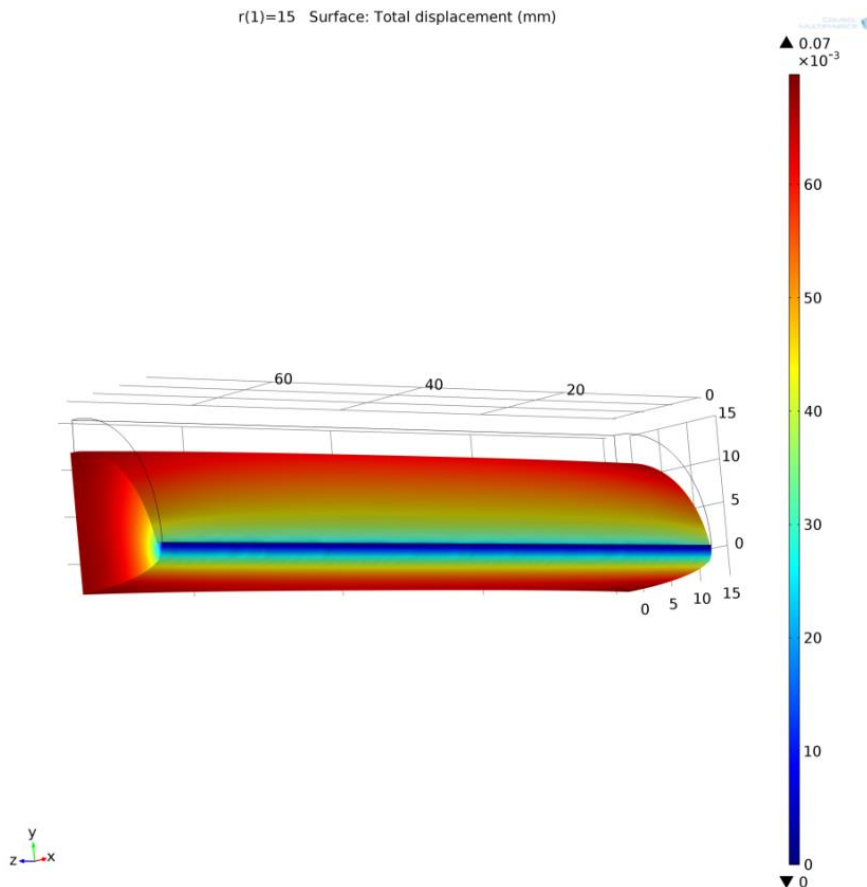


Figure. 4-1: Matrix displacement in response to overburden stress.

As figure 4-2 demonstrates, the displacements increase as the larger core plugs were flooded. It is worth mentioning that for the larger plugs the distance between the fixed boundary and the plug centre is increased and the stress concentration driven movement of matrix domain would be more pronounced. This conclusion remains valid with the assumption that fixed boundary remains at the outer plug boundary. Special attention should be drawn to the fact that for larger matrix blocks in a field scale investigation, more sparse fracture filling material can jeopardize the assumption of fixed boundary at the block edge only while up scaling the models.

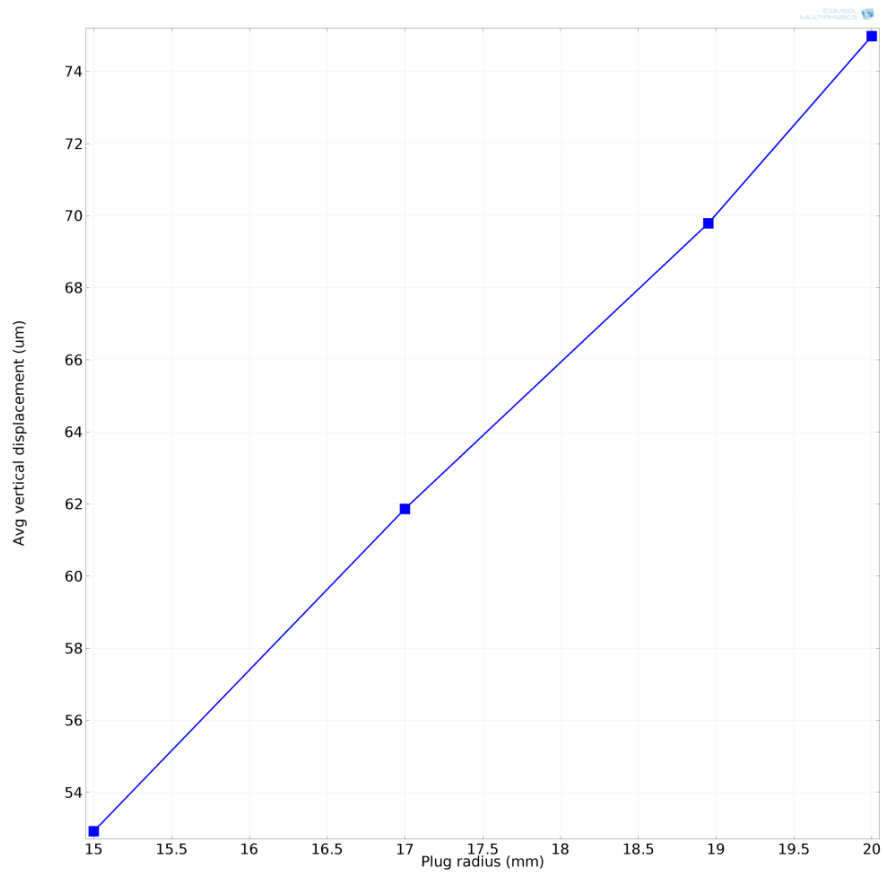


Figure 4-2: Stress affected fracture closure for various matrix plug sizes. Larger plugs undergo more severe strain.

Coupled sensitivity analysis results (Fig. 4-3) indicated that as the open-to-flow cross section area of the flooded sand stone plug increases the fracture flow decreases dominantly due to the reduced fracture aperture. The fracture flow decrease rate is reducing as the surface area increases. On the other hand matrix flow increases linearly for the larger porous media in accordance with Darcy law formulation.

Figure 4-3 reveals that for the flooded sandstone plug radius more than 1.8×10^{-2} (m) matrix flow exceeds fracture flow and becomes the dominant flow path provided all the remaining parameters are kept constant. This phenomenon can be of much interest when considering production strategies that can maximise large matrix blocks recovery factor in mature fractured hydrocarbon fields.

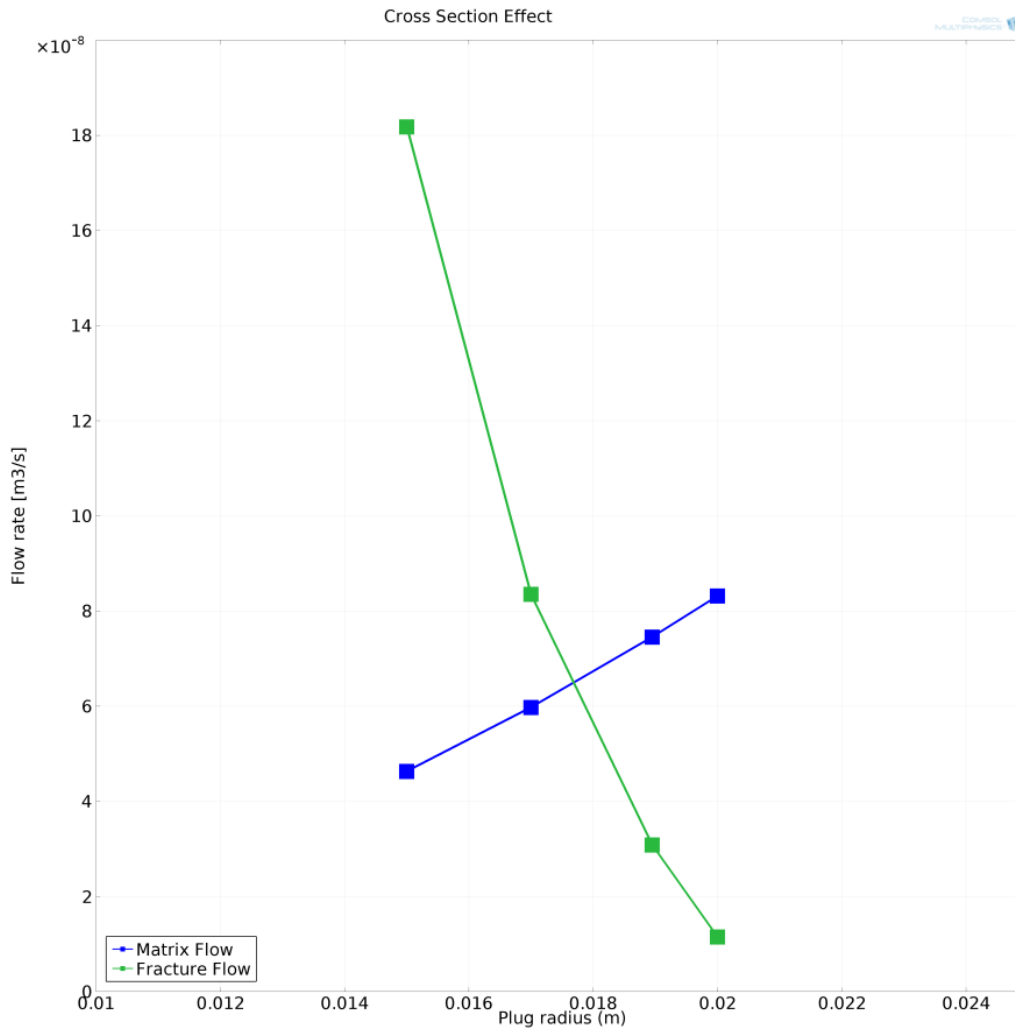


Figure 4-3: Fracture and Matrix flow versus plug radius. Enhanced matrix flow and reduced fracture flow resulted for larger plugs.

The other phenomenon responsible for the fracture flow decrease is the amount of cross flow discharged to the fracture through the fracture-matrix interface. Figure 4-4 reveals that the cross flow rate significantly decreases for the larger core plugs; indeed the larger matrix blocks tend to flow independently with minimum flow exchange with the fracture.

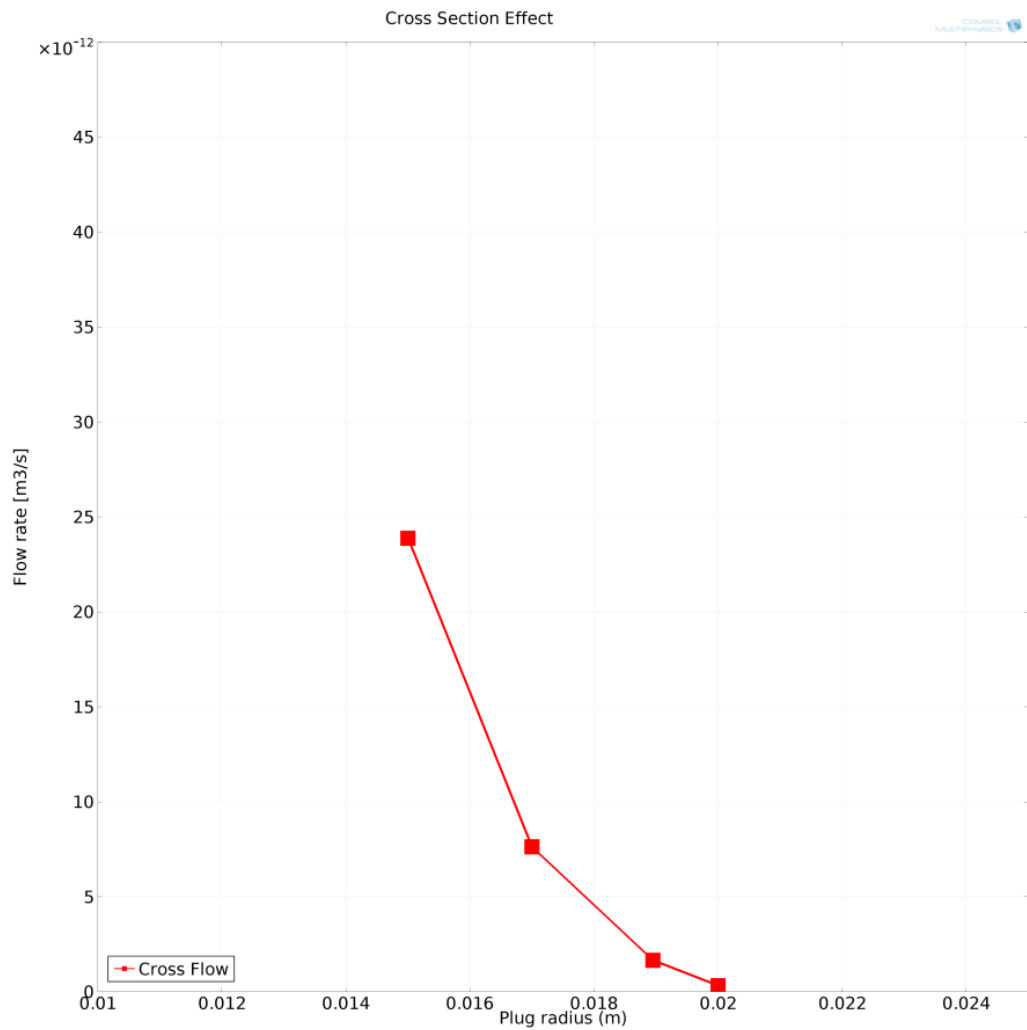


Figure 4-4: Fracture-matrix cross flow variation due to cross section area alteration. Note the significant decrease of the decline dip of the curve for extreme large plugs.

4.2.2 Initial rock matrix permeability

Initial permeability variation effect was taken into consideration as the other important component of Darcy law. Having applied the same numerical model, alternating initial permeability magnitudes were implemented and displacement and flow results were monitored.

As expected with regard to the stress-strain solid mechanics governing equations, permeability of the porous material would not affect the strain of the porous medium, hence the stability of the resulting fracture aperture while varying the permeability.

Despite the fact that the aperture size was not influenced by the matrix permeability, the fracture flow was changing. Enhanced initial permeability values resulted in incrementally increased fracture flow partitioning as can be seen in Fig. 4-5. The observed behaviour can be interpreted according to the infinitesimally intensified flow exchange between the fracture and matrix in more permeable porous media (Fig. 4-6) which enhances fracture flow intake from matrix at the interface.

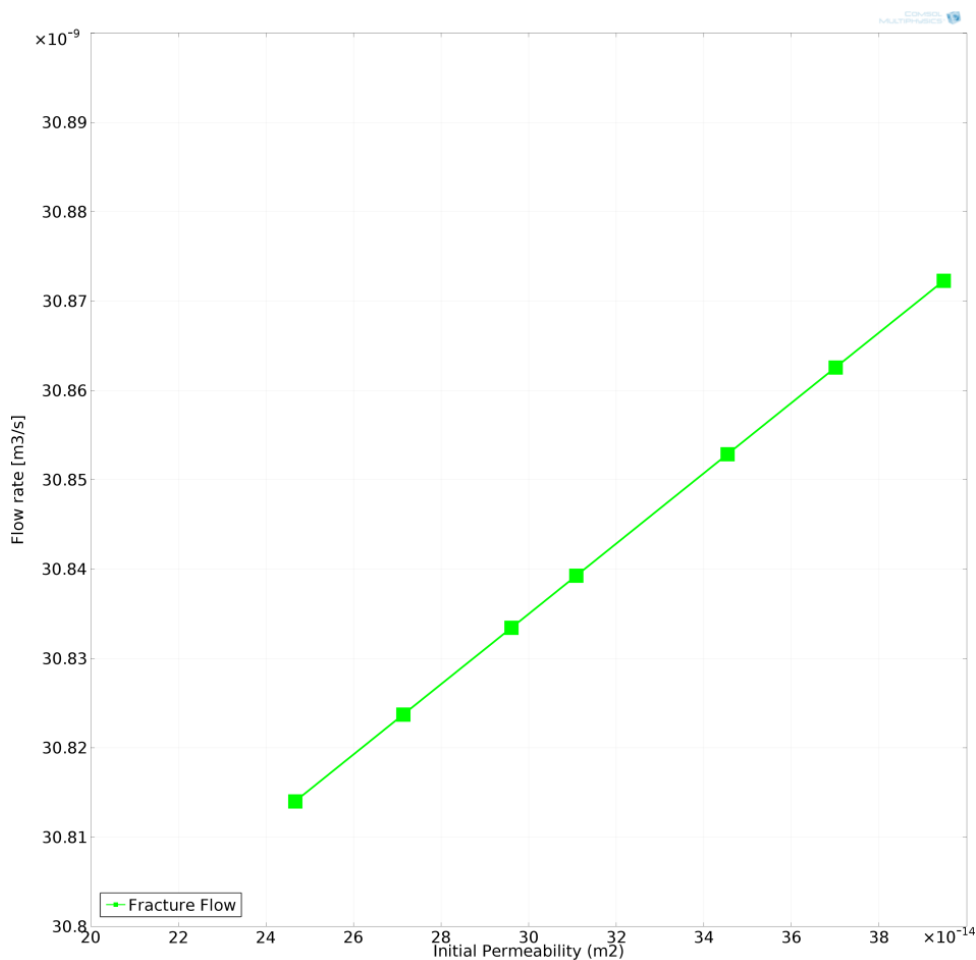


Figure 4-5. Incremental fracture flow response to various matrix permeabilities. Note the smaller graph scale which exaggerates the fracture flow fluctuation for better visibility.

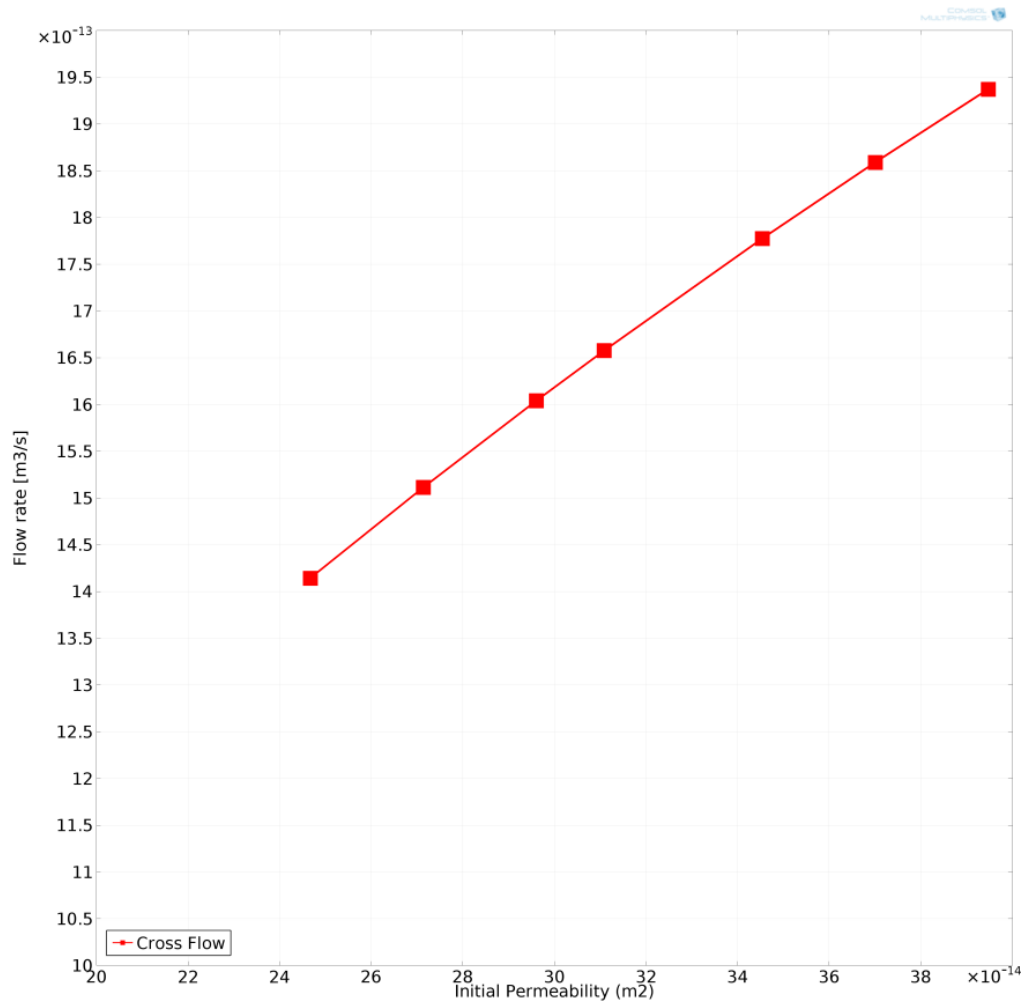


Figure 4-6. Cross flow infinitesimal change versus matrix permeability. Similar to the fracture flow graph the scale for cross flow also minimised for better variation resolution.

Matrix flow on the other hand, increases linearly in response to initial permeability magnitudes in accordance with Darcy law as figure 4-7 reveals.

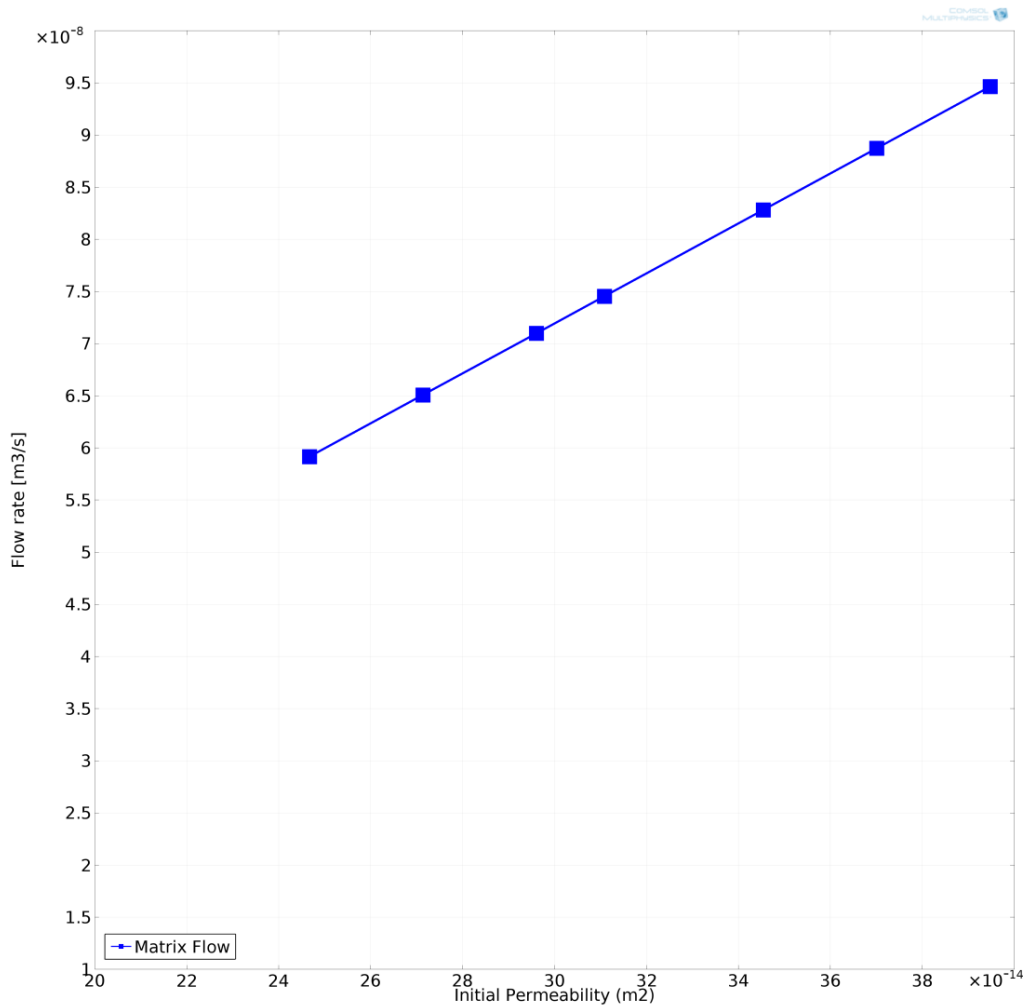


Figure 4-7. Matrix flow for various matrix permeabilities. Matrix flow increases linearly with the matrix permeability.

4.2.3 Core plug length

Core plug length is the other geometric parameter which is of prime importance in up scaling any coupled flow model to large field scale matrix blocks in addition to the open-to-flow cross section area of the matrix blocks. The parametric study for various core plug lengths indicates that for the more elongated plugs the fracture aperture size undergoes more reduction. This is more illustrated in Figure 4-8.

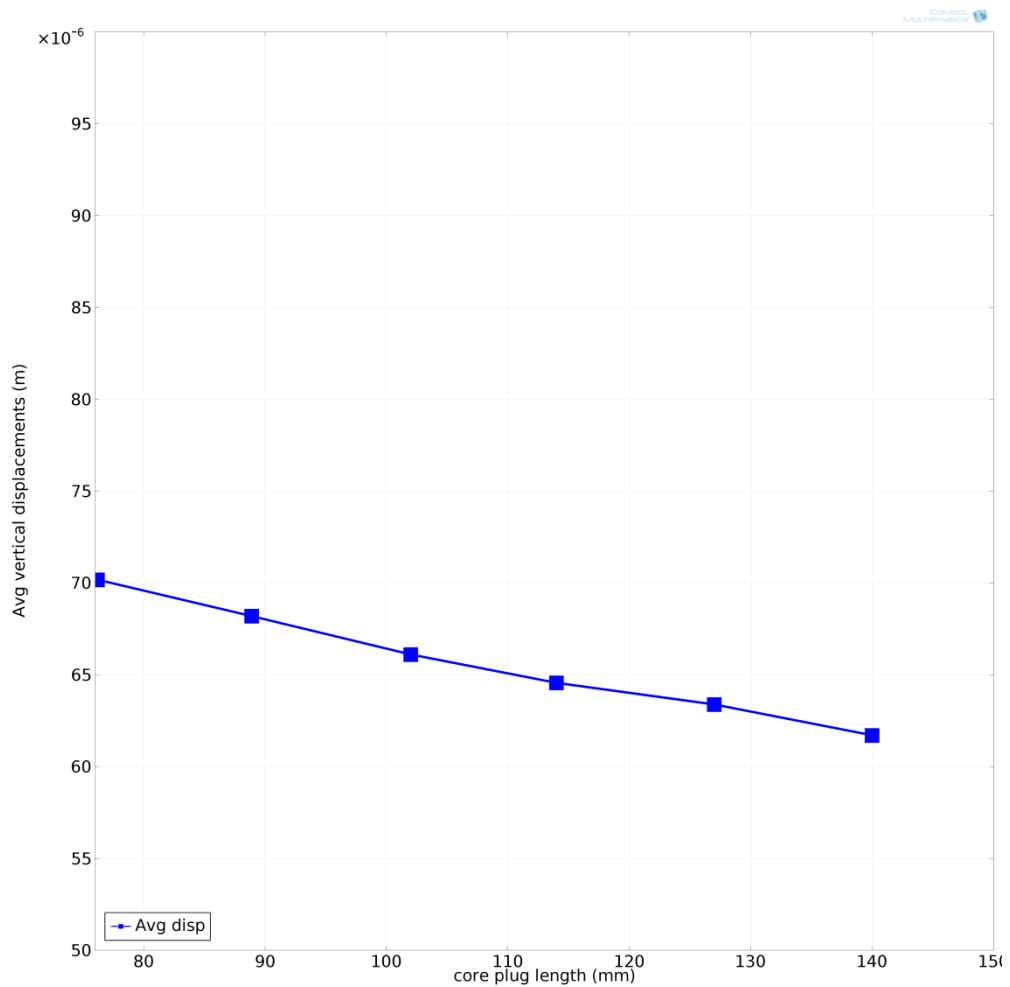


Figure 4-8. Core plug length effect on the mechanical displacements. Elongated core plug undergo less mechanical displacements.

Core plug length has an equally significant effect as the cross section area on the fracture-matrix flow partitioning in accordance with Darcy governing equations implemented. As the core plug length increases, at a particular plug length fracture and matrix compete equally for flow and fracture hydraulic conductivity overcomes matrix deliverability. As shown in Figure 4-9, this length threshold is around 1.2×10^{-1} m for currently investigated base case flooding. Such behaviour can explain how a single fracture can restrict matrix productivity if it can propagate extensively or intersect other fractures to form a fracture network.

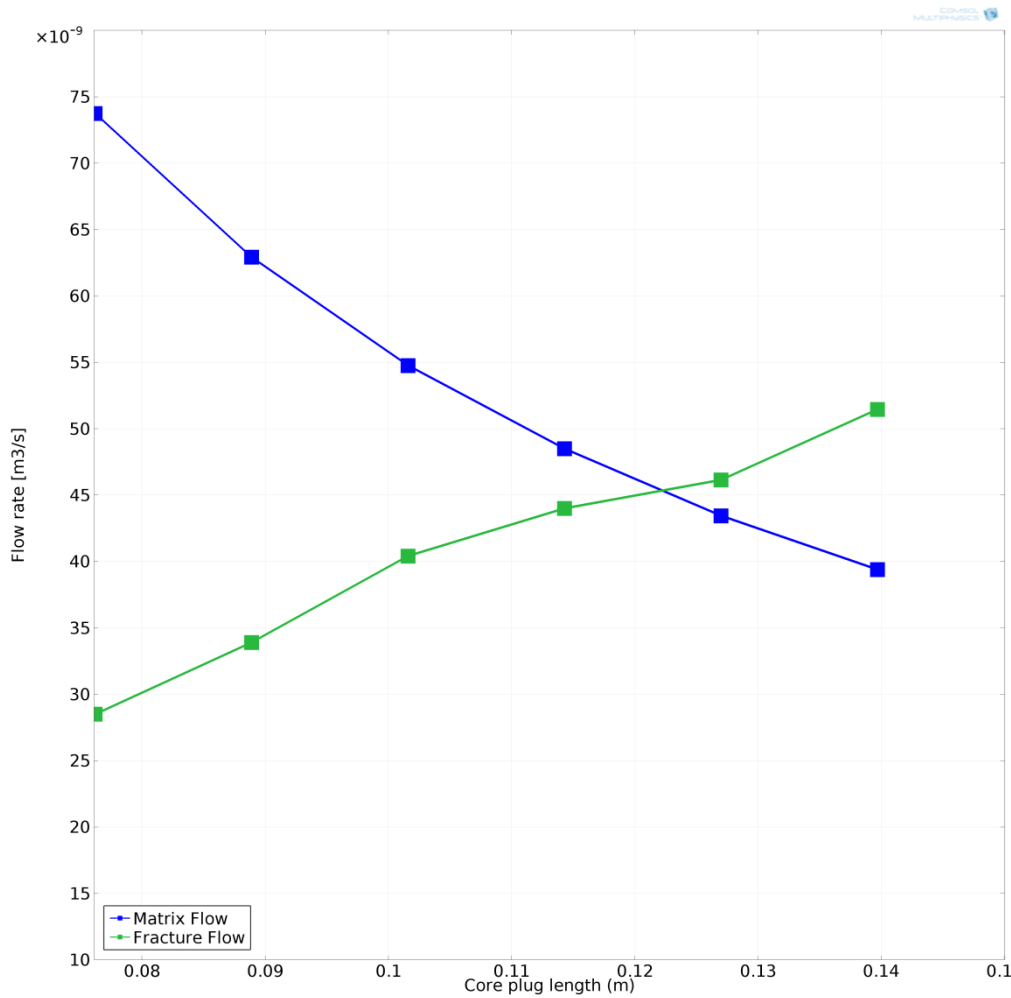


Figure 4-9. Fracture and matrix flow evolution versus core plug length. Note the switch of the dominant productive system at 1.2×10^{-1} m.

Careful review of the cross flow variation trend (Fig. 4-10), indicates a rather steady increase of the matrix-fracture flow exchange as the core plug length grows. This is initially related to the increase of the matrix-fracture interface due to the enlargement of the total fractured porous medium. A decrease in the cross flow right after the domination of fracture flow at 1.2×10^{-1} m, indicates how a hydrocarbon bearing block ceases feeding an adjacent conductive fracture. This is an immediate effect of the fracture flow dominance and a sudden increase in the fracture flow and consequently a back flow to the matrix block before reaching the flow stabilization bearing in mind that cross flow was defined as the summation of the vertical flow between fracture and matrix in either directions. The general cross flow variation trend is ascending

over the investigated range of core plug length; however generalization of the effect demands consideration over a wider range. Coupling several physics and extensive discretisation of the problem requires huge amount of numerical efforts that limited the extension of the analysis over a wider plug length range. This constraint should undergo a comprehensive investigation before up scaling the developed empirical models to larger scale scenarios.

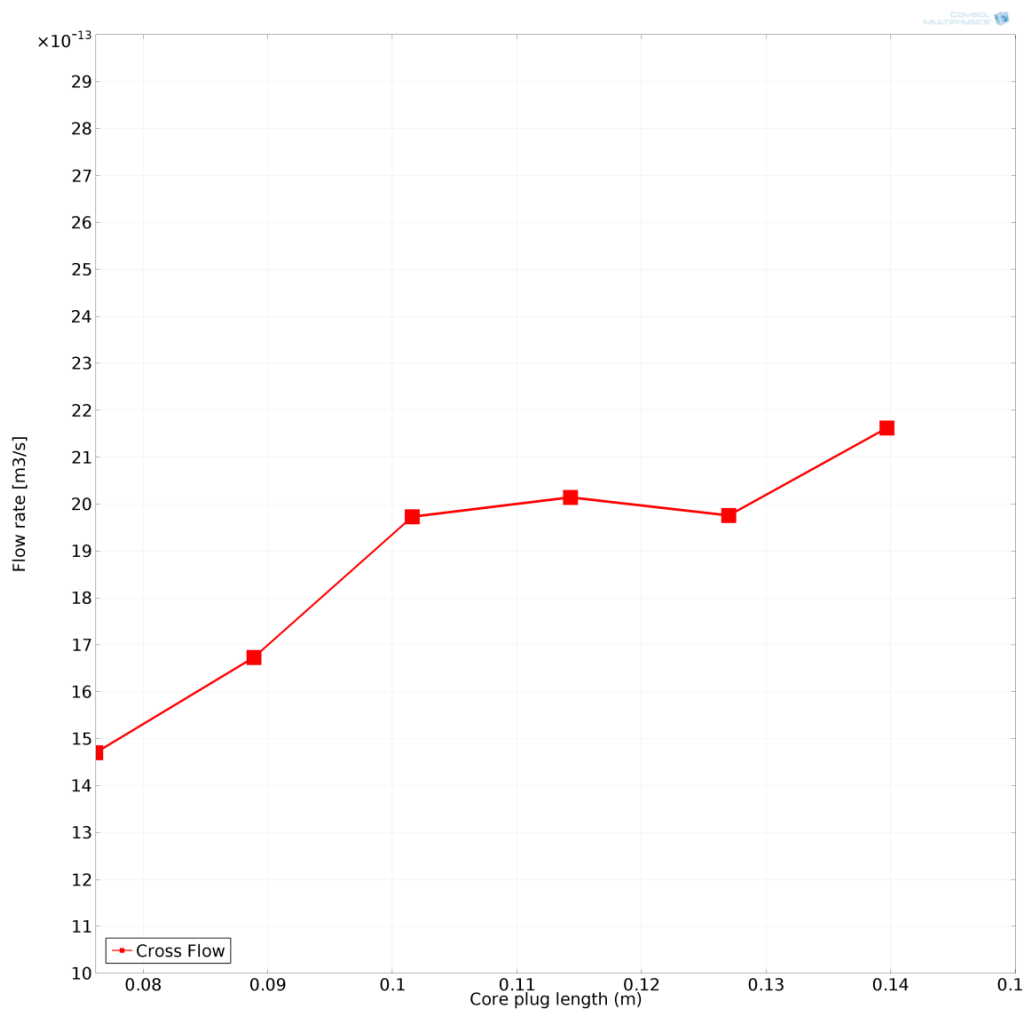


Figure 4-10. Cross flow variation as the plug length increases. General variation trend is ascending while a cross flow reduction after fracture flow domination is evident.

4.2.4 Fluid dynamic viscosity

Dynamic viscosity is the important parameter of all fluid flow formulations; nevertheless, it does not appear in the mechanical formulations for the rock mass deformation under overburden stress. Fracture aperture is not affected by fluid viscosity variation however, both Darcy law governing the matrix flow and Navier Stokes equation controlling flow within the fracture, deliver reduced amount of outflow for more viscous fluids. Figure 4-11 confirms that matrix and fracture flow magnitudes follow similar decreasing trend in response to enhanced fluid dynamic viscosity. Such a decreasing trend was anticipated due to the applied flow equations in Matrix and fracture; investigation of the dynamic viscosity effect was necessary for the desired sensitivity analysis though.

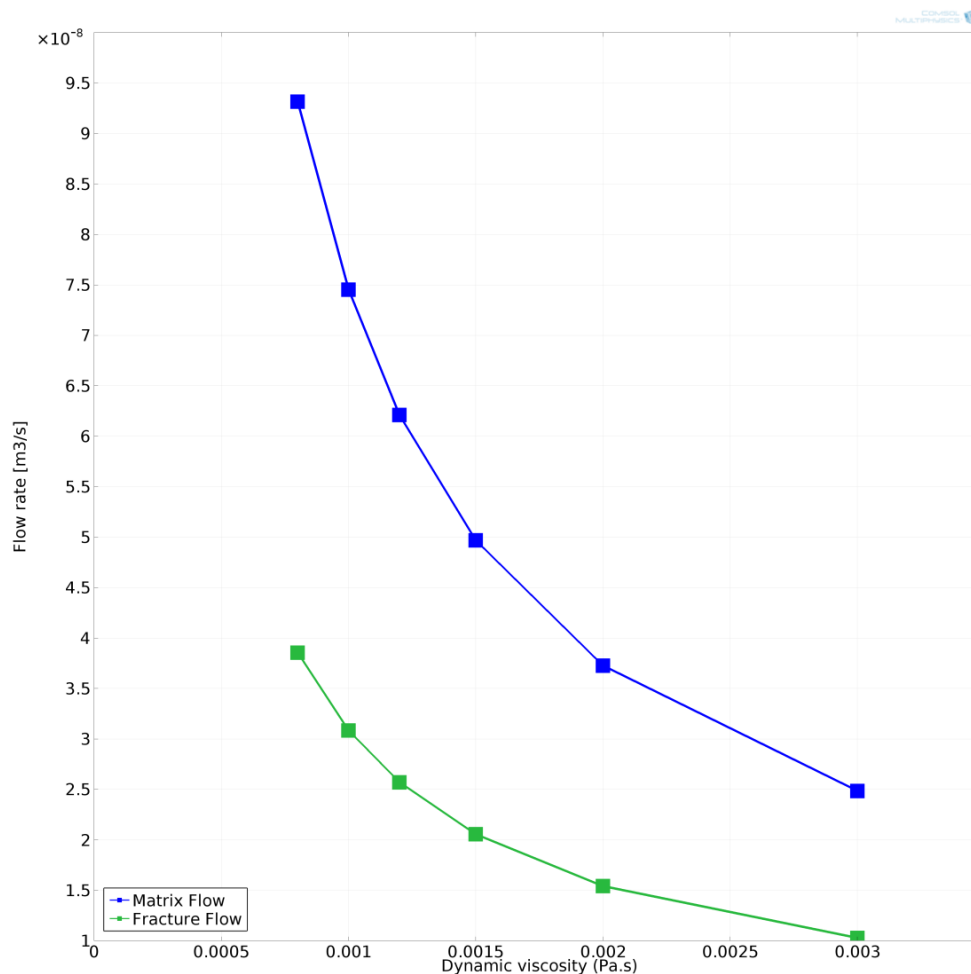


Figure 4-11. Effect of dynamic viscosity on fracture and matrix flow. Dynamic viscosity increase affects both matrix and fracture flow with an identical trend.

On the other hand, fluid dynamic viscosity effect on matrix-fracture cross flow requires more investigation. Although Brinkman equation which governs the flow at the fracture-matrix interface is derived from Darcy equation, the equivalent viscosity calculation utilized for the sake of flow consistency at the interface results in a suspicious concept of the viscosity effect. It can be inferred from figure 4-12 that matrix-fracture flow exchange also decreases as the dynamic viscosity of the flooding fluid increases following an identical trend as the variation of the flow within rock matrix and the fracture.

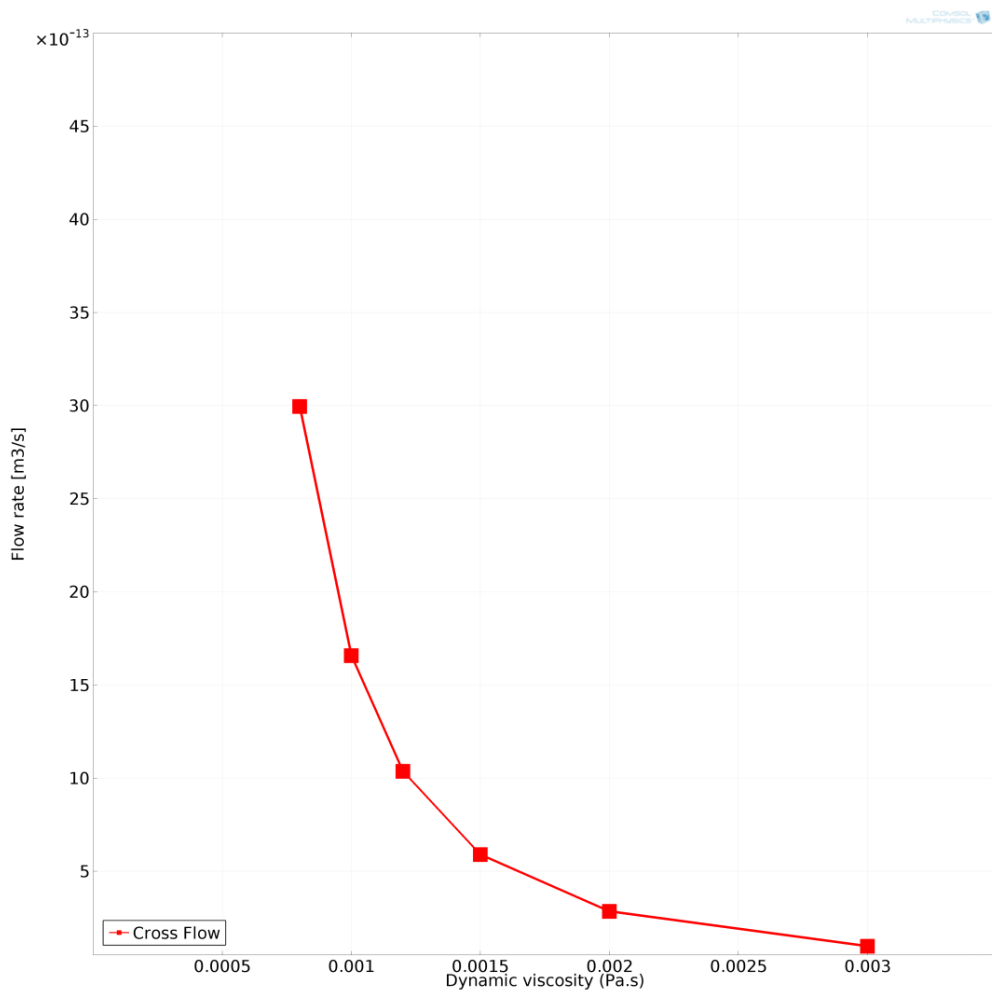


Figure 4-12. Effect of dynamic viscosity on fracture-matrix cross flow. Cross flow follows the same variation trend as matrix and fracture flow.

4.2.5 Differential pressure

Differential pressure across the formation is the main drive of viscous flow through the porous media. Porous media flow is a linear function of differential pressure. Structural mechanics formulation does not contain differential pressure term however in three dimensional analyses the differential pressure will be accounted for as a stress regime component. Therefore effect of differential pressure was evaluated in order to investigate its function in a coupled hydro-mechanical scenario. As shown in figure 4-13, the average fracture walls displacement is affected infinitesimally (Note the scale of Fig. 4-13) by differential pressure fluctuation. Enhanced differential pressure across the flooded core plug resulted in less severe strain although the overall effect is negligible. This is due to the fact that this differential pressure acts as a confining pressure that has stress elements normal to overburden.

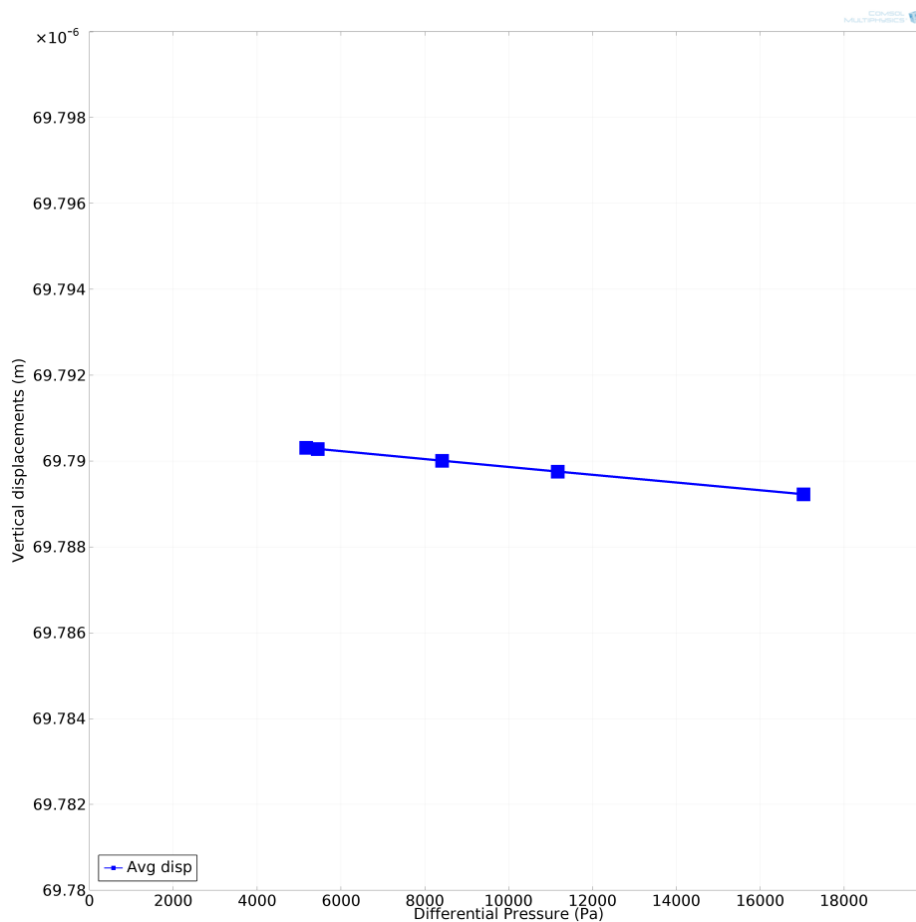


Figure 4-13. Matrix displacement versus differential pressure. Differential pressure affects matrix displacement infinitesimally.

Regarding the fracture and matrix flow investigation, in accordance with figure 4-14 and flow governing equations, increased differential pressure across the flooded core plug leads to increased fracture and matrix flow as expected from Darcy governing equations.

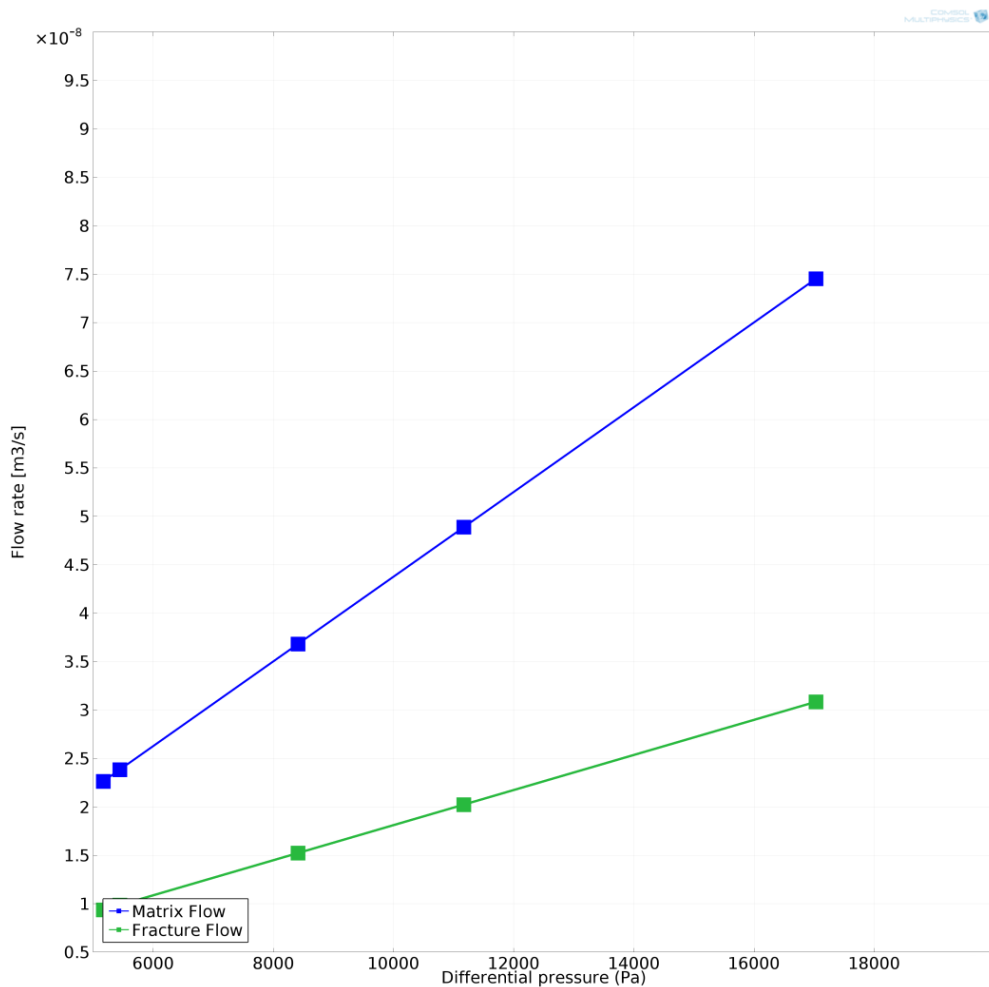


Figure 4-14. Fracture and matrix flow versus differential pressure. Matrix and fracture flows increase linearly with differential pressure.

Cross flow between matrix and fracture is also affected by the differential pressure magnitude. Logically as the amount of flow through fracture and matrix increases by differential pressure rise, the flow exchange between matrix and fracture also increases. This is demonstrated in figure 4-15.

However as the cross flow is derived from several interacting flow formulations at the interface, the trend is no longer.

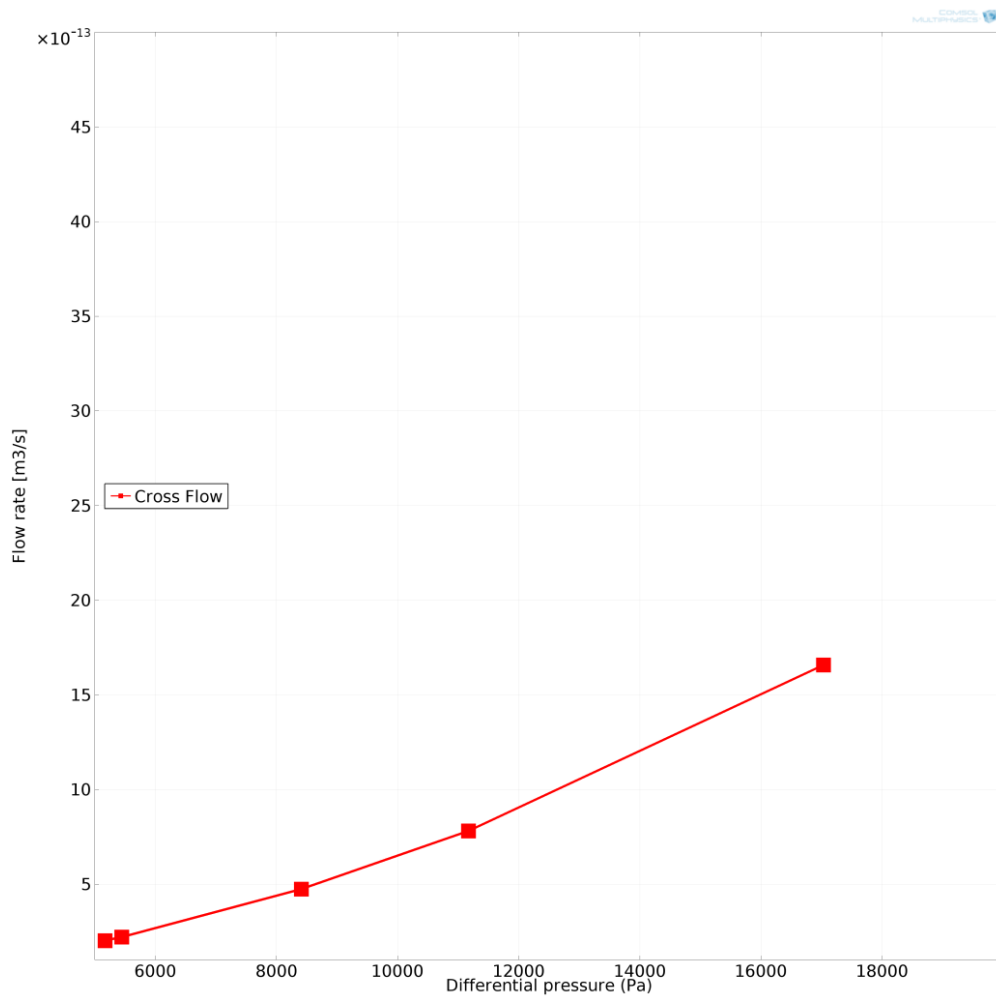


Figure 4-15. Cross flow as a function of differential pressure. More differential pressure causes more cross flow in an exponential form.

4.2.6 Overburden stress

Having investigated the hydraulic parameters, mechanical parameters were also considered in the sensitivity analysis to facilitate the ultimate goal of developing mechanistic flow models for fractured porous media. The most important mechanical parameter is the overburden stress which directly controls fracture aperture variation through stress-strain governing equations. As figure 4-16 confirms more intense overburden stresses results in more significant matrix displacement and leads to smaller fracture apertures.

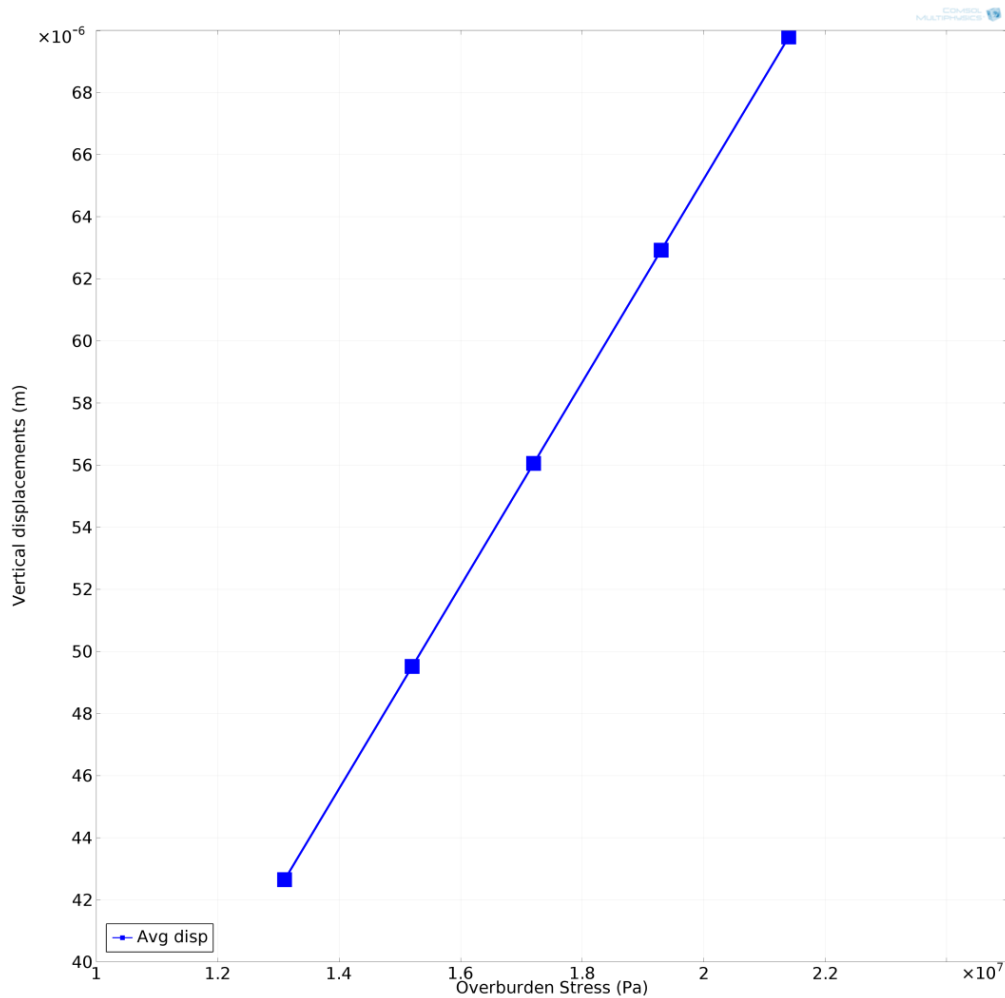


Figure 4-16. Matrix displacement in response to overburden stress. Matrix displacement increases linearly with the exerted overburden stress magnitude.

For lower overburden stresses fracture aperture is significant; as a result, fracture flow is responsible for the dominant fraction of production through the fractured core plug. As the overburden stress increases fracture flow decreases and at a an overburden stress threshold fracture aperture reaches a size beyond which rock matrix conducts flow stream more conveniently and matrix flow exceeds fracture flow. This overburden threshold for current analysis is about 2×10^7 Pa as can be inferred from figure 4-17. This threshold is so important in characterising stressed flow behaviour of a fractured rock mass and can influence the design of completion and production strategies.

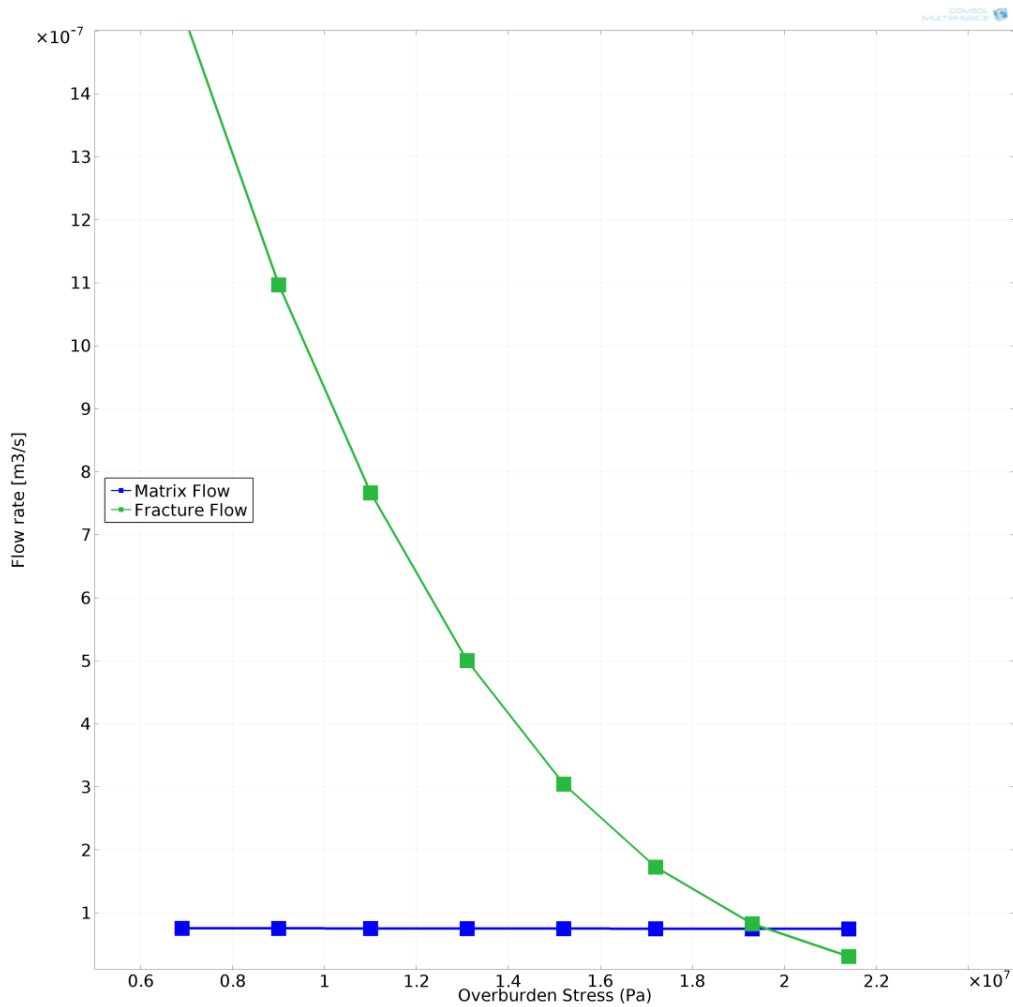


Figure 4-17. Fracture and matrix flow variation under different overburden stresses. Note the dominant flow path switches just below 2x10⁷ Pa overburden stress.

Although matrix flow seems to remain stable in figure 4-17, it is also decreasing in response to enhanced overburden stress in accordance with the stress dependent permeability formulation applied in the coupled simulation (Fig. 4-18). It is worth noting that fracture flow decreases in an exponential form as overburden stress increases while matrix flow follows a linear reduction.

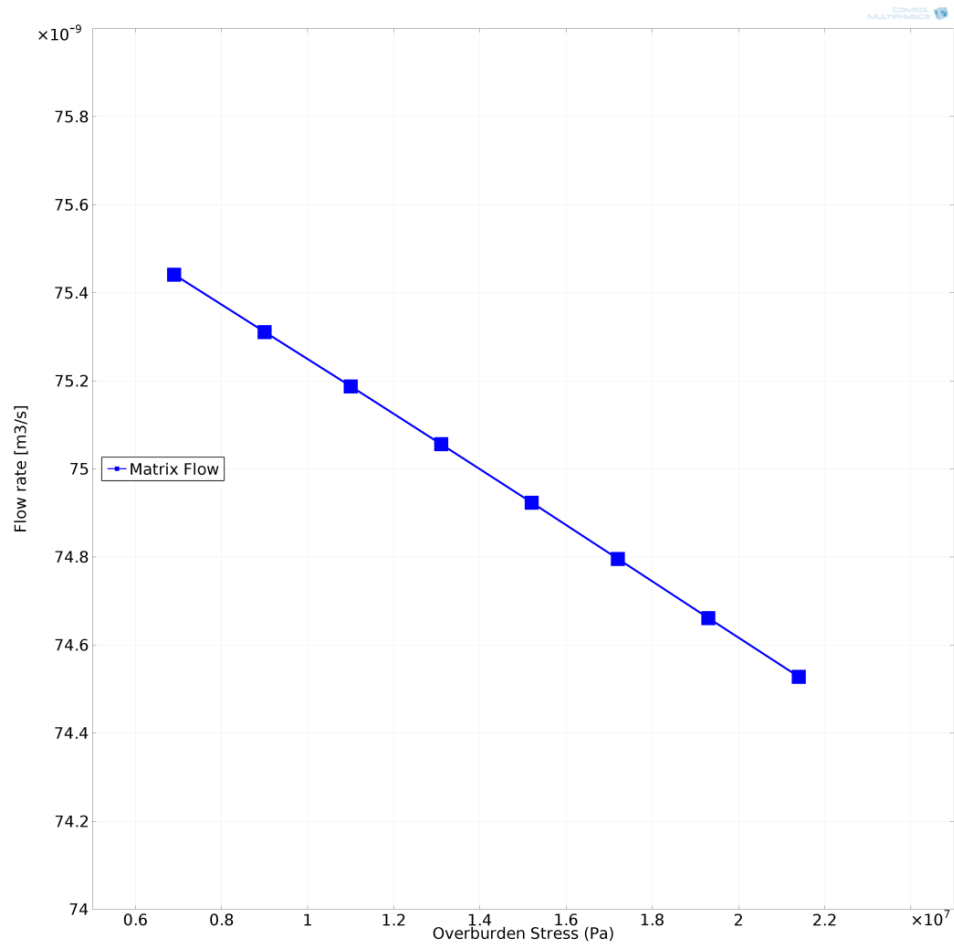


Figure 4-18. Matrix flow as a function of overburden stress. Matrix flow decreases linearly as the overburden stress increases.

Investigation of cross flow evolution during overburden stress increase revealed that matrix flow discharge into fracture decreases significantly as the overburden stress increases (Fig. 4-19). The exponential cross flow decrease trend is coincident with the fracture flow decrease trend. The previously mentioned fracture healing threshold is also evident from the cross flow change trend. Beyond the threshold matrix-fracture cross flow would reach a minimum confirming that the matrix rather flows as an isolated medium and fracture does not receive any influx from matrix anymore.

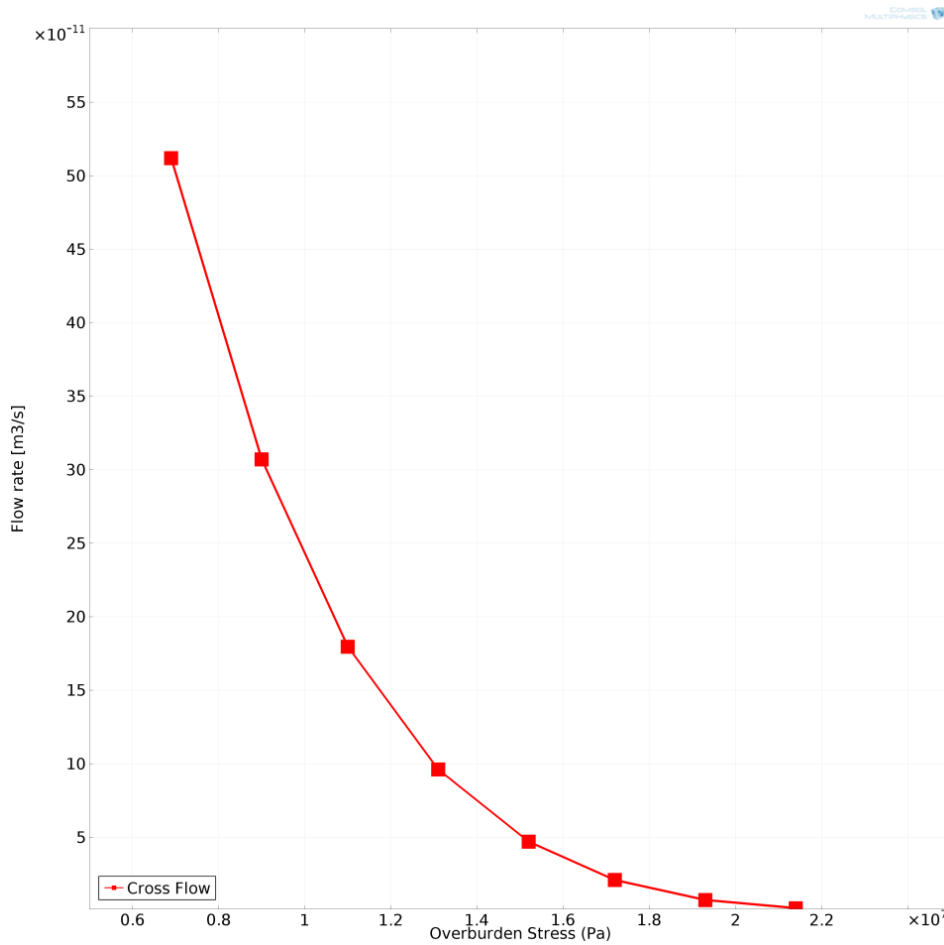


Figure 4-19. Cross flow change due to overburden stress variation. Note how the matrix-fracture cross flow reaches a minimum at fracture healing overburden stress.

4.2.7 Biot-Willis coefficient

Effective stress is the total body force responsible for the mechanical deformation of core plug under overburden stress in the modelling scenarios. Therefore Biot-Willis coefficient affects fracture geometry, and consequently fracture flow, as well as matrix flow infinitesimally through its controlling influence on pore pressure in effective stress calculations (Eq. 3-14). Matrix mechanical displacement is affected by change in Biot-Willis coefficient, over its total possible range of values from 0.1 to 0.9, only by maximum two tenth of a micron (Fig. 4-20) and this slight fracture aperture variation leads to a minor fracture flow fluctuation as can be inferred from figure 4-21. As the matrix displacement is slightly less for larger Biot-Willis coefficients, larger size fracture apertures deliver slightly increased fracture flow.

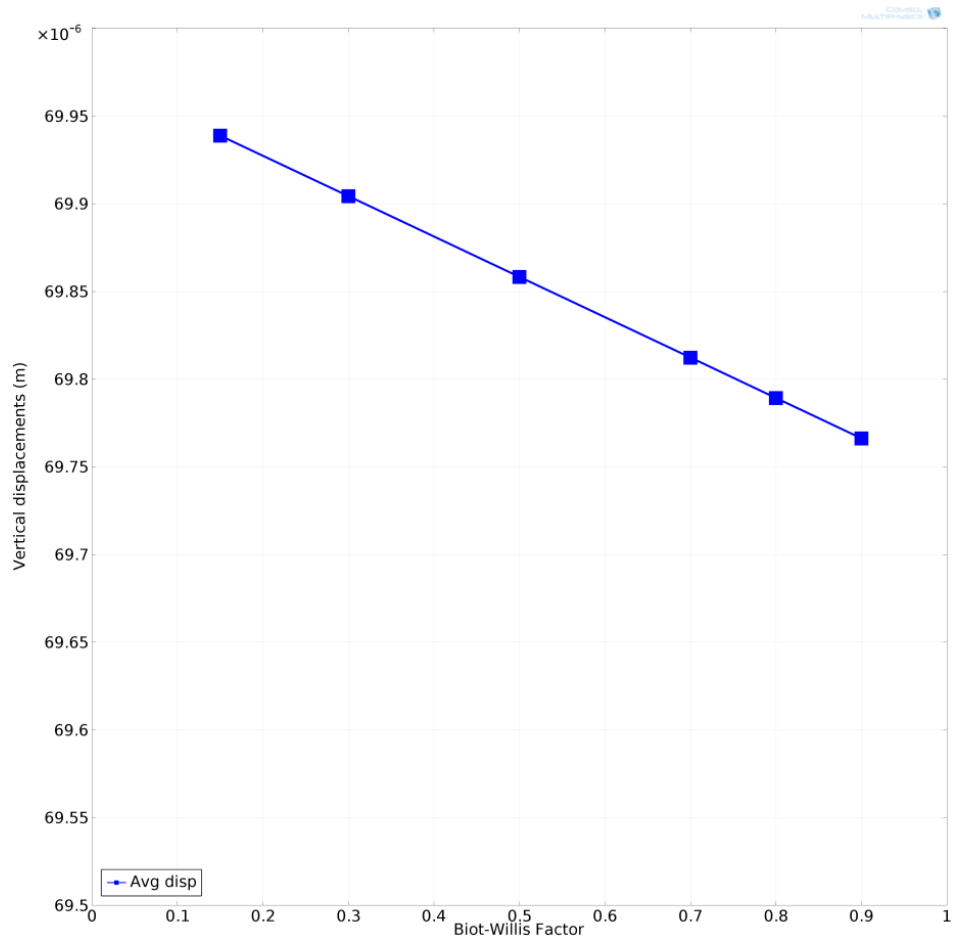


Figure 4-20. Biot-Willis coefficient driven matrix displacement. Larger Biot-Willis coefficient causes infinitesimally smaller displacements.

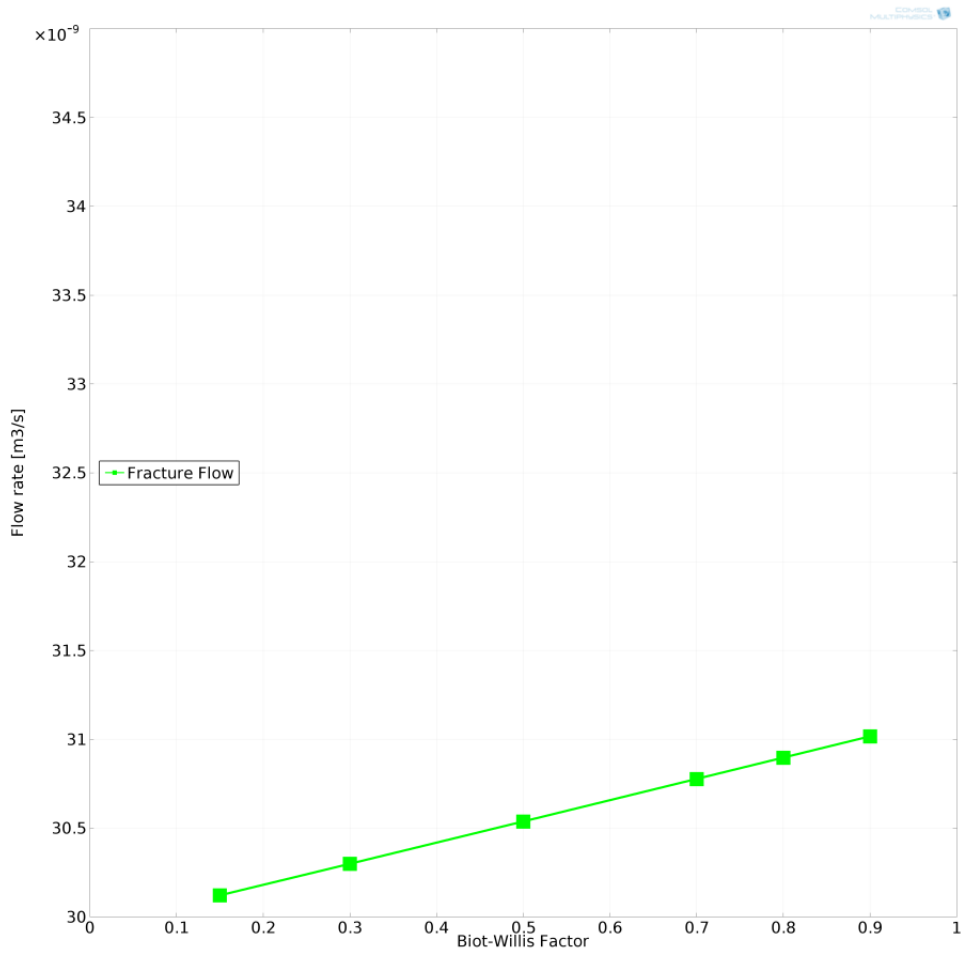


Figure 4-21. Fracture flow response to Biot-Willis coefficient. Larger fracture apertures result in slightly increased fracture flow.

On the other hand, increase in Biot-Willis coefficient causes matrix flow to increase incrementally due to reduction in effective stress and consequent increase in stress-dependent matrix permeability. This is illustrated in figure 4-22.

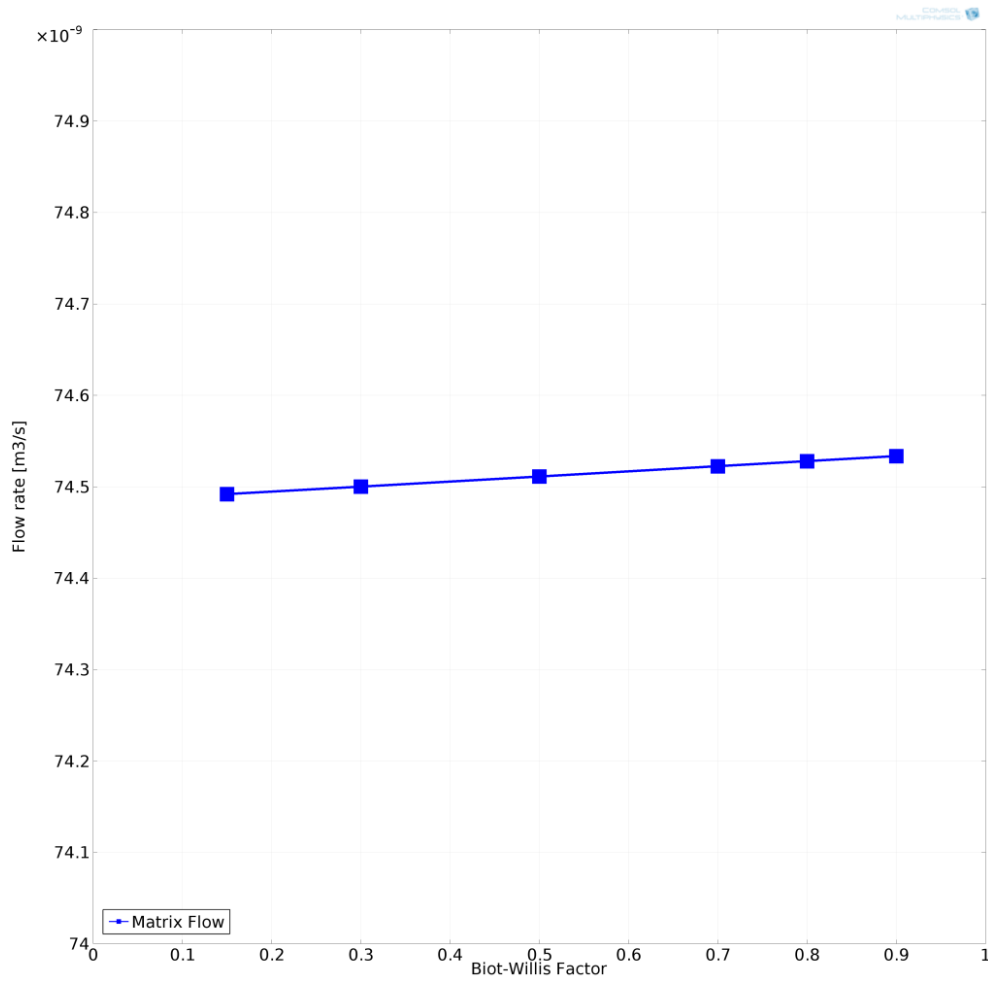


Figure 4-22. Effect of Biot-Willis coefficient variation on matrix flow. Larger Biot-Willis coefficients lead into infinitesimal increase in matrix flow.

This mechanical characteristic of core plug affects the matrix-fracture cross flow insignificantly similarly to the fracture and matrix flow (Fig. 4-23). It may seem that this parameter effect can be considered negligible however as it is desired to provide a mechanistic model that can be up scaled for field scale applications it is intended to investigate effects of all the parameters constituting the applied governing equations.

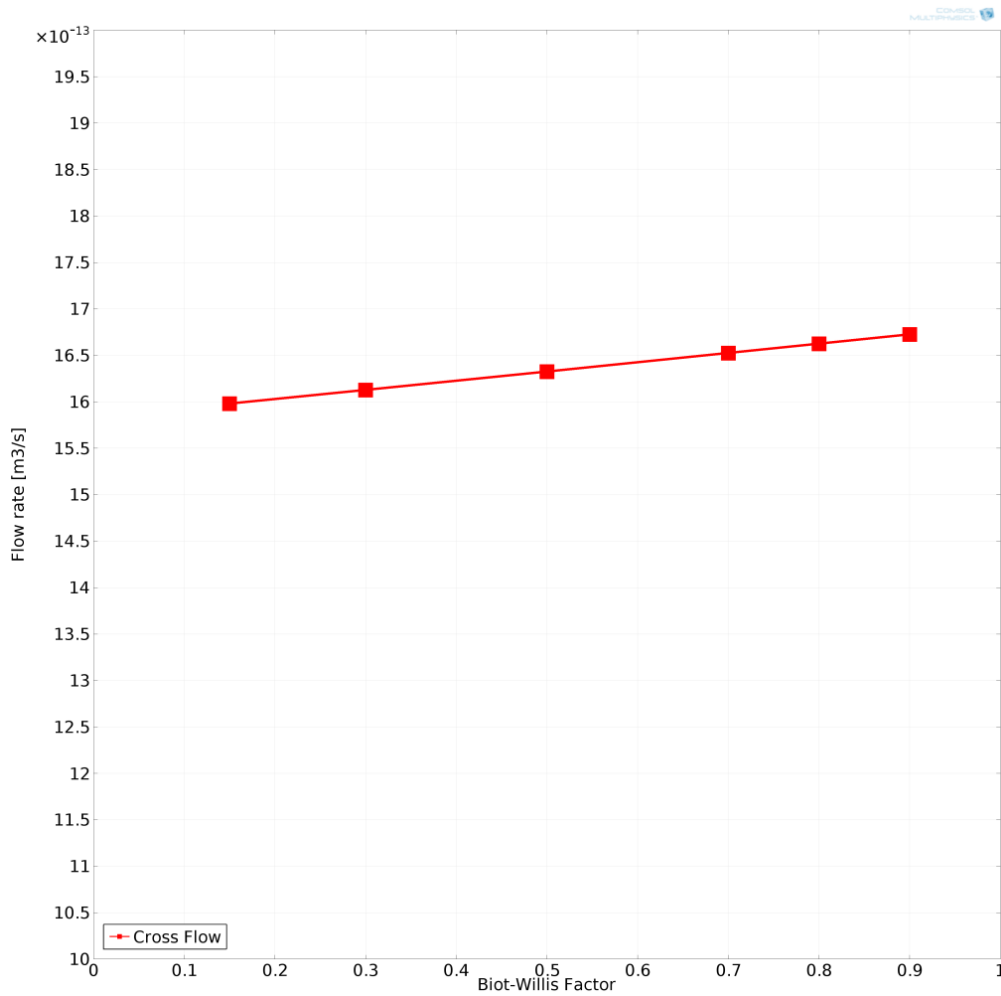


Figure 4-23. Cross flow alteration due to Biot-Willis coefficient change. Flow exchange between fracture and matrix follows the same trend as the fracture flow exhibits with different Biot-Willis coefficients.

4.2.8 Poisson’s ratio

Core plug Poisson’s ratio along with Young’s modulus is considered as the most important rock mechanical parameters that can provide an exact explanation of the flooded plug deformation. Poisson’s ratio directly affect the matrix displacement under overburden stress, therefore a range of common Poisson’s ratio for sandstones was analysed to achieve an understanding of its effect. Figure 4-24 indicates that larger Poisson’s ratios result in less matrix displacement in a descending polynomial form.

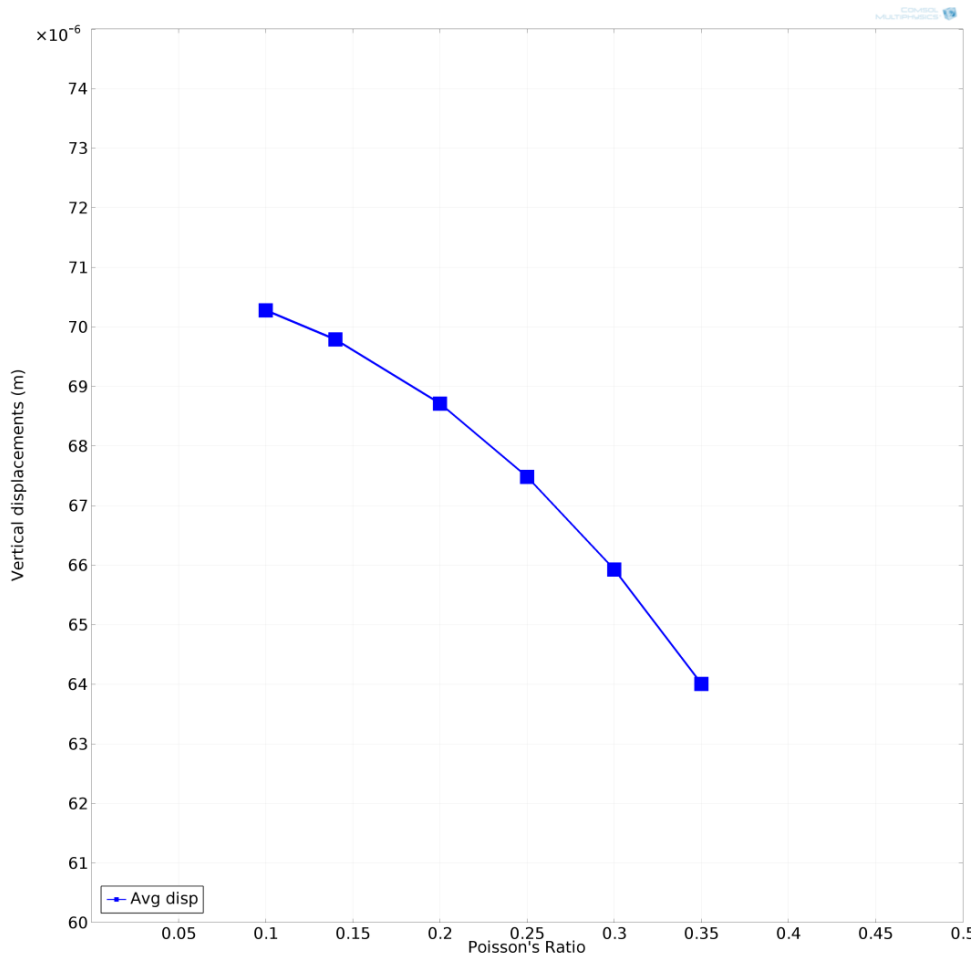


Figure 4-24. Poisson's ratio effect on matrix displacement under overburden stress. Less consolidated rocks with higher Poisson's ratio undergo more displacement under stress.

As the applied stress-dependent permeability formulation accounts for Poisson's ratio, increase of this parameter affects matrix flow insignificantly. The observed slight exponential growth of matrix flow (Fig. 4-25) can be considerable for larger blocks of hydrocarbon bearing reservoirs though.

Fracture flow, on the other hand, exhibits a more pronounced response to Poisson's ratio for the flooded sandstone (Fig. 4-26). This fact indicates how the rock mechanical characteristics of a fractured formation dictate flow behaviour under mechanical loading conditions.

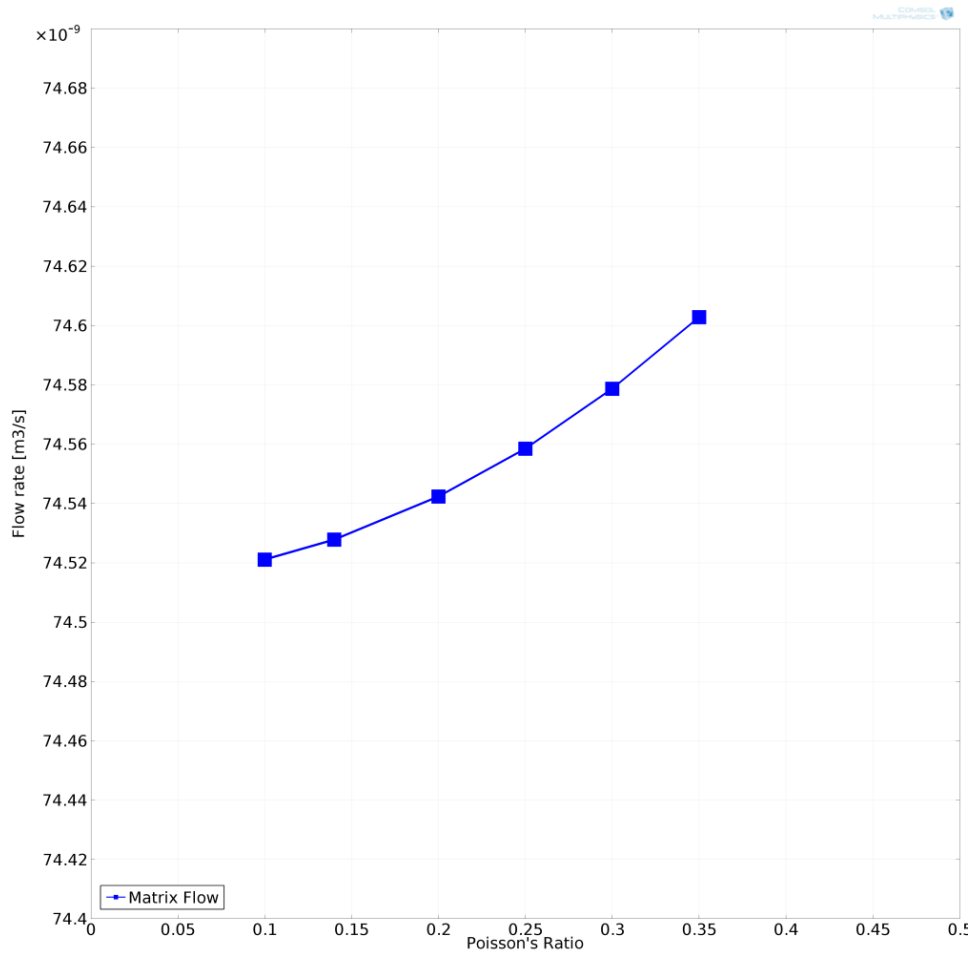


Figure 4-25. Poisson's ratio effect on matrix flow. Poisson's ratio affect matrix flow with an infinitesimal non-linear trend.

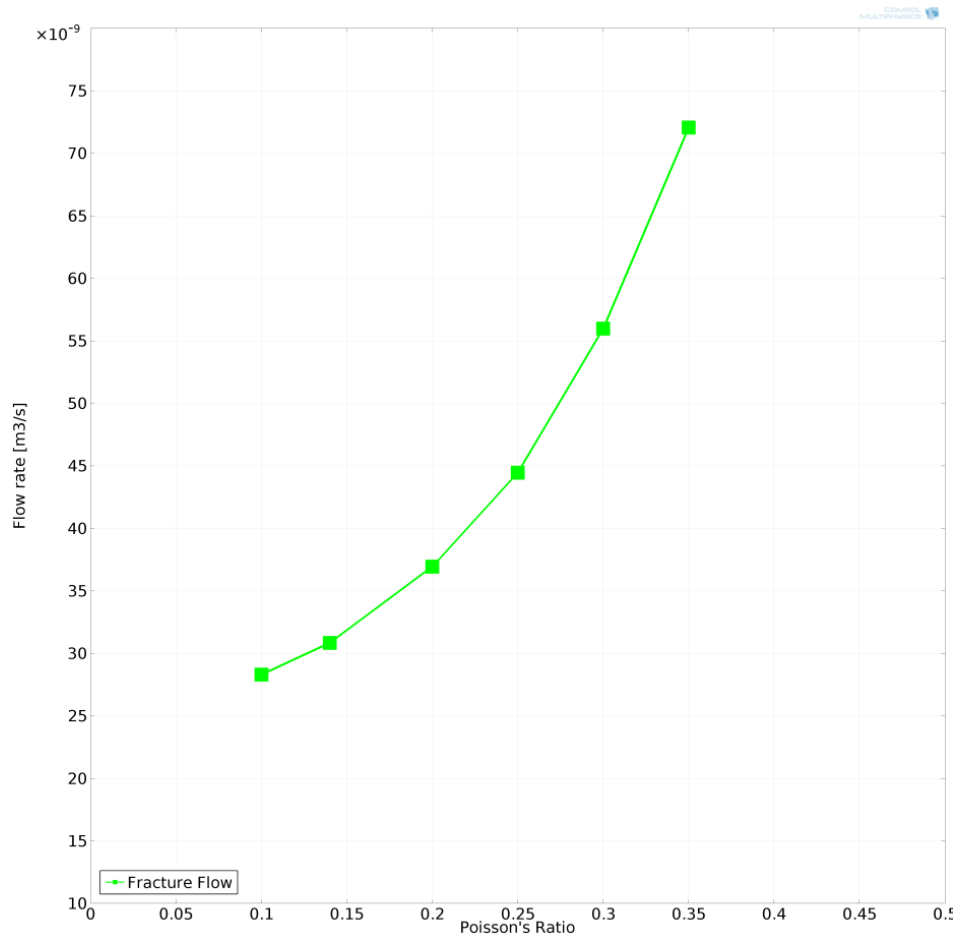


Figure 4-26. Poisson's ratio effect on fracture flow. Significantly less consolidated rocks with increased Poisson's ratio values alleviate flow through fractures.

In addition to the less fracture closure intensity due to reduced displacements, matrix-fracture cross flow monitoring (Fig. 4-27) can explain the significant observed effect of Poisson's ratio on fracture flow partitioning. Matrix-fracture flow exchange is enhanced to a comparable scale with fracture flow as the Poisson's ratio grows and this enhanced influx supports the higher fracture flow due to less matrix displacement and consequent larger fracture aperture size (Fig. 4-24).

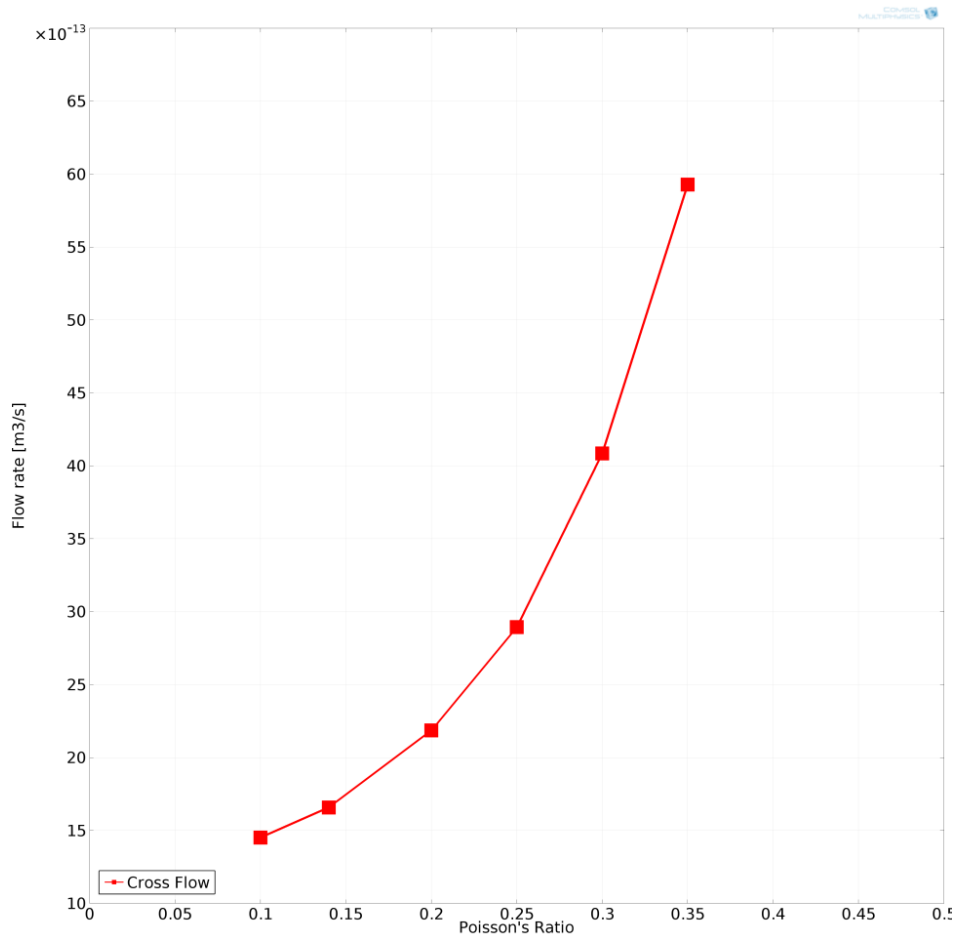


Figure 4-27. Matrix-fracture cross flow change due to various Poisson's ratio values. Cross flow increases significantly with increasing Poisson's ratio values in accordance with growth in fracture flow.

4.2.9 Young's Modulus

Young's modulus is the key mechanical parameter controlling the strain of any material under loading conditions. This parameter is the main parameter after the overburden stress that influences the matrix displacement and consequently the effective fracture aperture. It also appears in the poro-elasticity and the stress-dependent permeability formulation implemented in the coupled flow modelling scenario.

Young's modulus as an indication of rock stiffness is characterised by higher values for harder rocks; therefore expectation is to observe less matrix displacement under overburden loading for higher Young's modulus magnitudes. Figure 4-28 confirms this expectation.

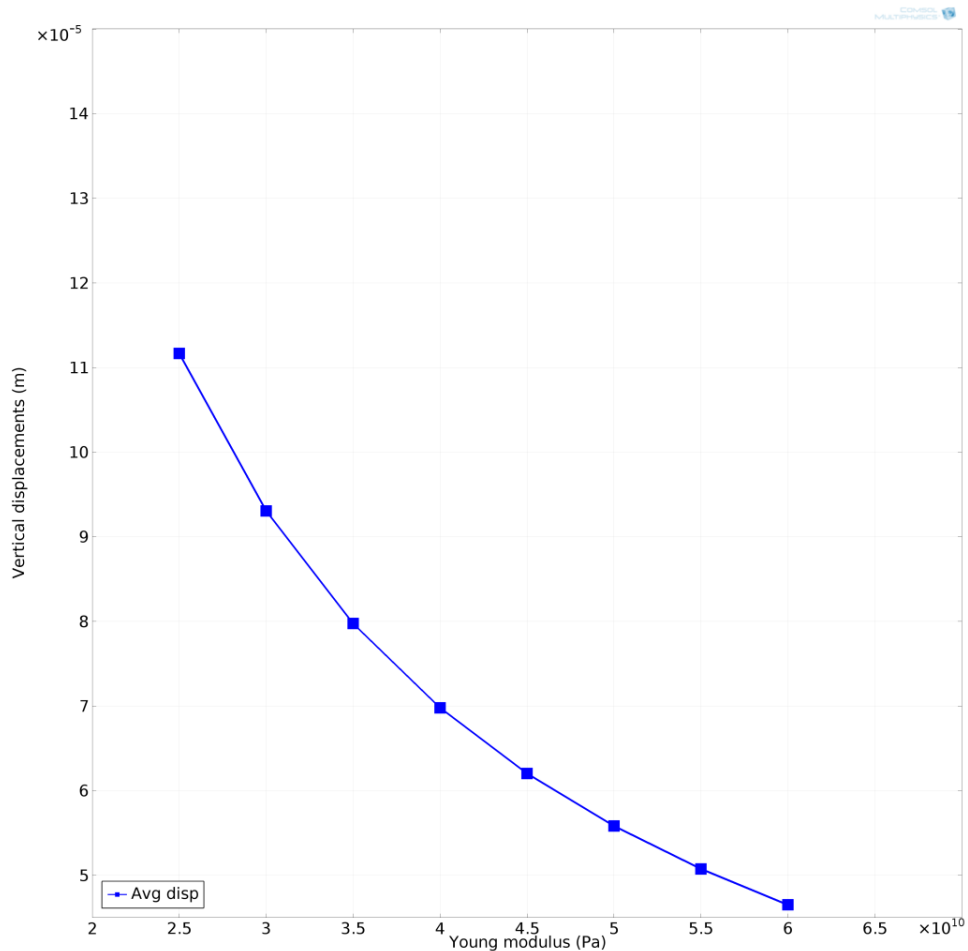


Figure 4-28. Less matrix displacement for higher Young’s modulus values. More robust formations with higher Young modulus undergo less strain in response to stresses.

Similar to other investigated parameters, the effect of Young’s modulus variation on Matrix flow is minimal; as can be inferred from Fig. 4-29, higher Young’s moduli result in slightly increased matrix flow. However variation of this modulus impacts fracture flow much more significantly (Fig. 4-30). This can be interpreted primarily with regard to the larger fracture aperture sizes due to enhanced resistance of harder rocks to loading conditions. It is worth mentioning that for current investigation, coupled numerical flow modelling at a Young’s modulus of just below 4.5×10^{10} Pa demonstrates a switch of dominant flow partitioning from matrix to fracture as can be seen in Fig. 4-30.

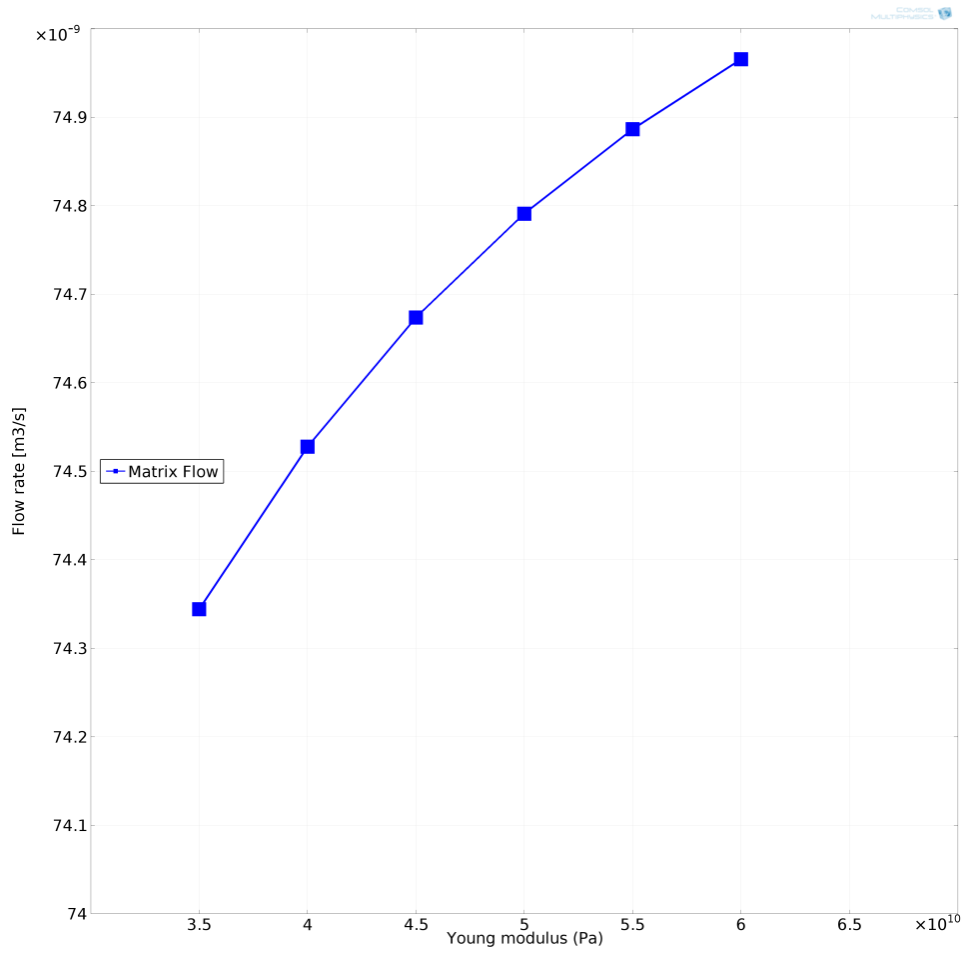


Figure 4-29. Minor increase of matrix flow for higher Young’s modulus core plugs. Young modulus effect on matrix flow rate is small just like the Poisson’s ratio effect.

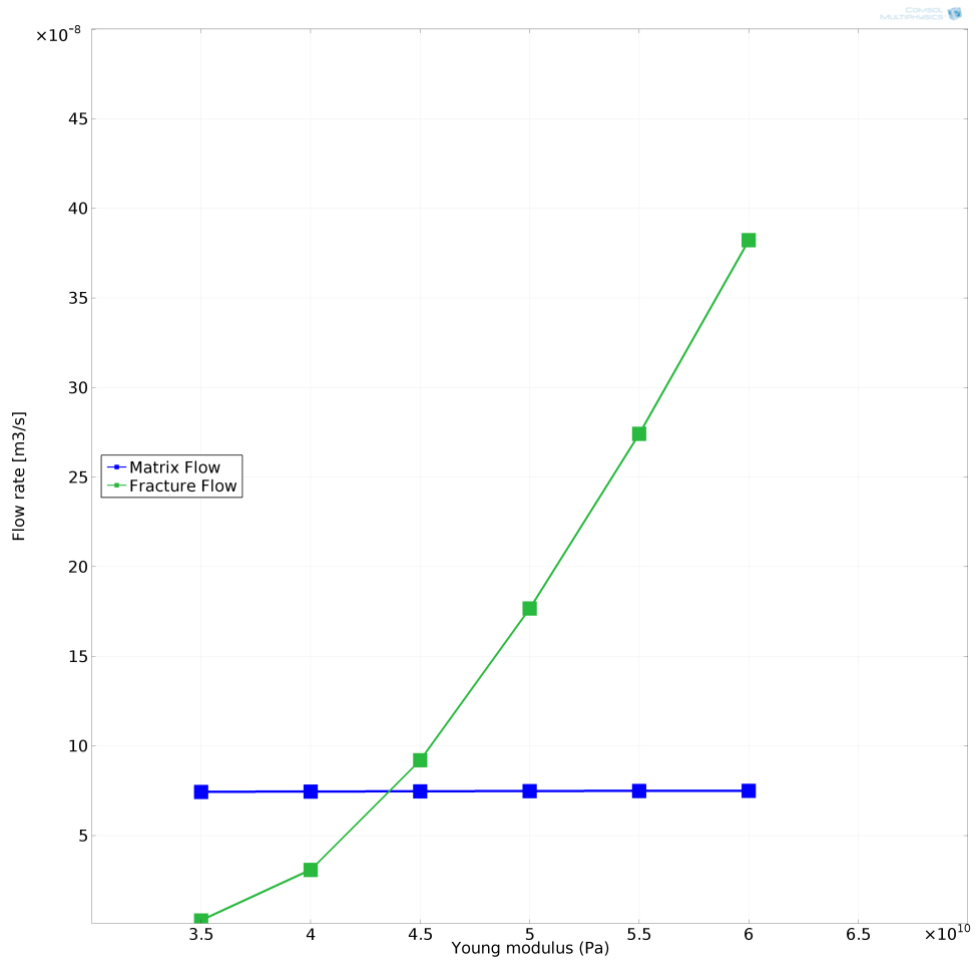


Figure 4-30. Young’s modulus effect on fracture and matrix flow. Note the dominant flow path switches below 4.5×10^{10} Pa.

Figure 4-30 reveals that Young’s modulus effect on matrix flow is negligible in comparison with its effect on fracture flow.

Significant increase of cross flow between matrix and fracture for rocks characterised by higher Young’s moduli, supports the reasoning for the observed fracture flow growth (Fig. 4-31).

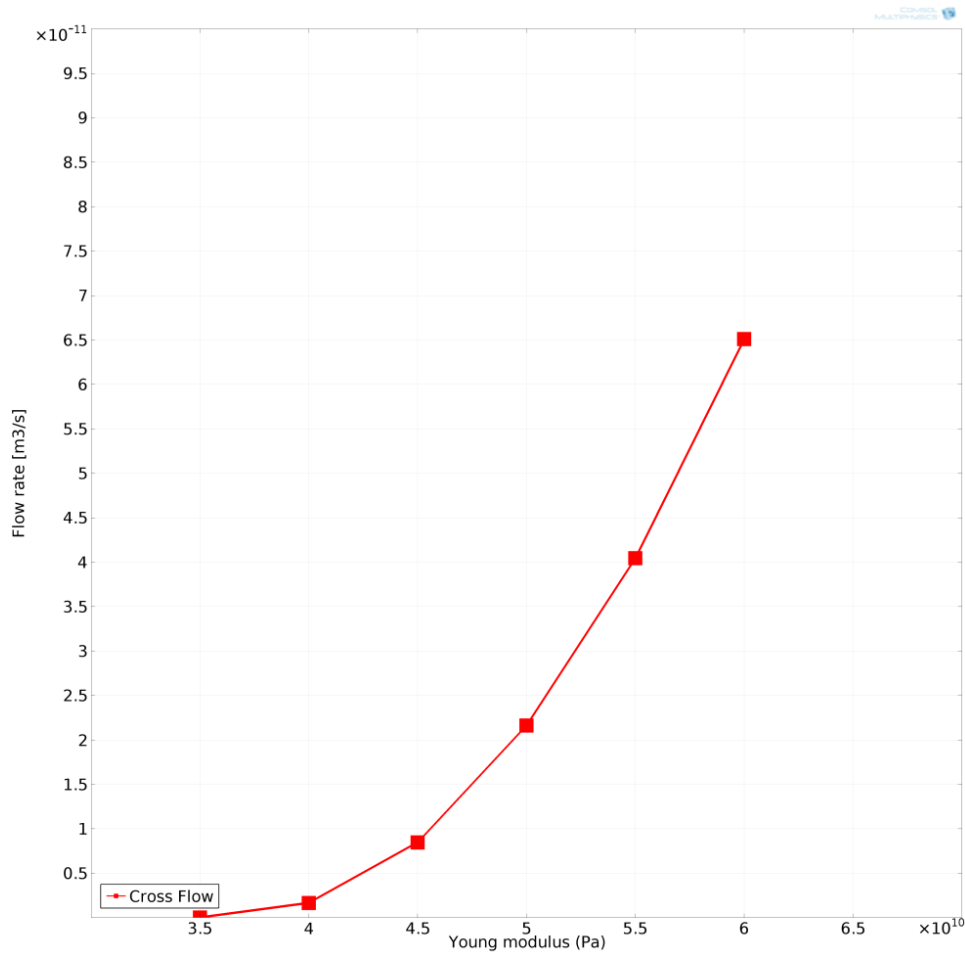


Figure 4-31. Significant increase of cross flow rate as Young’s modulus increases. Similar increasing effect of higher Young modulus values on fracture – matrix cross flow to the Poisson’s ratio.

This sensitivity analysis indicates that for hard reservoir formation rock types, possessing high Young’s Modulus magnitudes, fracture is the main production system and production planning should be much more focussed on fracture flow optimization rather than matrix flow.

4.2.10 Pore pressure

Reservoir pore pressure supports the formation against any overburden loading as it acts in the opposite direction to the overburden. As discussed in previous chapter, effective stress as the resultant net force vector is responsible for matrix deformation under loading conditions. Consequently, higher pore pressures lead to more resistance against overburden and as confirmed by Fig. 4-32 result in lower displacement magnitudes.

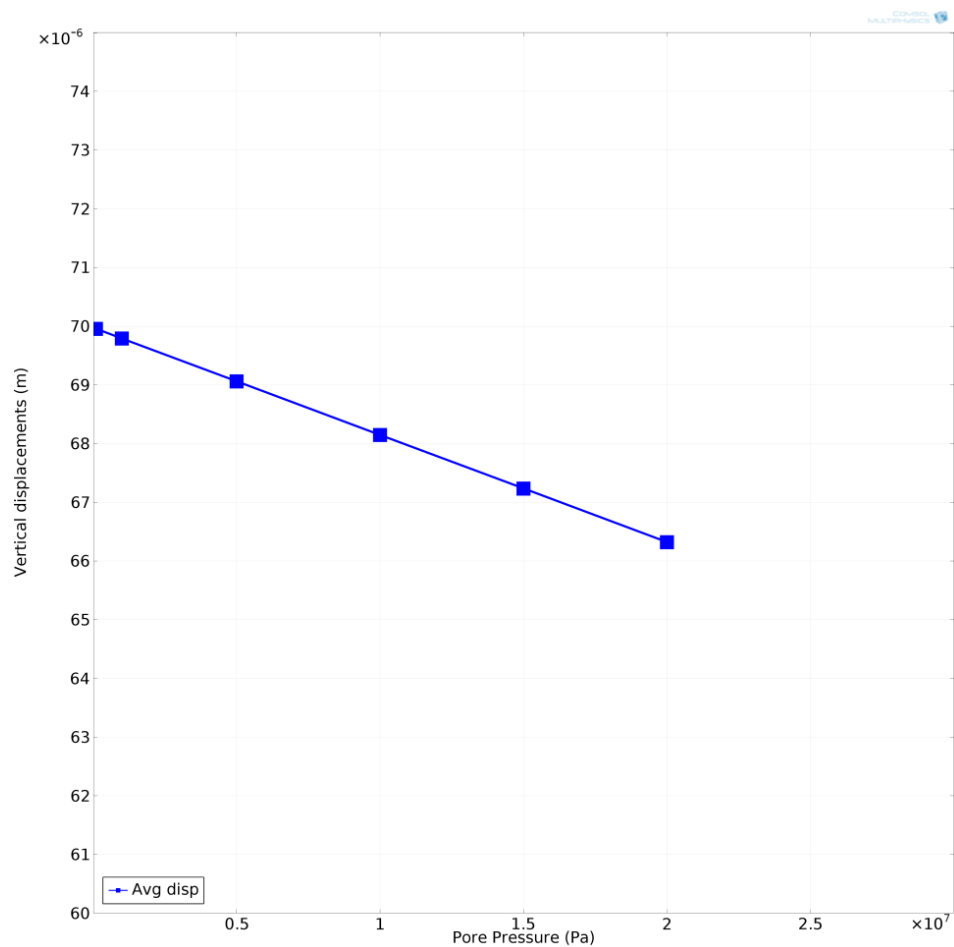


Figure 4-32. Pore pressure effect on matrix displacement. Matrix displacement decreases linearly as the pore pressure rises.

Logically as the pore pressure rise reduces the degrading effect of overburden stress on matrix permeability, matrix flow increases linearly in response to pore pressure amplification. This is illustrated in Fig. 4-33.

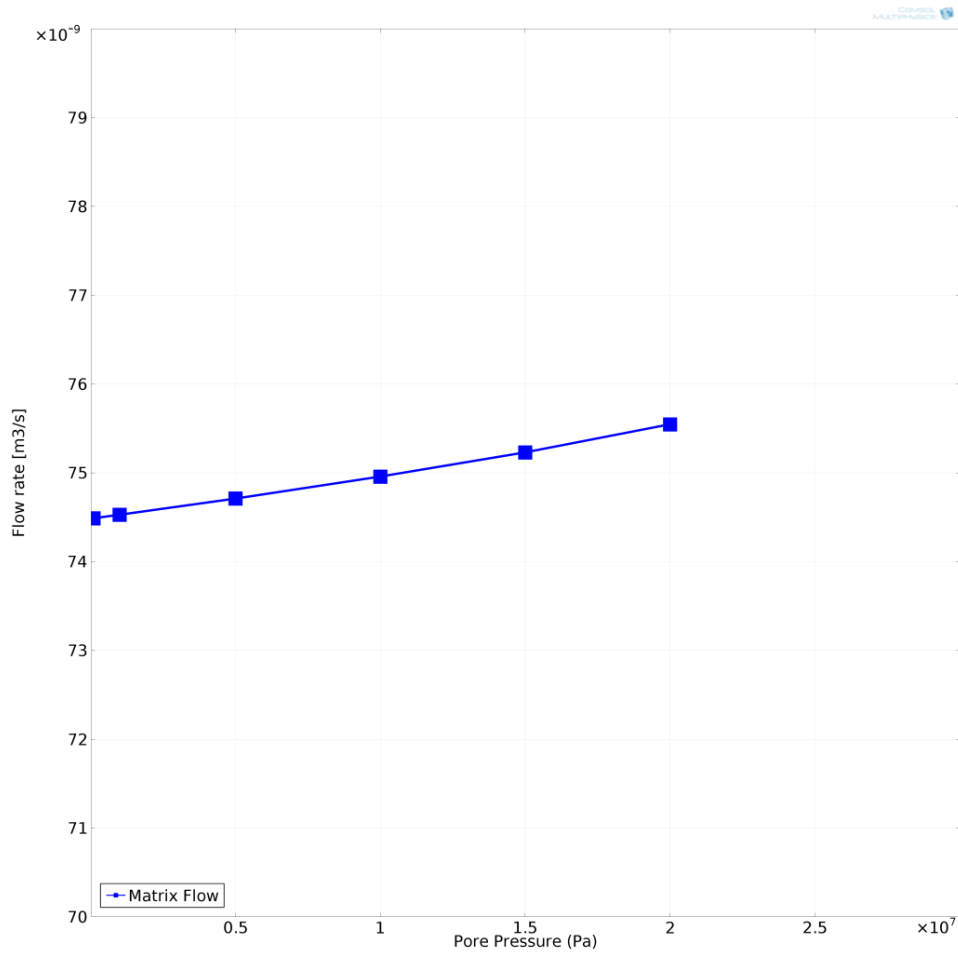


Figure 4-33. Matrix flow increases due to pore pressure rise.

In pace with the rock mechanical characteristics of the flooded plug, pore pressure increase imposes more severe effects on the fracture flow partitioning rather than matrix flow partitioning. Careful review of Fig. 4-34 reveals that the enhancing effect of pore pressure increase on fracture flow is less linear than its effect on matrix flow meaning that extra-large pore pressures that occur in high pressure deep reservoirs can enhance fracture flow significantly.

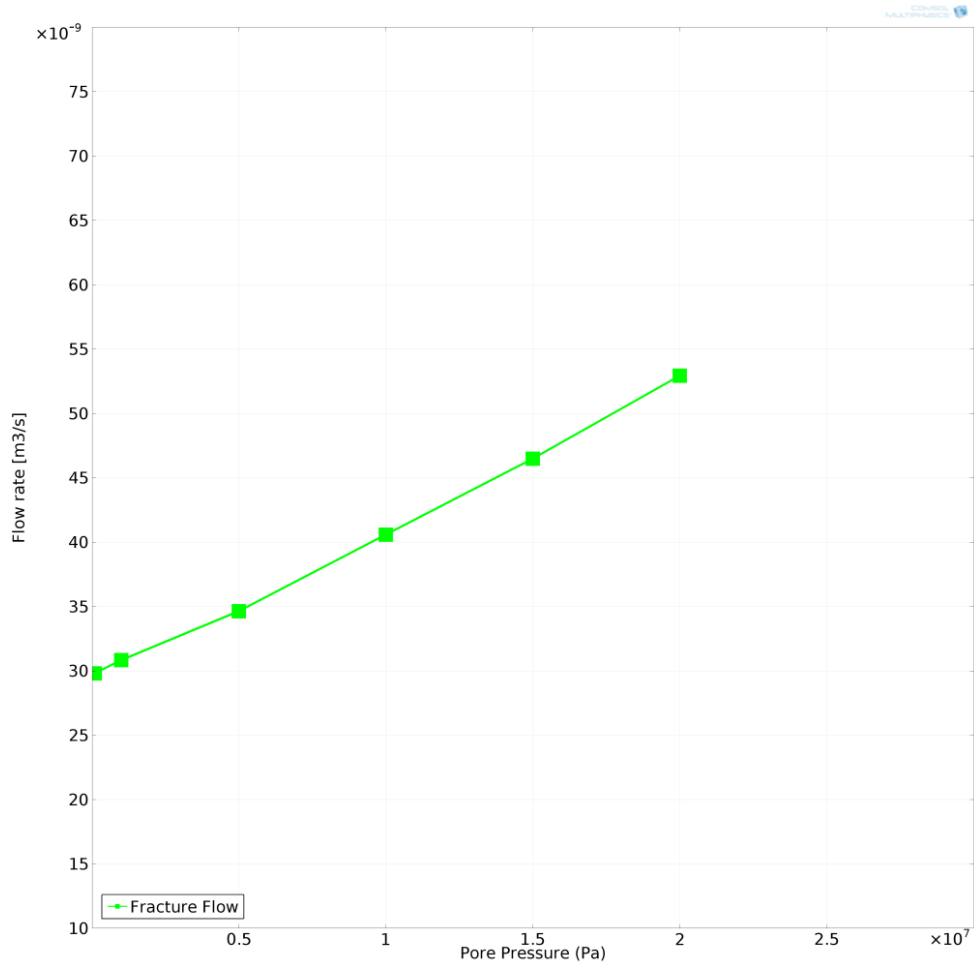


Figure 4-34. Fracture flow increases due to higher pore pressures. The higher fracture flow rates are in accordance with less fracture geometry decrease.

Increasing trend of matrix-fracture flow exchange follows more intense non-linear inclination rather than fracture flow growth in response to pore pressure enhancement (Fig. 4-35).

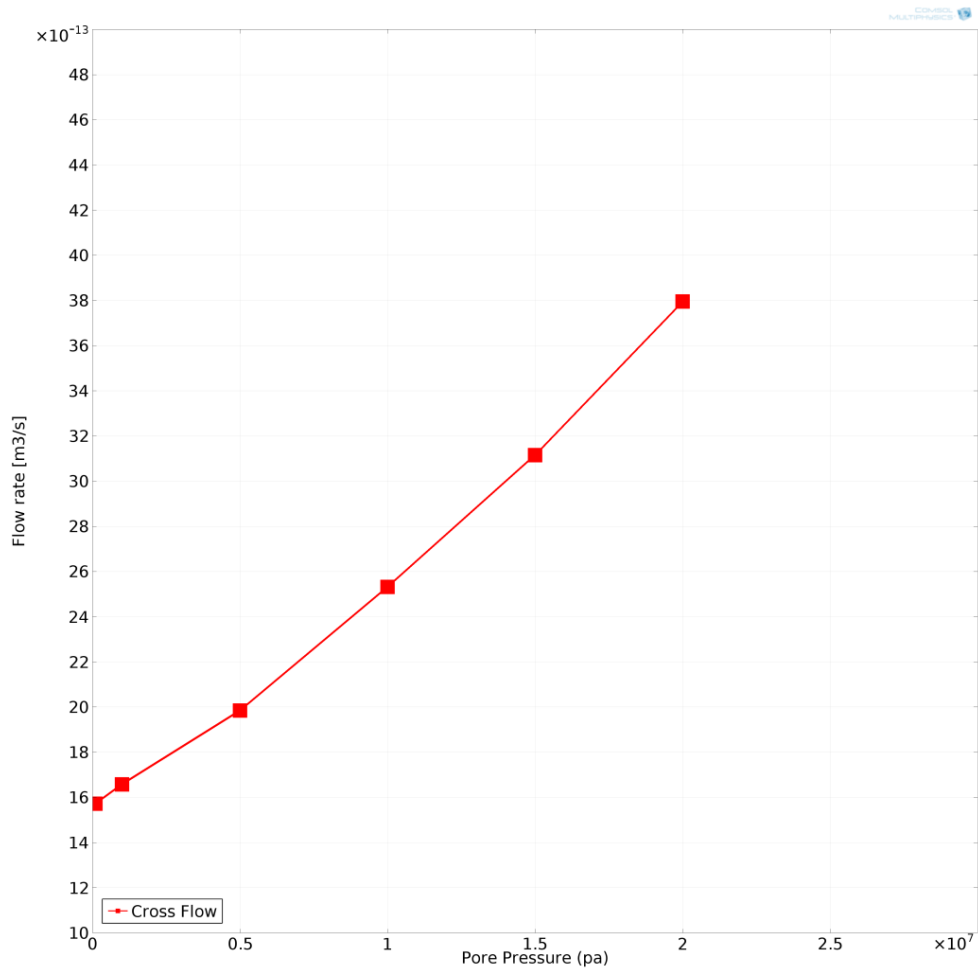


Figure 4-35. Matrix-fracture cross flow versus pore pressure. Enhanced pore pressure would result in increased fracture – matrix flow exchange.

As for the fracture flow case, exponential mode of cross flow increase with pore pressure indicates that for high pressure reservoirs cross flow between matrix and fracture will increase significantly.

4.2.11 Fluid density

Having analysed the parameters appearing in the flow equations and mechanical parameters contributing to structural mechanics and poro-elasticity equations, fluid density effect in the coupled fractured porous medium flow under loading conditions was investigated. Accounting for fluid density effects will extend the applicability of the developed coupled flow models to diverse hydrocarbon bearing reservoirs.

Fluid density does not impose any effect on the matrix displacement as it is not contributing to any mechanical governing equations. Density effect on matrix and fracture flow within the current plug scale sensitivity analysis, as can be seen in Fig.4-36 and Fig. 4-37 respectively, is also very limited. This minimal effect is due to the fact that gravity effect can be considered negligible for current core plug scale investigation.

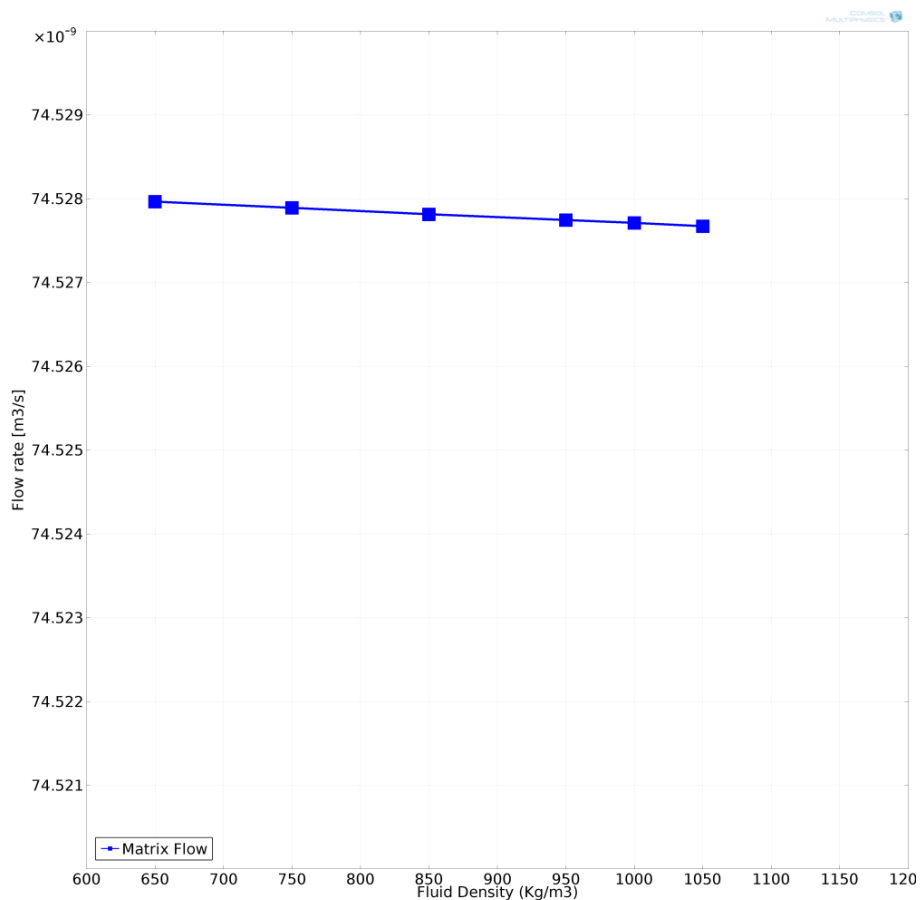


Figure 4-36. Matrix flow for various fluid densities. As can be seen fluid density exhibits very negligible effect on matrix flow as expected for such a small core plug.

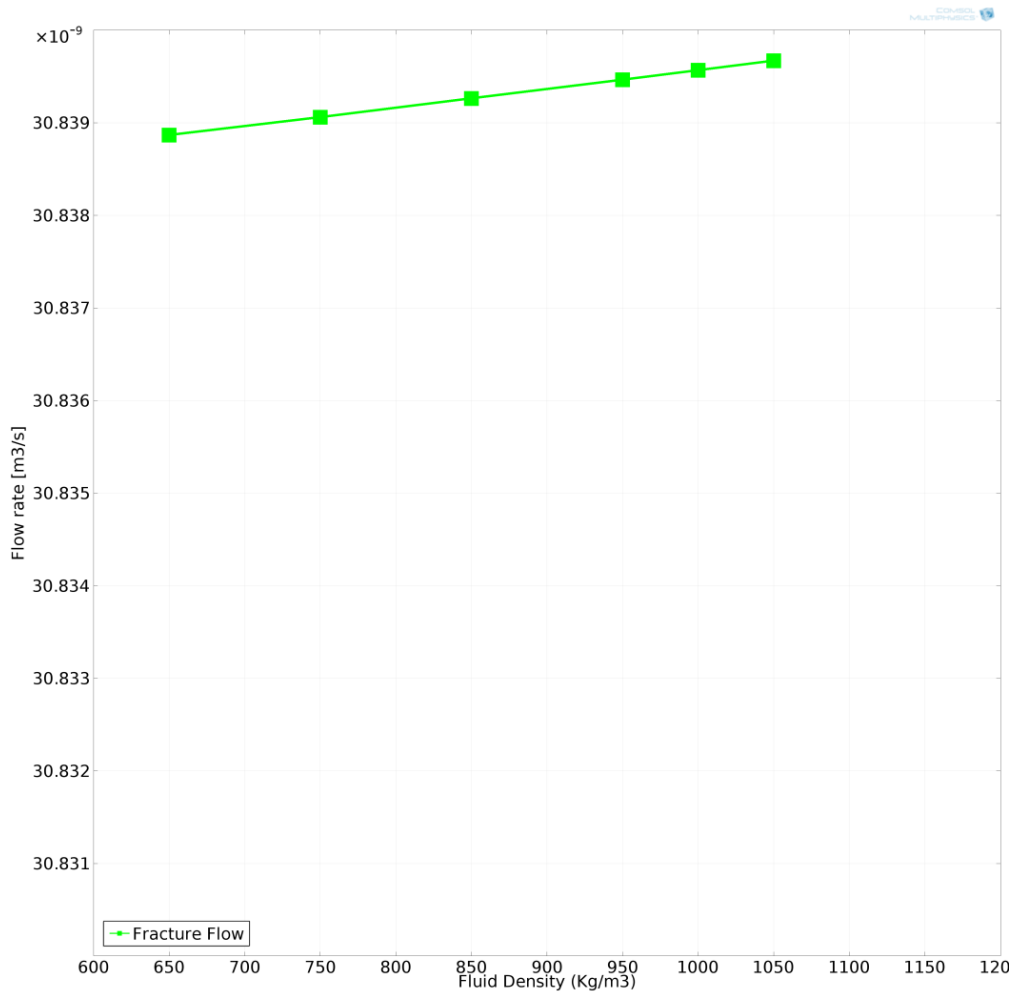


Figure 4-37. Incremental increase of fracture flow with fluid density. Similarly, fluid density does not show any significant effect on the fracture flow just like matrix flow.

Figures 4-36 and 4-37 indicate that denser fluids tend to increase the fracture flow and decrease matrix flow very infinitesimally. However it should be noted that denser hydrocarbon fluids like heavy oil are associated with increased dynamic viscosity; in this case, careful review of the flow variations against dynamic viscosity (Fig. 4-11) reveals that the decreasing effect of dynamic viscosity dominates the flow variations and therefore in case of heavy oil higher density fluids would not result in enhanced fracture and matrix flow.

On the other hand, fluid density impacts cross flow between rock matrix and fracture more significantly, in comparison to its effect on fracture and matrix flow, even in the case of the current core plug scale sensitivity analysis (Fig. 4-38).

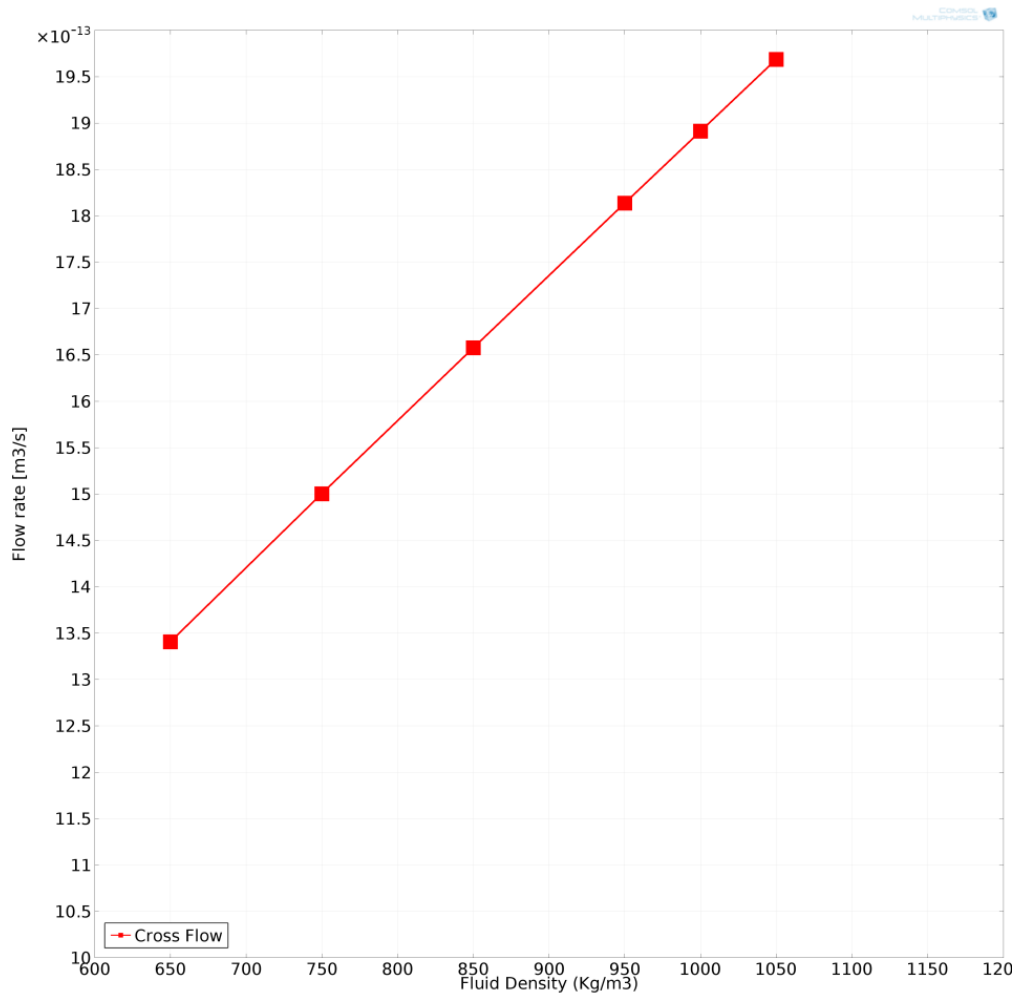


Figure 4-38. Matrix-fracture cross flow affected by fluid density. High fluid densities would result in increased cross flow between fracture and matrix however the effect is not outstanding comparing to other cross flow sensitivity plots.

As Fig. 4-38 confirms reservoir fluid influx from matrix to fracture increases linearly as the reservoir fluid density increases, however as discussed for fracture and matrix flow variations in case of heavy oil, comparison of Fig. 4-38 with Fig. 4-12 emphasizes the fact that the inverse effect of dynamic viscosity would be the dominant phenomenon and therefore fracture – matrix flow exchange would not be any improved for heavy oil.

4.2.12 Initial fracture aperture

Initial fracture aperture is a vital geometric parameter that impacts fracture – matrix flow interaction in a non-linear form under loading conditions. This non-linearity causes complexity in modelling this parameter effect to develop any coupled empirical flow model for fracture and matrix. This will be expounded more in section 4.3.

Matrix deformation is governed through mechanical stress-strain formulation and remains constant provided that the loading condition does not vary. Evidently, as the resulting fracture aperture after stress loading is the remaining aperture size after subtraction of the surface averaged matrix vertical displacement and this displacement is a function of overburden stress loading, the larger the initial fracture aperture the larger the remaining fracture aperture as a result of loading for every constant stress loading case.

In terms of matrix flow, as can be inferred from Fig. 4-39, enlargement of initial fracture aperture size initially results in an increase of matrix flow until a certain value of fracture aperture is reached (approximately 230 micron); beyond this value the matrix flow decreases with a much steeper rate. This critical aperture coincides with the start of significant increase in fracture flow as evident from Fig. 4-40. It is worth mentioning that since the current sensitivity analysis model was set by pressure boundary conditions corresponding to the 21.4 MPa Overburden stress loading, the total flow rate was so restricted for the initial fracture aperture sizes below 230 micron; as the initial fracture aperture increases initially both matrix and fracture flow increase until the point where total flow rate stabilizes and thereafter increase in fracture flow rate is reflected as an expected decrease in matrix flow rate. In addition, it should be noted that matrix flow response to the variation of initial fracture aperture sizes, has been exaggerated in Fig. 4-39 to emphasize its non-linear effect.

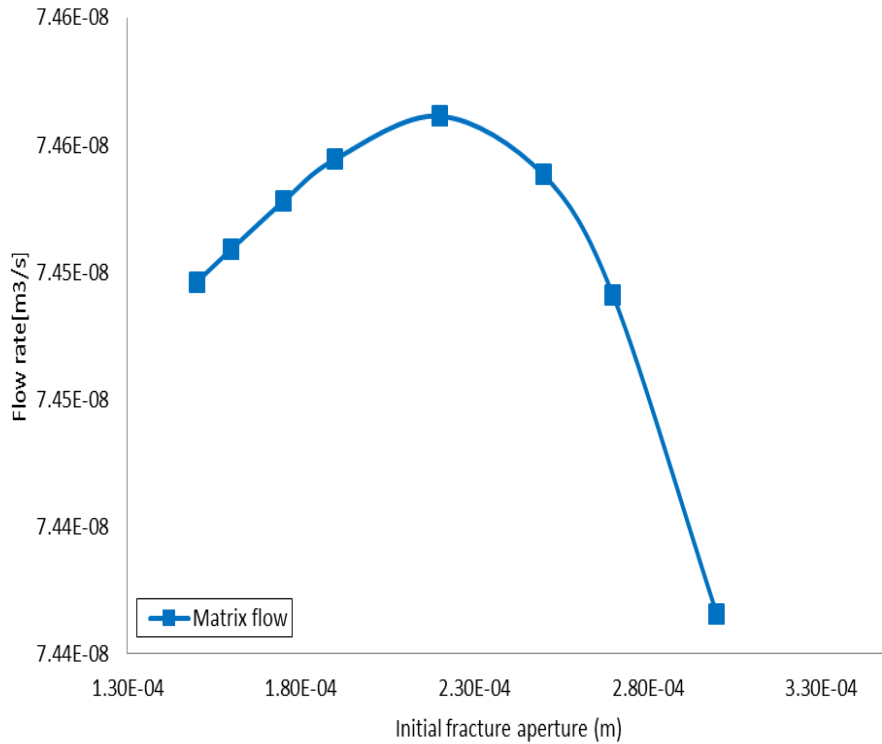


Figure 4-39. Matrix flow variation for different initial fracture aperture sizes. Initial fracture aperture effect is exaggerated to emphasize its non-linear effect on matrix flow for a small core plug.

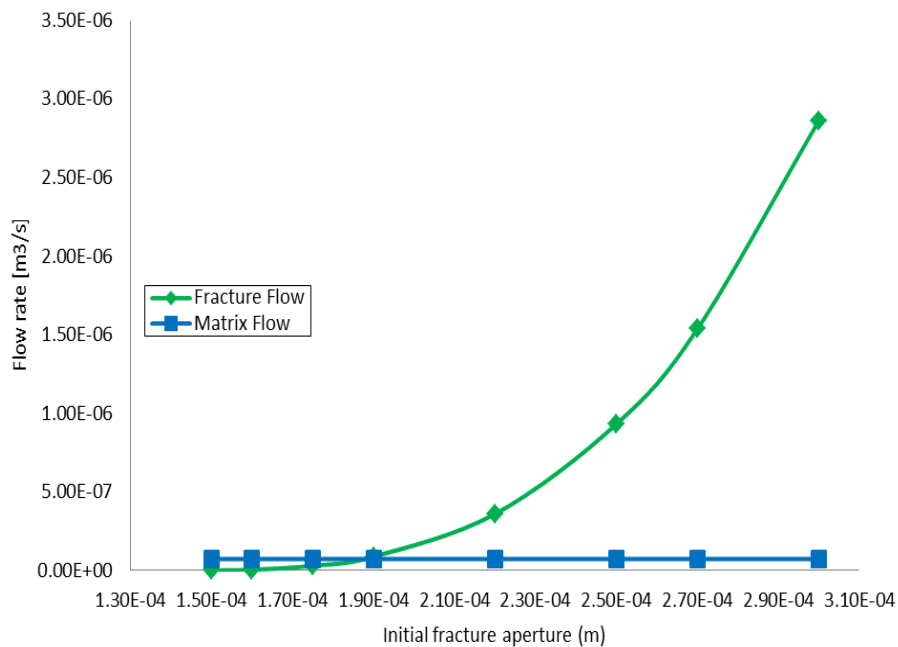


Figure 4-40. Matrix and fracture flow characterisation for different initial fracture aperture sizes. Initial fracture aperture has much more significant effect on fracture flow rather than on matrix flow.

Comprehensive review of Fig. 4-40 reveals that for the current analysed loading scenario, for fractures of lower than approximately 190 micron aperture size matrix conducts the main proportion of the overall influx that contradicts the assumption of fracture as the dominant production permeability in the cubic law (Bai and Elsworth, 1994) or Barton-Bandis (Bandis et al., 1983; Barton et al., 1985) or Rice (Rice, 1992) fracture permeability models; while as the initial aperture magnitudes enlarges more than this critical aperture, fracture flow takes over as the main production path. It is worth mentioning that since in case of less severe stress loading conditions matrix displacement is reduced; therefore the critical initial fracture aperture at which main flow path switches, would be reached at a lower magnitude.

Further evaluation of the matrix–fracture flow interaction also shows that cross flow increases exponentially beyond the critical initial fracture aperture size (Fig. 4-41).

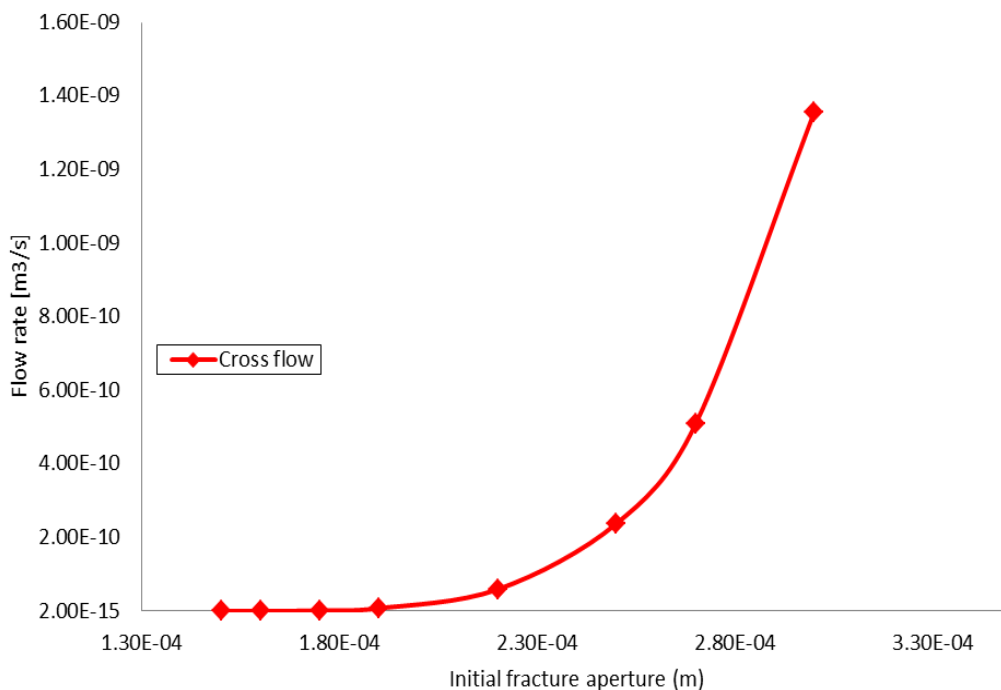


Figure 4-41. Matrix – fracture flow exchange evolution for various initial fracture aperture sizes. Cross flow is affected by the initial fracture aperture size with an identical trend to fracture flow.

The increase of cross flow in response to the initial fracture aperture size is in several orders of magnitude scale; this shows the most significant sensitivity of all the investigated parameters. This is so important when analysing fractured formations coupled flow problems as it demonstrates that if the fractures possess large aperture sizes, sufficiently larger than the discussed critical aperture size, matrix flow become a minor production domain and can be considered negligible in extreme cases; in such cases the fracture permeability models based on cubic models (Bai and Elsworth, 1994) or those introduced by Rice (Rice, 1992) and Barton-Bandis (Bandis et al., 1983; Barton et al., 1985) will be sufficiently predictive of fracture flow alterations. Mechanically coupled flow analyses can provide the engineers with the critical initial fracture aperture so that they can recognize the fracture flow significance with regard to the effect of reservoir depletion derived in-situ stress variation on the fracture aperture size alteration; this enables them to adopt an appropriate production scheme for the reservoir.

Figure 4-42 provides a snapshot of the sensitivity analysis for fracture, matrix and cross flow. The sensitivity percentage is the percentage of flow rate variation that the average value of each individual parameter makes comparing to the base case scenario. It is evident that Darcy law parameters significantly affect matrix flow while parameters like initial fracture aperture, overburden stress and rock mechanical parameters, in addition to the Darcy law parameters, have a remarkable effect on fracture flow and fracture-matrix interaction.

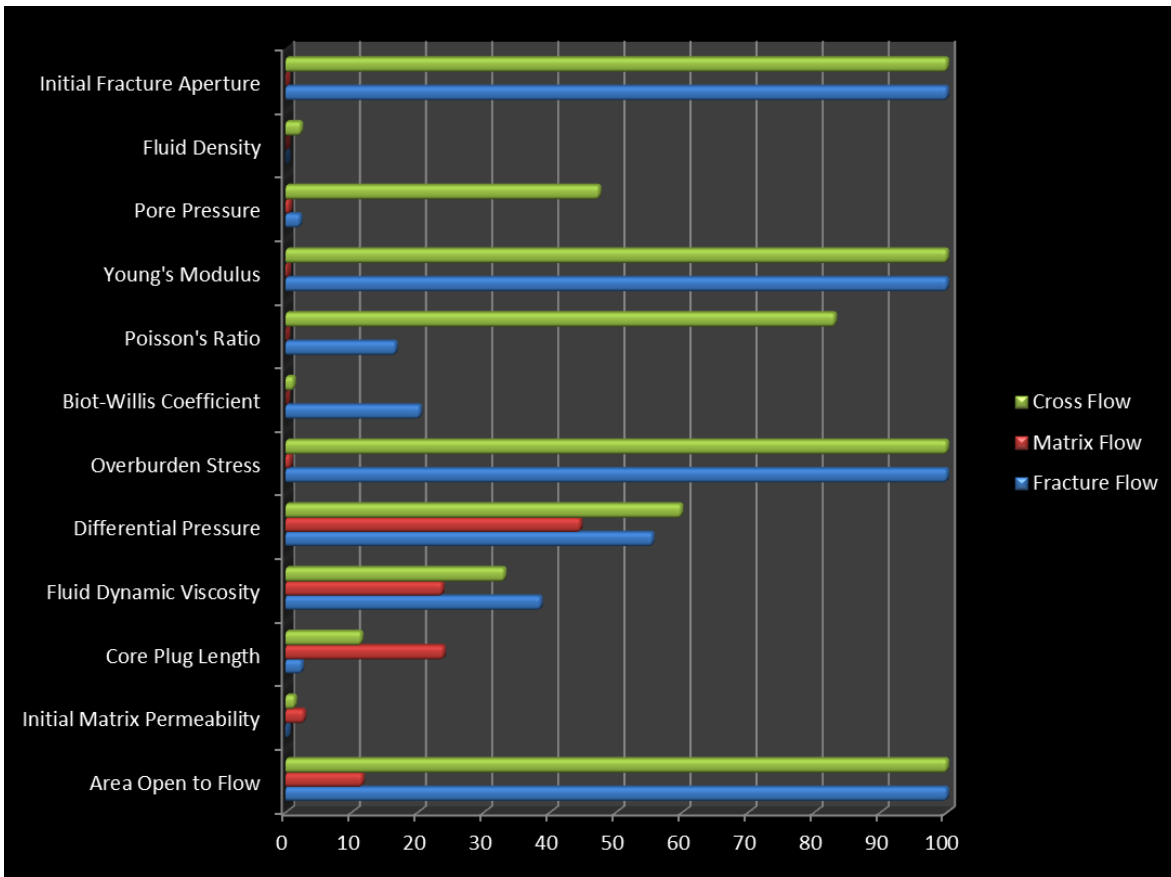


Figure 4-42. Sensitivity of various parameters appearing in governing equations on fracture, matrix and cross flow.

It is worth mentioning that all the flow rates reported in this chapter were calculated for a plug scale characterisation study; therefore specific attention need to be paid not to underestimate these flow rates' sensitivities. As an analogy, the lowest end of discussed flow rates, which were in range of 10^{-12} m^3/s for fracture – matrix interaction, are equivalent to 0.005 to 0.5 bbl/day for a typical fracture of 100 ft half-length in a 30 ft reservoir interval. Considering 10^4 times larger flow rates reported for fracture and matrix, the significance of the reported values to reservoir engineers is much better perceived.

4.3 Coupled empirical models for fracture and matrix flow

Having analysed the sensitivity of fracture, matrix and cross flow to all the hydraulic and mechanical parameters appearing in the coupled governing equations, the sensitivity analyses results were studied statistically to develop coupled mechanistic fracture and matrix flow models. Utilized analytical governing equations were considered while examination of a non-linear multi-parameter regression fitting investigation, in order to achieve the empirical flow models.

The statistical analysis was done utilizing an statistical package called Minitab which was originally developed by a group of researchers in Pennsylvania State University. As a user friendly general statistical analyses tool, Minitab initially considered as teaching assistive package. However it is efficient for analysing research data as well. The software is specifically powerful in regression modelling whether linear or non-linear. Ordinary least square method is the fundamental linear regression modelling technique and non-linear regression is also performed through an iterative algorithm which considers minimizing the sum of squares of the residual error between the predictions of a user-defined expectation function and the introduced data set.

4.3.1 Matrix flow model

Sensitivity analysis calculations were introduced to Minitab software as a prediction model development dataset in order to fit a multi-parameter non-linear regression model that can capture matrix flow variation under stress loading condition within a fractured porous formation.

Non-linear nature of the parameters' effects made the regression fitting a challenging mathematical effort. To overcome the complexity of the model fitting and enhance the physical reliability of the regression, the parameters were grouped together to form pseudo parameters based on the governing equations structure. Pseudo parameters which have been implemented in the regression analysis for matrix flow modelling are as follows:

Darcy flow term: $\frac{k_0 A \Delta P}{\mu L}$

Structural deformation term: $\sqrt[3]{\left(\pi \left(\frac{\sigma - \alpha P_p}{E}\right)\right)^2}$

Poisson's ratio term: $\sqrt[3]{1 - \nu^2}$

The pseudo parameters were defined in such a way that their mathematical relationship with matrix flow was linear as can be seen in Fig. 4-43.

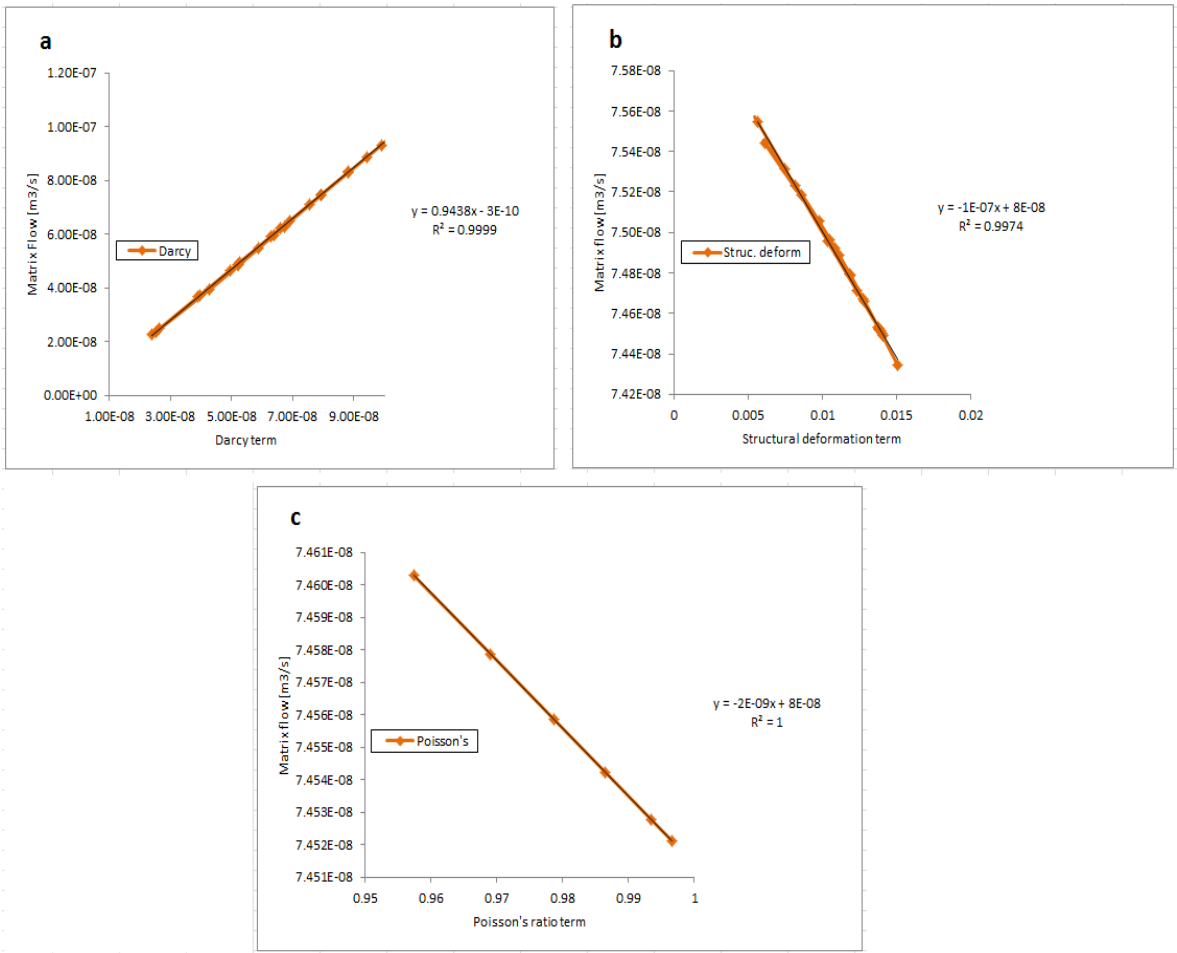


Figure 4-43. Matrix flow modelling pseudo parameters. Darcy (a), structural deformation (b) and Poisson's ratio (c) terms' effects on matrix flow variation.

As the regression fitting procedure is a multi-parameter one, the pseudo parameters' relationship with the target parameter, the matrix flow, should have been linear or otherwise a pre-assumed nonlinear function should have been introduced to the regression algorithm to start with. The pre-assumed non-linear relationship should provide a primitive approximation for the target

parameter. This was achieved through a single parameter linear regression, and if it was not possible a single parameter non-linear regression, over any individual sensitivity analyses parameter data set. These single parameter initiation relationships could be achieved via a simple curve fitting over the sensitivity analysis results of the desired parameter in a simple software suite like Microsoft Excel. The same procedure was also applicable to the considered pseudo parameters and their carefully extracted corresponding data sets. All the regression models for individual parameters as well as every pseudo-parameter which achieved owing to Excel statistical capabilities, were double checked for reliability via the coefficient of determination, R^2 , obtained for the regression models over all the dataset as well as over selected sub datasets.

Gauss-Newton algorithm was applied to perform the non-linear regression analysis over the generated matrix flow data set achieved via the discussed sensitivity analyses. Initial fracture aperture was the only parameter that could not be modelled linearly with any acceptable approximation taking into account the R squared and residual values for the linear fit model; therefore this parameter effect was incorporated in the regression modelling in a polynomial form. A variety of possible non-linear regression models was examined over the data and the regression-fitted values of the models were compared to the residual subtraction magnitudes of the sensitivity analysis data set and fitted models' predictions. Eventually the developed coupled matrix flow model (Eq. 4-1) demonstrated residuals of 2 order of magnitudes less than the matrix flow sensitivity analysis results, as can be inferred from Fig. 4-44. As evident from Fig. 4-44, the maximum observed residual magnitude for the developed model is about 7×10^{-10} while the matrix flow has a minimum value of 1×10^{-8} m³/s. This is considered as a robust indication of the model reliability.

$$MFLOW = 0.944729 \frac{k_0 A \Delta P}{\mu L} - 1.28282 \times 10^{-7} \sqrt[3]{\left(\pi \left(\frac{\sigma - \alpha P p}{E} \right) \right)^2} + 5.97705 \times 10^{-11} \sqrt[3]{1 - \vartheta^2} + 3.22002 \times 10^{-14} \rho - 0.0297833 b_0^2 + 1.29437 \times 10^{-5} b_0 \quad (4-1)$$

$MFLOW$ represents matrix flow and b_0 is the initial fracture aperture. SI units apply to all the parameters in eq. 4-1 in accordance with the sensitivity analyses applied units.

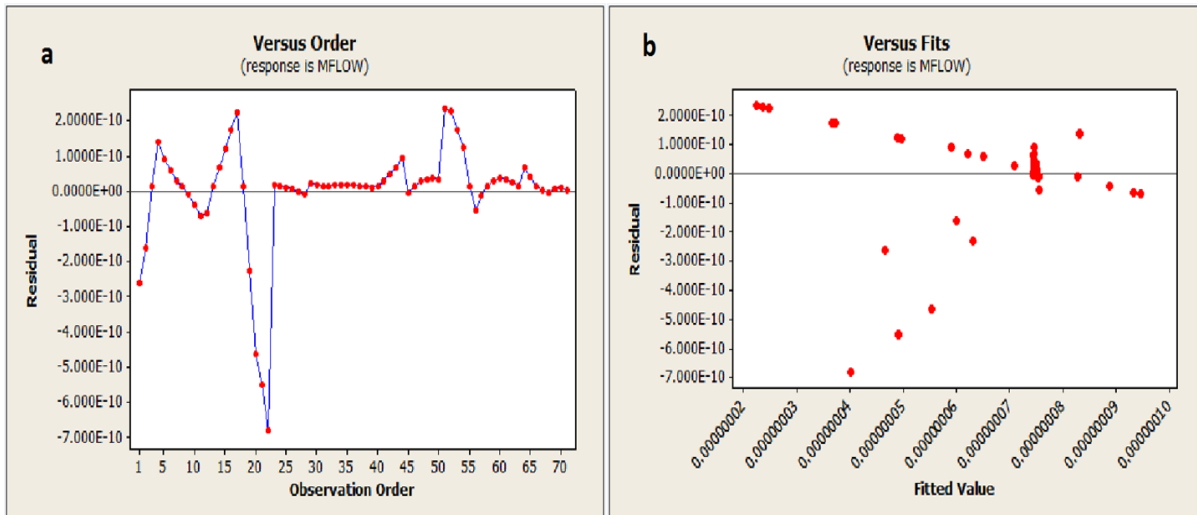


Figure 4-44. Matrix flow regression model residual magnitudes. Regression residuals versus data set order (a) and model fitted values (b).

As Fig. 4-44 reveals majority of the fitted regression values exhibits rather zero deviation from the sensitivity analysis data; the most considerable residual magnitudes correspond to the Darcy pseudo parameter and specifically the core plug length. Although the residuals are negligible compared to the matrix flow data set, extensive attention needs to be paid to up scaling and generalization of the developed models.

4.3.2 Fracture flow model

Using a similar approach to matrix flow regression modelling, the results of the sensitivity analysis of fracture flow were mathematically treated in order to develop a mechanically-coupled fracture flow model.

As several coupled flow equations associated with mechanical models are responsible for fracture flow, most of the constitutive parameters of the anticipated model exhibit non-linear effects on fracture flow. Therefore less comprehensive pseudo parameters could be defined and individual non-linear models for most of the parameters were introduced to Minitab to develop the final model instead.

Three pseudo parameters were implemented in the regression fitting analysis based on the sensitivity analysis results to overcome the limitation of non-linear regression fitting on a multi-parameter modelling. Young's modulus and fracture initial aperture were the most challenging non-linear parameters; their effects were implemented in the regression fitting via efficient definition of corresponding pseudo parameters as follows:

$$\text{Poisson's ratio term: } \frac{1}{\sqrt[3]{(1-\nu^2)}}$$

$$\text{Structural elasticity term: } 4 \times 10^{-28} E^2 - 2 \times 10^{-17} E$$

$$\text{Fracture aperture term: } 178.49 b_0^2 - 0.0622 b_0$$

Implementation of these pseudo parameters resulted in linearization of the Poisson's ratio, Young's modulus and initial fracture aperture effects on fracture flow as can be inferred from Fig. 4-45.

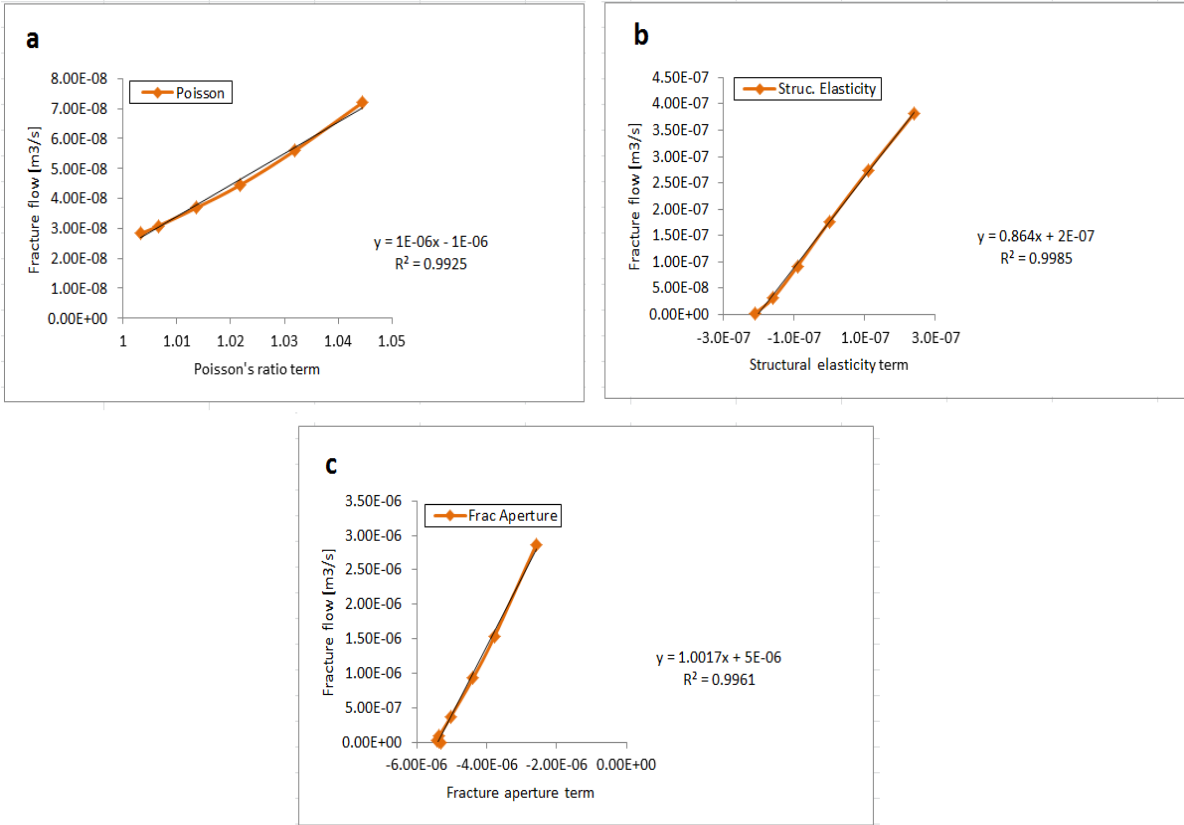


Figure 4-45. Fracture flow modelling pseudo parameters. Poisson’s ratio (a), structural elasticity (b) and fracture aperture (c) terms effects on fracture flow variation.

Having set the pseudo parameters and initial single parameter models, several possible regression models were examined on the fracture flow data set in Minitab. For each regression model, the residual magnitudes along with their statistical distribution were monitored to achieve the best predictive model (Eq. 4-2).

$$\begin{aligned}
 FFlow = & 163035k_0 + \frac{15.9364}{\sigma} + 173.9044b_0^2 - 0.06060b_0 + \frac{4.39713 \times 10^{-6}}{\sqrt[3]{(1-\theta^2)}} + 6.74519 \times 10^{-7}L + \\
 & \frac{1.38138 \times 10^{-13}}{A^2} + 5.7036 \times 10^{-11}\rho + 2.43839 \times 10^{-15}\alpha P_p + 8.14644 \times 10^{-16}\frac{\Delta P}{\mu} + 3.67928 \times \\
 & 10^{-28}E^2 - 1.83964 \times 10^{-17}E
 \end{aligned} \tag{4-2}$$

FFlow represents the fracture flow and SI system applies to all the constitutive parameters units. Fracture flow model accounts for more parameters effects as individual terms, in contrast to matrix flow, due to its more complex coupled multi-physics nature. This fact implicitly indicates a

lower accuracy compared to the matrix flow model; however, statistics of the regression fittings confirms that the model have predicted the sensitivity analysis results within an acceptable deviation margin. Fig. 4-46 provides the fracture flow model residuals statistics.

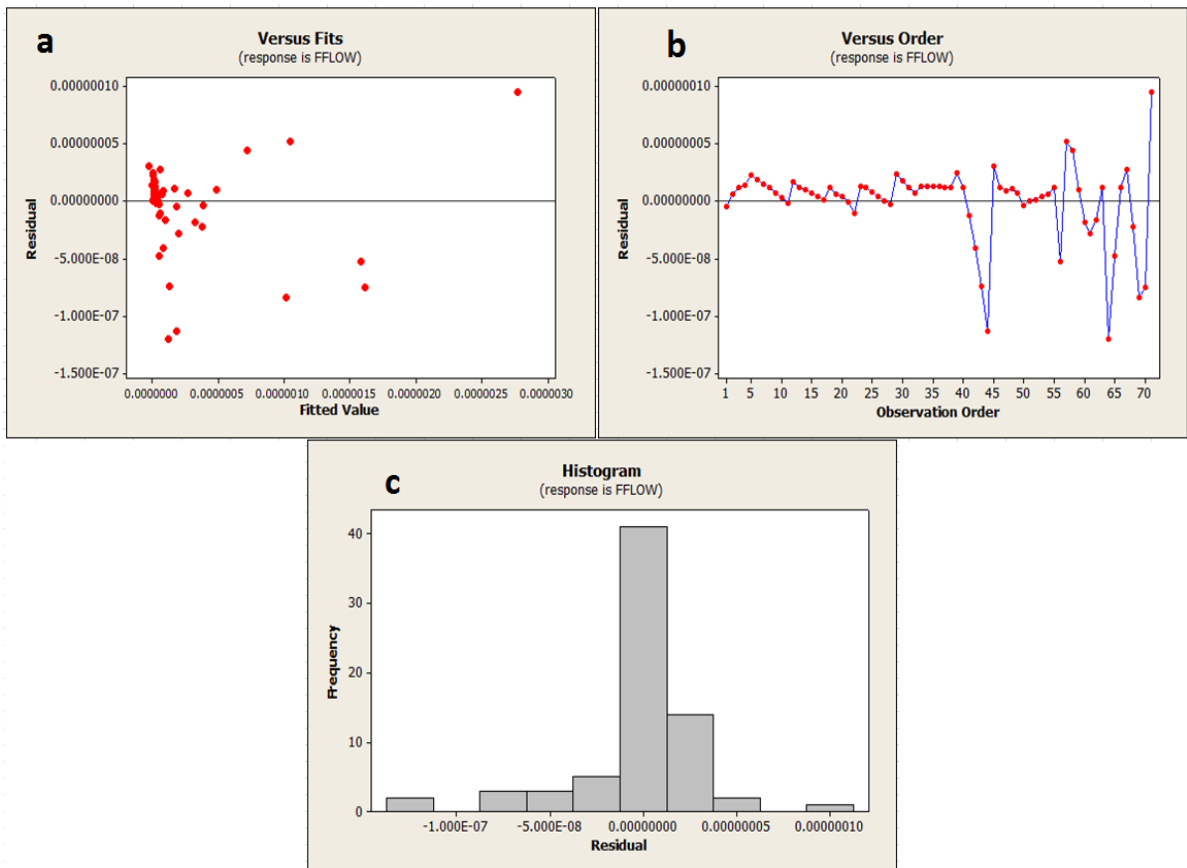


Figure 4-46. Fracture flow fitted model residuals statistics. a) Residual magnitudes versus fitted model predictions, b) Residual magnitudes versus the observation order of the data set and c) frequency of the residuals.

Fig. 4-46a exhibits the residuals of the fitted model predictions subtracted by the exact data from the previously performed sensitivity analyses versus the fitted values. As can be seen the majority of the residual magnitudes occur in the immediate vicinity of zero axis. This figure indicates that even for the extreme residual magnitude of below $10 \times 10^{-8} \text{ m}^3/\text{s}$, the fitted value, and logically the exact data point from data set, is approximately $30 \times 10^{-7} \text{ m}^3/\text{s}$ and

this indicates a residual of one order of magnitude less than the modelled data which is considered as an acceptable deviation margin.

In a similar manner, the largest residual values in Fig. 4-46b correspond to the largest simulated fracture flow results of significant fracture aperture values in case of the latest observation orders which are at least one order of magnitude larger than the residuals. The histogram shown in Fig. 4-46c also confirms the accuracy of the fitted regression model in terms of the frequency of the residuals which is pretty much dominantly distributed around zero.

The reliability of the provided regression models should be validated against laboratory data before they can be considered as a basis for larger-scaled scenarios or more complex multiphase flow systems. It should be taken into consideration that the achieved empirical models are only valid within the range of parameters that have been tested during the sensitivity analysis and is merely valid for the single fracture model analysed in the previous chapter. In section 4.4, the application of the coupled numerical analysis will be concisely examined in a multiphase time dependent flow scenario and the laboratory validation of the numerical results will be discussed in chapter 5.

4.4 Extension of coupling approach to two-phase flow matrix-fracture interaction

This section does not intend to provide a detailed modelling of two-phase flow interaction under stress loading scenarios in a fractured core plug similar to the previous analysis for single phase. Indeed this section aims at elaborating on the physics coupling for two-phase flow scenario and emphasizing extension of the adopted coupling approach to more realistic reservoir production cases.

Several considerations should be taken into account in dealing with two phase flow evolution under stress in a fractured porous media. Primarily it should be emphasized that linear piston-type water flooding of oil in the simulated core plug is the desired coupled problem discussed in this section. Movement of flooding front is a deterministic fact in this problem to recognize which phase is responsible for partitioning between matrix and fracture, and as a result, a

representative steady state flow regime cannot be considered while the initially present fluid is being displaced by the flooding fluid. Therefore water flooding of the oil saturated core plug demands a time dependent analysis in contrast to the single phase flow scenario. Indeed the time dependency of individual fluid phase saturations is crucial and should be analysed.

On the other hand, within the fracture piston-type displacement rate of the initial saturation is much more accelerated in comparison to the displacement rate of matrix fluid content. This fact leads to formation of a displacing fluid dominant two-phase mixture flow regime within the fracture at very early stage of flooding. The composition of the mixture varies by time as a result of two-phase capillary diffusion occurring at the matrix-fracture interface. In order to overcome the time-dependent continuity of the flow between matrix and fracture, a mixture flow model was considered for the physics coupling purposes within the fracture.

4.4.1 Two-phase flow governing equations

COMSOL Multiphysics was utilized for the two-phase flow physics coupling similar to the single phase flow investigations. Within the plug matrix, extended Darcy law governs the two-phase flow quality. The extended Darcy law applies an average density and viscosity calculated by means of individual phase's saturation and relative permeability as follows:

$$S_o + S_b = 1 \quad (4-3)$$

$$\rho_{tp} = S_o \rho_o + S_b \rho_b \quad (4-4)$$

$$\frac{1}{\mu_{tp}} = S_o \frac{k_{ro}}{\mu_o} + S_b \frac{k_{rb}}{\mu_b} \quad (4-5)$$

In the above equations S is the saturation and k_r is the relative permeability. tp , o and b subscripts represent two-phase, oil and brine properties accordingly.

The implemented relative permeability model is a Corey approximation based on the brine saturation and initial brine relative permeability of 0.8 as can be seen in Fig. 4-47.

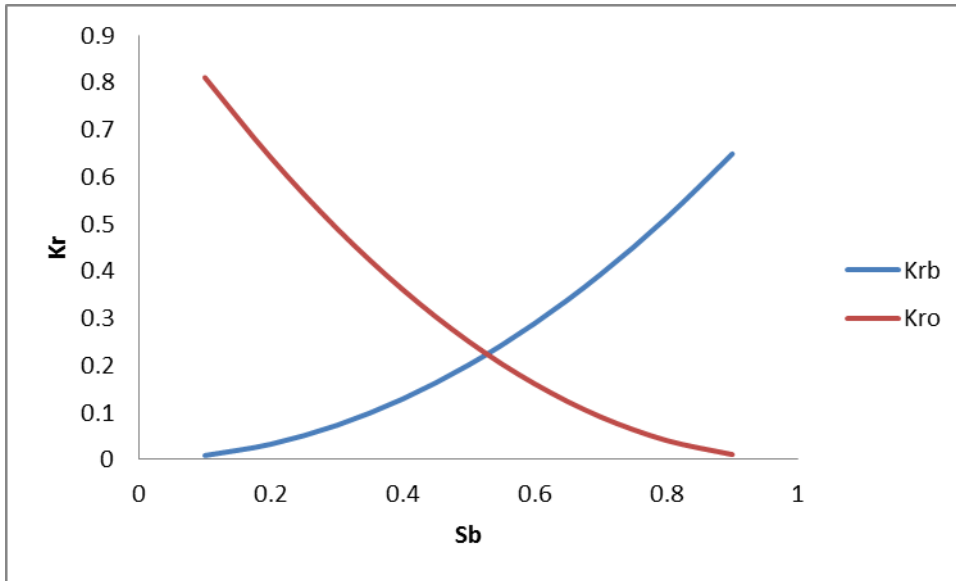


Figure 4-47. Typical relative permeability model implemented in the two-phase flow equations within core plug matrix.

Darcy law is combined with the continuity equation (eq. 4-6) as well as transport equation (eq. 4-7) for the fluid content $c_{o,b} = S_{o,b}\rho_{o,b}$.

$$\frac{\partial}{\partial t}(\rho\phi) + \nabla \cdot (\rho v) = 0 \quad (4-6)$$

$$\frac{\partial}{\partial t}(c_{o,b}\phi) + \nabla \cdot (c_{o,b}v) = \nabla \cdot D_c \nabla c_{o,b} \quad (4-7)$$

D_c denotes the capillary diffusion coefficient. The generalized governing equation (eq. 4-8) is the result of implementing Darcy law into the continuity equation (eq. 4-6):

$$\frac{\partial}{\partial t}(\rho\phi) + \nabla \cdot \rho \left[-\frac{k_0}{\mu} \nabla P \right] = 0 \quad (4-8)$$

As the considered two phases are brine and oil in this section for the current purpose, compressibility of the fluids was considered negligible.

On the other hand, fracture flow is governed by a mixture laminar flow model. This flow regime complies with the low Reynolds number of flow within the micro-scale fracture and also as it considers the flooded fluid as a dispersed phase in the continuous flooding phase; it therefore alleviates the time-dependent continuity concern discussed previously.

COMSOL mixture model calculates the averaged phase concentration, or volume fraction, and solves a single momentum equation (Eq. 4-9) for the mixture velocity.

$$\rho \frac{\partial v}{\partial t} + \rho(v \cdot \nabla)v = -\nabla P - \nabla \cdot \tau_{Gm} + \rho g + F - \nabla \cdot [\rho c_o(1 - c_o) \left(v_{Slip} - \frac{D_{md}}{(1-c_o)\varphi_o} \nabla \varphi_o \right) \left(v_{Slip} - \frac{D_{md}}{(1-c_o)\varphi_o} \nabla \varphi_o \right)] \quad (4-9)$$

In the above equation c_o is the oil (dispersed phase) mass fraction (Kg/Kg), v_{Slip} is the relative velocity vector between the two phases, τ_{Gm} is the summation of viscous and turbulent stresses (Kg/m.s²), φ_o denotes oil volume fraction and F represents any additional body force (N/m³). D_{md} is a turbulent dispersion coefficient (m²/s) accounting for extra diffusion due to turbulent effects. When no turbulence model is applied, like the current analysis, D_{md} is equal to zero.

v_{Slip} is calculated by means of Hadamard-Rybczynski drag model (eq. 4-10). This model is valid for droplets with particle Reynolds number (Re_p) less than 1 in accordance with the current study conditions. Hadamard-Rybczynski model provides the drag coefficient for oil droplets (C_o) as below:

$$C_o = \frac{24}{Re_p} \left(\frac{1 + \frac{2\mu_b}{3\mu_o}}{1 + \frac{\mu_b}{\mu_o}} \right) \quad (4-10)$$

Re_p is the particle Reynolds number as defined by eq. 4-11:

$$Re_p = \frac{d_o \rho_b |v_{Slip}|}{\mu} \quad (4-11)$$

d_o is the diameter of an equivalent sphere volume to the oil droplets.

The dispersed phase, oil in current two-phase scenario, is treated as moving droplets within the flooding medium current, water in our two-phase flooding scenario. Both mixture model phases share the same pressure field and relative velocity between them is accounted for by assuming a balance between the pressure gradient and viscous drag.

The applied drag model (eq.4-10) yields the following explicit expression (eq. 4-12) for slip velocity as a result of balancing viscous drag and buoyancy forces acting on the oil phase.

$$v_{Slip} = -\frac{(\rho-\rho_o)d_o^2}{18\rho\mu_b} \left(\frac{1+\frac{\mu_b}{\mu_o}}{1+\frac{2\mu_b}{3\mu_o}} \right) \nabla P \quad (4-12)$$

v in the momentum equation is the mass-averaged mixture velocity that is calculated using eq. 4-13:

$$v = \frac{\varphi_b \rho_b v_b + \varphi_o \rho_o v_o}{\rho} \quad (4-13)$$

φ_b represents brine (continuous phase) volume fraction. The two phases' velocities follow a relationship defined by eq. 4-14 below:

$$v_o - v_b = v_{bo} = v_{Slip} - \frac{D_{md}}{(1-c_o)\varphi_o} \nabla \varphi_o \quad (4-14)$$

Mixture density is a volume averaged one calculated using eq. 4-15 and the oil (dispersed phase) mass fraction term appearing in eq. 4-9 and eq. 4-14 is given by eq. 4-16.

$$\rho = \varphi_b \rho_b + \varphi_o \rho_o \quad (4-15)$$

$$c_o = \frac{\varphi_o \rho_o}{\rho} \quad (4-16)$$

Summation of the viscous and turbulent stresses is considered using eq. 4-17 where μ_T , the turbulent viscosity, equals zero as no turbulence model was used.

$$\tau_{Gm} = (\mu + \mu_T)[\nabla v + \nabla_v^T] \quad (4-17)$$

Eq. 4-18 provides the transport formulation accounting for oil volume fraction.

$$\frac{\partial}{\partial t}(\varphi_o \rho_o) + \nabla \cdot (\varphi_o \rho_o v_o) = -m_{ob} \quad (4-18)$$

Where m_{ob} is the mass transfer rate from the oil to the continuous brine phase and the summation of oil and brine volume fractions equals unity. The general continuity equation for the mixture is eq. 4-19; however when it is combined to eq. 4-18 and taking the constant phases densities into consideration, the specific continuity equation is derived (eq. 4-20).

$$\frac{\partial \rho}{\partial t} + \nabla \cdot (\rho v) = 0 \quad (4-19)$$

$$(\rho_b - \rho_o) \left[\nabla \cdot (\varphi_o (1 - c_o) v_{slip} - D_{md} \nabla \varphi_o) + \frac{m_{ob}}{\rho_o} \right] + \rho_b (\nabla \cdot v) = 0 \quad (4-20)$$

4.4.2 Two-phase scenario physics coupling

As emphasized previously, it is intended to demonstrate how the two-phase flow physics within the plug matrix and fracture can be coupled to poro-elasticity rather than analysing a real-case two phase flow scenario within the fractured plug.

In order to perform coupled analysis of the initially oil saturated brine flooding of the same Clashach sandstone plug that has been extensively investigated for single phase scenario, three comprehensive physics of geomechanics, two phase Darcy flow and mixture flow was coupled.

The starting stage of the numerical modelling was to perform the two-phase Darcy flow in the matrix geometry applying the two-phase governing equations. Initialization of the simulation was achieved through implementing the following pressure and saturation conditions (i subscript indicate initial condition):

$$P_i = 1e6$$

$$S_{oi} = 0.9$$

$$S_{oi}^{inlet} = 0.1$$

Similar to the single phase flooding scenario, stress dependent permeability was introduced to the two-phase flow physics with the Clashach plug matrix. The flooding phase, brine, was set to sweep the matrix geometry through the inlet of the plug geometry which was the same left-hand side boundary of the plug. Flooding inlet pressure boundary conditions were similar to the ones implemented in the single phase analysis. Two-phase flow initialization diffusivity coefficient was adopted from published literature of similar analyses (Bidlack and Anderson, 1964; Pentland, 2010; Wesselingh and Bollen, 1997) for the current demonstration purpose.

Matrix-fracture interface boundary was considered as an additional outlet boundary within the simulation problem settings because of the low prospects of applying Brinkman equation and the equivalent viscosity concept incorporated in the single-phase analysis (Fig. 4-48).

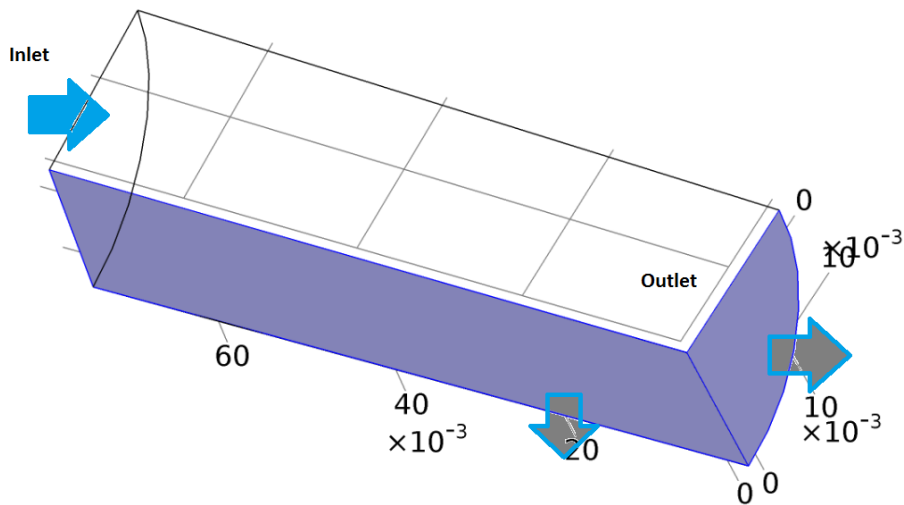


Figure 4-48. Outlet boundaries incorporated for the two-phase Darcy law physics. Note the fracture-matrix interface, bottom boundary, is considered as an outlet

Two-phase Darcy law physics derived average fluid density and viscosity along with the vertical component of capillary diffusion (D_{cyy}) at the fracture-matrix interface for each time step, was later incorporated in the poro-elasticity physics at the second stage of the simulation to calculate the plug matrix vertical displacement and therefore the fracture volume geometry. The geomechanics physics was set with identical specification as the single-phase analysis. Stress-dependent permeability was taken into account in this stage and effect of external overburden stress was analysed on the fracture geometry.

The derived capillary diffusion vertical component from matrix two-phase Darcy calculations for each time step was coupled to the fracture-matrix interface as a boundary condition. This coupled boundary condition enabled defining the fracture-matrix interface boundary as an outlet for the geomechanics physics geometry in line with the two-phase Darcy law physics settings.

In the final stage of the simulation, fracture volume geometry was updated by surface averaged matrix displacement calculated through application of poro-elasticity physics via the already discussed moving mesh capability, in section 3.5.1, utilized for the single phase scenario. The updated fracture geometry was then utilized for mixture flow model computations. The initial pressure and saturation conditions for fracture volume were identical to matrix initializing conditions. Brine was introduced to the mixture model as the continuous phase from the fracture's flooding inlet (left-hand side fracture geometry boundary). Oil phase was the initial dominant ($\varphi_{oi} = 0.9$) fracture saturation however oil flux at the flooding inlet was zero. On the other hand, the fracture-matrix interface was introduced as another inlet for the fracture volume via coupling of the vertical component of capillary diffusion derived from two phase Darcy law physics of matrix domain.

Fig. 4-49 and 4-50 demonstrate how the flooding front progresses along the matrix and fracture respectively.

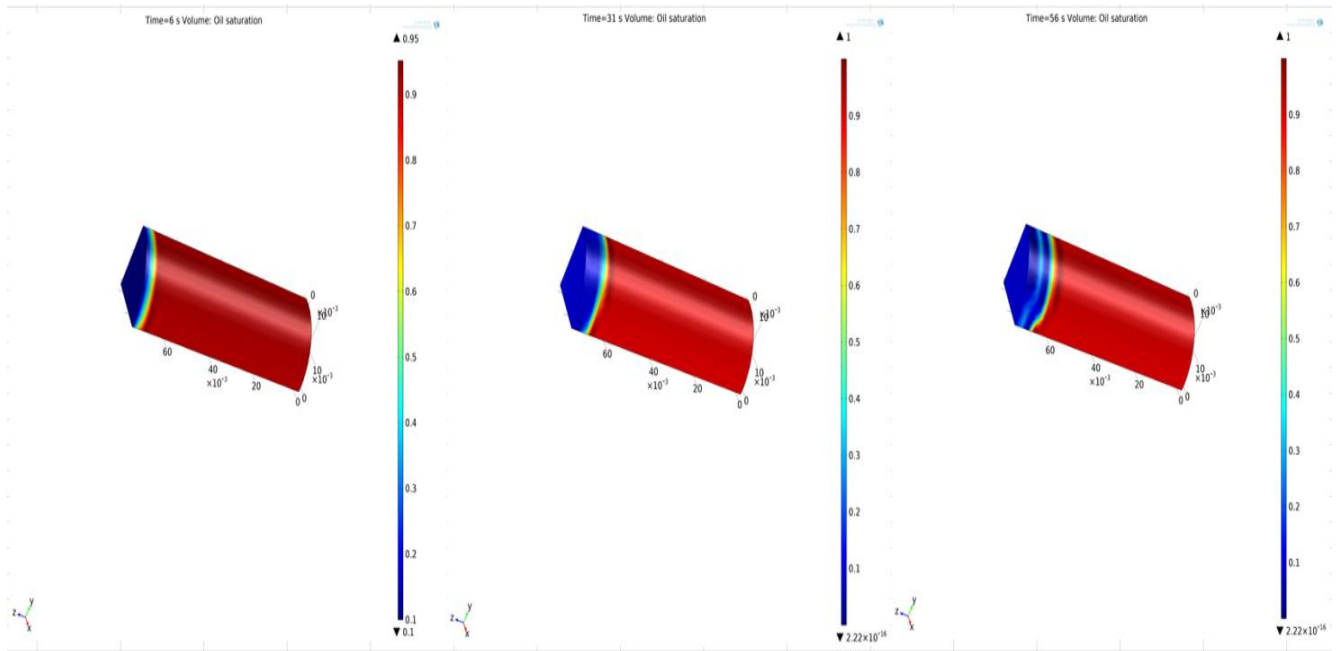


Figure 4-49. Oil saturation profile versus time within matrix. Brine front progresses after 6, 31 & 56 seconds from left to right.

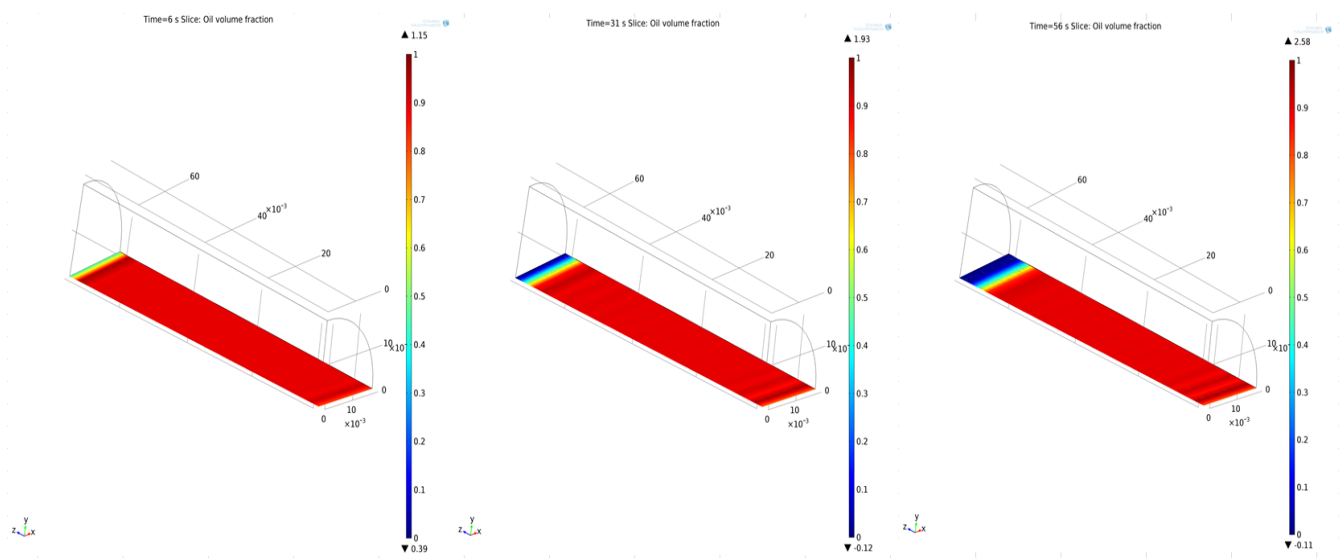


Figure 4-50. Oil saturation profile versus time within fracture. Brine front progresses after 6, 31 & 56 seconds from left to right.

Such coupled modelling analysis would provide matrix and fracture flow results similar to the single phase scenario study (Fig. 4-51). However interpretation of these outflow results should take brine breakthrough time into account.

Brine breakthrough is the fact clarifying when the matrix or fracture outflow switches from oil production to brine production.

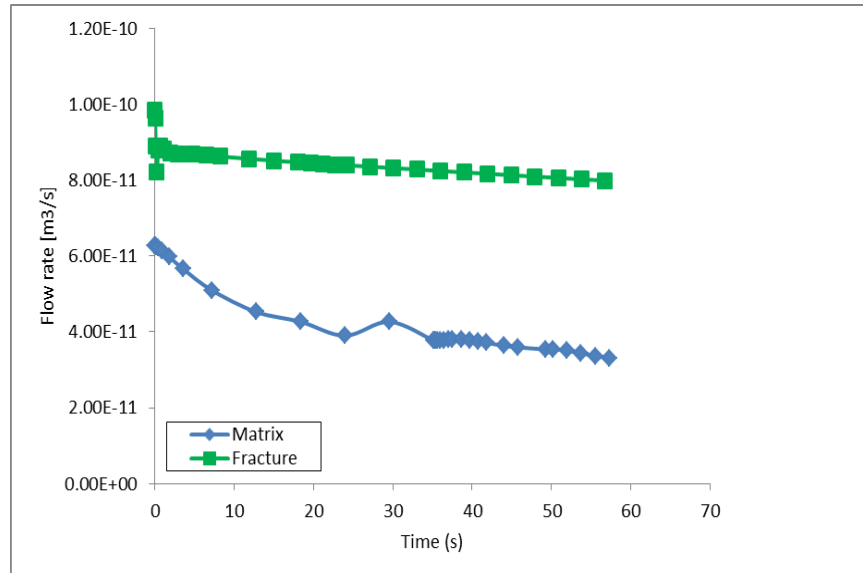


Figure 4-51. Two-phase flow fracture and matrix flow partitioning for the oil phase.

The illustrated coupling strategy demonstrates how the numerical coupling of the physics can be extended to multiphase scenarios. It is worth mentioning that as the multi-phase analyses require more constitutive physics to be coupled, the numerical computation effort for large scale problems can be significantly excessive. Developing empirical coupled models such as those provided for the single phase scenario can assist to overcome such concerns; however, the empirical formulations would need to be validated against laboratory data before application.

Coupling strategies adopted in this chapter along with the developed empirical models require validation against laboratory data in order to be qualified for further up scaling. The following chapter will focus on the design of a special core analysis rig capable of providing laboratory validation data on fracture-matrix flow partitioning. Moreover, single phase laboratory analysis of flow under various overburden stress levels is provided for a fractured Buff Berea sandstone core plug. The laboratory results are compared with the numerical findings to evaluate their reliability.

Chapter 5.0

Laboratory analysis of matrix-fracture flow interaction under mechanical loading conditions

5.1 Introduction

Adopted coupling techniques of various flow models to the structural mechanics and poro-elasticity within the fractured core plug flooding scenarios discussed in chapter 3 and 4, demands a laboratory validation. Furthermore, the developed empirical correlations should also be evaluated against laboratory data in order to be considered reliable for up scaling.

Laboratory validation of the numerical simulations required distinct measurement of fracture and matrix flow during a fractured core plug flooding under overburden stress. Lack of any appropriate experimental procedure along with absence of a capable core flooding rig, has initially been drawn to attention through the literature review of the current research. Therefore there was a need to design and implement a fit to purpose flooding rig; performed coupled numerical analyses enabled designing rig elements specifications and definition a proper laboratory procedure.

This chapter discloses the design of the special fractured core analysis rig which enables analysis of fracture-matrix flow partitioning. In addition, the chapter discusses experimental investigation of fractured core flooding. Having achieved a capable flow partitioning measurement rig and procedure, authenticity of the developed empirical matrix and fracture flow models were evaluated.

5.2 Laboratory fractured porous media flow analyses background

As previously discussed in chapter 2, laboratory techniques applied in fractured porous media flow investigations so far can be categorized into two major types.

First category involves characterising fracture flow by utilizing variety of natural and artificial glass-made fracture planes (Chen, 2005). Although fracture flow can be characterised comprehensively using this technique, effects of rock matrix hydraulic interaction and consequently hydraulic interaction alteration due to overburden stress change cannot be investigated thoroughly in this category of laboratory studies.

On the other hand, there were several fractured core flooding analyses reported in the literature characterising hydro-mechanical behaviour of fractured core plugs as unified double porosity or double permeability porous media (Polak et al., 2004; Wang et al., 2011). This category of laboratory studies cover the rock matrix and fracture hydraulic interaction and considered as more realistic fractured reservoirs characterisation technique. However, flow characterisation is a cumulative result of both matrix and fracture specifications in this category; consequently, distinguished hydraulic contribution of matrix and fracture is not the focus of this laboratory analysis category.

Therefore in order to obtain laboratory data relating to fracture and matrix flow contributions while flooding under overburden stress, there was a need to design a novel flow analysis rig.

5.3 Core flood Rig design and implementation

Conventionally routine core analysis set-ups are used to characterise hydraulic storage and conductivity of various reservoir rock types including fractured ones. However, investigation of fractured plugs flow dynamics requires specific attention to several issues due to the additional physics involved.

Presence of fracture as a conductive flow path jeopardizes a desired sweep efficiency over the complete core plug length. Matrix-fracture hydraulic interaction can be immature due to fluid early breakthrough via fracture. Increased overburden stresses and consequent fracture aperture reduction constrains fracture conductivity; limited fracture conductivity supports improved sweep efficiency in permeable rock matrix however, it is of prime importance to monitor the flooding front in order to ensure flow exchange from matrix into the fracture at the matrix-fracture interface and characterise developed flow regimes.

It was decided to use a special core holder that benefited from several pressure ports at 1 inch spacing along its length to enable efficient monitoring of flooding front progress. The differential pressure transducers mounted on these pressure ports indicate the pressure disturbance front movement along the flooded core plug. This functionality eliminates the need for a CT scanning device implementation that can be significantly costly.

Transducers reading range specification was another challenging task in laboratory set-up design stage. The complexity of specifying appropriate transducers for fractured plugs flooding rises from the significantly reduced differential pressures observed across the flooded plug due to the enhanced fracture conductivity. Accordingly very low-range differential pressure transducers are required to be implemented on the flow line to achieve reliable measurement accuracy. On the other hand, overburden stress loading and saturation procedure requirements demand significant line pressure tolerance for transducers. This enormous difference between the transducers' measurement range and line pressure specification results in a challenging core flooding operation.

The coupled sensitivity analyses discussed in chapter 4 provided the guidelines for differential pressure transducers measurement range specification.

Differential pressures were monitored in the simulations along the plug length and extreme pressures observed in the pressure ports were taken into consideration. Different range of differential pressure transducers were implemented on the rig to provide differential pressures in equal spacing along the flooded plug as well as across the whole flooded plug considering a reasonable safe margin over the numerically observed differential pressures. Moreover, all the differential pressure transducers were protected using shut-off valves across them. Such a consideration conveniently permitted saturation of the plugs and over-pressure security of the transducers. These shut-off valves also facilitate testing core plugs with various lengths appreciating the maximum length of 12 inches for the plugs with constant diameters of 1.5 inches. It is worth mentioning all the analysed tests in this dissertation were examining 1.5 inches diameter and 3 inches length core plugs.

In accordance with the numerical simulations, sandstone plugs were cut longitudinally into halves to generate a smooth artificial fracture within the plug in laboratory (Fig. 5-1) prior to performing any flooding test.

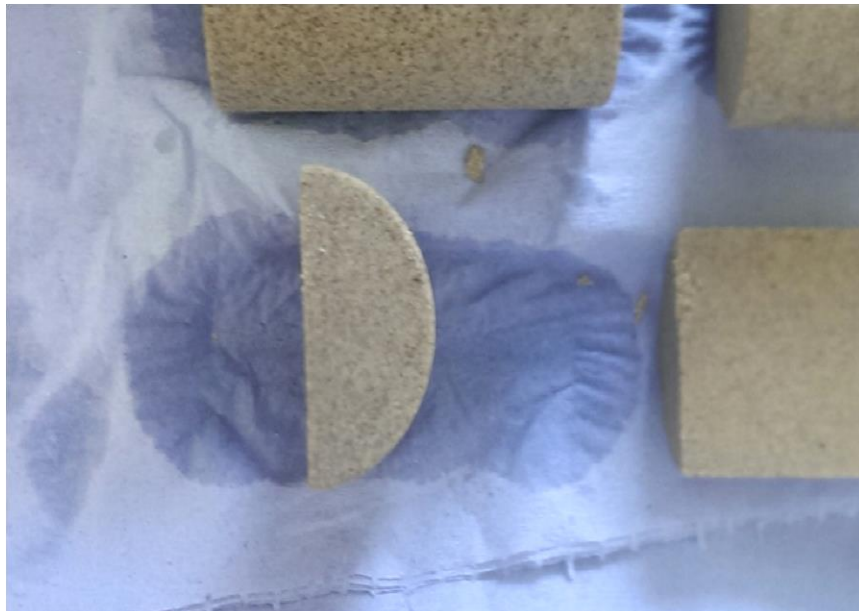


Figure 5-1. Cut core plugs. Fracture is artificially created by cutting core plugs in halves longitudinally.

Steel shims were set initially at the edge of the fracture plane providing the initial fracture aperture size and preventing total closure of the smooth-walled fracture under loading conditions (Fig. 5-2). Two metallic shims were set symmetrically on the half plugs' edges to form an open fracture when the whole fractured plug was being set for flooding within the core holder sleeve.



Figure 5-2. Set metallic shim. Metallic shims were set symmetrically on the plug halves' edges. Note the attachment of flow accumulating cap (Left) to the sandstone plug (right) and use of the shims on the metallic plug as well as the sandstone plug.

To fulfil the requirements of measuring fracture and matrix flow separately, two metallic flow accumulating plugs were designed and machined (Fig. 5-3). These flow accumulating plugs were glued using an epoxy resin to the sandstone plugs (Fig. 5-4) and subsequently inserted into the core holder sleeve for each flooding test. Metallic flow accumulating plugs' wall thickness, material and machining technique were considered resilient enough to accommodate the increased overburden pressures while high pressure flooding. The plugs were intentionally designed to collect the outflow from the sandstone plugs. Since the accumulating plugs access screws are seal-tight while flooding, the collected matrix flow was preserved inside the accumulating plug until termination of each test. Having performed an individual flooding test, the accumulating plugs are retrieved and the collected

matrix flow is measured. Any amount of flow produced from the core holder while flooding is measured as the fracture flow. This technique enabled distinct measurement of fracture and matrix flow for any investigated stressed core flooding test.

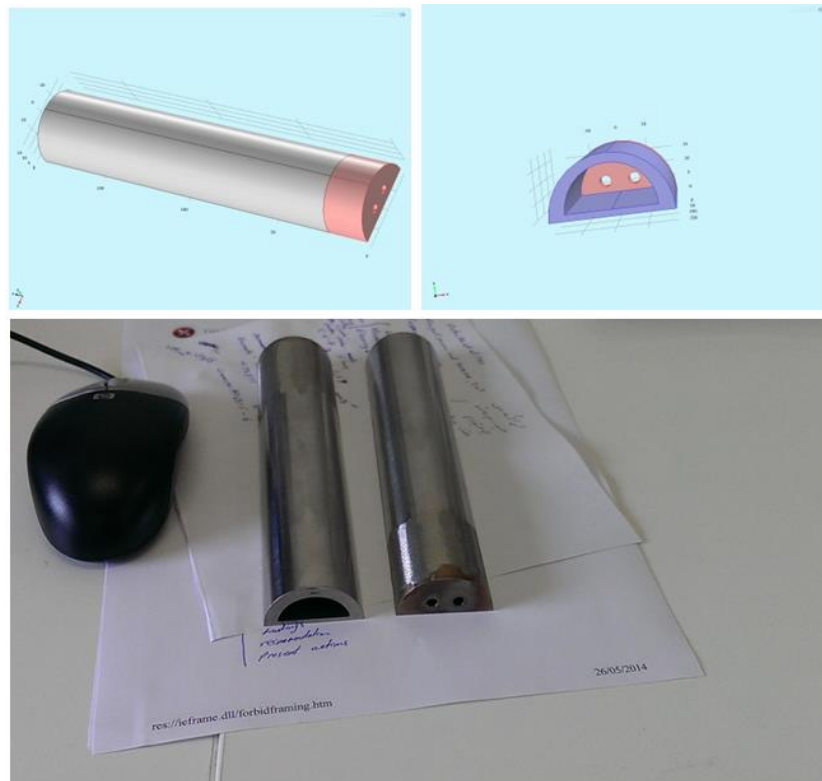


Figure 5-3. Metallic flow accumulating plugs.

It is worth mentioning that the open end of the accumulating plugs are glued to the sandstone plugs and serve as the inlet for collection of matrix flow. A single pair of flow accumulating plugs can be used iteratively for analysing numerous core plugs' hydro-mechanical behaviour.



Figure 5-4. Sandstone half plugs attached to the flow accumulating plugs ready for flooding test.

Having developed a laboratory technique of measuring matrix and fracture flow associated with flooding front monitoring capability utilizing several differential pressure transducers, fractured cores flooding rig was designed, built and pressure tested. As evident from Fig. 5-5, the rig is augmented with an accumulator that not only dampens the HPLC pump pressure pulses but also safeguards the pump through prevention of the flooding fluid contact with the sensitive pump pistons. Augmentation of the rig with accumulator facilitates multi-phase flow experiments which are beyond the scope of this research.

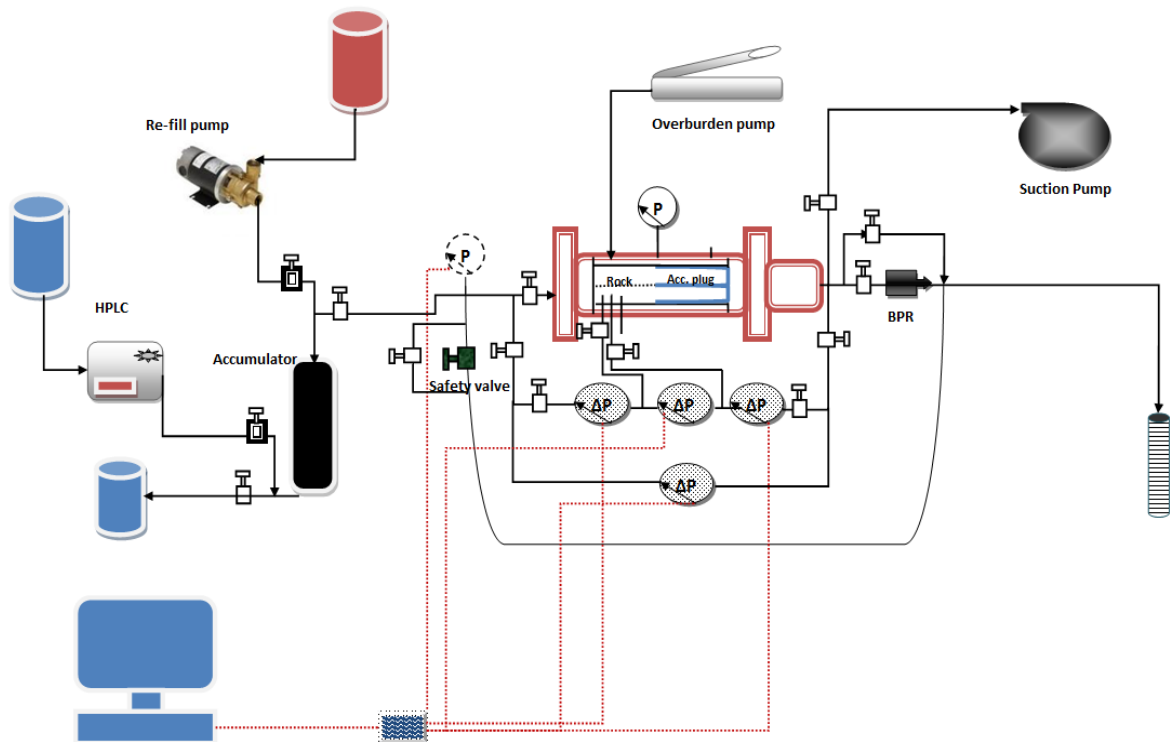


Figure 5-5. Core flood rig design. Designed and implemented rig used to analyse flow behaviour of fractured core plugs under overburden stress loading.

Mounted manual pressure gauges equipped with digital pressure monitoring capability enables data gathering, recording and analysis. Differential pressure transducers' specifications were considered based on the numerical analyses results. All the differential pressure transducers as well as the line pressure transmitter readings were digitized by means of Labview software to provide the controlling functionality for the rig operator. Manual gauges in addition to the mounted safety valve and several transducers protection shut-off valves, ensure the safe operation of the rig in high pressures. Technical and operational excellence of the rig was acknowledged by the Scotland Chartered Quality Institute (CQI) 2014 award.

The implemented rig is equipped with an electric re-fill pump that charges the accumulator with the flooding fluid initially; consequently, an HPLC pump pressurizes the accumulator fluid content to be injected into the core holder. The core holder itself is pressurized externally by a hydraulic hand pump to exert up to 5000 psi overburden stress on the core plugs enclosed in the core

holder sleeve. Line pressure and differential pressures across core holder pressure ports are monitored while flooding on a computer (Fig. 5-6). An implemented back pressure regulator enables the rig operator to perform the experiment at any desired pore pressure up to 2000 psi.

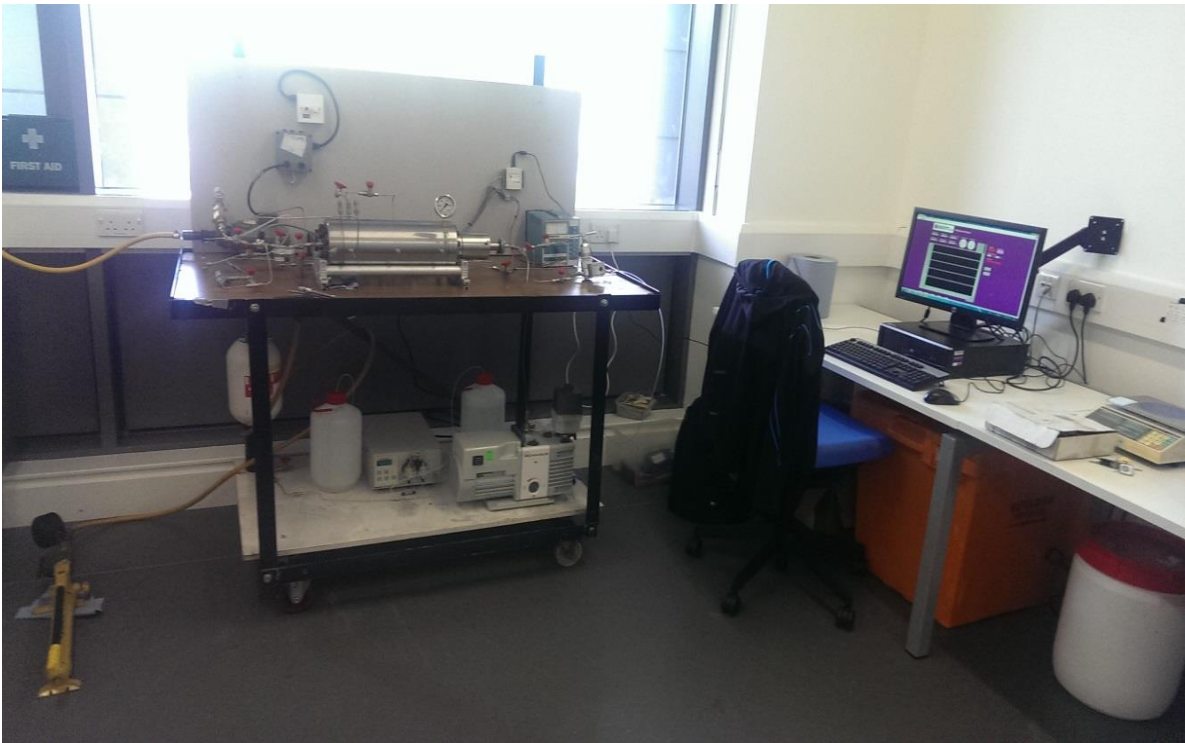


Figure 5-6. Core flood rig equipped with digital pressure monitoring. Differential pressures are monitored digitally and line pressure is monitored both digitally and manually for safety.

5.4 Matrix-fracture flow partitioning laboratory analysis procedure

Having implemented and pressure tested the SCAL rig, measurement of fracture-matrix flow partitioning in laboratory flooding analyses under various overburden stress loading were made convenient to perform. These experiments enabled evaluation of the developed empirical models derived from applied sensitivity analyses reported in chapter 4.

Buff Berea sandstone core plugs were considered appropriate to perform the laboratory analyses due to their proper homogenous permeability (300 – 400 mD) and rather high uniaxial compressive strength of 3800 psi, suitable for overburden stress loading conditions; On the other hand, this sandstone has close porosity and permeability values to the Clashach sandstone used in the benchmarking published paper and utilized for validation of the numerical approaches in chapter 3. Furthermore, the other hydro-mechanical characteristics of the Buff Berea core plugs which is reported in Table 5-1, fall within the examined range in the numerical sensitivity analysis which served as the foundation of the developed empirical models and therefore the models should be able to predict the stress-related production from these core plugs.

5.4.1 Plug samples physical properties

Plug samples porosity and permeability were measured by the supplier prior to splitting them in order to generate the artificial fractures. Physical properties of the laboratory tested plugs are provided in table 5-1. Plugs were cut using precision cutting machines which give zero kerf down the middle and consequently smooth fracture walls and constant fracture aperture throughout the whole plug length.

Table 5-1. Buff Berea sandstone plugs and laboratory used brine specification.

<i>Buff Berea plugs & Brine specification</i>	
Plugs diameter	3.81×10^{-2} m
Plugs length	7.65×10^{-2} m
Porosity	22%
UCS	3800 Psi
Permeability	200 mD
Poisson's ratio	0.17
Young's Modulus	14.6×10^9 Pa
Brine Density	1020 Kg/m ³
Brine Viscosity	4.45; 4.20 cp
Initial fracture aperture	160×10^{-6} m

Rock mechanical data of the plugs also needed to be measured in order to account for these parameters effect in the empirical fracture and matrix flow models validation. Plugs dimensions and weight were initially measured prior to compressional and shear sonic wave velocity measurements. Consequently the Young's modulus and Poisson's ratio were calculated using equations 5-1 and 5-2 (After Mavko et al., 1998).

$$\nu = \frac{V_c^2 - 2V_s^2}{2(V_c^2 - V_s^2)} \quad (5-1)$$

$$E = \frac{\rho V_s^2 (3V_c^2 - 4V_s^2)}{V_c^2 - V_s^2} \quad (5-2)$$

V_c and V_s represent compressional and shear wave velocities respectively. Fig. 5-7 provides the sonic measurements driven rock mechanical data used in the laboratory analyses.

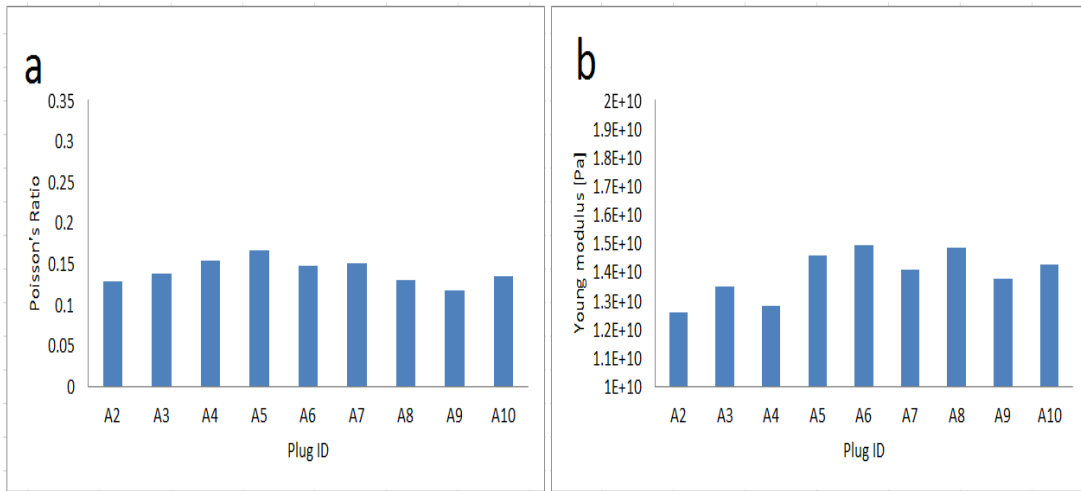


Figure 5-7. Rock mechanical properties of Buff Berea sandstone. a) Poisson's ratio and b) Young's modulus.

5.4.2 Brine preparation

To achieve a realistic production scenario in the core flood laboratory experiments, it was decided to use a formation water composition in preparing the flooding fluid. Therefore a reported North Sea formation brine composition in the literature which was previously utilized in Berea sandstone core flooding was selected (McGuire et al., 2005). The brine composition is provided in Table 5-2.

Table 5-2. Brine composition after McGuire et al., 2005.

<i>Brine composition</i>	<i>mg/L</i>
Na	5626
K	56
Ca	58
Mg	24
Cl	8249
HCO ₃	1119
SO ₄	16

The prepared North Sea formation brine was analysed and its rheological data is reported in table 5-1. This brine was used for all laboratory flooding tests in ambient temperature reported in this dissertation. All the wet parts of the rig, including the core holder internal sleeve and gaskets, were considered resilient to corrosiveness of the applied brine in ambient temperature. These wet parts were also compatible for mineral oil flooding in increased temperatures in order to provide the possibility of multi-phase flooding in further sophisticated analyses beyond scope of this research.

5.4.3 Laboratory fractured core flooding tests

Having prepared the brine, the first step in running laboratory flooding tests was to seal-attach the flow accumulating caps to the half Buff Berea plugs. Robust resin epoxy glue was applied to attach the open end of the accumulating plugs to the half core samples giving the resin epoxy an appropriate acting time of at least 24 hours. Resin epoxy adhesive was precisely applied not to leave any residual on the outer periphery of the attachment position; any epoxy residual would either leave a gap between the core holder sleeve and the plugs or reduce the fracture aperture size.

Metallic shims with specified thickness, equal to initial fracture aperture size (160 Micron for current analyses), were set along the sandstone plugs as well as the accumulating caps in order to provide a constant initial fracture aperture size throughout the whole length in the second step. Same resin epoxy adhesive was utilized in setting the shims. Shims were set on opposing longitudinal edges of half-core plugs capped with the accumulating caps as can be seen in Fig. 5-4.

Having capped the half-core plugs with the accumulating plugs and set the metallic shims, the samples were ready for saturation. The accumulating plugs' screws are removed in the saturation phase to allow complete saturation of the sandstone plugs. Buff Berea plugs were put under vacuum overnight prior to flooding under high pressure (approximately 2000 psi) for at least 24 hours.

After achieving an efficient saturation, the accumulating plugs' screws were fitted and the desired flooding tests under overburden stress loading were run. Figure 5-8 demonstrates the initial and boundary conditions of the desired tests after achieving complete saturation of the core plugs. An HPLC pump was providing the injection pressure which maintained equal to the intended pore pressure magnitudes across core plugs (1.5" diameter and 3" length) using a back pressure regulator just before the flooding outlet line. The overburden stress was exerted using a hydraulic hand pump. Sandstone plugs were 3 inches long and differential pressure along them was monitored by three transducers in 1 inch spacing.

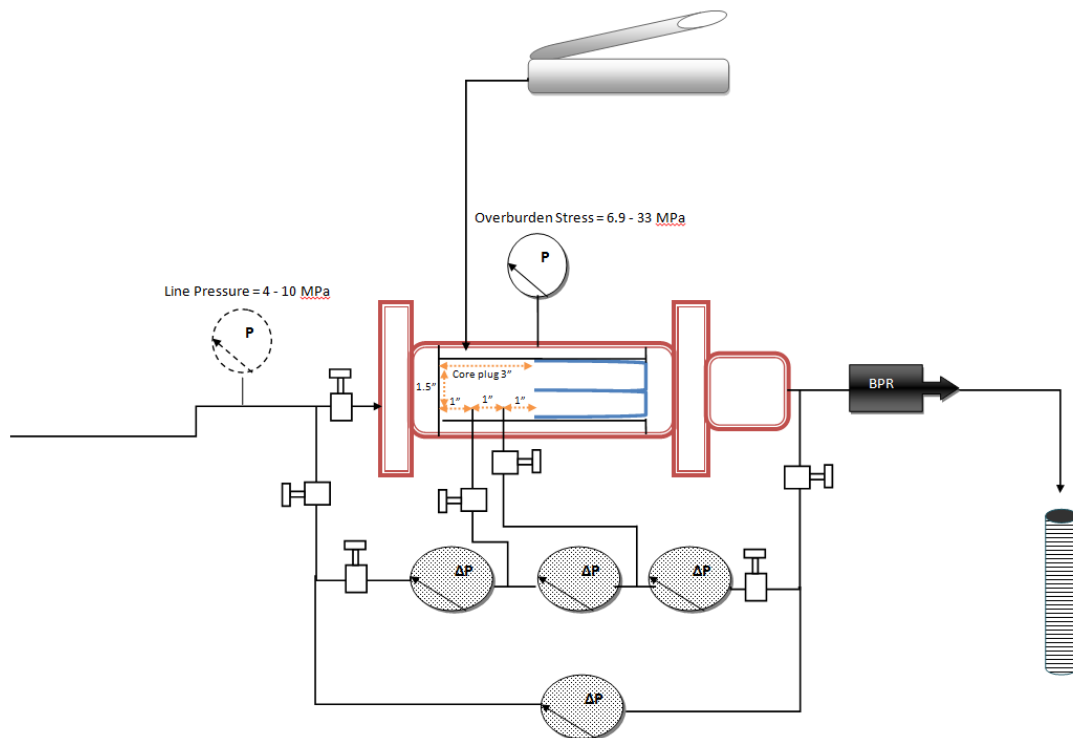


Figure 5-8. Laboratory implemented initial and boundary conditions for the flooding tests.

It takes a while for the pressure front to sweep the whole core plug length prior to matrix production initiation into the accumulating plugs. Although the core plugs were completely saturated prior to the tests, fracture channel

necessitates to be filled before less permeable plug matrix commences flow intake. For each flooding test, the pressure front was monitored based on interpretation of differential pressures data as can be inferred from Fig. 5-9.

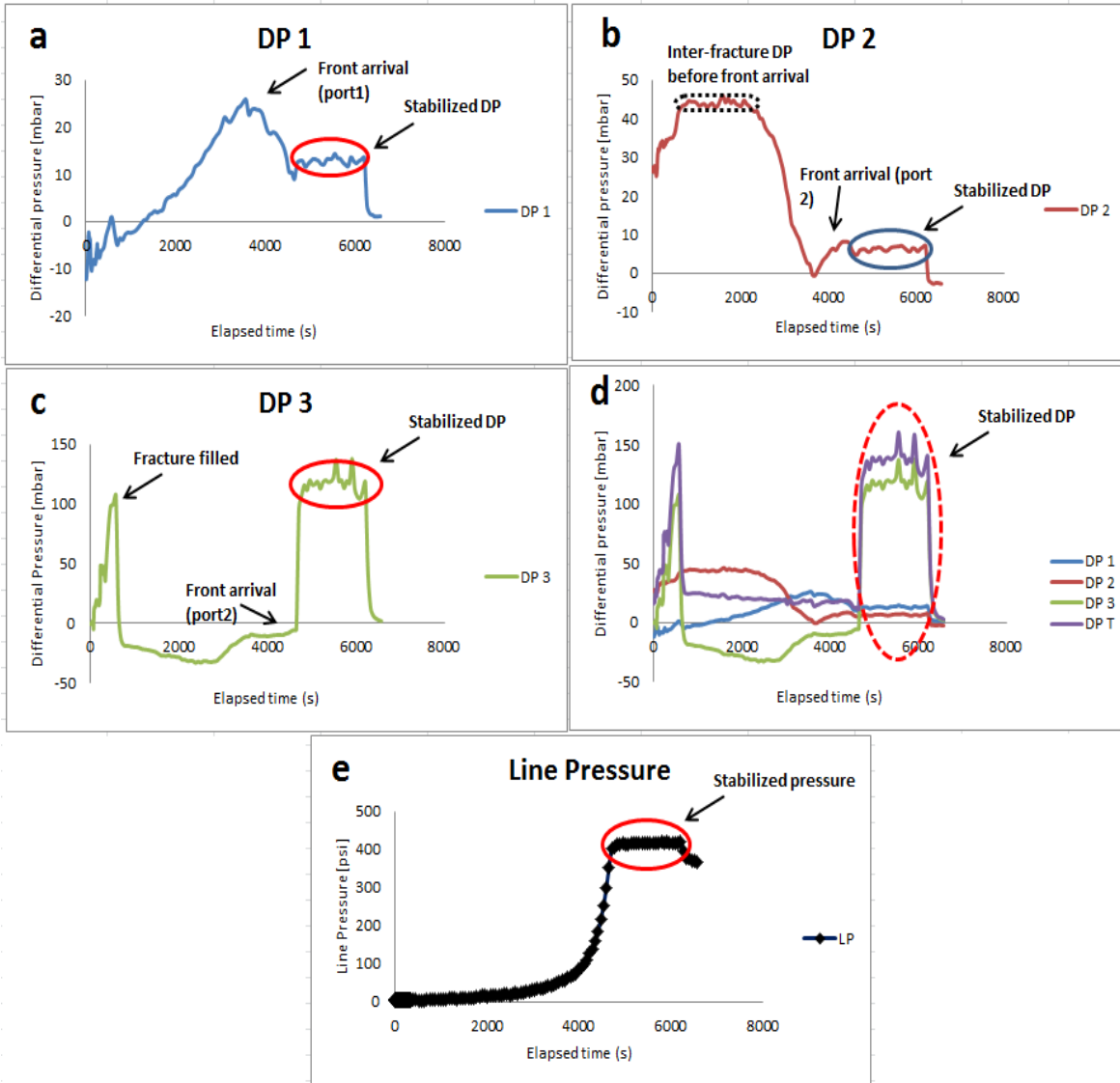


Figure 5-9. Typical differential pressures while flooding. a) differential pressure 1, b) differential pressure 2, c) differential pressure 3 d) all differential pressures including total differential pressure (DP T) and e) line pressure

DP 1, DP 2, DP 3 and DP T in Fig. 5-8 indicate differential pressure between core holder inlet and first pressure port, between first and second pressure port, between second pressure port and the core holder outlet and the

cumulative differential pressure over the whole plug respectively. The first pressure port is positioned at one inch spacing from the core holder inlet and this spacing is maintained between the pressure ports along the core holder length as demonstrated in Fig. 5-8.

During a flooding test, fluid stream initially bypasses the core plug via the more conductive fracture space, even though the fracture aperture is reduced as a result of overburden stress loading; This is happening due to the fact that fracture space is not saturated initially and the line pressure hasn't been build up completely. Consequently, DP 1 reads a negative value initially in Fig. 5-9a (note the line pressure build up trend in Fig. 5-9e). It is worth mentioning that fracture filling and consequent fracture flow commencement at the outlet takes a short time to accomplish. DP 3 which is the indication of differential pressure between the last pressure monitor port and the core holder outlet would clearly reveal when fracture filling occurs. It is the time at which DP 3 suddenly reads negative values after an initial rising trend (Fig. 5-9c). This is due to the fact that flow stream at this time breakthrough outlet while pressure front hasn't reached the 2nd pressure monitoring port within the matrix yet; hence a negative differential pressure. When the fracture space was filled completely with brine, due to the presence of back pressure regulator at the outlet of the core holder, line pressure build up occurs from the outlet towards the flow inlet. Hence, the negative pressure drop indicating a reverse flow direction toward the last pressure port (Fig. 5-9c).

As the pore pressure starts to build up (Fig. 5-9e) flow stream starts sweeping through the matrix pore volume and stable differential pressures are developed. All the monitored differential pressures follow an ascending trend until the point at which the fluid stream pressure front reaches the corresponding outlet port for which the differential pressure is monitored. At this time the differential pressure stabilizes. For the flooding case shown in Fig. 5-9, the pressure front arrived at first pressure monitoring port at about 3500s (Fig. 5-9a) and the second port at about 4000s (Fig. 5-9b). The initial differential pressure plateau evident in Fig. 5-9b, indicates the inter-fracture bypassed flow driven differential pressure between the first and second pressure monitoring ports prior to arrival of the pressure front in Berea sandstone plug matrix.

DP 3 exhibits the differential pressure between the second port and the outlet of core holder and since the rate of pore (line) pressure increase is faster than the pressure front movement along the Buff Berea matrix, the outlet pressure is higher, hence a negative reading prior to arrival of the pressure front at the second port. As a matter of fact, arrival of the pressure front at the second port is more visible in DP 3 readings (Fig. 5-9c) as a sharp increase to the stable differential pressure plateau. Achieving stable differential pressures (Fig. 5-9d) in combination with the stabilization of pore pressure ensures matrix flow initiation. As evident from Fig. 5-9d and Fig. 5-9e, this flow dynamic state has been reached at approximately 5000s for the typical case reported in the figure.

It is extremely important to reach this stabilized differential pressure window among all transducers' readings to ensure that the matrix is flowing into the accumulating plugs and fracture flow is calculated from that point in order to be compared with the matrix flow. The time interval of the discussed stabilized dynamic state was recorded to provide the flow rates which can consequently be validated against numerical findings. Based upon test specific flow rate and the capacity of the accumulating caps, the measurement time interval should have been defined in a way not to pressurize the accumulating caps excessively and cause a backflow into matrix or fracture from the plugs. This measurement window was maximum 45 minutes within our experimental set-up specification considering a safe operating margin.

Having measured matrix flow (through time recording and subsequent retrieval of the accumulating plugs) and fracture flow (outflow of the core holder within the measurement interval) rates, the last step is to depressurize the core holder to retrieve the accumulating plugs and finalize matrix flow measurement. When the samples are retrieved, the accumulating plug screws are unscrewed and the matrix flow rate is calculated based on the time recorded and the plugs content measurement.

The pore pressure at which the stabilized dynamic state is achieved depends on several factors among which are the test flow rate and the overburden stress. Several flooding tests covering a range of overburden stress loadings

have been analysed and their data are compared in the next section with the provided empirical models' predictions.

5.5 Experimental analysis results and empirical models validation

Matrix-fracture dynamic flow interaction has been analysed in laboratory following the previously discussed procedure for saturating and flooding through the Buff Berea sandstone core plugs. The tests were run for several overburden stress loading scenarios to investigate how overburden stress affects fracture-matrix hydraulic exchange. Twenty flooding tests were performed in total for various overburden stresses and pore pressures. Successful tests provided similar flow partitioning results. Therefore typical representation of a successful series of tests on a single core plug is investigated in this chapter. Successive tests with variable overburden stress loadings on a single core plug is a major laboratory challenge as the core sample undergoes persistent creep under each loading and flooding test and considering the fact that any subsequent test cannot be performed less than 48 hours from the previous test, due to the need for re-saturation, the core plugs mechanical strength would be adversely affected. On the other hand, the same core plug should be tested under different loading scenarios in order to maintain the plug characteristics such as porosity and permeability in an attempt to examine the effect of overburden stress on matrix – fracture hydraulic interaction.

Laboratory flow measurements for an identical core plug are provided in Fig. 5-10. As evident, matrix flow increases as the overburden stress increases while fracture flow decreases significantly in response to excessive overburden stress loading.

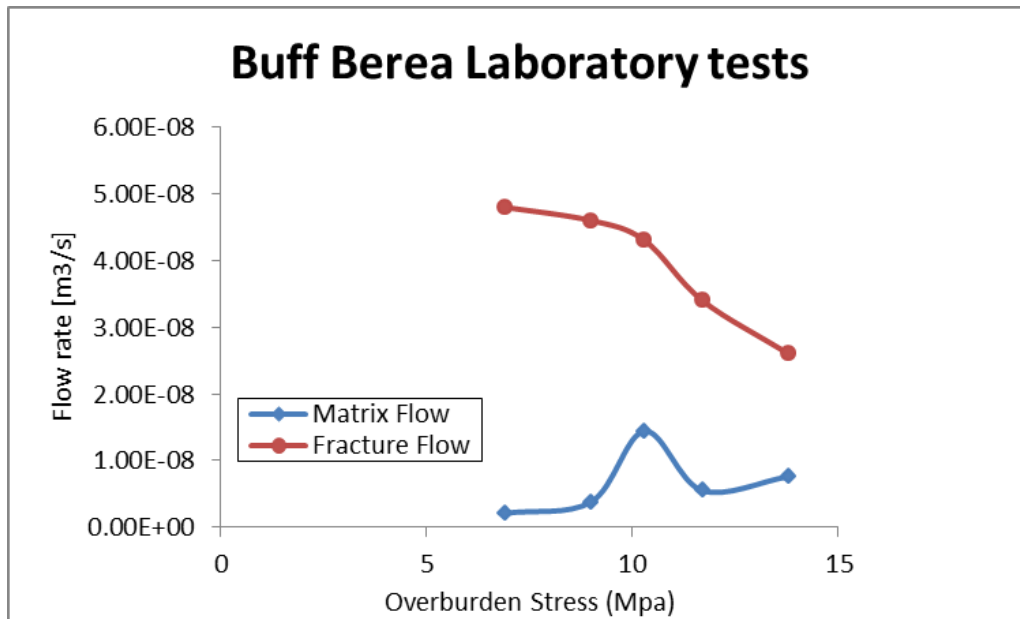


Figure 5-10. Matrix and fracture laboratory flow measurements.

The abnormal measurement observed at 10.3 MPa overburden stress is due to the larger test flow rate and consequently enhanced differential pressure over the plug length. Operational difficulties prevented the test to reach a stable flow for this stress level at the desired reduced flow rate similar to the other stress loading test cases shown in Fig. 5-10. Despite the fact, fracture flow did not show an abnormality corresponding to the higher flow rate. It is inferred that fracture flow is more dependent on the overburden stress, and consequently fracture aperture, rather than the experiment flow rate.

It is worth mentioning that even for the same core plug, the measured matrix and fracture flow rates were cumulative results of overburden stress, differential pressure and pore pressure simultaneous alteration. Due to the very low differential pressure rating of the transducers, it was difficult to keep pore pressure constant for all the stress loading tests. In fact, any minor increase of the pore pressure was causing a back pressure on the transducers that could damage the transducer diaphragm if not controlled; on the other hand, as soon as stable differential pressures were achieved and the pressure disturbance front swept all the core plug pore volume, the measurement should take place since matrix flow into the accumulating plugs is initiated.

Consequently the desired pore pressure should have been achieved with extra care and in very small increments.

Obtaining laboratory flow partitioning measurements provided the chance to validate the empirical models, discussed previously in chapter 4, efficiency. Fig. 5-11 and Fig. 5-12 provide the comparison of the matrix and fracture empirical models flow predictions with the laboratory measurements respectively. As can be seen, the Matrix flow model could predict matrix flow contribution appropriately within a 16% error margin.

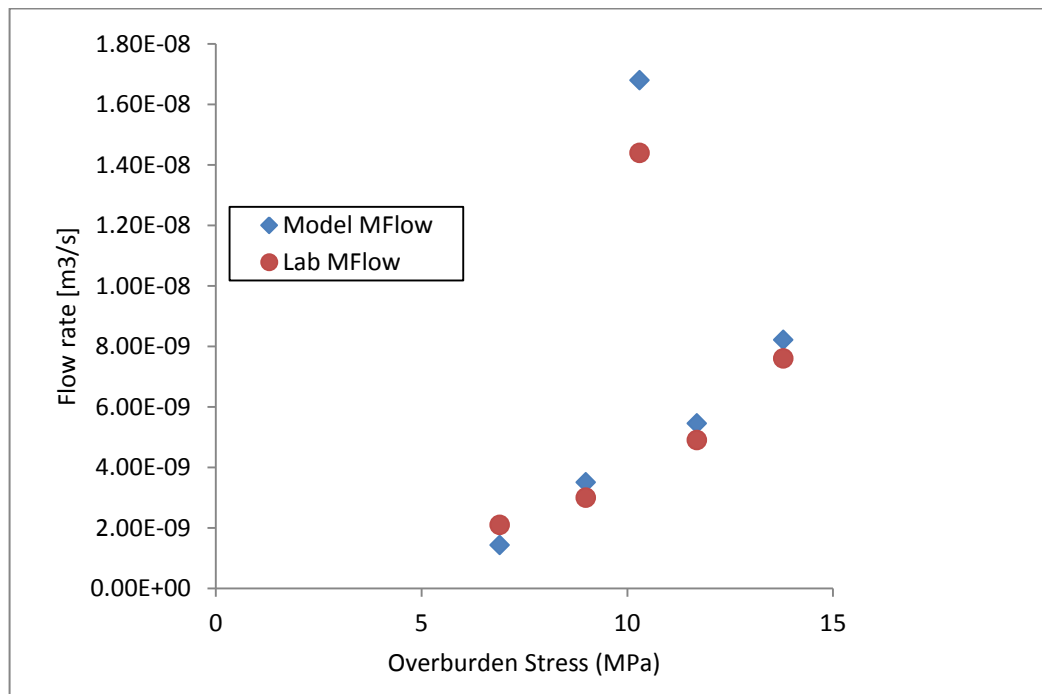


Figure 5-11. Matrix flow model evaluation. Comparison of the model prediction with laboratory data.

The reliability of the empirical matrix flow model (Eq. 4-1) is further supported by considering the fact that overburden stress has little effect on matrix flow accounted for using the stress dependent permeability equation. As a result, matrix flow quality is dominated by Darcy's law and the empirical model can accommodate the stress effect reasonably.

In contrast to matrix flow model, fracture flow model predictions are not as much accurate. In fact, fracture flow model overestimated actual fracture flow measurements by one order of magnitude. This discrepancy, observed among all laboratory tests, challenged the reliability of the developed fracture flow model. This model should undergo more numerical refinement to provide more accuracy.

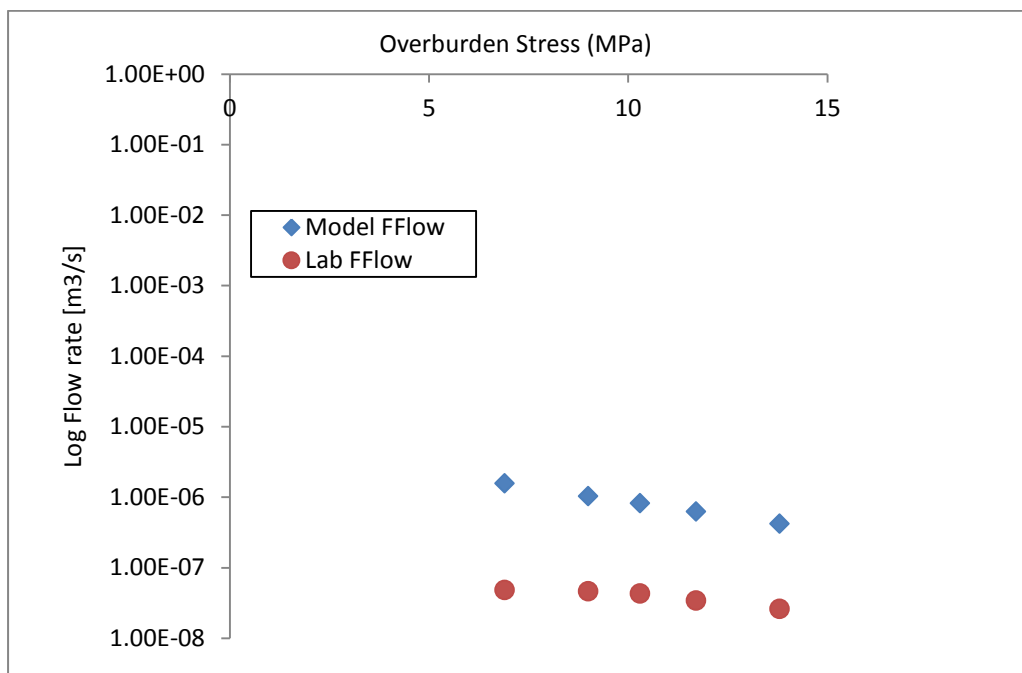


Figure 5-12. Fracture flow model evaluation. Comparison of the model prediction with laboratory data. Note the logarithmic scale of the flow rate axis.

In addition to the uncertainties imposed from estimating Biot-Willis coefficient, instead of its direct laboratory measurement, the main source of imperfect fracture flow model prediction can be the averaging technique applied in fracture aperture calculations within the coupled sensitivity analyses. A planar averaging strategy on the fracture-matrix interface plane was adopted for the current research; however, such technique seemed to be inadequate. A careful consideration of fracture aperture effect on fracture flow reveals that, inaccuracy in determining fracture aperture size affect the fracture permeability by a power of three as can be seen in Eq. 2-6. Therefore a better averaging procedure can be implementing average fracture permeability

magnitudes instead of averaging fracture aperture size. This can be achieved through computation of local fracture permeability values based on local fracture aperture change, e.g. near the shims and at the core plug's centreline, and then implementation of these local permeability values into the flow equations. This technique can be useful specifically if fracture surface visualization scanning devices are available.

Furthermore, a proportion of sand particles was visible in both matrix and fracture flux during all the tests, while no sand particle transport has been taken into consideration in formulating the analytical governing equations of the coupled numerical analyses in chapter 3 and 4. The produced sand in the fracture flow measurements is most likely a result of fracture-matrix interface mechanical failure under overburden stress. Detachment of these particles is expected to cause a variable fracture aperture over the fracture-matrix interface which hasn't been accounted for in the sensitivity analyses.

On the other hand, running a coupled numerical simulation such as the one applied in chapter 4 analyses, would be so time consuming and not feasible for some of the laboratory tests. Lack of numerical modelling possibility is due to the fact that for some excessive overburden stresses the fracture walls' vertical displacement average exceeds the initial fracture aperture and hence no possibility of fracture flow calculation; while in the laboratory experiments, the overburden stress can be counteracted partially via reaction forces created at the grain to grain contact area of opposing fracture walls and often the immediate aperture in the vicinity of the shims remains open. Therefore it is necessary to further enhance the quality of introduction of stress driven fracture aperture variation to the fracture flow calculations in the sensitivity analyses.

An extensive laboratory analysis can assist in adoption of the best way to couple the fracture walls displacement to the fracture flow equations. Another alternative would be composing a discretized formulation that can be introduced as a sub-routine to COMSOL subsurface module that enables applying exact displacement per grid within every calculation step for all the matrix-fracture interface grids; this would add to the numerical complexity of the simulations though.

In addition to the discussed limitation of the empirical models, special attention needs to be paid into the fact that in order to apply the empirical models in a reservoir simulation scenario more complex fracture network consisting of intersecting, hydraulically connected fractures should be investigated in the sensitivity analysis in order to achieve universal empirical models. Moreover, the discussed workflow assumes that the reservoir model is a dual permeability model and rock matrix can be producing as well as the fracture network; as a result, the adopted procedure of developing the empirical models may not be valid for tight carbonate reservoirs which rely only on the fracture network for hydrocarbon production.

Although such comprehensive laboratory review or sub-routine composition is beyond the scope of this work, the well-equipped laboratory set-up is now available and the matrix flow model proved to be efficient to be applied in mechanically coupled flow scenarios of fractured porous medium. The fracture flow model provides the similar trend of variation under overburden stress as the fracture flow laboratory measurements and can be further improved for enhanced efficiency taking the advantages of a comprehensive laboratory analysis that can specify the best averaging technique for stress-driven fracture aperture variation coupling to the flow equations.

Chapter 6.0

Discussion, Conclusions and Recommendation for Further Research

6.1 Introduction

In this chapter, technical challenges encountered at each stage of geomechanical analysis of flow partitioning between rock matrix and fracture volume are evaluated in order to highlight the rationale behind the adopted numerical coupling and laboratory strategies. The chapter also sets the scene for further promotion of the analysis taking the advantages of developed numerical and laboratory infrastructure to enhance the reliability of empirical models.

Physics coupling techniques applied in the open fracture concept is discussed first, followed by the evaluation of the methodology leading to the empirical models development. Consequently, the laboratory challenges which could have influenced the deviation between the empirical models' predictions and laboratory measurements are discussed. Finally the research results are summarized followed by further research opportunities that worth being pursued to achieve more reliable models specifically for fracture flow to conclude the chapter.

6.2 Discussion

6.2.1 Coupling techniques of open fracture modelling approach

Due to lack of any existing core flood experimental data on isolated fracture and matrix outflow, it was decided to apply the most reliable coupled physics in simulations of chapter 3 and compare the cumulative outflow calculated from simulation to the laboratory data on a fractured core plug flooding which was available in the literature.

Conventionally numerical analyses involving coupling physics require availability of experimental data for ease of fine tuning the couplings. This

data requirement was recognised in this research and consequently designing a laboratory set-up capable of distinguished flow measurements was addressed. Available cumulative outflow data provided a foundation for physics coupling validation and design specification requirements of the laboratory set-up.

Comprehensive set of flow equations including porous media flow and Navier-Stokes flow were implemented in the adopted numerical analysis approach in chapter 4. These equations were coupled by defining an equivalent viscosity term that could maintain the continuity of flow and pressure field at the fracture-matrix interface. Such coupling enabled monitoring the evolution of cross flow between the porous matrix and the fracture.

The flow couplings were further augmented with structural mechanics, poro-elasticity and stress dependent permeability formulations to fulfil the requirements of stress effects analysis on the flow dynamics between matrix and fracture. The model geometry and mesh was allowed to move in response to the exerted overburden stress by surface average of the displacement magnitudes calculated for the fracture-matrix interface grids in each stress loading scenario. In this way the geometry and mesh were adjusted per each stress loading and fracture volume contracted to accommodate stress structural effect. Surface averaging of displacements was taken into consideration in an attempt to overcome the computational limitations of coupling all fracture-matrix interface numerical grids displacement to the model complex geometry. The model geometry complexity was an inevitable consequence of a significant size contrast between the fracture aperture and the porous matrix dimensions. Surface averaging seemed not to be an appropriate way of coupling matrix displacements to the fracture geometry when laboratory measurements of matrix and fracture flow were made possible in the last phase, chapter 5, of this study; however, in the beginning that seemed to be an effective technique.

Although applying symmetry boundaries and surface averaging of the interface displacement alleviated the computational works in tackling the mechanistic flow dynamics of the fractured sandstone core flooding, the simulations however were taking days to run on a computationally upgraded computer.

Provided that the laboratory set-up can be augmented with scanning equipment, then more appropriate averaging methods can be implemented after a thorough review of the aperture variation in response to overburden stress. This will upgrade the fracture flow empirical model accuracy.

In terms of cumulative outflow, the coupling strategy proved to be reliable in comparison to the available Clashach sandstone flooding data set. This strengthened the confidence to apply the coupled open fracture concept modelling results in design and implementation of the laboratory set-up.

The only physics which was not accounted for within the numerical simulations was mass transfer governing equations. Mass transfer was considered to be negligible as the scenarios simulated were defined based on the assumption of complete initial saturation of the core plugs. While this assumption was valid for the fluid phase due to complete saturation of the plugs during laboratory analysis, it was not so accurate for the solid phase as a limited amount of sand production was observed in the effluents from both matrix and fracture outflow. Although the produced sand was so much limited, accounting for their production in the simulations governing equations might be another factor to be considered in improving the accuracy of numerical modelling.

6.2.2 Sensitivity analysis and empirical models

Having developed the best modelling approach to evaluate and analyse the mechanistic flow dynamics problem of a stressed fractured porous medium, all the individual parameters contributing to the governing equations implemented in the coupled numerical simulation approach were subjected to a sensitivity study in chapter 4 to enable development of the empirical models provided in section 4.3.

Some of the analysed parameters are inter-related in nature and the methodology applied in this research which considers their effects as independent variables, is questionable; however, it is worth mentioning that the physical governing equations were taken into consideration while the individual effects were addressed comprehensively at the empirical modelling stage.

The overarching objective of the parametric study was to develop empirical models that can be applied with an acceptable accuracy for discontinuous media flow dynamics. This is more significant when considering the several days of computational effort for the single-fracture plug scale problem investigated.

The challenge encountered in developing the empirical models was obtaining a non-linear multi parameter regression fitting. Commercial regression-fitting packages were unable to provide the regression specifically as there was not even a close approximation of the regression needed to initialize the iterative regression fitting procedure. At this stage effects of each set of parameters which were related based on the governing equation were analysed to provide non-linear initial formulation guess for the regression fitting software to process.

On the other hand, individual relationships of the parameters with the modelling target parameter, matrix flow or fracture flow, should have been linear initially for the regression fitting algorithm to function properly. In order to overcome this challenge, for each parametric study that had returned non-linear relationships, pseudo parameters were defined based on an extensive analysis of physical governing equations and individual parameters regression models. In all cases, regression quality parameters like the mean squared error indicator were checked to ensure definition of the best pseudo-parameter for the main regression fitting algorithm.

Various types of formulation in combination with different regression fitting techniques, least prescribed deviation tolerance values and residual confinement criteria were examined in developing the empirical matrix and fracture flow models. Prior to finalization of the models, the residual values as well as the best regression models' predictions distribution over the whole data set, were monitored as a tool in shortlisting the most accurate models.

As figures 4-44 and 4-46 indicate, despite all the mentioned quality assurance considerations, there were still some numerical data points that couldn't be predicted accurately with the regression models. Nevertheless, these data points were found to be sparse numerical data with values significantly larger than the dataset median range and the residuals corresponding to the models'

predictions, when carefully reviewed, fell within one order of magnitude lower than the actual numerical data points. Taking this fact into consideration, the developed empirical models were deemed able to predict the sensitivity analysis results to a reasonable degree of confidence.

In the next step the developed models were validated against laboratory data in an attempt to evaluate their reliability in estimating experimental results, considering the fact that coupled numerical simulations were extremely time consuming if at all numerically responsive. Empirical models fine-tuned against laboratory data can be further generalized to more complex fractured porous formations.

6.2.3 Laboratory validation of the developed empirical models

Several challenges were required to be addressed prior to actual designed experimental procedure in order to run experimental analyses that could reasonably comply with the numerical modelling assumptions and achieve robust laboratory measurements. Designed laboratory techniques assisting in overcoming these challenges are discussed in the following subsections.

6.2.3.1 Plug samples preparation and saturation

In the core plugs saturation phase, flow accumulating plugs should have been initially attached to the core plugs before vacuum suction due to the necessary immediate saturation right after vacuum. Flow accumulating plugs were needed to be glued using a resin epoxy adhesive in order to be compliant with the high pressure operating condition requirements. Any amount of residual epoxy adhesive on the perimeter of the core or flow accumulating plugs, results in a gap generated between the plugs and the core holder sleeve. This gap conducts the flow over the core and flow accumulating plugs and leads to a fluid breakthrough and flaws differential pressure readings. On the other hand, the epoxy resin consolidation time was within few hours; as a result the epoxy application was performed within a precision adhesive application tool

to ensure an aligned smooth circumference over the core plug-flow accumulating plug joints.

When the flow accumulating plugs were fitted, the core plugs were put under vacuum overnight and consequently a high pressure, 1800 psi, low rate flooding for another 24 hours to ensure complete saturation. Absence of bubbles in the outflow and stabilized pressure readings were indicators of complete saturation of the core plugs.

6.2.3.2 Core flooding procedure challenges

There were several operational complexities in implementing a conventional flooding procedure on the custom-designed rig. One of the challenges was exerting the confining pressure over the core plugs. Exerting the required overburden stress at once was a challenge due to the delicate pressure rating of the differential pressure transducers. To protect the transducers, desired overburden was achieved in stages whilst paying attention to the rise of the differential pressures. However, the progressive stress loading stages were completed in early stages of flooding tests and consequently the analysed pressure readings and flow measurements were recorded while the desired overburden stress was achieved.

Differential pressure transducers with extremely low differential pressure ratings selected as a result of presence of fracture also necessitated careful monitoring of the whole flow lines while line pressure was building up. Any minor leakage in the flow line can cause an abnormality in the differential pressures and can cause transducers diaphragm rupture. Even when the transducers can tolerate the leakage effects, they have to undergo re-calibration to provide reliable readings. This concern is one of the major factors contributing to the extended testing time for fractured core laboratory analyses.

Another challenge arising from reduced differential pressure rating of transducers was the core flooding inflow rate control. This concern, in combination with the limited flow accumulating plugs capacity, required the pressure readings to be recorded as soon as the flooding front reached outlet

and stable differential pressures were achieved across the monitoring ports. Although bypass lines were considered for all the transducers, built-up pressure was a major concern in maintaining the integrity of the flooding procedure.

Fracture plane surfaces undergo a wash out for each overburden stress loading tested. Produced sand in both matrix and fracture flows proved that the smooth saw-cut fracture-matrix interface became rougher for successive flooding tests. Gradual erosion of the fracture surfaces caused the averaging of the fracture aperture for numerical analyses to be more erratic. The empirical model for fracture flow is significantly influenced by fracture aperture magnitude. Core plugs cannot be changed for different stress loading scenarios as the key requirement for the tests was to maintain all the rock physical characteristics throughout the entire test regimes. As pointed out previously, scanning the fracture aperture alteration can significantly improve the accuracy and reliability of the numerical simulations and the resulting empirical models.

6.3 Conclusions

Numerical, analytical and experimental analyses carried out during this study improved the understanding of fractured porous medium flow dynamics under various stress loading scenarios. These analyses resulted in developing intrinsically-coupled fracture and matrix flow models which can be employed in characterising near well-bore flow in open-hole completions within fractured reservoirs. Developed models are particularly applicable to reservoirs with permeable rock matrices and with rather parallel fracturing surfaces perpendicular to the wellbore axis (Fig. 1-2).

The empirical models also describe the quality of hydraulic interaction between fractures and rock matrix as the dominant stress loading alters e.g. through reservoir depletion. In case of unconventional tight reservoirs which are brought into production taking the advantages of horizontal drilling and hydraulic fracturing, the models applicability is limited as the formation matrix is unable to flow into the reservoir due to its ultra-low permeability. However

the developed models are capable of evaluating shale oil reservoirs with micro-scale permeability. It is worth mentioning that best parallel pattern for fractures are generated in case of developing unconventional resources via hydraulic fracturing and consequently within permeability magnitudes of higher than micro-scale, the models are so efficient.

Application of the empirical models requires the investigated completion scenario to be comparable to a parallel-pattern fractured scenario in the near wellbore region. In addition, the formation matrix permeability range should be in micro-scale or higher in order to maintain the validity of the parametric study assumptions. Moreover, the formation matrix should be also capable of production into the wellbore in an open hole completion design.

Therefore the empirical models are best suitable for analysing unconventional shale and tight reservoirs which are brought into production via parallel-pattern hydraulic fractures. It is worth mentioning that empirical models can be developed for further complicated fractured reservoirs through modifying the parametric study followed by adjusted corresponding validating laboratory tests.

Specific achievements of the research can be summarised as follows:

1. The best numerical coupling approach for flow in fractured sandstone core plugs has been identified, through validation against published core flooding data, in which fracture domain was simulated as a volume interacting with the matrix in terms of flow. The coupling strategy accounts for Darcy flow within the rock matrix and Navier-Stokes flow within the fracture domain. The two physics maintain pressure and velocity continuity at the matrix fracture interface. Flow governing equations were further coupled with structural mechanics responsible for fracture aperture variation, poro-elasticity and stress dependent permeability physics to account for overburden stress effects.
2. A sensitivity analysis was performed providing the effect of all hydraulic and mechanical factors independently on flow dynamics of a fractured porous medium. This analysis promotes production planning from fractured formations.

3. Empirical models have been developed for fracture and matrix flow accounting for rock mechanical effects. Reference was made to physical governing equations to develop the empirical models; in addition the reliability of the models was checked against the generated numerical data set during the sensitivity analysis in order to ensure a robust regression modelling and avoid compromising the physics coupling authenticity.
4. A novel experimental set-up has been designed and implemented to enable the analysis of flow partitioning between rock matrix and fracture domain under various overburden stresses. Matrix and fracture flow models' efficiencies were evaluated using the data that this custom-designed set-up provided. Matrix flow model proved to be considered reliable, through laboratory validation, as a practical alternative for complex coupled numerical simulations; fracture flow model was not as accurate as the matrix flow model however, improvement studies were identified to fine tune this model further specifically by taking the advantages of the available laboratory set-up. Such models would significantly reduce numerical complexities in predicting hydraulic behaviour of complicated fractured reservoirs.

6.4 Recommendation for further work

Implementing the fit for purpose laboratory set-up that takes into consideration grounds for further upgrade due its thorough initial design, enables analysis of further sophisticated scenarios such as multiphase flooding and matrix-fracture cross flow in fractured core plugs flooding experiments. Furthermore the numerical coupling strategies employed for single phase and multiphase analyses in this dissertation can be further promoted based on the laboratory observations. The current research can be further investigated in the following aspects, to mention just a few, to provide similar empirical models as alternatives for computationally complicated coupled simulations:

1. In accordance with the laboratory observations of sand production, the coupled simulations can be further enriched by addition of mass transport physics to the governing equations.

2. Adopting other averaging techniques for the coupling of stress-induced displacements to the fracture geometry in the fracture flow governing equations can significantly enhance the accuracy of the fracture flow empirical model which is so dependent on fracture aperture size. Fracture asperities and fillings effect can also be incorporated in the numerical simulations via implementing displacements averaging techniques representative of the asperities occurrence pattern on the fracture plane surfaces.
3. A demonstration discussed in chapter 4 proved the applicability of the current research numerical approach to time-dependent multi-phase flow scenarios. The study can be further analysed for these complicated flow dynamic problems within fractured porous media to achieve mechanically coupled empirical models for multi-phase flooding regimes.
4. The numerical approach can be extended to several intersecting fractures model to develop empirical models that can be used for coupled flow analyses in fracture networks. Up-scaling can be facilitated through fracture planes relative angles and apertures which in turn can be considered as functions of in-situ stress regime.
5. The laboratory set-up can be conveniently upgraded by adding another pump for further flooding phases due to the presence of the accumulator and two other inlet ports that have been considered on the core holder. The core holder can also be utilized for a tri-axial stress scenario as the core holder outlet is equipped with a hydraulically moving rod that can exert axial stress to the core plug by means of a hydraulic power source. This will provide the chance for evaluating more complex and realistic mechanical conditions.
6. Augmentation of the laboratory set-up with CT scanning devices will improve the tracking of the flooding front specifically for multiphase scenarios. It will also improve the understanding of the stress-induced displacements that can be referred to when deciding on averaging technique suitable for the physics coupling.

References

Agar, S. M., Geiger, S., Matthai, S., Alway, R., Tomas, S., Immenhauser, A., Shekhar, R., Paul, J., Benson, G. and Kabiri, L. (2010) The impact of hierarchical fracture networks on flow partitioning in carbonate reservoirs: examples based on a Jurassic carbonate ramp analogue from the High Atlas, Morocco. Society of Petroleum Engineers, doi:10.2118/135135-MS.

Akin, S. and Kovscek, A. R. (1998) Imbibition studies of low-permeability porous media. Society of Petroleum Engineers, doi:10.2118/54590-MS.

Alajmi, A. F. and Grader, A. S. (2000) Analysis of fracture-matrix fluid flow interactions using X-ray CT. Society of Petroleum Engineers, doi:10.2118/65628-MS.

Ameri Ghasrodashti, A., Farajzadeh, R., Verlaan, M., Suicmez, V. S. and Bruining, H. (2013) Dynamic interactions between matrix and fracture in miscible solvent flooding of fractured reservoirs. 17th European Symposium on Improved Oil Recovery, St. Petersburg, Russia.

Apaydin, O. G., Bertin, H., Castanier, L. M. and Kovscek, A. R. (1998) An experimental investigation of foam flow in homogenous and heterogeneous porous media. U.S. Department of Energy Topical Report, SUPRI TR 112.

Aziz, K. and Settari, A. (1979) Petroleum reservoir simulation. Applied Science Publishers Ltd, London.

Baghbanan, A. (2008) Scale and stress effects on hydro-mechanical properties of fractured rock masses. PhD dissertation, Land and Water Resources Engineering Department, KTH Royal Institute of Technology, Sweden.

Bai, M. and Elsworth, D. (1994) Modelling of subsidence and stress-dependent hydraulic conductivity for intact and fractured porous media. *Rock Mechanics and Rock Engineering*, 27, 4, 209-234.

Bai, M., Meng. F., Elsworth, D. and Rogiers, J. C. (1999) Analysis of stress-dependent permeability in nonorthogonal flow and deformation fields. *Rock Mechanics and Rock Engineering*, 32, 3, 195-219.

Bai, M., Meng. F., Elsworth, D., Zaman, M. and Rogiers, J. C. (1997) Numerical modeling of stress-dependent permeability. *Int. J. Rock Mech & Min. Sci.*, 34, 3-4, Paper No. 020.

Bai, M., Roegiers, J. C. and Elsworth, D. (1995) Poromechanical response of fractured-porous rock masses. *Journal of Petroleum Science and Engineering*, 13, 155-168.

Bandis, S. C., Lumsden, A. C. and Barton, N. R. (1983) Fundamentals of rock joint deformation. *International Journal of Rock Mechanics and Mining Sciences & Geomechanical Abstracts*, 20(6), 249-268.

Barton, C. A., Moos, D., Hartley, L., Baxter, S., Foulquier, L., Holl, H. and Hogarth, R. (2013) Geomechanically coupled simulation of flow in fractured reservoirs. *Proceedings, Thirty-eighth Workshop on Geothermal Reservoir Engineering*, Stanford, USA.

Barton, N. R., Bandis, S. C. and Bakhtar, K. (1985) Strength, deformation and conductivity coupling of rock joints. *International Journal of Rock Mechanics and Mining Sciences & Geomechanical Abstracts*, 22(3), 121-140.

Bayani Cardenas, M. and Wilson, J. L. (2007) Hydrodynamics of coupled flow above and below a sediment-water interface with triangular bedforms. *Advances in Water Resources*, 30, 301-313.

Berryman, J. G. (2004) Poroelastic fluid effects on shear for rocks with soft anisotropy. University of California, Lawrence Livermore National Laboratory, UCRL-JRNL-203522.

Bertin, H. J., Apaydin, O. G., Castanier, L. M. and Kavscek, A. R. (1999) Foam flow in heterogeneous porous media. *Society of Petroleum Engineers*, doi:10.2118/56009-PA.

Beydoun, Z. R. (1998) Arabian plate oil and gas: why so rich and so prolific?, *Episodes Journal of International Geoscience*, 21, 74-81.

Bidlack, D. L. and Anderson, D. K. (1964) Mutual diffusion in the liquid system Hexane-Hexadecane. *The Journal of Physical Chemistry*, 68, 1, 206-208.

Biot, M. A. (1941) General theory of three-dimensional consolidation. *Journal of Applied Physics*, 12, 155-164.

Biot, M. A. (1955) Theory of elasticity and consolidation for a porous Anisotropic solid. *Journal of Applied physics*, 26, 2, 182-185.

Biot, M. A. (1956a) General solutions of the equations of elasticity and consolidation for a porous material. *Journal of Applied Mechanics*, March, 91-96.

Biot, M. A. (1956b) Thermoelasticity and irreversible thermodynamics. *Journal of Applied Physics*, 27, 3, 240-253.

Biot, M. A. (1962) Mechanics of deformation and acoustic propagation in porous media. *Journal of Applied physics*, 33, 4, 1482-1498.

Bourbiaux, B., Basquet, R., Cacas, M. C., Daniel, J. M. and Sarda, S. (2002, January1) An integrated workflow to account for multi-scale fractures in reservoir simulation models: implementation and benefits. Society of Petroleum Engineers. doi:10.2118/78489-MS.

Burchette, T. (2012) Carbonate rocks and petroleum reservoirs: A geological perspective from industry. Geological Society, Special Publications 2012, London, 370, 17-37.

Chacon, A. and Tiab, D. (2007) Impact of pressure depletion on oil recovery in naturally fractured reservoirs. Society of Petroleum Engineers, doi:10.2118/108107-MS.

Chen, C. Y. (2005) Liquid-gas relative permeabilities in fractures: effects of flow structures, phase transformation and surface roughness. Stanford Geothermal Program interdisciplinary Research in Engineering and Earth Sciences, Stanford University, Stanford, USA, SGP-TR-177.

Cito, S. (2009) Numerical and experimental study of flow and wall mass transfer rates in capillary driven flows in microfluidic channels. PhD dissertation, Department of Mechanical Engineering, Universitat Rovira I Virgili, Spain.

Coumou, D., Matthai, S., Geiger, S. and Driesner, T. (2008) A parallel FE-FV scheme to solve fluid flow in complex geologic media. *Computers & Geosciences*, 34, 1697-1707.

Crandall, D., Ahmadi, G. and Smith, D. H. (2010) Computational modelling of fluid flow through a fracture in permeable rock. *Transp. Porous Med.*, 84, 493-510.

Crawford, B. R., Smart, B. G. D., Main, I. G. and Liakopoulou-Morris, F. (1995) Strength characteristics and shear acoustic anisotropy of rock core subjected to true triaxial compression. *International Journal of Rock Mechanics and Mining Sciences & Geomechanics Abstracts*, 32, 3, 189-200.

Dershowitz, B., LaPointe, P., Eiben, T., and Wei, L. (2000, April 1). Integration of discrete feature network methods with conventional simulator approaches. Society of Petroleum Engineers. doi:10.2118/62498-PA.

Detournay, E. and Cheng, A. H. D. (1993) Fundamentals of poro-elasticity. In: *Comprehensive Rock Engineering: Principles, Practice and Projects*, Vol. II, Analysis and Design Method, C. Fairhurst [Ed.], Pergamon Press, 113-171.

Detwiler, R. L. (2008) Experimental observations of deformation caused by mineral dissolution in variable-aperture fracture. *Journal of Geophysical research*, 113, No. B08202.

Detwiler, R. L. and Rajaram, H. (2000) Solute transport in variable-aperture fractures: An investigation of the relative importance of Taylor dispersion and macrodispersion. *Water Resources Research*, 36, 1611-1625.

Detwiler, R. L., Pringle, S. E. and Glass, R. J. (1999) Measurement of fracture aperture fields using transmitted light: An evaluation of measurement errors and their influence on simulations of flow and transport through a single fracture. *Water Resources Research*, 35, 2605-2617.

Detwiler, R. L., Rajaram, H. and Glass, R. J. (2002) Experimental and simulated solute transport in a partially-saturated variable-aperture fracture. *Geophysical Research Letters*, 29, No. 8.

Diaz-Viera, M. A., Lopez-Falcon, D. A., Moctezuma-Berthier, A. and Ortiz-Tapia, A. (2008) COMSOL implementation of a multiphase fluid flow model in porous media. *Proceedings of the COMSOL Conference, Boston 2008, USA*.

Di Donato, G. and Blunt, M. J. (2004) Streamline-based dual-porosity simulation of reactive transport and flow in fractured reservoirs. *Water Resour. Res.*, 40, W04203, doi:10.1029/2003WR002772.

Dutra Jr, T. V. and Aziz, K. (1992) A new double-porosity reservoir model for oil/water flow problems. *Society of Petroleum Engineers*. doi:10.2118/21248-PA.

Elfeel, M. A., Couples, G., Geiger, S. and Ma, J. (2010) Upscaled multi-phase flow properties of fracture corridors. *Society of Petroleum Engineers*, doi:10.2118/139463-MS.

Elkhoury, J. E., Ameli, P. and Detwiler, R. L. (2013) Dissolution and deformation in fractured carbonates caused by flow of CO₂-rich brine under reservoir conditions. *International Journal of Greenhouse Gas Control*, 16S, S203-S215.

Evans, R. D. (1982) A proposed model for multi-phase flow through naturally fractured reservoirs. *Society of Petroleum Engineers*, doi:10.2118/9940-PA.

Faoro, I., Elsworth, D. and Marone, C. (2012) Permeability evolution during dynamic stressing of dual permeability media. *Journal of Geophysical Research*, 117, B01310, doi:10.1029/2011JB008635.

Faoro, I., Niemeiger, A., Marone, C. and Elsworth, D. (2009) Influence of shear and deviatoric stress on the evolution of permeability in fractured rock. *Journal of Geophysical Research*, 114, B01201, doi:10.1029/2007JB005372.

Faoro, I., Vinciguerra, S., Marone, C., Elsworth, D. and Schubnel, A. (2013) Linking permeability to crack density evolution in thermally stressed rocks under cyclic loading. *Geophysical Research Letters*, 40, 2590-2595.

Ferer, M., Crandall, D., Ahmadi, G. and Smith, D. H. (2011) Two-phase flow in a rough fracture: Experiment and modelling. *Physical Review E*, 84, No. 016316.

Fleming, S. W. and Haggerty, R. (2001) Modelling solute diffusion in the presence of pore-scale heterogeneity. *Journal of Contaminant Hydrology*, 48, 3-4, 253-276.

Frampton, A. (2010) Stochastic analysis of fluid flow and tracer pathways in crystalline fracture networks. PhD dissertation, Land and Water Resources Engineering Department, KTH Royal Institute of Technology, Sweden.

Franquet, J. A. and Abass, H. H. (1999) Experimental evaluation of Biot's poroelastic parameter – three different methods. In: Rock Mechanics for Industry. Amadei, Kranz, Scott & Smeallie [Eds], Balkema, Rotterdam, ISBN: 9058090523, 349-355.

Gambolati, G., Ferronato, M., Teatini, P., Deidda, R. and Lecca, G. (2001) Finite element analysis of land subsidence above depleted reservoirs with pore pressure gradient and total stress formulations. *Int. J. Numer. Anal. Meth. Geomech.*, 25, 307-327.

Griso, G. and Rohan, E. (2007) On the homogenization of a diffusion-deformation problem in strongly heterogeneous media. *Recherche mat.*, 56, 161-188.

Han, D. (1996) Flow systems and dispersion characteristics of fractured core samples. PhD dissertation, School of Petroleum and Geological Engineering, University of Oklahoma, USA.

Hoteit, H. and Firoozabadi, A. (2008) An efficient numerical model for incompressible two-phase flow in fractured media. *Advances in Water Resources*, 31, 891-905.

Hughes, R. G. and Blunt, M. J. (2001) Pore-scale modelling of multiphase flow in fractures and matrix/fracture transfer. Society of Petroleum Engineers, doi:10.2118/71297-PA.

Ito, K. and Seol, Y. (2003) A 3-dimensional discrete fracture network generator to examine fracture-matrix interaction using TOUGH2. Proceedings of TOUGH Symposium 2003, Berkeley, USA.

Jaffre, J., Mnejja, M. and Roberts, J. E. (2011) A discrete fracture model for two-phase flow with matrix-fracture interaction. *Procedia Computer Science*, 4, 967-973.

Jamshidi, E. and Amani, M. (2014) Numerical wellbore stability analysis using discrete element models. *Petroleum Science and Technology*, 32, 8, 974-982.

Jones, C. and Somerville, J. M. (2001) Attenuation changes during oilflood experiments. *Society of Core Analysis*, SCA 2001-54.

Karpyn, Z. T., Alajmi, A., Radaelli, F., Halleck, P. M. and Grader, A. S. (2009) X-ray CT and hydraulic evidence for a relationship between fracture conductivity and adjacent matrix porosity. *Engineering Geology*, 103, 139-145.

Kazemi, H., Gillman, J. R. and Elsharkawy, A. M. (1992) Analytical and numerical solution of oil recovery from fractured reservoirs with empirical transfer functions (includes associated papers 25528 and 25818). *Society of Petroleum Engineers*, doi:10.2118/19849-PA.

Kazemi, H. and Gilman, J. R. (1993) Multiphase flows in fractured petroleum reservoirs. *Flow and Contaminant Transport in Fractured Rocks*, (eds J. Bear, Tsang, C. F. and De Marsily, G.), Academic Press, New York.

Keller, A. A. (1996) Single and multiphase flow and transport in fractured porous media. PhD dissertation, Department of Civil Engineering, Stanford University, USA.

Kovscek, A. R., Zhou, D., Jia, L. and Kamath, J. (2000) Scaling of counter-current imbibition processes in low-permeability porous media. U.S. Department of Energy Topical Report, SUPRI TR 121.

Laurent, J., Bouteica, M. J., Sarda, J. P. and Bary, D. (1993) Pore pressure influence in the poroelastic behaviour of rocks: Experimental studies and results. Society of Petroleum Engineers, doi:10.2118/20922-PA.

Lee, S. H., Jensen, C. L. and Lough, M. F. (2000) Efficient finite-difference model for flow in a reservoir with multiple length-scale fractures. Society of Petroleum Engineers, doi:10.2118/56752-MS.

Liu, J., Bodvarsson, G. S. and Wu, Y. S. (2003) Analysis of flow behaviour in fractured lithophysal reservoirs. *Journal of Contaminant Hydrology*, 62-63, 189-211.

Liu, J., Chen, Z., Elsworth, D., Miao, X and Mao, X. (2011) Evolution of coal permeability from stress-controlled to displacement-controlled swelling conditions. *Fuel*, 90, 2987-2997.

Malik, Q. M., da Rocha, B. R. P., Marsden, J. R. and King, M. S. (1998) High pressure electromagnetic fractal behaviour of sedimentary rocks. *Progress in Electromagnetics Research*, PIER 19, 223-240.

Martys, N. S. and Hagedorn, J. G. (2002) Multi scale modelling of fluid transport in heterogeneous material using discrete Boltzmann methods. *Materials and Structures*, 35, 650-659.

Matthai, S. K. and Belayneh, M. (2004) Fluid flow partitioning between fractures and a permeable rock matrix. *Geophysical research Letters*, 31, L07602.

Matthai, S. K., Mezentsev, A. and Belayneh, M. (2007) Finite element-node-centred finite-volume two-phase-flow experiments with fractured rock represented by unstructured hybrid-element meshes. Society of Petroleum Engineers, doi:10.2118/93341-PA.

Mavko, G., Mukerji, T. and Dvorkin, J. (1998) *The rock physics handbook: Tools for seismic analysis in porous media*. Cambridge University Press.

McGuire, P. L., Chatham, J. R., Paskvan, F. K., Sommer, D. M. and Carini, F. H. (2005) Low salinity oil recovery: An exciting new EOR opportunity for Alaska's north slope. Society of Petroleum Engineers, doi:10.2118/93903-MS.

Min, K. B., Rutqvist, J. and Elsworth, D. (2009) chemically and mechanically mediated influences on the transport and mechanical characteristics of rock fractures. *International Journal of Rock Mechanics & Mining Sciences*, 46, 80-89.

Mogilevskaya, S. G., Rothenburg, L. and Dusseault, M. B. (2000) Growth of pressure-induced fractures in the vicinity of a wellbore. *International Journal of Fracture*, 104, L25-L30.

Montaron, B. (2008) Carbonate evolution. *Oil & Gas Middle East*, August, 26-31.

Nelson, R. A. (2001) Geological analysis of naturally fractured reservoirs, 2nd edition, Gulf Professional Publishing, 1-100.

Ojala, I. O. (2003) Stress corrosion crack growth in porous sandstones. PhD dissertation, College of Science and Engineering, School of Geoscience, University of Edinburgh, UK.

Oluyemi, G. F. and Ola, O. (2010) mathematical modelling of the effects of in-situ stress regime on fracture-matrix flow partitioning in fractured reservoirs. Society of Petroleum Engineers, doi:10.2118/136975-MS.

Ozkan, E., Raghavan, R. and Apaydin, O. G. (2010) Modeling of fluid transfer from shale matrix to fracture network. Society of Petroleum Engineers, doi:10.2118/134830-MS.

Palciauskas, V. V. and Domenico, P. A. (1989) Fluid pressures in deforming porous rocks. Water Resources Research, 25, 2, 203-213.

Paluszny, A. (2009) Numerical simulation of fracture pattern development and implications for fluid flow. PhD dissertation, Earth Science and Engineering Department, Imperial College, London, UK.

Paul, P., Zoback, M. and Hennings, P. (2007) Fluid flow in a fractured reservoir using a geomechanically-constrained fault zone damage model for reservoir simulation. Society of Petroleum Engineers, doi:10.2118/110542-MS.

Pentland, C. H. (2010) Measurements of non-wetting phase trapping in porous media. PhD dissertation, Earth Science and Engineering Department, Imperial College, London, UK.

Petchsingto, T. and Karpyn, Z. T. (2009) Deterministic modelling of fluid flow through a CT-scanned fracture using computational fluid dynamics. *Energy Sources, Part A*, 31, 897-905.

Petchsingto, T. and Karpyn, Z. T. (2010) Simulation of fluid percolation in a rough-walled rock fracture. *Hydrogeology Journal*, 18, 1583-1589.

Philip, Z. G., Jennings Jr., J. W., Olson, J. E., Laubach, S. E. and Holder, J. (2005) Modelling coupled fracture-matrix fluid flow in geomechanically simulated fracture networks. *Society of Petroleum Engineers*, doi:10.2118/77340-MS.

Piller, M., Casagrande, D., Schena, G. and Santini, M. (2014) Pore-scale simulation of laminar flow through porous media. *Journal of Physics, Conference Series* (512), 012010.

Piri, M. and Karpyn, Z. T. (2007) prediction of fluid occupancy in fractures using network modelling and x-ray microtomography. *Physical Review E*, 76, No. 016316.

Polak, A., Elsworth, D., Liu, J. and Grader, A. S. (2004) Spontaneous switching of permeability changes in a limestone fracture with net dissolution. *Water Resources Research*, 40, W03502.

Pruess, K. and Wu, Y. S. (1991) A new empirical method for numerical simulation of fluid and heat flow in fractured reservoirs. Society of Petroleum Engineers, doi:10.2118/18426-PA.

Rangel-German, E. R., Akin, S. and Castanier, L. (1999) Multiphase flow properties of fractured porous media. Society of Petroleum Engineers, doi:10.2118/54591-MS.

Rangel-German, E. R. and Kavscek, A. R. (2000) Matrix-fracture interaction in single matrix blocks. Twenty-fifth Workshop on Geothermal Reservoir Engineering, Stanford, USA.

Rangel-German, E. R. and Kavscek, A. R. (2001) Experimental and analytical study of multidimensional imbibition in fractured porous media. U.S. Department of Energy Topical Report, SUPRI TR 129.

Raven, K. G. and Gale, J. E. (1985) Water flow in a natural rock fracture as a function of stress and sample size. International journal of Rock Mechanics Mining Sciences and Geomechanics Abstracts, 22, 251-261.

Reynolds, D. A. and Kueper, B. H. (2001) Multiphase flow and transport in fractured clay/sand sequences. Journal of Contaminant Hydrology, 51, 41-62.

Rice, J. R. (1992) Fault mechanics and transport properties of rocks. Edited by Bryan Evans and Teng-Fong Wong, Academic Press Ltd, 475-503.

Rice, J. R. and Cleary, M. P. (1976) Some basic stress diffusion solutions for fluid saturated elastic porous media with compressible constituents. *Reviews of Geophysics and Space Physics*, 14, 2, 227-241.

Rubin, B. (2010) Accurate simulation of non-Darcy flow in stimulated fractured shale reservoirs. Society of Petroleum Engineers, doi:10.2118/132093-MS.

Rutqvist, J., Wu, Y. S., Tsang, C. F. and Bodvarsson, G. (2002) A modelling approach for analysis of coupled multiphase fluid flow, heat transfer and deformation in fractured porous rock. *International Journal of Rock Mechanics and Mining Sciences*, 39, 429-442.

Sanaee, R., Oluyemi, G. F., Hossain, M. and Oyeneyin, M. B. (2012) Fracture-matrix flow partitioning and cross flow: Numerical modelling of laboratory fractured core flood. In: *Proceedings of 2012 COMSOL Multi-Physics Conference*, Milan, Italy.

Sanaee, R., Oluyemi, G. F., Hossain, M. and Oyeneyin, M. B. (2013) Stress effects on flow partitioning in fractured reservoirs: Equivalent porous media versus poro-elasticity coupled modelling. American Rock Mechanics Association, In: *Proceedings of 47th US Rock Mechanics/ Geomechanics Symposium*, San Francisco, USA.

Sanaee, R., Shadizadeh, S. R. and Riahi, M. A. (2010) Determination of the stress profile in a deep borehole in a naturally fractured reservoir. *International Journal of Rock Mechanics and Mining Sciences*, 47, 4, 599-605.

Sarda, S., Jeannin, L., Basquet, R. and Bourbiaux, B. (2002) hydraulic characterization of fractured reservoirs: simulations on discrete fracture models. Society of Petroleum Engineers, doi:10.2118/66398-MS.

Sarkar, S., Toksoz, M. N. and Burns, D. R. (2002) Fluid flow simulation in fractured reservoirs. Massachusetts Institute of Technology, Earth Resources Laboratory Industry Consortia Annual Report, 2002-12.

Schembre, J., Akin, S. and Kovscek, A. R. (1998) Spontaneous imbibition in low permeability media. U.S. Department of Energy Topical Report, SUPRI TR 114.

Settari, A., Walters, D. A. and Behie, G. A. (2001) Use of coupled reservoir and geomechanical modelling for integrated reservoir analysis and management. Petroleum Society of Canada. doi:10.2118/01-12-04

Shafer, J. L., Boitnott, G. N. and Ewy, R. T. (2008) Effective stress laws for petrophysical rock properties. SPWLA 49th Annual Logging Symposium, May 2008, Edinburgh, UK.

Slough, K. J., Sudicky, E. A. and Forsyth, P. A. (1999) Numerical simulation of multiphase flow and phase partitioning in discretely fractured geologic media. *Journal of Contaminant Hydrology*, 40, 107-136.

Souley, M., Boulon, M., Rahmani, I. and Thoraval, A. (2007) laboratory measurements of hydraulic exchanges and associated hydromechanical couplings between fracture and rock mass in the case of a sandstone. In: Rebeiro e Sousa, Olalla & Grossmann [Ed.] 11th Congress of the International Society for Rock Mechanics. Taylor & Francis Group, London, 327-330.

Stalker, R., Graham, G. M. and Oluyemi, G. (2009) Modelling stage diversion treatments and chemical placement in the presence of near-wellbore fractures. Society of Petroleum Engineers, doi:10.2118/121683-MS.

Stalgorova, E. and Babadagli, T. (2012) Field-scale modelling of tracer injection in naturally fractured reservoirs using the random-walk particle-tracking simulation. Society of Petroleum Engineers, doi:10.2118/144547-PA.

Suzuki, A., Niibory, Y., Fomin, S. A., Chugunov, V. A. and Hashida, T. (2014) Characterisation of mass/heat transfer in fractured geothermal reservoirs using mathematical model of complex dynamical system. Proceedings of Thirty-ninth Workshop on Geothermal Reservoir Engineering, Stanford, USA.

Tamayol, A. and Bahrami, M. (2008) Numerical investigation of flow in fibrous porous media. ECI International Conference on Heat Transfer and Fluid Flow in Microscale, Whistler, Canada.

Taniguchi, T. and Fillion, E. (1996) Numerical experiments for 3-dimensional flow analysis in a fractured rock with porous matrix. *Advances in Water Resources*, 19, 97-107.

Terzaghi, K. V. (1923) Die Berechnung der Durchlässigkeitsziffer des tones aus dem verlauf der hydrodynamischen spannungerscheinungen. *Sitzber. Akad. Wiss. Wien, Abt. IIa*, 132, 125-138.

Thorenz, C. (2001) Model adaptive simulation of multiphase and density driven flow in fractured and porous media. PhD dissertation, Institute of Fluid Mechanics and Environmental Physics in Civil Engineering, University of Hannover, Germany.

Tidwell, V. C., Glass, R. J. and Peplinski, W. (1995) Laboratory investigation of matrix imbibition from a flowing fracture. *Geophysical Research Letters*, 22, 11, 1405-1408.

Tran, N. H. and Ravoof, A. (2007) Coupled fluid flow through discrete fracture network: A novel approach. *International Journal of Mathematics and Computers in Simulation*, 1, 3, 295-299.

Unsal, E., Matthai, S. K. and Blunt, M. J. (2010) Simulation of multiphase flow in fractured reservoirs using a fracture-only model with transfer functions. *Computational Geosciences*, 14, 4, 527-538.

Van Golf-Racht, T. D. (1982) *Fundamentals of fractured reservoir engineering (Developments in petroleum science)*. Elsevier Scientific Publishing Company, Amsterdam – Oxford – New York, ISBN-13: 978-0444420466, 147-169.

Van Oort, E. (1994) A novel technique for investigation of drilling fluid induced borehole instability in shales. *Society of Petroleum Engineers*, doi:10.2118/28064-MS.

Vasquez, G. F., Junior, E. A. V., Ribeiro, C. J. B., Leao, M. and Justen, J. C. R. (2009) Experimental determination of the effective pressure coefficients for Brazilian limestones and sandstones. *Brazilian Journal of Geophysics*, 27, 1, 43-53.

Voelker, J. (2004) A reservoir characterization of Arab-D super-K as a discrete fracture network flow system, Ghavar field, Saudi Arabia. PhD dissertation, Department of Petroleum Engineering, Stanford University, USA.

Wang, S., Elsworth, D. and Liu, J. (2011) Permeability evolution in fractured coal: The roles of fracture geometry and water content. *International Journal of Coal Geology*, 87, 13-25.

Warren, J. E. and Root, P. J. (1963) The behaviour of naturally fractured reservoirs. Society of Petroleum Engineers. doi:10.2118/426-PA.

Weatherill, D., Graf, T., Simmons, C. T., Cook, P. G., Therrien, R. and Reynolds, D. A. (2008) Discretizing the fracture-matrix interface to simulate solute transport. *Ground Water*, 46, 4, 606-615.

Wesselingh, J. A. and Bollen, A. M. (1997) Multicomponent diffusivities from the free volume theory. *Trans IChemE*, 75, A, 590-602.

Wu, Y. S. and Pruess, K. (2005) A physically based numerical approach for modelling fracture-matrix interaction in fractured reservoirs. *Proceedings World Geothermal Congress 2005, Antalya, Turkey*.

Wu, Y. S. and Qin, G. (2009) A generalized numerical approach for modelling multiphase flow and transport in fractured porous media. *Communications in Computational Physics*, 6, 1, 85-108.

Wu, Y. S., Pan, L. and Pruess, K. (2004) A physically based approach for modelling multiphase fracture-matrix interaction in fractured porous media. *Advances in Water Resources*, 27, 875-887.

Wu, Y. S., Zhang, K., Ding, C., Pruess, K., Elmroth, E. and Bodvarsson, G. S. (2002) An efficient parallel computing method for modelling nonisothermal

multiphase flow and multicomponent transport in porous and fractured media. *Advances in Water Resources*, 25, 243-261.

Zhang, J., Bai, M. and Roegiers, J. C. (2003) Dual-porosity poroelastic analyses of wellbore stability. *International Journal of Rock Mechanics and Mining Sciences*, 40, 473-483.

Zhu, W. C., Liu, J., Sheng, J. C. and Elsworth, D. (2007) Analysis of coupled gas flow and deformation process with desorption and Klinkenberg effects in coal seams. *International Journal of Rock Mechanics and Mining Sciences*, 44, 971-980.

Zinn, B., Meigs, L. C., Harvey, C. F., Haggerty, R., Peplinski, W. J. and Von Schwerin, C. F. (2004) Experimental visualization of solute transport and mass transfer processes in two-dimensional conductivity fields with connected regions of high conductivity. *Environmental Science Technology*, 38, 3916-3926.

Appendix A: Publications

Proceedings of 2012 COMSOL Multi-Physics Conference, Milan, Italy

Fracture-Matrix Flow Partitioning and Cross Flow: Numerical Modeling of Laboratory Fractured Core Flood

R. Sanaee*, G. F. Oluyemi, M. Hossain, and M. B. Oyeneyin

Robert Gordon University

*Corresponding author: Clarke Building, RGU, Schoolhill, Aberdeen, U.K, AB10 1FR, r.sanaee@rgu.ac.uk

ARMA 13-442



Stress effects on flow partitioning in fractured reservoirs: equivalent porous media versus poro-elasticity coupled modeling

Sanaee, R.

Robert Gordon University, Aberdeen, United Kingdom

Oluyemi, G.F. and Hossain, M.

Robert Gordon University, Aberdeen, United Kingdom

Oyeneyin, M.B.

Robert Gordon University, Aberdeen, United Kingdom

****Please refer to the printed version of the thesis to access the full articles.**